Modelling of Power System Transformers in the Complex Conjugate Harmonic Space

A thesis
presented for the degree of
Doctor of Philosophy in Electrical Engineering
in the
University of Canterbury,
Christchurch, New Zealand

by

Enrique Acha Daza

1988

Vobis Aliquid Propono:

finxit deus mulierem huius ex ventre est natus vir

Maria Teresa

Monica Joan

Emily Susana

Monica Siobhan

Contents

List of Figures

List of Main Symbols

ψ,X	Magnetic fluxes
i,y	Magnetizing currents
ΔI,ΔY	Vectors of superimposed harmonic currents
ΔV,ΔU	Vectors of superimposed harmonic voltages
I_N,Y_N	Norton equivalent current sources
$[G]$,$[F]$,$[H]$	Matrices of magnetic admittances
$\{Y\}_t$,$\{Y_l\}$	Diagonal matrices of leakage admittances of transformer
$\{Y\}$	Diagonal matrix of transfer admittances of the line
$[Z]$	Lumped series impedance matrix of a multiconductor line
$[\psi]$	Matrix of potential coefficients
$[T_v]$,$[T_i]$	Matrices of modal transformations
$[Y_J]$	Harmonic admittance-Jacobian matrix of the entire network
z_c	Characteristic impedance
τ	Propagation characteristic
l	Length of the line
h	Harmonic order
s_e,t_e,u_e,v_e	Coefficients for the evaluation of ground impedances
s_c,t_c,u_c,v_c	Coefficients for the evaluation of conductor impedances(skin effect)

The present research has given place to the publications cited below:

J. Arrillaga, E. Acha, T.J. Densem and P.S. Bodger. Ineffectiveness of transmission line transpositions at harmonic frequencies. Proceedings IEE Part C, 133(2):99-104,March 1986.

A. Semlyen, E. Acha and J. Arrillaga. Harmonic Norton equivalent for the magnetizing branch of a transformer. Proceedings IEE Part C, 134(2):162-169, March 1987.

A. Semlyen, E. Acha and J. Arrillaga. Newton-type algorithms for the harmonic analysis of non-linear power circuits in periodical steady state with special reference to magnetic non-linearities. In PES Winter Meeting, IEEE Power Engineering Society, New Orleans, Louisiana, November 17 1987.

J. Arrillaga, E. Acha, N. Watson and N. Veale. Ineffectiveness of transmission line VAR compensation at harmonic frequencies. Accepted for presentation in ICHPS-IEEE to be held in Nashville, Indiana in September, 1988.

E. Acha, J. Arrillaga. Modal analysis of harmonic propagation with particular reference to the effect of transmission line transpositions. Accepted for presentation in ICHPS-IEEE to be held in Nashville, Indiana in September, 1988.

E. Acha, J. Arrillaga. An efficient algorithm for the analysis of harmonic propagation in long transmission lines. Accepted for publication in the Australian Journal of Electrical Engineering.

Abstract

Magnetizing harmonics in power systems have received limited attention. The general belief is that they do not reach harmful levels in interconnected networks. Moreover the modelling of non-linearities is not a straightforward procedure and so there has been little motivation to develop appropriate methodologies that allow a thorough investigation to take place.

In this thesis the problem of magnetizing harmonics in power systems is investigated. The results obtained show that, contrary to expectations, magnetizing currents can give rise to a considerable harmonic distortion in the voltage wave form of power networks operating under loaded conditions.

The method adopted in this research linearizes each magnetic non-linearity around a base operating point.The linearization exercise takes place in the complex-conjugate harmonic space and the individual linearized equations may be interpreted as harmonic Norton equivalents. These equations combine easily with each other and with the transfer admittances representing the linear part of the network. The overall process of linearization may be seen as a linearization of the entire network and can also be interpreted as a multi-nodal, polyphase harmonic Norton equivalent.

This problem is non-linear and the harmonic solution is reached by an iterative process. A re-linearization of the network takes place at each iterative step and so the solution is found through a Newton-type procedure. Several iterative strategies are tested, including unified and sequential solutions with either single or multi-evaluated Jacobians.

A hitherto neglected problem which also receives attention is the harmonic modelling of non-homogenous transmission lines. A novel approach to the modelling of the frequence dependent part of the transmission line is also presented. The equations proposed are shown to be the fastest to date and yet maintain a high degree of accuracy.

Acknowledgements

It is true that even a modest contribution, such as the present one, could not have been possible without a pleasent enviroment and the excellent resources provided by the University of Canterbury. Equally important has been the support and advice given by many people. In particular, I wish to thank Professor Josu Arrillaga, who has been a cornerstone in the development of this work.

At a very early stage in this research I was also also fortunate to work under the guidance of Professor Adam Semlyen. The knowledge gathered during that brief period has proved to be the backbone of this thesis. I wish to extend my warmest thanks to Professor Semlyen.

Much earlier, at the beginning of my professional education, Salvador Acha pointed out power engineering to me as an area of rewarding endeavours. He also taught me many of the basic concepts that have been useful resource when dealing with the intricacies of this research. I hope the time is correct and this space is appropriate to express my gratitude to him.

The generous help of M.G. Derrington is truly appreciated. His detailed reading of the first part of the manuscript resulted in changes that have greatly enhanced the presentation of many of the arguments contained in this thesis.

Finally, I wish to express a word of gratitude to Sandeep Chugh, Andrew Elder, Bruce Davey, Vadivelu Rahuraman and Aurelio Medina . Without their kind and timely help this thesis could not have been completed in its present form.

Chapter 1

Introduction

1.1 General

The last quarter of the nineteen century saw the development of the electricity supply industry as a new, promising and fast growing activity[1]. Since that time electrical power networks have undergone immense transformations.

Owing to the relative safety and cleanliness of electricity, it quickly became established in man's environment. Nowadays it is closely linked to primary activities such as industrial production, transport, communications and agriculture. Population growth, expectations of higher standards of living, technological innovation and higher capital gains are just a few of the factors that have maintained the momentum of the power industry.

Clearly it has not been easy for the power industry to reach its present status. Throughout its development innumerable technical and economic problems have been overcome, enabling the supply industry to meet the ever increasing demand for energy with electricity at competitive prices. The generator, the incandescent lamp and the industrial motor were the basis of the success of the earliest schemes. Soon the transformer provided a means for improved efficiency of distribution so that the generation and transmission of alternating current over considerable distances provided a major source of power in industry and also in domestic applications. More recently the power converter has permitted the transmission of a large amount of power over very great distances, and the interconnection of individual systems having different frequencies.

Under ideal operating conditions the electrical wave of AC networks is expected to be sinusoidal with constant amplitude and frequency. In practice, however, to a greater or lesser extent, all power plant components possess the undesirable property of distorting the electrical wave from its ideal sinusoidal form. This phenomenon, known as harmonic distortion of the wave form, has been aggravated by the number of electrical loads capable of producing considerable wave distortion. These include all forms of electric transport, arc-electric lamps, metal reduction devices and, more recently, the thyristor which, owing to its versatility and economy, has flooded the industrial and domestic markets [Gauper,Harnden and McQuarrie 1971].

Various adverse effects have been traced to the existence of non- sinusoidal waves. The most common being additional losses in the system, reduction in the useful life of power plant equipment, ill-tripping of protection devices, ripple spill-over and interference in communication circuits by power lines.

The problem of harmonics in power systems is not new. It is as old as the power network itself and the first reports can be traced to the beginning of this century [Clinker 1914] when transformers were the major source of harmonic distortion. Interference in communication circuits by power lines was the first problem which indicated the necessity of reducing the harmonic content of electrical waves.

[1]This development took place in both Europe and The United States, simultaneously.

In spite of the inadequacies of measuring equipment and computation facilities, reductions in harmonic distortion were achieved through a series of practices such as the use of different three phase transformer connections, phase transpositions, the use of filters and improvements in transformer designs. Furthermore, communication equipment less susceptible to noise was developed, the circuits were insulated and different rights of way were chosen wherever possible. These remedies were sufficient, for example, to reduce the telephonic interference to tolerable levels.

The measures adopted were both technically and economically successful thanks to the operational and structural properties of the early electric networks. Low operational voltages, radial systems and short-distance transmission lines produced a low degree of imbalance and made the excitation of an harmonic resonance difficult. The harmonic sources of that time could only produce low order harmonic injections, generally up to the thirteenth harmonic. Such is the case of saturated transformers, electric machinery connected to unbalanced circuits and rectified loads for electric traction purposes [Joint committee on electromagnetic interference 1914].

From the point of view of the supply industry the problem of harmonic distortion of the electric wave was considered to be solved and a phenomenum of the past. For several decades the problem was forgotten and practically no serious research was reported. It was regarded, if at all, as a purely academic exercise.

For most practical purposes the electrical wave was considered to be sinusoidal and the quality of the electrical energy delivered to the consumer was measured only in terms of constant voltage magnitude and constant frequency.

More recently, however, the design and operating conditions of modern power systems have changed radically. Owing to the very high voltages required to transmit the large amount of electrical energy demanded, the network has suffered extreme imbalance. Furthermore, the technological innovations of our time have created new and more powerful sources of harmonic. The distortion of the waveform has reappeared as a problem having practical significance. This time, however, the picture appears to be considerably more complicated than in the past. The new sources of harmonics generate both low and high order harmonics and the resonant points are difficult to estimate because of the highly interconnected nature of modern networks.

The use of power semiconductor devices and modern appliances has grown very rapidly indeed and this, coupled with the traditional sources of harmonics and the proliferation of DC links has become a real challenge to the power engineer who has to operate and supply electricity to a large and varied number of devices characterized by their risk of causing major harmonic distortion into the network [Emanuel 1977].

Very little progress has been made in finding new remedies for the problem; the methods used at the beginning of the century are the same utilised today. However in this occasion extreme care must be exercised when such measures are applied. Large imbalance, continuous expansion of the network and tight interconnection may reduce their effectiveness. Moreover, due to the higher voltages involved, costs have also increased and those measures may consume an important proportion of the overall investment [Robinson 1966].

Because of its implications the problem has attracted the attention of both the supply industry and the large consumers. Several countries have adopted regulations to limit the permissible level of harmonic distortion [Bradley,Morfee and Wilson 1985]

Significant progress has been made in the development of accurate and versatile instrumentation to monitor the harmonic behaviour of the network at the point of measurement, thus enabling effective enforcement of the legislation [Arrillaga 1981].

Measurements , however, become increasingly difficult to coordinate and increasingly expensive as the number of points simultaneously monitored increases [Breuer et al 1982].

In planning and system analysis the problem must be addressed in a different way because measurements may not be economic or sufficiently versatile, or the network might not even exist.

Simulation, based on modern digital computers and powerful numerical techniques, provides answers which satisfy some of the requirements. A considerable effort has being devoted worldwide over the last ten years to finding the answer and several approaches which represent the problem more or less accurately have been reported but no solution so far put forward copes with it satisfactorily in all its complexities.

On one hand, transient studies and dynamic models for most of the power system components are already well advanced and, in principle, they could be used to determine the harmonic solution of the network [Dommel 1969]. In practice the technique is rendered impractical for determining the harmonic solution because of the computational burden which arises when a large range of conditions is required or an interactive environment is sought. On the other hand, steady state solutions using harmonic phasor analysis have emerged as the natural alternative. A great deal of experience has been accumulated in the fundamental frequency solution of very large non-linear systems. Highly efficient numerical techniques of the Newton-Raphson type, together with sparsity and diakoptics facilities, have enabled the solution of large networks in a matter of seconds.

These developments have encouraged a similar line of thinking for harmonic analysis. However, the problem undertaken is not a straightforward extension of the practices in current use at the fundamental frequency but is one of a more general philosophy and a greater degree of complexity.

Conventional studies are formulated on the premise that the sources are the system generators. When viewed in the harmonic perspective, however, they behave as sources at some harmonic frequencies (among them the fundamental) and as sinks at other harmonic frequencies and, in general, they will act as harmonic frequency converters [Semlyen,Eggleston and Arrillaga 1986]. This is a change from tradition as power plant components such as the static converter and the power transformer which were seen as loads at fundamental frequency analysis are now seen in harmonic operations in a dual source-sink role.

Transmission lines do not exhibit these properties. they act as passive admittances that vary with frequency in a non-linear fashion. Lumped transmission line models based on the nominal pi concept are no longer valid when dealing with harmonic frequencies, and long-line effects have to be incorporated. Moreover, modern power transmission lines are very unbalanced and the unquestioned practice of transposing the line as a means of restoring geometrical balance could not only render ineffective but also deteriorate further the symmetry of the harmonic voltages at the far end of the line [Arrillaga,Acha,Densem and Bodger 1986].

The accurate and reliable harmonic solution of a power system network incorporating all the above and other important effects requires the development of a new generation of mathematical models for all the power plant component. Scattered contributions to this developments have appeared in the technical literature recently and the research program of this department can be seen to be an important contribution towards the understanding and solution of problems which are of paramount importance to the present and future of the electrical power industry, worldwide.

A powerful principle behind the developments taking place in this department is that all power plant components are amenable to a nodal terminal description in the form of either a harmonic transfer admittance or a harmonic Norton equivalent. Linear components are represented by transfer admittances while non-linear components, in a linearized form, are modelled by Norton equivalents. Because of this it is possible to represent a wide range of power plant components, polyphase busbars and harmonics of interest in the complex-conjugate harmonic space which acts as a unified frame of reference. The associated linearized, harmonic equations provide a means for the iterative solution of the non-linearities through a Newton-Raphson procedure. In contrast, other institutions have adopted a simpler alternative which models the non-linearity as a set of harmonic current sources and leaves no option but to carry the numerical solution in a sequential fashion of the Gauss-Seidel type.

Power transformers have long been the subject of widespread research. Early studies were largely confined to qualitative discussions drawn from practical observations and more recently, passive harmonic models have been proposed. In practice, however, the magnetic core of the transformer is an active source of harmonic generation. It has the property of acting simultaneously as both harmonic source and sink. Moreover, it is not possible to anticipate particular values or limits in the amount of magnetizing current that a transformer can draw, as this is critically dependent on the magnitude and waveform of the excitation voltage and the quality of the transformer core.

Thus, a realistic transformer model suitable for power system harmonic analysis should not only incorporate voltage and frequency dependent effects, but also take proper account of the electrical connection and ability to combine easily with the external network.

Transformer models incorporating all these features are presented for the first time in this thesis. A parallel development to the harmonic Norton equivalent presented in this thesis models the transformer as a set of harmonic current sources [Dommel,Yan and Shi-Wei 1986].

Due to its characteristic as a very heavy distorter, the static power converter has received a great deal of attention and, although establishing accurate harmonic models for the converter taking due account of its control parameters is not an easy task, an outstanding model which represents the converter as a set of harmonic currents is in active use [Yacamini and De Oliveira 1980]. Also a way of representing the static converter in the complex harmonic space has been reported [Mizuma,Sagisaka,Neri and Sekine 1985].

Serious attention has recently been given to the synchronous generator [Semlyen,Eggleston and Arrillaga 1986] and [Mizuma,Sagisaka,Neri and Sekine 1985]. It behaves as an active source of harmonics both when supplying an unbalanced network and when operating in saturated conditions. The former case involves a harmonic conversion process between the stator and the salient poles rotor and is a function of both the degree of saliency of the rotor and the degree of unbalance of the external network.

Successful models which include the mechanism of harmonic conversion and which take place in the complex harmonic space are already available. Furthermore, harmonic studies of the interaction generator-converter have been reported.

1.2 Main aims

The main objectives of the thesis are:

1. To formulate new mathematical tools for the periodic, steady state solution of non-linear, dynamic circuits described by ordinary differential equations.

2. To develop harmonic, three phase transformer models which represent correctly the voltage and the frequency dependent effects of the magnetic core as well as the electrical connection. Furthermore, they should combined easily with the external network.

3. To improve both the versatility and the efficiency of present harmonic transmission line models and to investigate the behaviour of non-homogeneous transmission lines at harmonic frequencies.

4. To propose a new and more general frame of reference suitable for the unified harmonic solution of power system networks.

1.3 Chapter Presentation

The material studied in this research project is organized as follows:

Chapter 2 introduces the concept of non-linear, steady state relationships into the harmonic analysis and discusses its suitability in modelling magnetic non-linearities of the transformer type. It also gives guidelines for the modelling of other power system elements amenable to similar treatment.

Although it is not explicitly mentioned as such, the approach to the harmonic modelling of power network elements on the basis of their input-output behaviour is already a favoured approach. Some elements of the system such as power converters are described by analytical equations which allow their response to be determined. Some other elements, however, may not have such equations available and alternative ways of quantifying their response have to be established. Magnetic non-linearities are in this category but, fortunately, the relevant information is contained in their associated experimental magnetizing characteristics.

A clear understanding of the mechanics of magnetizing characteristics is essential when modelling power transformers. Magnetizing characteristics depend critically on the excitation voltage and they contain one part which is frequency dependant and another which is frequency independent.

Chapter 3 Presents a linearization procedure that takes place in the real harmonic space and is suitable for determining the periodic steady state response of a class of non-linear circuits.

This is a more restricted development than the formulation presented in the next Chapter, because it is strictly valid only for cases of sinusoidal excitation plus a DC term. In practice, however, it has been shown to work well under cases of non-sinusoidal excitation.

Chapter 4 presents the derivation of new and efficient mathematical techniques for the harmonic solution of non-linear circuits subjected to periodic excitations.

The formulation is based on incremental linearization, which take place in the complex-conjugate harmonic space. The linearized model is not related to discretization in the time domain. It is valid for any length of time as steady state solution. It is approximate because of the truncation of higher order terms in the process of linearization. It provides, however, a mean for the iterative solution of the circuit in a steady state by use of a harmonic Newton-Raphson method. After convergence, the harmonics will be in balance.

Chapter 5 develops three phase transformer models suitable for determining the steady state response under any kind of periodic excitation.

The magnetic circuit of the transformers is well modelled by using the technique of linearization in the complex-conjugate harmonic space. The double philosophy of operation source-sink and voltage and frequency dependence effects are included correctly. Moreover, the resultant three phase linearized model combines easily with the electric circuit of the transformer, and also with the external network.

Chapter 6 proposes alternative transmission line models that, owing to their versatility and reduced time of response, are suitable for interactive analysis of power system. Furthermore, it shows how linear elements also can be modelled in the complex conjugate-harmonic space.

Accurate harmonic models for homogeneous transmission lines are already available. Such models are based on the equivalent pi concept and properly include geometric imbalance, frequency dependence and long-line effects. However, it appears that adequate representation of discontinuities such as transpositions and var compensation plant have received no attention.

Harmonic transmission line models based on transfer functions, rather than the equivalent pi concept are shown to be more efficient. New formulae for the frequency dependant part of the line are also proposed. These formulae are shown to be the fastest to date yet maintain a high degree of accuracy, and, coupled with the transfer function approach, provide the means for an interactive solution.

Chapter 7 presents the complex-conjugate harmonic space as a new frame of reference where, in principle at least, all the plant components of the power system can be framed. It offers a more general frame than the one provided by the phases and it is intended, only, for the harmonic analysis of power systems.

Here the harmonic space concept is further extended so that any number of multi-phase busbars can be accommodated. The resultant harmonic matrix equation couples all the busbars, phases and harmonics present in the network. Furthermore, any number and type of both linear and non-linear plant components represented by either a harmonic Norton equivalent or a harmonic admittance can be framed into it.

Chapter 8 presents the major conclusions reached by the present research project.

Chapter 2

Non-linear Excitation-Response Relationships

2.1 Introduction

Power networks are built up from a large number of elements of widely different natures and it may not be practical from a system point of view to establish harmonic models based on a detailed representation of their internal behaviour. On the other hand, all of them are amenable, in principle at least, to a nodal terminal description in the form of either a harmonic transfer admittance or a harmonic Norton equivalent. Linear components are modelled by transfer admittances while non-linear components are represented by Norton equivalents. This philosophy of modelling relies on the assumption that means exist for quantifying the responses of each of the elements.

Some non-linear components, such as static power converters, have explicit equations associated with their responses [Yacamini and De Oliveira 1980]. Other non-linear elements, however, may not have explicit equations. Magnetic non-linearities, for instance, belong to the class of elements for which analytical solutions are only feasible in a very restricted number of cases. Nevertheless, numerical solutions based on their steady state magnetizing characteristic are possible and are completely general. Both approaches to the problem are presented in this chapter.

Magnetizing characteristics are central to the harmonic solution of magnetic non-linearities and an overview of their physics, along with experimental ways of recording them, is presented in this chapter. In addition, analytical and numerical algorithms which may be used to calculate the harmonic currents and the magnetic admittances from the magnetizing characteristics are given.

2.2 Excitation-Response Characteristics

Consider the power plant component shown in figure 2.1, where only a single port is available for both the excitation and measurement of a response.

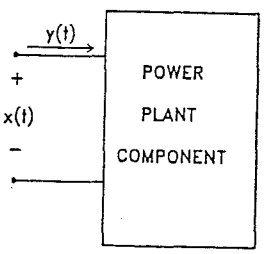

Figure 2.1: Single port representation of a power plant component

When a periodic,sinusoidal excitation $x(t)$ is placed across the terminals of the plant component a periodic response $y(t)$ takes place which could be either sinusoidal or non-sinusoidal. A sinusoidal response will be produced by a plant component with linear impedance and a non-sinusoidal response will be produced by a plant component with non-linear impedance.

Furthermore, the excitation-response characteristic of the plant component can be determined by supplying both the periodic excitation and the periodic response to any suitable device, e.g. an oscilloscope. The general characteristic exhibited by a linear power plant component is an ellipse, as shown in figure 2.2, which can degenerate into a straight line.

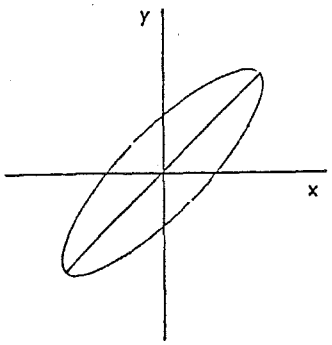

Figure 2.2: General x-y characteristic for a linear component

2.2.1 Idealized characteristics

The response associated with most of the non-linear elements of the power system is difficult to determine by analytical calculations, except for very simple and idealized cases. For instance, the non-linear response of a lossless ferromagnetic core acting under moderate saturating conditions can be adequately represented by a polynomial equation, as shown in figure 2.3 (a).

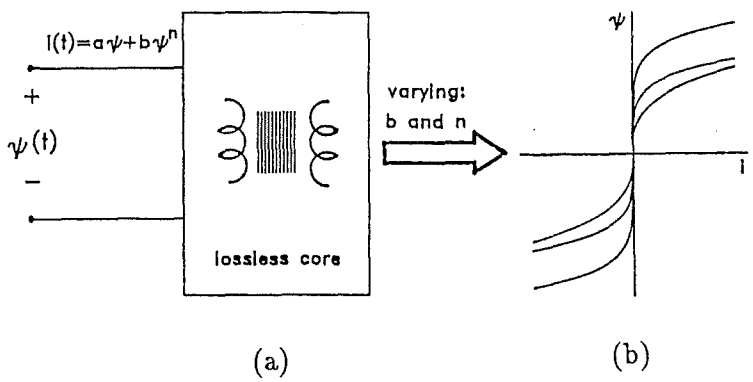

Figure 2.3: Polynomial characteristics corresponding to lossless cores
(a) Schematic representation (b) Idealized characteristics

It will be shown in a later section of this chapter that the coefficients a, b and n are determined by experimental measurements and a fitting exercise. In general, such coefficients are expected to be different for each magnetic material. Figure 2.3 (b) shows the excitation-response characteristics for different values of the coefficients b and n.

The static power converter acting under sinusoidal AC voltage excitation, infinite DC inductance and zero reactance on the AC side, presents another example of an idealized case. If the DC side current is free of harmonics, the AC line currents (the response) will consists of a series of rectangular blocks of current. In that case the response can be expressed conveniently by the series shown in figure 2.4 (a), while figure 2.4 (b) shows the excitation-response characteristic.

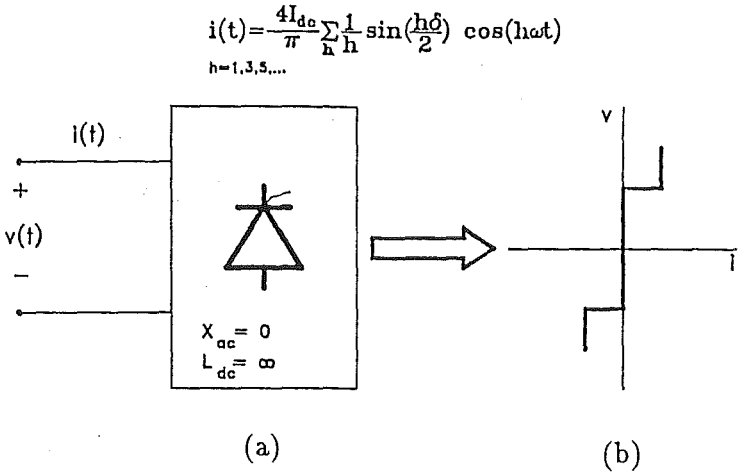

Figure 2.4: v-i characteristic for one phase of the static power converter
(a) Schematic representation (b) idealized characteristic

2.2.2 More realistic characteristics

When more realistic conditions are considered, the excitation-response characteristics of the non-linear power plant components will differ from those given above.

The characteristics of ferromagnetic cores will exhibit a looped form if there are losses. Figure 2.5 shows the looped characteristic resulting from plotting, point by point, a given sinusoidal excitation and the corresponding non-linear response.

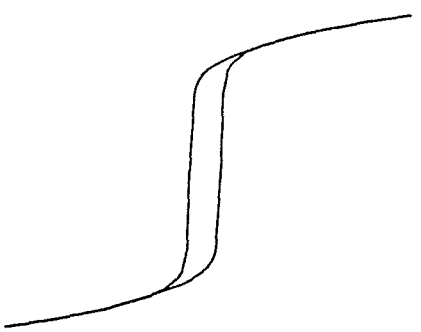

Figure 2.5: Magnetizing characteristic of a single phase transformer

The AC system to which the static power converter is connected will contain a certain amount of reactance rather than the zero value assumed for the idealized case of figure 2.4. This reactance, termed commutating reactance, plays an important role in the operation of the converter and its overall effects are to reduce the harmonic content of the current drawn by the converter [Arrillaga 1983] and to turn the idealized circuit of figure 2.4 into a *lossy* one.

Figure 2.6 (a) shows the v-i characteristic for one phase of the static power converter. It has been obtained by plotting a sinusoidal voltage and the current shown in figure 2.6 (b).

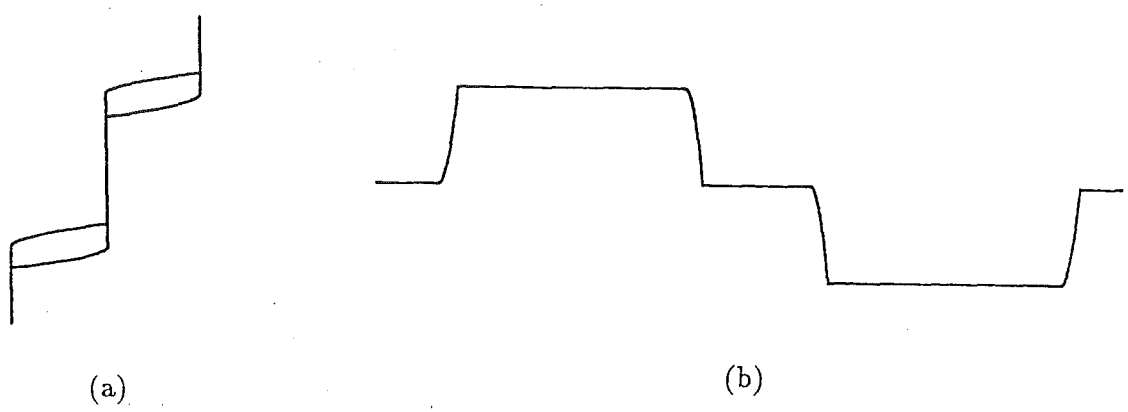

Figure 2.6: v-i characteristic of a converter including commutating reactance effects
(a) *Lossy* characteristic (b) A full cycle of the current

A more realistic characteristic can be obtained by considering a static power converter connected to a DC link with a finite amount of inductance. The v-i characteristic is shown in figure 2.7 (a), while figure 2.7 (b) shows the cycle of current being drawn by the converter.

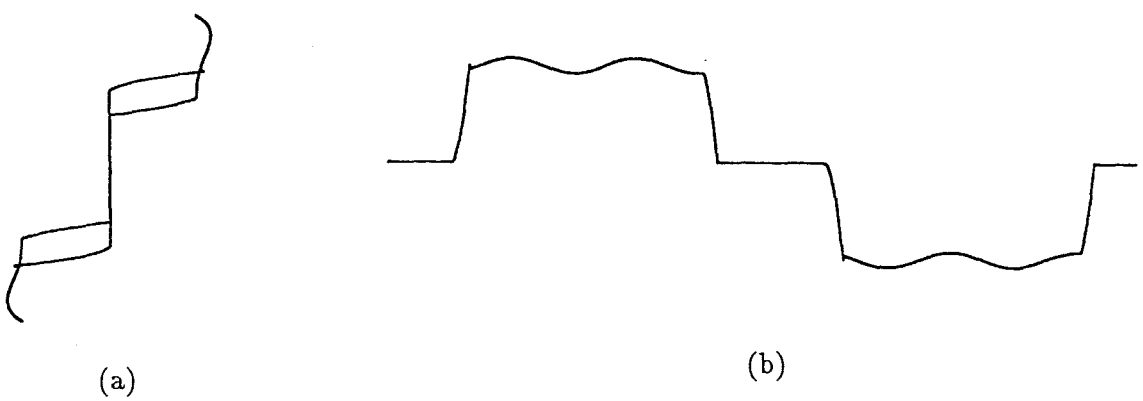

Figure 2.7: v-i characteristic of a converter including commutating reactance effects and DC ripple
(a) *Lossy* characteristic (b) A full cycle of the current

2.3 An Overview Of The Magnetizing Characteristic

2.3.1 The non-linear effects

Three non-linear effects are introduced by ferromagnetic cores, namely, saturation, hysteresis and Eddy currents. These three effects are exhibited by the magnetizing characteristic shown in figure 2.8, which corresponds to a small transformer and was obtained with a 50 Hz, sinusoidal excitation.

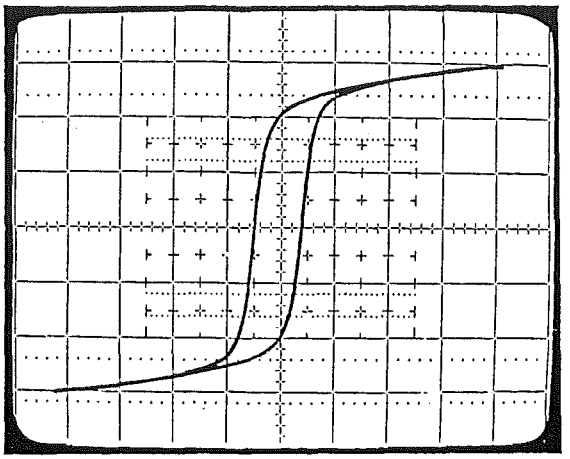

Figure 2.8: Magnetizing characteristic recorded in the laboratory
for a transformer of small rating

The magnetizing characteristic above can be divided into two main components, as shown in figure 2.9.

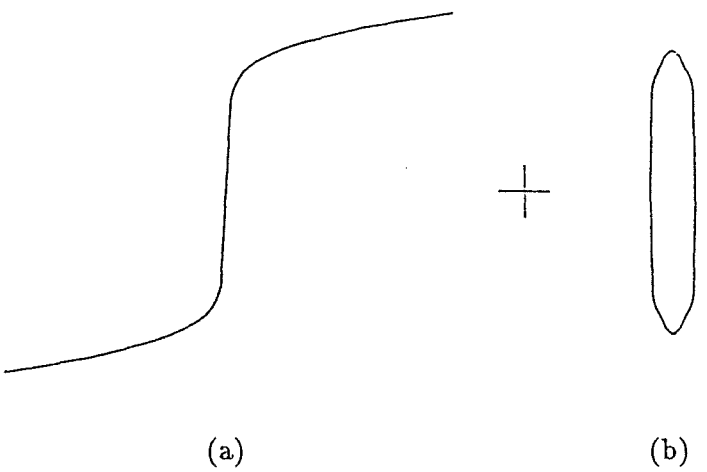

Figure 2.9: Main components of the magnetizing characteristic
(a) Characteristic of a lossless core (b) Loss cycle

The single line curve of figure 2.9 (a) represents the behaviour of a lossless core acting under saturated conditions. The looped curve of figure 2.9 (b) is dependant on the rate at which the contour is traversed. It is frequency dependant, and includes the effects of hysteresis and Eddy currents. The latter curve relates to the core losses and could be refered to as the loss cycle.

The hysteresis phenomenom consists of two parts, a part which is frequency independent and is attributable to domain wall movements, non-magnetic inclusions and imperfections [Boon and Robey 1968] and a part which is frequency dependant and is refered to as the *anomalous losses* [Brailsford and Fogg 1964]. Losses associated with hysteresis are expected to be small in modern power transformers. Eddy currents, on the other hand, are not present when very slow (essentially zero frequency) traverses of the loop occur but any increase beyond zero frequency will give rise to Eddy currents which increase the loss per cycle. At power frequencies and above, this effect can account for two to three times as much loss as hysteresis does [Swift 1971].

2.3.2 Experimental magnetizing characteristics

The experimental magnetizing characteristics of transformers of small rating can be recorded in the laboratory by means of the arrangement shown in figure 2.10.

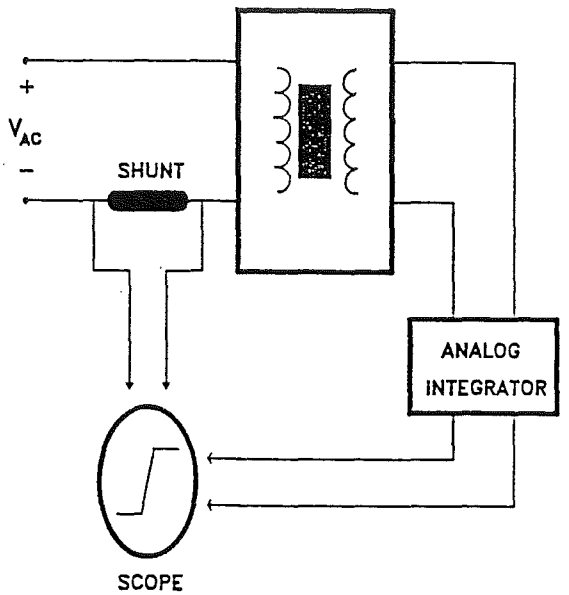

Figure 2.10: Basic arrangement for the recording of magnetizing characteristics

The method is approximate because the voltage drop due to the resistance of the windings is not accounted for. It is based on a changing current being applied to one winding while the instantaneous voltage appearing across a second winding is integrated to determine the flux linkage. Both current and integrated voltage are supplied to either an oscilloscope or an X-Y plotter and the magnetizing characteristic is recorded.

The basic circuit in figure 2.10 can be modified to allow for greater accuracy and versatility. For instance, the resistive drop can be taken into account and, if voltage and current measurements are carried out in the same winding, the technique can be applied to both transformers and reactors. Furthermore, a digital integrator can be used instead of the analog one [Calabro,Coppadoro and Crepaz 1986].

Of the non-linear effects associated with ferromagnetic cores, saturation is the one of most interest but generally it is also the most difficult to measure. For instance, large units can be driven into saturation through AC excitation only if high power sources are used and, moreover, the rated voltage of the source must exceed considerably the rating of the unit under test. Such sources are not easily available for experiments.

A practical alternative lies in the use of a reversible DC supply rather than an AC source [Dick and Watson 1981]. This method can be seen as excitation by very low frequency AC whereby high flux levels can be obtained with the application of low voltage and low power. Magnetizing characteristics measured using this approach will include saturation correctly and most of the hysteresis effect but their loss cycle will be very narrow. This is particularly true for ferromagnetic cores built of high quality materials. The reason for narrow loops is that neither Eddy currents nor *anomalous losses* are included.

Figure 2.11 shows the positive half of an experimental magnetizing characteristic for a modern three phase 25 MVA, 110/44/4 KV, Y/Y/D power transformer measured using DC excitation [Dick and Watson 1981].

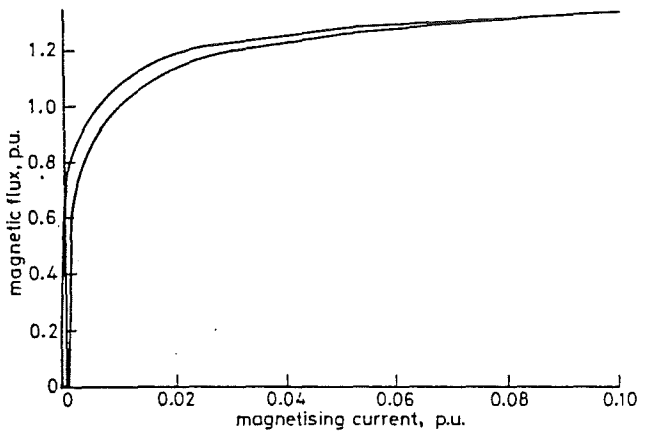

Figure 2.11: Positive half of an experimental magnetizing characteristic of a modern three phase power transformer

2.3.3 Polynomial magnetizing characteristics

Finding analytical expressions to describe experimental magnetizing characteristics has been an area of active research [Hale and Richardson 1953]. Fitted polynomial and exponential equations containing a large number of terms have been proposed to represent lossless magnetizing characteristics [De Carvalho 1984]. Alternatively, a simple procedure suitable for a class of harmonic distortion problems is possible.

A fitted polynomial equation of the form

$$i = a\psi + b\psi^n \tag{2.1}$$

is determined, with the coefficients a, b and n being derived from the following basic information, corresponding to the lossless magnetizing characteristic:

- Coordinates of the knee
- Coordinates of the maximum point to be considered
- Slope of the linear part

For example, a polynomial fitting for the magnetizing characteristic of figure 2.11 is shown below. The coefficients of the polynomial are taken from the *experimental* lossless curve as follows:

- Knee point $\psi_{nom} = 1.0$ p.u. $i_{nom} = 0.008$ p.u.
- Maximum point $\psi_{max} = 1.2$ p.u. $i_{max} = 0.026$ p.u.
- Linear slope $M = 1700$

Substituting these parameters in equation (2.1) yields

$$0.026 = \frac{1.2}{1700} + b \times 1.2^n \tag{2.2}$$

Therefore

$$b = \frac{0.025294}{1.2^n} \tag{2.3}$$

so that

- for $n = 3$ $b = 0.014638$
- for $n = 5$ $b = 0.010165$
- for $n = 7$ $b = 0.007057$

The selected magnetizing characteristic requires a current $i = 0.008$ when $\psi = 1$ and therefore $n = 7$ is the best approximation. The chosen fitting is then

$$i = \frac{1}{1700} + 0.007059\,\psi^7 \tag{2.4}$$

Figure 2.12 compares the *actual* transformer magnetizing characteristic with that obtained by the polynomial of equation (2.1). They are shown to be in good agreement in the region $0 \leq \psi \leq 1.2$ p.u.

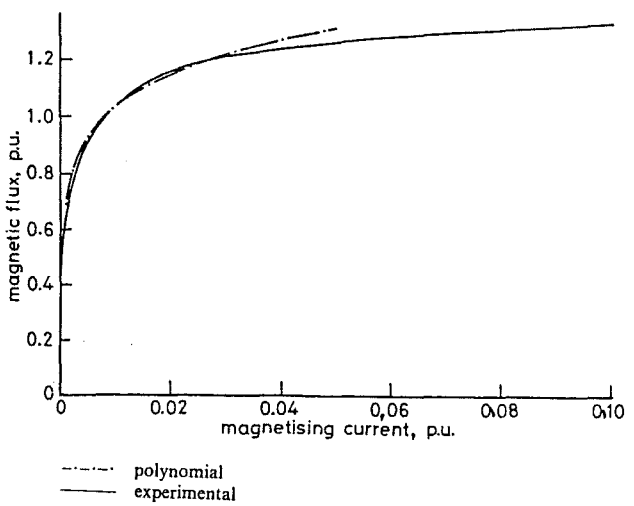

Figure 2.12: Comparison of the *actual* transformer magnetizing characteristic with that obtained through the polynomial approach

2.4 Derivation Of The Harmonic Information Of Magnetizing Characteristics

2.4.1 Analytical representation of the magnetizing characteristic

It was shown in the previous section that an *experimental* magnetizing characteristic can be approximated by the polynomial form

$$i = a\psi + b\psi^n \tag{2.5}$$

where n is an odd integer. Since equation (2.5) has odd symmetry, the magnetizing characteristic can be well fitted to *experimental* curves by noting that

- the coefficient a corresponds to the initial slope
- the exponent n is a measure of the sharpness of the knee
- after a and n have been selected, the coefficient b can be obtained so that the curve passes through the point i_{max}, ψ_{max}

Once the coefficients a, b and n have been found, Equation (2.5) is evaluated at a particular base operating flux ψ_b,

$$f(\psi_b) = a\psi_b + b\psi_b^n \tag{2.6}$$

and also its derivative,

$$f'(\psi_b) = a + n\,b\psi_b^{n-1} \tag{2.7}$$

It must be noted that

$$\psi_b^m = \psi_{b,max}^m(\sin(\omega t) + \alpha)^m \tag{2.8}$$

which can be expanded into

$$\psi_b^m = \psi_{b,max}^m \sum_{i=0}^{m}(\beta_i' \sin(i\omega t) + \beta_i'' \cos(i\omega t)) \tag{2.9}$$

where

$$\alpha = \frac{\psi_{dc}}{\psi_{b,max}} \tag{2.10}$$

To obtain equation (2.9) consider the more general expression

$$(\sin(x) + \alpha)^m = \sum_{j=0}^{m} C_m^j \alpha^{m-1} \sin^j(x) \tag{2.11}$$

The binomial coefficients C_m^j are given below arranged in the triangle of Pascal to show how they can be calculated recursively:

$$
\begin{array}{ccccccccccccc}
 & & & & & 1 & & & & & & & \\
 & & & & 1 & & 1 & & & & & & \\
 & & & 1 & & 2 & & 1 & & & & & \\
 & & 1 & & 3 & & 3 & & 1 & & & & \\
 & 1 & & 4 & & 6 & & 4 & & 1 & & & \\
1 & & 5 & & 10 & & 10 & & 5 & & 1 & & \\
 & 6 & & 15 & & 20 & & 15 & & 6 & & 1 & \\
7 & & 21 & & 35 & & 35 & & 21 & & 7 & & 1 \\
 & & & & & etc & & & & & & &
\end{array}
\tag{2.12}
$$

If the expression (2.12) is seen as a lower triangular matrix L_1, then equation (2.11) can be written as

$$
(\sin(x)+\alpha)^m = \alpha^m \times (\text{row m of } L_1) \times diag\{\alpha^{-j}\} \times \text{col}\{\sin^j(x)\} \qquad j = 0,1,2,\ldots \tag{2.13}
$$

The powers of $\sin(x)$ are given as

$$
\begin{aligned}
\sin^0 x &= 1 \\
\sin^1 x &= \sin x \\
\sin^2 x &= \frac{1}{2}(1-\cos 2x) \\
\sin^3 x &= \frac{1}{4}(3\sin x - \sin 3x) \\
\sin^4 x &= \frac{1}{8}(3-4\cos 2x+\cos 4x) \\
\sin^5 x &= \frac{1}{16}(10\sin x - 5\sin 3x + \sin 5x) \\
\sin^6 x &= \frac{1}{32}(10-15\cos 2x + 6\cos 4x - \cos 6x) \\
\sin^7 x &= \frac{1}{64}(35\sin x - 21\sin 3x + 7\sin 5x - \sin 7x)
\end{aligned}
\tag{2.14}
$$

It is noted that the coefficients in equation (2.14) can be obtained from the right half of the triangle in expression (2.12), split vertically. Moreover,they can be accommodated in a lower triangular matrix and change signs where appropriate:

$$
L_2 = \begin{pmatrix}
\frac{1}{2} & & & & & & & \\
0 & 1 & & & & & & \\
1 & 0 & -1 & & & & & \\
0 & 3 & 0 & -1 & & & & \\
3 & 0 & -4 & 0 & 1 & & & \\
0 & 10 & 0 & -5 & 0 & 1 & & \\
10 & 0 & -15 & 0 & 6 & 0 & -1 & \\
0 & 35 & 0 & -21 & 0 & 7 & 0 & -1
\end{pmatrix}
\tag{2.15}
$$

Now equations (2.14) can be written as:

$$\text{col}\{\sin^j(x)\} = 2 \times \text{diag}\{2^{-j}\} \times L_2 \times \text{col}\left\{\begin{array}{c}\cos(ix)\\ \sin((i+1)x)\end{array}\right. \tag{2.16}$$

$$i = 0, 2, 4, \ldots, m-1$$
$$j = 0, 1, 2, \ldots, m$$

Substitution of equation (2.16) into (2.13) yields

$$(\sin(x)+\alpha)^m = 2^{1-m} \times (\text{row m of } L_1) \times diag\{(2\alpha)^{m-j}\} \times L_2 \times \text{col}\left\{\begin{array}{c}\cos(ix)\\ \sin((i+1)x)\end{array}\right. \tag{2.17}$$

$$i = 0, 2, 4, \ldots, m-1$$
$$j = 0, 1, 2, \ldots, m$$

If $\alpha = 0$, equation (2.16) can be used directly. Both equations (2.16) and (2.17) can be written more simply:

$$\sin^m(x) = c_1 \times \text{col}\left\{\begin{array}{c}\cos(ix)\\ \sin((i+1)x)\end{array}\right. \tag{2.18}$$

$$i = 0, 1, 2, \ldots, m$$

and

$$(\sin(x)+\alpha)^m = c_2 \times \text{col}\left\{\begin{array}{c}\cos(ix)\\ \sin((i+1)x)\end{array}\right. \tag{2.19}$$

$$i = 0, 1, 2, \ldots, m$$

where

$$c_1 = 2^{1-m} \times (\text{row m+1 of } L_2)$$

$$c_2 = 2^{1-m} \times (\text{row m+1 of } L_1) \times \text{diag}\{(2\alpha)^{m-j}\} \times L_2$$

$$j = 0, 1, 2, \ldots, m$$

2.4.2 Numerical example 1

For a given characteristic $i = f(\psi_b) = 0.001\psi_b + 0.0743\psi_b^3$ and $\psi_b = \sin(x) + \alpha$

$$(\sin(x)+\alpha)^3 = \frac{1}{4}\begin{pmatrix} 1 & 3 & 3 & 1 \end{pmatrix} \begin{pmatrix} (2\alpha)^3 & & & \\ & (2\alpha)^2 & & \\ & & (2\alpha)^1 & \\ & & & (2\alpha)^0 \end{pmatrix} \begin{pmatrix} \frac{1}{2} & & & \\ 0 & 1 & & \\ 1 & 0 & -1 & \\ 0 & 3 & 0 & -1 \end{pmatrix} \begin{pmatrix} 1 \\ sinx \\ cos2x \\ sin3x \end{pmatrix} \quad (2.20)$$

and for the particular case when $\alpha = 0.5$ then

$$(\sin(x)+0.5)^3 = \frac{1}{4}\begin{pmatrix} 1 & 3 & 3 & 1 \end{pmatrix} \begin{pmatrix} \frac{1}{2} & & & \\ 0 & 1 & & \\ 1 & 0 & -1 & \\ 0 & 3 & 0 & -1 \end{pmatrix} \begin{pmatrix} 1 \\ sinx \\ cos2x \\ sin3x \end{pmatrix} \quad (2.21)$$

or

$$(\sin(x)+0.5)^3 = 7/8 + 3/2\sin(x) - 3/4\cos(2x) - 1/4\sin(3x) \quad (2.22)$$

and substituting into the polynomial characteristic,

$$i = f(\psi) = 0.0655 + 0.11246\sin(x) - 0.05573\cos(2x) - 0.01858\sin(3x) \quad (2.23)$$

The harmonic content, in phasor form, is readily available from the above result,

$$\begin{aligned} i_{dc} &= 0.0655 \\ i_1 &= 0.0 - j0.11246 \\ i_2 &= -0.05573 + j0.0 \\ i_3 &= 0.0 + j0.01858 \end{aligned}$$

also

$$(\sin(x)+0.5)^2 = 3/4 + \sin(x) - 1/2\cos(2x) \quad (2.24)$$

and

$$f'(\psi_b) = 0.16818 + 0.222915\sin(x) - 0.11146\cos(2x) \quad (2.25)$$

2.4.3 Point by point representation of the magnetizing characteristic

As an alternative, a full cycle of the magnetising current can be derived from the experimental magnetizing curve using discrete values of flux as shown in figure 2.13 and the derivative of the function $i = f(\psi)$ can be derived by numerical analysis.

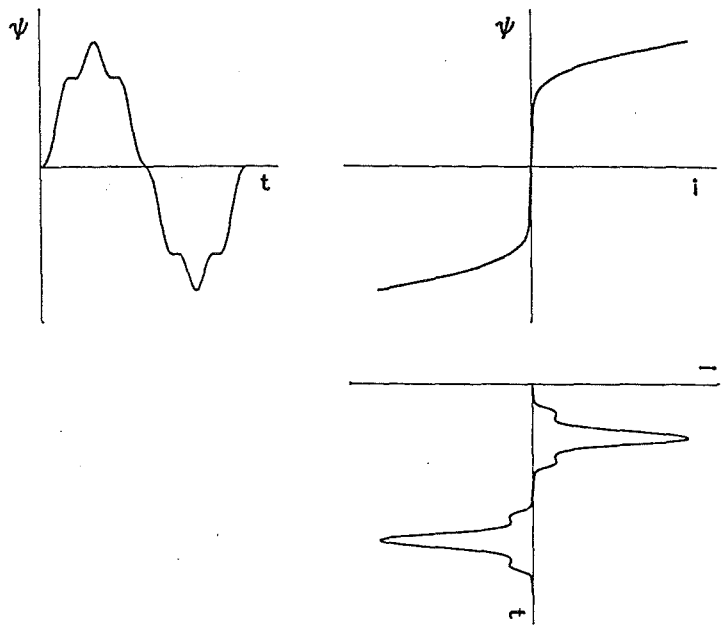

Figure 2.13: Point by point derivation of magnetizing current from the flux waveform and magnetizing characteristic

The current and derivative wave-shapes are then subjected to a fast Fourier transform. This procedure is the numerical version of the analytical solution based on equations (2.6) and (2.7). The solution requires the following steps:

1. A full period of the flux wave is impressed, point by point, upon the experimental characteristic $\psi - i$ and the corresponding magnetizing current $i_b(t)$ is thus determined in the time domain.
2. By means of the complex Fourier transform (*FFT* version), the magnetizing current $i_b(t)$ is solved in the frequency domain and the real and imaginary coefficients of the harmonic currents are obtained.
3. Using the magnetizing current and the magnetic flux, the derivative of the function $i = f(\psi)$ is evaluated.
4. The Fourier transform is applied to the slope shape in 3, and the real and imaginary coefficients of the harmonic magnetic admittances are obtained.

2.4.4 Numerical example 2

Figure 2.14 (a) shows a full period of the magnetizing current resulting from impressing, point by point, a full period of the magnetic flux

$$\psi_b = \sin(\omega t)$$

upon the experimental magnetizing characteristic of figure 2.8 (reproduced here as figure 2.14 (b)).

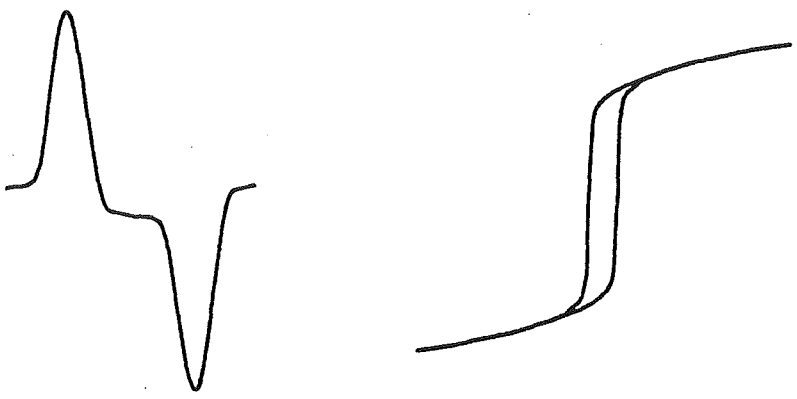

(a) (b)

Figure 2.14: Current resulting from applying a sinusoidal excitation to a lossy transformer
(a) A full cycle of the current (b) Magnetizing characteristic

An *FFT* exercise is applied to the above magnetizing current and the harmonic content is given below.

$$\begin{aligned}
i_1 &= 0.003669 - j0.033906 \\
i_3 &= 0.001365 + j0.018590 \\
i_5 &= -0.000514 - j0.005185 \\
i_7 &= -0.000466 - j0.000166 \\
i_9 &= 0.000251 + j0.000202 \\
i_{11} &= 0.000253 + j0.000165 \\
i_{13} &= -0.000110 - j0.000039 \\
i_{15} &= -0.000111 - j0.000019
\end{aligned}$$

As expected, the magnitude of the harmonic content decreases rapidly with the harmonic order and, due to the symmetry of the excitation and the response, no even harmonics are present. For this level of the excitation it is observed that the real component of the harmonic content (losses) is significant when compared with the imaginary part and such significance increases with the harmonic order, although it decreases with the excitation level, e.g. $i_7 = 0.000563 - j0.003917$ when $\psi = 1.2\sin(\omega t)$.

On the other hand, figure 2.15 (a) shows the resultant magnetizing current when a full cycle of the magnetic flux

$$\psi_b = \sin(\omega t)$$

is impressed, point by point, upon the lossless magnetizing characteristic of figure 2.9 (a) (reproduced here as figure 2.15 (b)).

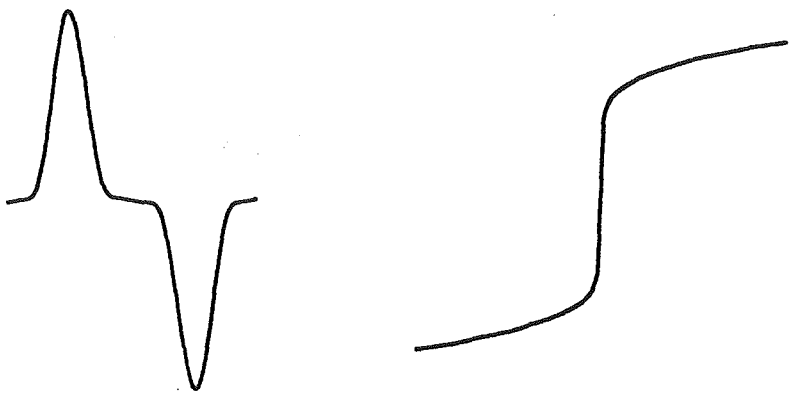

(a) (b)

Figure 2.15: Current resulting from applying a sinusoidal excitation to a lossless transformer (a) A full cycle of the current (b) Magnetizing characteristic

The corresponding harmonic content is given below,

$$\begin{aligned}
i_1 &= 0.0 - j0.033906 \\
i_3 &= 0.0 + j0.018590 \\
i_5 &= 0.0 - j0.005185 \\
i_7 &= 0.0 - j0.000166 \\
i_9 &= 0.0 + j0.000202 \\
i_{11} &= 0.0 + j0.000165 \\
i_{13} &= 0.0 - j0.000039 \\
i_{15} &= 0.0 - j0.000019
\end{aligned}$$

In this case the imaginary component of the harmonic content equals that involving the complete magnetizing characteristic but it contains no real part. It may also be observed that in the process of neglecting the loss cycle, the most important component of the higher order harmonics (real part) has been dropped. However, the magnitude of these harmonics is very small and it is unlikely that they will have a major effect in actual computations.

2.5 Conclusions

It was stated in the introduction to this chapter that, in principle, harmonic models for all the plant components of the power system based on the concept of excitation-response relationships, are possible. This philosophy of modelling avoids the complexities associated with the internal mechanisms of the power components and only requires them to have explicit equations, or other suitable means, for the description of their response.

The above approach is the one pursued in the present research and, aiming at this, some fundamental concepts have been presented in this chapter and the ground work has been prepared for the application of non-linear excitation-response characteristics to actual computations.

A wide range of both idealized and realistic characteristics has been presented for the transformer and the static power converter. While magnetizing characteristics have been used by electrical engineers for almost a century, no attention has been paid so far to the characteristics of static power converters.

A probable reason is that converters possess explicit equations for the evaluation of their responses and thus their explicit $v-i$ characteristic may play no role in actual computations. However, the use of converter $v-i$ characteristics has been shown to provide greater insight into their steady state operation

On the other hand, it has been shown that ferromagnetic cores present the opposite problem but, in the absence of explicit equations, their response can be determined by using a suitable magnetizing characteristic which is usually derived experimentally.

Several techniques, with different degrees of accuracy, are available for the derivation of magnetizing characteristics. However, from the three non-linear effects introduced by ferromagnetic cores, saturation is the effect that plays the major part in the harmonic distortion process.

Magnetizing characteristics contain the relevant information needed for the harmonic solution of magnetic non-linearities and analytical and numerical procedures have been presented here for the determination of both magnetizing currents and magnetic admittances.

The analytical approach, based on the Pascal's triangle, provides an elegant and easy way of extracting the relevant harmonic information from a polynomial representing the magnetizing characteristic. However, its range of applicability is limited to cases of sinusoidal excitation, plus a DC term, and its accuracy relies on the ability of the polynomial to match the lossless magnetizing characteristic.

On the other hand, the numerical approach based on interpolation, the central difference formulae and the use of the *FFT* algorithm provides a more general solution to the problem of magnetizing currents and magnetic admittances. It applies to both double- and single-valued magnetizing characteristics and cases of symmetrical and asymmetrical over-excitation.

Chapter 3

The Real Harmonic Space

3.1 Introduction

An essential part of the computer-aided analysis of networks containing non-linearities is the evaluation of their steady-state response when subjected to a periodic excitation. This has been a topic of active research in the areas of circuit theory, control engineering and electronics over the last twenty years.

In principle, the periodic solution can always be found by integrating the differential equations that describe the system until the transient response dies out; but this **brute force** approach becomes prohibitively expensive whenever the transients are governed by time constants that are much larger than the period of the driving force [Director and Wayne 1976].Nevertheless, integrating the differential equations was the first approach adopted for the solution of this kind of problems, partly because numerical integration techniques have been reasonably well known by most engineers over many years but also because an alternative solution was not straightforward to formulate [Nakhla and Branin 1977]. It was necessary to carry the integrations for a considerable number of periods before the transient became small enough to be ignored. Clearly, better methods of solution were needed.

More efficient formulations, intended for electrical and electronic circuits, exist nowadays. In very general terms they can be classified into harmonic balance techniques, **shooting** methods and the describing function approach. The former two solve the problem to a specified accuracy level and are valid for cases of arbitrary (periodic) excitation.

Shooting methods take the approach of integrating the dynamic equations over one or two full periods and then solving the two point boundary-value problem by iteration. The methods are reported to be well-behaved and yield the initial state of the transient response in addition to the final harmonic solution. However, numerical integration of the dynamic equations is still required.

The harmonic balance technique is based on an iterative, steady state approach where each state variable is represented by a Fourier series that satisfies the requirement of periodicity. In order to ensure convergence, an optimization algorithm is used to adjusts the coefficients of the Fourier series. Thus, the system equations are satisfied with least error and with a minimum number of iterations. A number of examples corresponding to electronic circuits have been solved and in every case successful convergence was achieved with a smaller execution time than that required for the integration of the corresponding dynamic equations over two full periods [Nakhla and Vlach 1976].

In general harmonic balance techniques are better suited than **shooting** methods to the solution of large networks because they do not require time-domain modelling and numerical integrations. However, the usefulness of the harmonic balance techniques also deteriorates with the number of non-linearities present in the network. The reason being that the number of variables to be optimized grows with the number of non-linearities and convergence problems occur in optimization techniques when dealing with high order systems [Aprille and Trick 1972].

In the past two decades, the determination of the periodic response of a non-linear networks has not been a problem of major concern for the power engineer. When the need for a solution first arose, methods based on the integration of the differential equations describing the non-linearity were used [Dommel 1969].

Owing to the growing number of new and powerful harmonic sources being connected to the transmission grid as well as the traditional sources of harmonics the problem of evaluating the periodic response of power networks has now been acknowledged as a priority and ambitious research programs have been initiated, worldwide, to achieve it.

Non-linearities in power systems, as well as linear components, are multi-phase and frequency-dependant. In general, the problems they produce are more difficult to solve than their electronic counterparts. The solutions proposed for electric and electronic circuits are not always either suitable or directly applicable to the case of power circuits and although some of the fundamental ideas are similar, the problem of power system non-linearities must be addressed in a different way.

For most steady-state operating conditions the problem of power system harmonics can be viewed as one of a fundamental voltage with a superimposed ripple because the harmonic voltages existing in the network are only a few per cent of the fundamental.

Thus, when an iterative approach (harmonic balance technique) is adopted for the harmonic solution of the non-linear power system, the undistorted load flow solution provides a very good initial estimate of the final solution with harmonics. If no resonant conditions are involved the harmonic solution is reached in a reduced number of iterations (less than five), even if no optimization techniques are used to adjust the coefficients of the Fourier series. However, convergence problems are expected to occur when poorly damped resonances are present.

An algorithm, which exploits the points mentioned above, has been proposed recently [Dommel,Yan and Shi Wei 1986] and applied to the problem of magnetic non-linearities of the transformer type. It is a sequential iterative algorithm that models the transformer magnetizing branch as a set of harmonic current sources calculated from a point by point representation of the magnetizing characteristic. It uses nodal analysis to represent the linear part of the network.

Dommel's algorithm is very simple and represents a major step forward in the development of more efficient tools for the harmonic solution of non-linear power systems. However, the proposed algorithm is based on a Gauss-Seidel numerical procedure and, it is worth considering the development of an alternative model based on Newton-Raphson procedures.

In this research harmonic Newton-type algorithms have been developed that are suitable for the solution of both single and multi-phase circuits. They belong to the class of steady-state solutions and fully exploit the nodal analysis which has been used so successfully by power system engineers for most of their traditional studies. These formulations are based on local linearization as opposed to the describing function, which is based on global linearization and the process takes place in the harmonic space. Moreover, the resultant linearized equations may be interpreted as harmonic Norton equivalents that combine easily with the linear network in a unified frame of reference when that linear part is also represented in the harmonic space.

One of these formulations, to be presented in the next chapter, is valid for any kind of symmetrical or asymmetrical, periodic excitation and provides a solution to a specified level of accuracy. It takes place in the complex-conjugate harmonic space [Semlyen,Acha,Arrillaga 1987(a)].

The other formulation is presented in this chapter. In theory it has a more restricted scope because it is strictly valid only for cases of sinusoidal excitation plus a DC term. In practice, it can also be used for cases of non-sinusoidal excitation [Semlyen,Acha,Arrillaga 1987(b)].

The proposed methods can be applied to many excitation-response characteristics but, because the main concern of this research is with power system non-linearities of the transformer type, the non-linearity chosen for the derivation of the method discussed in this chapter is a magnetizing characteristic. A presentation of the linearized equation to be obtained is given below, and the remaining sections contain the mathematical derivations and examples.

This solution is based on linearization of the magnetizing characteristic around a base operating point using small increments of voltages and currents of the fundamental and harmonic frequencies. This permits the postulation (for guidance at this stage-proof is given in the next section) that the following linear equation exists:

$$I = I_b + [G]\Delta V \tag{3.1}$$

where I is the vector of resultant harmonic currents
I_b is the base vector of harmonic magnetizing currents
ΔV is the vector of superimposed harmonic voltages
$[G]$ is an admittance matrix to be derived from a given magnetizing curve

The variables I,I_b and ΔV include the increments of fundamental frequency and have both a longitudinal component (i.e. in phase with the base flux) and a transversal component (i.e. leading the longitudinal component by 90°).

The multi-input/multi-output diagram of figure 3.1 shows a conceptual representation of equation (3.1).

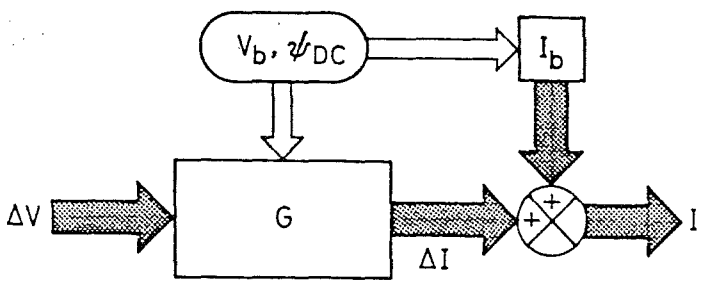

Figure 3.1: Harmonic input/output relations in a non-linear device

3.2 Harmonic Norton Equivalent

3.2.1 General procedure

Given the magnetizing characteristic

$$i = f(\psi) \tag{3.2}$$

a base flux linkage is assumed

$$\psi_b = \psi_{b,max} \sin(\omega t) + \psi_{dc} \tag{3.3}$$

with an increment of small terms

$$\Delta\psi = \sum_{h=1}^{\infty} \Delta\psi'_{max,h} \sin(h\omega t) + \sum_{h=0}^{\infty} \Delta\psi''_{max,h} \cos(h\omega t) \tag{3.4}$$

The resultant flux linkage is

$$\psi = \psi_b + \Delta\psi \tag{3.5}$$

so that i of equation (3.2) becomes, by a Taylor expansion around ψ_b truncated after the first order term,

$$i = f(\psi_{b,max}\sin(\omega t) + \psi_{dc}) + f'(\psi_{b,max}\sin(\omega t) + \psi_{dc})\Delta\psi \tag{3.6}$$

In equation (3.6) both functions $f(\psi_b)$ and $f'(\psi_b)$ are periodic in t. Therefore they can be represented by Fourier series in $\sin(k\omega t)$ and $\cos(k\omega t)$. Substituting equation (3.4) into equation (3.6) yields:

$$\begin{aligned} i &= \sum_{k=1}^{\infty} I'_{max,k}\sin(k\omega t) + \sum_{k=0}^{\infty} I''_{max,k}\cos(k\omega t) \\ &+ \left(\sum_{i=1}^{\infty} a'_{max,i}\sin(i\omega t) + \sum_{i=0}^{\infty} a''_{max,i}\cos(i\omega t)\right) \\ &\times \left(\sum_{h=1}^{\infty} \Delta\psi'_{max,h}\sin(h\omega t) + \sum_{h=0}^{\infty} \Delta\psi''_{max,h}\cos(h\omega t)\right) \end{aligned} \tag{3.7}$$

Here the products of sine and cosine functions yield more sine and cosine functions so that the second term on the right hand side of equation (3.7) will have the form:

$$\Delta i = \sum_{h=1}^{\infty} \Delta I'_{max,h}\sin(h\omega t) + \sum_{h=0}^{\infty} \Delta I''_{max,h}\cos(h\omega t) \tag{3.8}$$

If all current and flux linkage harmonics of equations (3.8) and (3.4) are assembled into the vectors

$$\Delta I = [\cdots \Delta I'_{max,k} \cdots \mid \cdots \Delta I''_{max,k} \cdots]^t \tag{3.9}$$

$$\Delta\psi = [\cdots \Delta\psi'_{max,k} \cdots \mid \cdots \Delta\psi''_{max,k} \cdots]^t \tag{3.10}$$

then, comparing the coefficients in equations (3.7) and (3.8) corresponding to the same sine and cosine functions, yields

$$\Delta I = [A]\Delta\psi \tag{3.11}$$

where the elements of the matrix $[A]$ are linear combinations of a'_i and a''_i of equation (3.7).

3.2.2 Matrix [A] identification

The matrix $[A]$ can be identified by taking all elements of the vector $\Delta\psi$ of equation (3.10) equal to zero, except one which is set to unity. Let this be $\Delta\psi'_{max,h}$. Then in equation (3.7) the following multiplication is to be performed,

$$(\sum_{i=1}^{\infty} a'_i \sin(i\omega t) + \sum_{h=0}^{\infty} a''_i \cos(i\omega t)) \times \sin(h\omega t) \tag{3.12}$$

which yields

$$\begin{aligned} &\frac{1}{2}\sum_{i=0}^{\infty} a'_i \cos((i-h)\omega t) - \sum_{h=0}^{\infty} a'_i \cos((i+h)\omega t) + \\ &\frac{1}{2}\sum_{i=1}^{\infty} -a''_i \sin((i-h)\omega t) + \sum_{h=1}^{\infty} a''_i \sin((i+h)\omega t) \end{aligned} \tag{3.13}$$

Similarly, for $\Delta\psi''_{max,h}$, the multiplication

$$(\sum_{i=1}^{\infty} a'_i \sin(i\omega t) + \sum_{h=0}^{\infty} a''_i \cos(i\omega t)) \times \cos(h\omega t) \tag{3.14}$$

yields

$$\begin{aligned} &\frac{1}{2}\sum_{i=1}^{\infty} a'_i \sin((i-h)\omega t) - \sum_{h=1}^{\infty} a'_i \sin((i+h)\omega t) + \\ &\frac{1}{2}\sum_{i=0}^{\infty} -a''_i \cos((i-h)\omega t) + \sum_{h=0}^{\infty} a''_i \cos((i+h)\omega t) \end{aligned} \tag{3.15}$$

The coefficients of the sine and cosine terms of equations (3.13) and (3.15) have to be arranged in columns numbered h and rows numbered k to obtain the partitioned matrix

$$[A] = \frac{1}{2}\begin{pmatrix} [A]_{ss} & [A]_{sc} \\ [A]_{cs} & [A]_{cc} \end{pmatrix} \tag{3.16}$$

where the subscripts s and c refer to sine and cosine function inputs and outputs.

The four submatrices are given below in an explicit form.

$$[A]_{ss} = \begin{pmatrix} 2a''_0 - a''_2 & a''_1 - a''_3 & a''_2 - a''_4 & a''_3 - a''_5 & \cdots \\ a''_1 - a''_3 & 2a''_0 - a''_4 & a''_1 - a''_5 & a''_2 - a''_6 & \cdots \\ a''_2 - a''_4 & a''_1 - a''_5 & 2a''_0 - a''_6 & a''_1 - a''_7 & \cdots \\ a''_3 - a''_5 & a''_2 - a''_6 & a''_1 - a''_7 & 2a''_0 - a''_8 & \cdots \\ \vdots & \vdots & \vdots & \vdots & \ddots \end{pmatrix} \tag{3.17}$$

$$[A]_{sc} = \begin{pmatrix} 2a'_1 & a'_2 & -a'_1 + a'_3 & -a'_2 + a'_4 & -a'_3 + a'_5 & \cdots \\ 2a'_2 & a'_1 + a'_3 & a'_4 & -a'_1 + a'_5 & -a'_2 + a'_6 & \cdots \\ 2a'_3 & a'_2 + a'_4 & a'_1 + a'_5 & a'_6 & -a'_1 + a'_7 & \cdots \\ 2a'_4 & a'_3 + a'_5 & a'_2 + a'_6 & a'_1 + a'_7 & a'_8 & \cdots \\ \vdots & \vdots & \vdots & \vdots & \vdots & \ddots \end{pmatrix} \tag{3.18}$$

$$[A]_{cs} = \begin{pmatrix} a'_1 & a'_2 & a'_3 & a'_4 & \cdots \\ a'_2 & a'_1 + a'_3 & a'_2 + a'_4 & a'_3 + a'_5 & \cdots \\ -a'_1 + a_3 & a'_4 & a'_1 + a'_5 & a'_2 + a'_6 & \cdots \\ -a'_2 + a_4 & -a'_1 + a'_5 & a'_6 & a'_1 + a'_7 & \cdots \\ -a'_3 + a_5 & -a'_2 + a'_6 & -a'_1 + a'_7 & a'_8 & \cdots \\ \vdots & \vdots & \vdots & \vdots & \ddots \end{pmatrix} \tag{3.19}$$

$$[A]_{cc} = \begin{pmatrix} 2a''_0 & a''_1 & a''_2 & a''_3 & a''_4 & \cdots \\ 2a''_1 & 2a''_0 + a''_2 & a''_1 + a''_3 & a''_2 + a''_4 & a''_3 + a''_5 & \cdots \\ 2a''_2 & a''_1 + a''_3 & 2a''_0 + a''_4 & a''_1 + a''_5 & a''_2 + a''_6 & \cdots \\ 2a''_3 & a''_2 + a''_4 & a''_1 + a''_5 & 2a''_0 + a''_6 & a''_1 + a''_7 & \cdots \\ 2a''_4 & a''_3 + a''_5 & a''_2 + a''_6 & a''_1 + a''_7 & 2a''_0 + a''_8 & \cdots \\ \vdots & \vdots & \vdots & \vdots & \vdots & \ddots \end{pmatrix} \tag{3.20}$$

Sufficient terms have been written in each matrix to permit writing any number of additional terms.

The number of columns of these matrices are obviously equal to the number of input harmonics h_{max} considered. The number of rows is

$$k_{max} = h_{max} + i_{max}$$

where i_{max} is the number of harmonics in $f'(\psi_b)$ of equation (3.7).

3.2.3 Voltage inclusion

In addition, two other vectors are defined, one for the harmonics of the resultant i and one for the harmonics of the first right hand side term of equation (3.7).

$$I = [\cdots I'_{max,k} \cdots \mid \cdots I''_{max,k} \cdots]^t \tag{3.21}$$

$$I_b = [\cdots I'_{b,max,k} \cdots \mid \cdots I''_{b,max,k} \cdots]^t \tag{3.22}$$

Substituting equation (3.8) into (3.7) and breaking down the resultant equation into coefficients of $\sin(k\omega t)$ and $\cos(k\omega t)$ yields the vector equation

$$I = I_b + \Delta I \tag{3.23}$$

or, with equation (3.11) included,

$$I = I_b + [A]\Delta\psi \tag{3.24}$$

In order to introduce voltages into the above equations, the following relation is used,

$$\Delta V = \frac{d\Delta\psi}{dt} \tag{3.25}$$

where $\Delta\psi$ is given in equation (3.4) and

$$\Delta V = \sum_{i=1}^{\infty} \Delta V'_{max,h} \sin(h\omega t) + \sum_{h=0}^{\infty} \Delta V''_{max,h} \cos(i\omega t) \tag{3.26}$$

Substituting equation (3.26) into (3.25) and comparing the coefficients of $\sin(h\omega t)$ and $\cos(h\omega t)$ yields:

$$\begin{pmatrix} \Delta V'_{max,h} \\ \Delta V''_{max,h} \end{pmatrix} = h\omega \begin{pmatrix} 0 & -1 \\ 1 & 0 \end{pmatrix} \begin{pmatrix} \Delta\psi'_{max,h} \\ \Delta\psi''_{max,h} \end{pmatrix} \tag{3.27}$$

and

$$\begin{pmatrix} \Delta\psi'_{max,h} \\ \Delta\psi''_{max,h} \end{pmatrix} = \frac{1}{h\omega} \begin{pmatrix} 0 & 1 \\ -1 & 0 \end{pmatrix} \begin{pmatrix} \Delta V'_{max,h} \\ \Delta V''_{max,h} \end{pmatrix} \tag{3.28}$$

Clearly, the vector

$$\Delta V = [\cdots \Delta V'_{max,k} \cdots \mid \cdots \Delta V''_{max,k} \cdots]^t \tag{3.29}$$

is related to the vector $\Delta\psi$ of equation (3.10) by the relations

$$\Delta V = [\Omega]\Delta\psi \tag{3.30}$$

and

$$\Delta\psi = [\Omega]^{-1}\Delta V \tag{3.31}$$

where $[\Omega]$ is a block-diagonal with blocks

$$[\Omega] = h\omega \begin{pmatrix} 0 & -1 \\ 1 & 0 \end{pmatrix} \tag{3.32}$$

Substitution of equation (3.31) into (3.24) yields the linearized equation

$$I = I_b + [A][\Omega]^{-1}\Delta V \tag{3.33}$$

or

$$I = [G]V + I_N \tag{3.34}$$

where $[G]$ is a conductance matrix which can be assembled from the submatrices of $[A]$,

$$[G] = \begin{pmatrix} -[A]_{sc} & [A]_{ss} \\ -[A]_{cc} & [A]_{cs} \end{pmatrix} \begin{pmatrix} diag\{\frac{1}{2h\omega}\} & 0 \\ 0 & diag\{\frac{1}{2h\omega}\} \end{pmatrix} \tag{3.35}$$

and

$$I_N = I_b - [G]V_b \tag{3.36}$$

If, in equation (3.3), $\psi_{dc} = 0$, then $[A]_{sc}$ and $[A]_{cs}$ in equation (3.35) are both zero and, in addition, the odd and even harmonics in $[A]_{ss}$ and $[A]_{cc}$ become decoupled. This fact may be significant in practical applications as illustrated later in a numerical example because the even harmonics will not appear in the system if they are not independently excited.

Both I_b and $[G]$ are controlled by the fundamental voltage and the DC flux. However, ΔV and ΔI include also a small fundamental frequency component, thus allowing some tolerance for the selection of the base voltage V. In this way the fundamental frequency analysis (load flow) and harmonic analysis are effectively decoupled.

The real matrix $[G]$ is constant for a given V_b and ψ_{dc} but it is not symmetrical. Also it is not possible to combine the two components corresponding to sine and cosine functions into complex variables (i.e. phasors and complex admittance matrix).

3.2.4 Equivalent circuit

Equation (3.33) represents the linearized model of the non-linear magnetizing characteristic $f(\psi)$ around a base operating point and it is shown in figure 3.2 that it may be considered as an harmonic Norton equivalent.

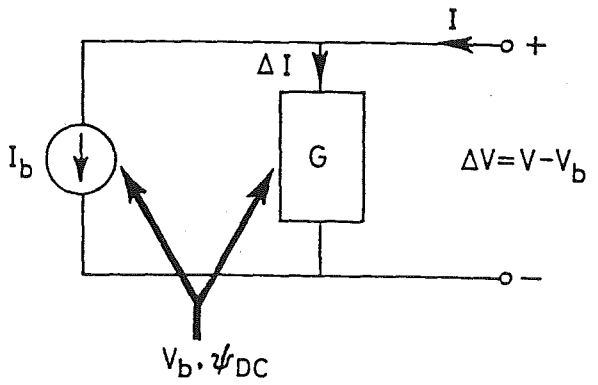

Figure 3.2: Harmonic Norton equivalent of non-linear magnetizing branch

3.3 Numerical Examples

3.3.1 Example 1

When a sinusoidal flux excitation

$$\psi_b = \sin(\omega t) \tag{3.37}$$

is impressed upon the magnetizing characteristic described by the analytical expression

$$i = f(\psi) = 0.001\psi + 0.0743\psi^3 \tag{3.38}$$

the harmonically related response is,

$$f(\psi_b) = 0.0567\sin(\omega t) - 0.0186\sin(3\omega t) \tag{3.39}$$

while,

$$f'(\psi_b) = 0.1125 - 0.1115\sin(2\omega t) \tag{3.40}$$

The coefficients of $f(\psi_b)$ make up the base current vector I_b,

$$I_b = \begin{pmatrix} 0.0567 & 0.0 & -0.0186 & 0.0 & 0.0 & 0.0 \end{pmatrix}^t \tag{3.41}$$

and the coefficients of $f'(\psi_b)$ are used in order to assemble the $[A]$ matrix,

$$[A]_{ss} = \begin{pmatrix} 0.3364 & 0.0 & -0.1115 \\ 0.0 & 0.2249 & 0.0 \\ -0.1115 & 0.0 & 0.2249 \end{pmatrix} \tag{3.42}$$

$$[A]_{cc} = \begin{pmatrix} 0.1135 & 0.0 & -0.1115 \\ 0.0 & 0.2249 & 0.0 \\ -0.1115 & 0.0 & 0.2249 \end{pmatrix} \tag{3.43}$$

Once the base vector I_b and the matrix $[A]$ are determined, the linearized model may be written out as follows,

$$\begin{pmatrix} I_1^s \\ I_2^s \\ I_3^s \\ I_1^c \\ I_2^c \\ I_3^c \end{pmatrix} = \begin{pmatrix} & & & 0.1682 & & -0.0186 \\ & & & & 0.0563 & \\ & & & -0.0557 & & 0.0375 \\ -0.0567 & & 0.0186 & & & \\ & -0.0563 & & & & \\ 0.0557 & & -0.0375 & & & \end{pmatrix} \begin{pmatrix} V_1^s \\ V_2^s \\ V_3^s \\ V_1^c \\ V_2^c \\ V_3^c \end{pmatrix} + \begin{pmatrix} -0.1115 \\ 0.0 \\ 0.0372 \\ 0.0 \\ 0.0 \\ 0.0 \end{pmatrix} \tag{3.44}$$

3.3.2 Example 2

The test system of figure 3.3 illustrates the use of the Norton equivalent for a single phase transformer. The transformer secondary side is open circuited and its primary side is fed from an infinite busbar through a 63 kV single-phase transmission line.

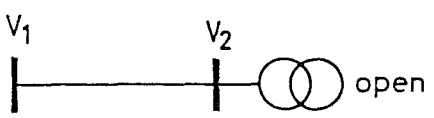

Figure 3.3: Single phase test system

The excitation voltage at the infinite busbar is given as $V_1 = \sin(\omega t - \frac{\pi}{2})$ and the magnetizing characteristic of the single phase core is assumed to be that of figure 2-12, while the transmission line parameters at 50 Hz are:

The characteristic impedance, $z_c = 393 \angle 11\ \Omega$

The propagation characteristic, $\gamma = 0.0002 + j0.0011\ km^{-1}$

The length of the line is assumed to vary from 5 to 600 km and the transformer's leakage reactance is 10 per cent.

The transformer is represented by a T-nominal equivalent circuit while a transfer function approach is used for the transmission line, which incorporates earth return and skin effects. The test system of figure 3.3 may be represented by the circuit of figure 3.4.

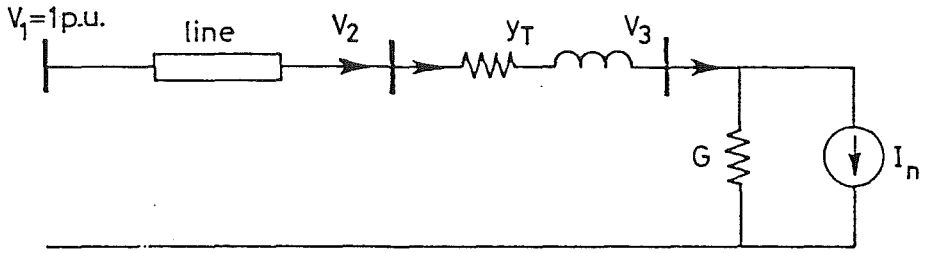

Figure 3.4: Equivalent circuit of the test system

Using nodal analysis the following matrix equations may be written for the relevant transformer nodes in the circuit of figure 3.4.

node 2

$$-\{Y\}''V_1 - \{Y\}'V_2 = \{Y\}_t(V_2 - V_3) \tag{3.45}$$

node 3

$$\{Y\}_t(V_2 - V_3) = [G]V_3 + I_N \tag{3.46}$$

or in combined form

$$\begin{pmatrix} \{Y\}_{22} & \{Y\}_{23} \\ \{Y\}_{32} & [Y]_{33} \end{pmatrix} \begin{pmatrix} V_2 \\ V_3 \end{pmatrix} = \begin{pmatrix} I_2 \\ I_3 \end{pmatrix} \tag{3.47}$$

where $\{Y\}_{22} = \{Y\}' + \{Y\}_t$
$\{Y\}_{23} = \{Y\}_{32} = -\{Y\}_t$
$[Y]_{33} = \{Y\}_t + [G]$
$I_2 = -\{Y\}''V_1$
$I_3 = I_N = I_{b,3} - [G]V_{b,3}$
$\{Y\}_t$ is a diagonal matrix of leakage admittances of the transformer
$[G]$ is a matrix of magnetic conductances of the core
$\{Y'\}$ and $\{Y''\}$ are diagonal transfer admittance matrices for the line
I_N represents the Norton equivalent current sources
V_b and I_b are the base voltages and currents, respectively

The two components of the $[G]$ matrix elements can not be combined into complex variables. The whole system must therefore be solved in terms of sine and cosine components and the previous nodal equation must be expressed as

$$\begin{pmatrix} I_2^s \\ I_3^s \\ I_2^c \\ I_3^c \end{pmatrix} = \begin{pmatrix} Re\{Y\}_{22} & Re\{Y\}_{23} & Im\{Y\}_{22} & Im\{Y\}_{23} \\ Re\{Y\}_{32} & Re[Y]_{33} & Im\{Y\}_{32} & Im[Y]_{33} \\ -Im\{Y\}_{22} & -Im\{Y\}_{23} & Re\{Y\}_{22} & Re\{Y\}_{23} \\ -Im\{Y\}_{32} & -Im[Y]_{33} & Re\{Y\}_{32} & Re[Y]_{33} \end{pmatrix} \begin{pmatrix} V_2^s \\ V_3^s \\ V_2^c \\ V_3^c \end{pmatrix} \tag{3.48}$$

The linear elements of the system (transmission line and transformer leakage admittance) have a diagonal matrix structure. The non-linear element (magnetizing branch) has submatrices with a banded Toeplitz matrix structure (equal elements on a diagonal). The bandwidth is determined by the sharpness of the non-linear magnetizing characteristic.

The nodal harmonic admittance matrix equation given above represents explicitly all the harmonics and busbars of interest. The dimensions of the admittance matrix are therefore $2nh \times 2nh$ where n is the number of busbars and h the number of harmonics.

Two sets of results are presented below. Figure 3.5 shows results corresponding to the case when the experimental magnetizing characteristic has been fitted to a polynomial curve, while the results of figure 3.6 correspond to the case when the actual experimental magnetizing characteristic has been used in a point by point representation. As expected, both results are in good agreement because a polynomial equation exists that fits closely the magnetizing characteristic in the region $0 \leq \psi \leq 1.2$.

The use of a transmission line of varying length provides information of the resonance points at all the harmonics of interest. Figure 3.5(a) and 3.6(a) show the fundamental, third, fifth and seventh harmonic frequency components of the magnetizing current of the transformer connected at the end of a line of varying length. As the line length increases, the fundamental voltage grows and with it the harmonic currents resulting from transformer saturation.

The harmonic voltage magnitudes at the transformer terminals are shown in figures 3.5(b) and 3.6(b) with the fundamental and harmonic components plotted at different scales. The transmission line being used in this example is not really a single-phase line but the positive sequence equivalent of a three-phase transmission line. Accordingly, lengths of line corresponding to quarter-wavelength frequencies produce the highest harmonic voltages, e.g. a 300 km length of line produces a one per cent voltage peak at the fifth harmonic and a 500 km length produces a four per cent voltage peak at the third harmonic. For the level of excitation and magnetizing characteristic being used, the seventh harmonic voltage is seen to be negligibly small. A different result would be expected for the case when a true single phase transmission line is considered. See Appendix B.

The magnitude of the harmonic voltage depends on the excitation level being applied at the transformer terminals, the magnetizing characteristic and the amount of resistance in the transmission circuit.

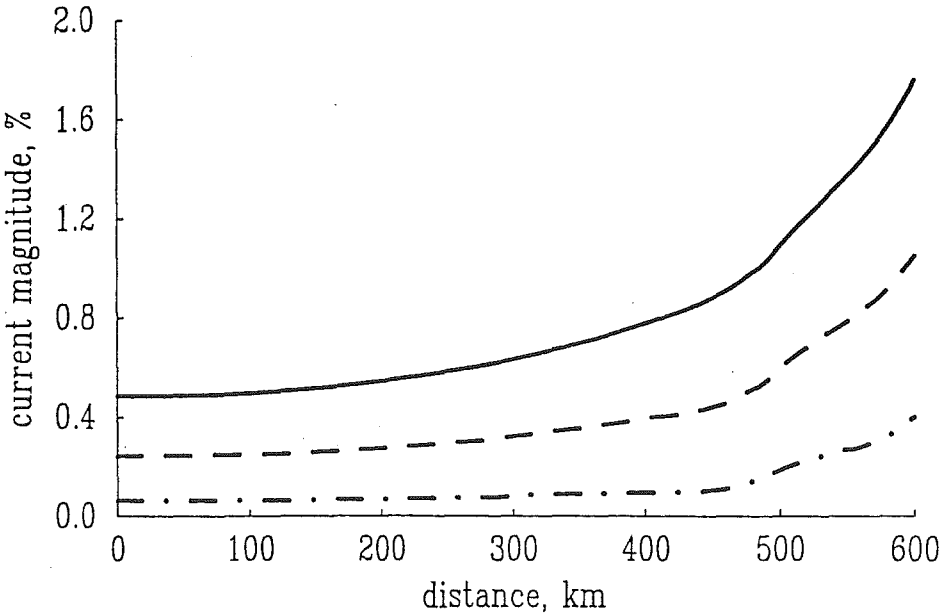

(a)

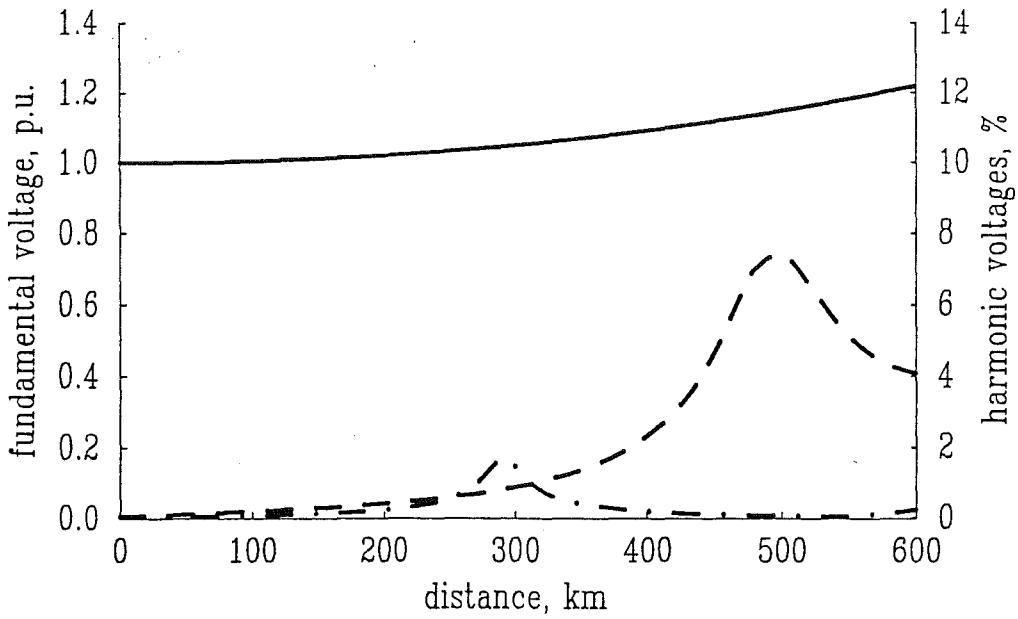

(b)

Figure 3-5: Fundamental and harmonic information against line length at busbar 2, polynomial representation of the characteristic. (a) Currents (b) Voltages

fund. ———
third — — —
fifth — · —

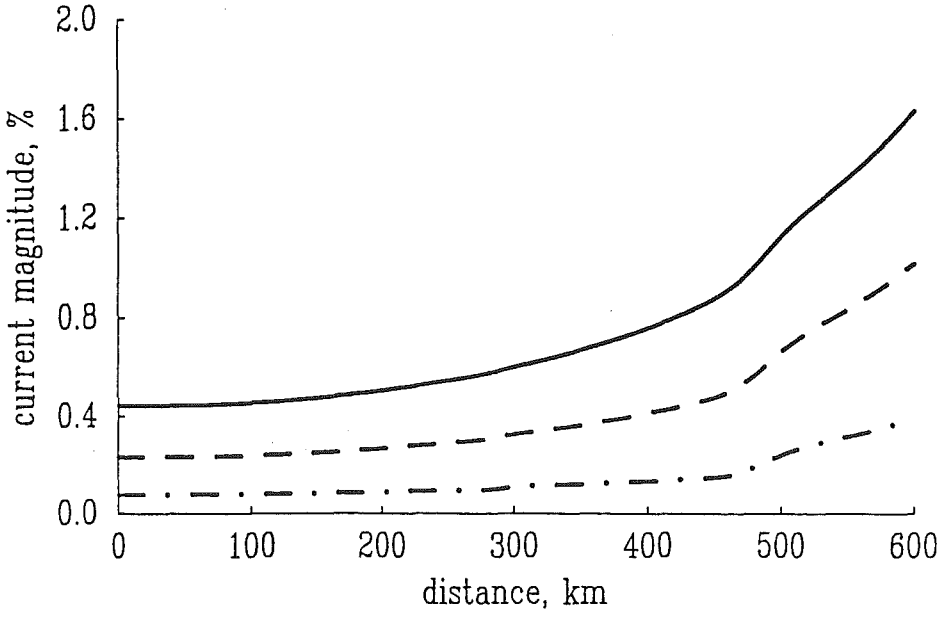

(a)

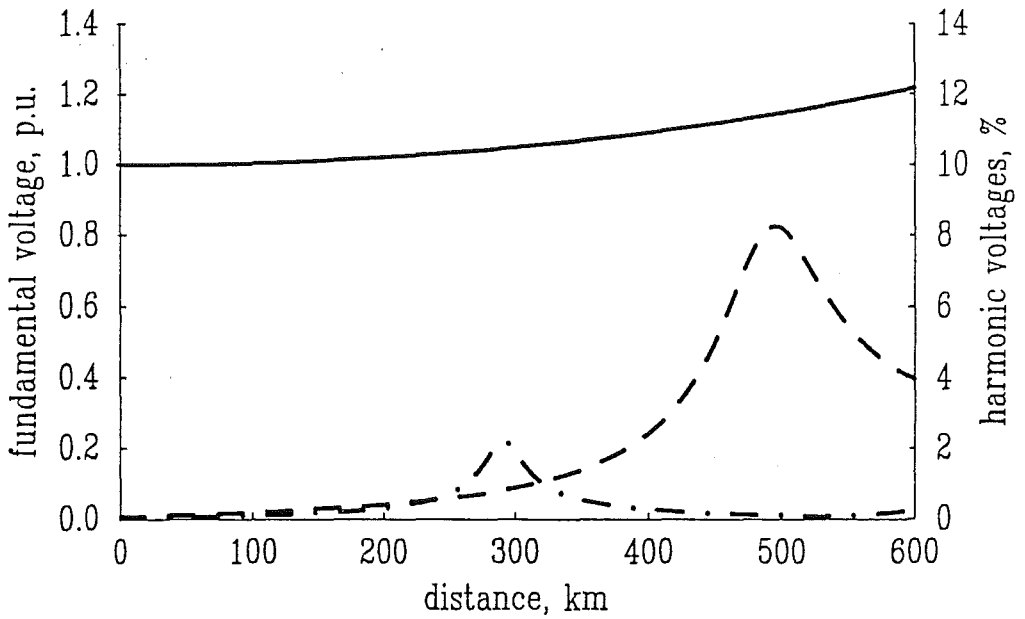

(b)

Figure 3-6: Fundamental and harmonic information against line length at busbar 2, point by point representation of the characteristic. (a) Currents (b) Voltages

fund. ——————
third — — —
fifth — · —

3.4 Conclusions

A new mathematical technique in the form of a linearized equation has been developed that allows the periodic solution of non-linear circuits to be determined. Sufficient proofs of the existence of the linearized equation have been given along with a physical interpretation and detailed numerical examples.

The technique is based on local linearization around a base operating point with the linearization taking place in the real harmonic space where all the harmonics are coupled. However, the resultant linearized equation does not satisfy the field structure of the complex numbers and therefore it is not possible to combine the two components corresponding to sine and cosine functions into complex variables, i.e. phasors and complex admittance matrices.

The linearized equation may be considered as an harmonic Norton equivalent and it may easily be combined with the admittances of the linear part of the network. This requires the linear components to be expressed in terms of sine and cosine functions, rather than the customary phasors. Any number of harmonics can be modelled simultaneously.

In practice, the technique can be applied in the presence of non-sinusoidal excitation but, in theory, it is strictly valid only for cases of sinusoidal excitation plus a DC term. A more general formulation will be presented in the next chapter.

The effect of the harmonic Norton equivalent has been demonstrated in a test system consisting of an unloaded transformer at the end of a transmission line. It has been shown that magnetizing currents can cause substantial voltage distortion which can not be ignored in harmonic penetration studies.

Chapter 4

The Complex-Conjugate Harmonic Space

4.1 Introduction

It was mentioned in the previous chapter that several techniques are already available for the determination of the periodic response of non-linear circuits of the electric and electronic type. However, it was also mentioned that such techniques are not entirely suitable or directly applicable to the case of power system non-linearities.

This chapter describes new proposals suitable for the harmonic solution of large networks which are applicable to both single and multiphase non-linear circuits. These techniques are based on linearization of the excitation-response characteristic around a base operating point, with the linearization taking place in the harmonic space. The linearized equations may be interpretated as an harmonic Norton equivalent.

The previous chapter was devoted to the technique of linearization in the real harmonic space which is, strictly speaking only valid for cases of sinusoidal excitation plus a DC term. However, a more general formulation is possible by relaxing this restriction. The linearization process then takes place in the complex-conjugate harmonic space and the resulting linearized equation may be used for the iterative solution of the network by Newton-type approximations. This is the approach to be discussed in this chapter.

This approach has many potential applications and, therefore, the non-linearity and the notation chosen in this chapter will be more general than that used for the derivation of the technique of linearization in the real harmonic space. A general description of the formulation is presented below.

The periodic steady-state behaviour of non-linear circuits can be described by the general state equations

$$\dot{x} = f(x, u)$$

$$y = g(x, u) \tag{4.1}$$

where in the case of a transformer non-linearity, the state variable x are magnetic fluxes and u and y are the voltages and currents required to interconnect the transformer with the transmission network.

In power system applications it is desirable to obtain from equation (4.1) algebric input-output relations of the form

$$y = h(u) \tag{4.2}$$

by eliminating the state variable x.

This implies a step-by-step numerical integration or, in the case of sinusoidal excitation of a single frequency, algebraization by means of phasors which is only possible for the linearized approximation of equations (4.1). If the input is periodical then instead of phasors of a single frequency the fundamental and its harmonics will be present and the problem becomes one of linearization of equations (4.1) in the complex-conjugate harmonic space which would yield

$$Y = [H]U + Y_N \tag{4.3}$$

where the Y and U are vectors of all the harmonics of y and u, respectively.

The linearized, algebraic model is, clearly, not related to discretization in the time domain. Rather, it is valid for any length of time as a steady-state solution but it is approximate because of the truncation of higher order terms in the process of linearization. It is therefore a means for the iterative solution of the network in steady-state through a Newton-type approach. When converged the harmonics will be in balance.

After a review of the behaviour of non-linear circuits under harmonic excitation the basic non-linear relationship

$$y = f(x) \tag{4.4}$$

is analyzed for periodic $x(t)$. This relationship is fundamental in the solution of equation (4.1) and its linearization turns out to yield a simple (Toeplitz-type) band-diagonal, Jacobian matrix $[F]$, so that

$$Y = [F]X + Y'_N \tag{4.5}$$

With this building block, equations (4.1) are then easily brought to the form of equation (4.3).

4.2 The Basic Formulation

4.2.1 Real and complex transfer functions for harmonics in linear circuits

Consider first an algebraic linear circuit with the input

$$u(t) = \sum_0^\infty u_h(t) = \sum_1^\infty (U'_h \sin(h\omega t) + U''_h \cos(h\omega t)) + U_o \tag{4.6}$$

and the output

$$y(t) = \sum_0^\infty y_h(t) = \sum_1^\infty (Y'_h \sin(h\omega t) + Y''_h \cos(h\omega t)) + Y_o \tag{4.7}$$

The Fourier series for equations (4.6) and (4.7) can be written in complex form as

$$u(t) = \sum_0^\infty u_h(t) = \sum_{-\infty}^\infty U_h e^{jh\omega t} \tag{4.8}$$

$$y(t) = \sum_0^\infty y_h(t) = \sum_{-\infty}^\infty Y_h e^{jh\omega t} \tag{4.9}$$

corresponding for $h = 1, 2, ..., \infty$, to

$$u_h(t) = U_h e^{jh\omega t} + U_{-h} e^{-jh\omega t} \tag{4.10}$$

$$y_h(t) = Y_h e^{jh\omega t} + Y_{-h} e^{-jh\omega t} \tag{4.11}$$

where

$$U^*_{-h} = U_h = \frac{j}{2}(U'_h + jU''_h) \tag{4.12}$$

$$Y^*_{-h} = Y_h = \frac{j}{2}(Y'_h + jY''_h) \tag{4.13}$$

In equations (4.12) and (4.13) the asterisk denotes the conjugate and equations (4.10) and (4.11) define, in addition to the customary phasors U_h and Y_h, the phasors U_{-h} and Y_{-h}. If U_h and Y_h are related by the transfer function H_h, and U_{-h} and Y_{-h} by H_{-h}, i.e.

$$Y_h = H_h U_h \tag{4.14}$$

$$Y_{-h} = H_{-h} U_{-h} \tag{4.15}$$

then, taking into account equations (4.12) and (4.13), for linear circuits

$$H_{-h} = H^*_h \tag{4.16}$$

In addition, it is possible to combine the equations (4.14) and (4.15) into a single matrix equation

$$Y = [H]U \tag{4.17}$$

where

$$U = [\cdots U_{-h} \cdots U_{-2}, U_{-1}, U_0, U_1, U_2 \cdots U_h \cdots]^t \tag{4.18}$$

$$Y = [\cdots Y_{-h} \cdots Y_{-2}, Y_{-1}, Y_0, Y_1, Y_2 \cdots Y_h \cdots]^t \tag{4.19}$$

$$[H] = diag\{\cdots H_{-h} \cdots H_{-2}, H_{-1}, H_0, H_1, H_2 \cdots H_h \ldots\} \tag{4.20}$$

By substituting equations (4.12) and (4.13) into (4.14) and (4.15) and separating the real and imaginary parts,

$$\begin{pmatrix} Y'_h \\ Y''_h \end{pmatrix} = \begin{pmatrix} H'_h & -H''_h \\ H''_h & H'_h \end{pmatrix} \begin{pmatrix} U'_h \\ U''_h \end{pmatrix} \tag{4.21}$$

The matrix of equation (4.21) is the real equivalent of the complex transfer function H_h of a linear circuit. If the structure of equation (4.21) is not satisfied, the real transfer function matrix cannot be converted into a complex one. Similarly, if equation (4.16) is not valid, equation (4.14) will not in itself be enough.

From equation (4.21) the block-diagonal real matrix

$$[H] = diag\{H_h\} \tag{4.22}$$

can be assembled to give the complete set of harmonics. It may be noted that for the complex form (4.20), the structural property of equation (4.16) is valid while for the real form (4.22), the structural property (4.21) is true. It will be seen later that these properties are not valid for linearized, non-linear circuits. Because of this, in combined circuits the full forms (4.20) or (4.22) have to be retained, even for the linear part.

4.2.2 Linearization of $y = f(x)$ in the Form $Y = [F]X + Y_N$

Consider the non-linear relation

$$y = f(x) \tag{4.23}$$

between the periodic variables x and y, where

$$x(t) = \sum_{-\infty}^{\infty} X_h e^{jh\omega t} \tag{4.24}$$

$$y(t) = \sum_{-\infty}^{\infty} Y_h e^{jh\omega t} \tag{4.25}$$

Let X and Y be the vectors of X_h and Y_h. Substitution of equation (4.24) and (4.25) into (4.23) shows that y is a function of x, i.e.

$$Y = f(X) \tag{4.26}$$

If the non-linear relation (4.23) between the periodical variables x and y is differentiable then, for small increments about x_b and y_b,

$$\Delta y = f'(x_b)\Delta x \tag{4.27}$$

where

$$\Delta x = \sum_{-\infty}^{\infty} \Delta X_h e^{jh\omega t} \tag{4.28}$$

$$\Delta y = \sum_{-\infty}^{\infty} \Delta Y_k e^{jk\omega t} \tag{4.29}$$

$$f'(x_b) = f'(x(t)) = \sum_{-\infty}^{\infty} c_i e^{ji\omega t} \tag{4.30}$$

In order to identify the matrix [F], first, only a single term in the expansion of (4.28) is considered, i.e.

$$\Delta x = \Delta X_h e^{jh\omega t} \tag{4.31}$$

Substituting this term together with equations (4.29) and (4.30) into equation (4.27) yields

$$\sum_{-\infty}^{\infty} \Delta Y_k e^{jk\omega t} = (\sum_{-\infty}^{\infty} c_i e^{j(i+h)\omega t}) \times \Delta X_h \tag{4.32}$$

To identify like exponents in equation (4.32), we write

$$k = i + h \tag{4.33}$$

and break down equation (4.32) into the equation of coefficients

$$\begin{pmatrix} \cdot \\ \cdot \\ \cdot \\ \Delta Y_{-2} \\ \Delta Y_{-1} \\ \Delta Y_0 \\ \Delta Y_1 \\ \Delta Y_2 \\ \cdot \\ \cdot \\ \cdot \end{pmatrix} = \begin{pmatrix} \cdot \\ \cdot \\ \cdot \\ c_{-2-h} \\ c_{-1-h} \\ c_{-0-h} \\ c_{1-h} \\ c_{2-h} \\ \cdot \\ \cdot \\ \cdot \end{pmatrix} \times \Delta X_h \tag{4.34}$$

This identifies one column of the matrix [F] in the complete linear relation

$$\Delta Y = [F]\Delta X \tag{4.35}$$

to be obtained if all terms ΔX_h of equation (4.28) are considered. It may be noticed that $[F]$ represents the Jacobian of equation (4.26).

In equation (4.35)

$$\Delta X = [\cdots \Delta X_{-h} \cdots \Delta X_{-2}, \Delta X_{-1}, \Delta X_0, \Delta X_1, \Delta X_2, \cdots \Delta X_h \cdots]^t \tag{4.36}$$

$$\Delta Y = [\cdots \Delta Y_{-k} \cdots \Delta Y_{-2}, \Delta Y_{-1}, \Delta Y_0, \Delta Y_1, \Delta Y_2, \cdots \Delta Y_k \cdots]^t \tag{4.37}$$

and

$$[F] = \begin{pmatrix}
\ddots & \ddots & \ddots & \ddots & & & & & & & \\
\ddots & c_0 & c_1 & c_2 & c_3 & & & & & & \\
\ddots & c_{-1} & c_0 & c_1 & c_2 & c_3 & & & & & \\
\ddots & c_{-2} & c_{-1} & c_0 & c_1 & c_2 & c_3 & & & & \\
 & c_{-3} & c_{-2} & c_{-1} & c_0 & c_1 & c_2 & c_3 & & & \\
 & & c_{-3} & c_{-2} & c_{-1} & c_0 & c_1 & c_2 & c_3 & & \\
 & & & c_{-3} & c_{-2} & c_{-1} & c_0 & c_1 & c_2 & & \\
 & & & & c_{-3} & c_{-2} & c_{-1} & c_0 & c_1 & \ddots & \\
 & & & & & c_{-3} & c_{-2} & c_{-1} & c_0 & \ddots & \\
 & & & & & & \ddots & \ddots & \ddots & \ddots &
\end{pmatrix} \tag{4.38}$$

If the linearization is about a point X_b,Y_b in the space of complex conjugate harmonics,i.e.

$$\Delta X = X - X_b \tag{4.39}$$

$$\Delta Y = Y - Y_b \tag{4.40}$$

then substitution of equations (4.39) and (4.40) into (4.35) yields

$$Y = [F]X + Y_N \tag{4.41}$$

where

$$Y_N = Y_b - [F]X_b \tag{4.42}$$

The subscript N draws attention to the possibility of interpreting the linearized equation (4.41) as a Norton equivalent in the complex-conjugate harmonic space.

It is noted that not only are the harmonics complex conjugate pairs, but so also are the entries

$$c_{-i} = c_i^*$$

of the Jacobian matrix $[F]$, which makes it Hermitian. It can be seen that it consists of equal elements on all diagonals, thus, $[F]$ is a Toeplitz matrix. Often the band of side-diagonals will be of limited width or it will be truncated so that $[F]$ is a banded Toeplitz matrix. In all practical cases $[F]$ will be of finite dimensions due to simplifying assumptions, to truncation or to discretization in computer evaluation.

It may be seen from the matrix (4.38) that c_0 represents an output of the same order to any unit harmonic input and c_i represents the side harmonic, which is also the same for a unit input of any harmonic.

4.2.3 Numerical Example 1

Linearize

$$i = f(\psi) = \psi + \psi^3$$

around

(a) $\psi_b = \sin(\omega t)$

and

(b) $\psi_b = \sin(\omega t) + \sin(3\omega t)$

The derivative of the non-linear function is

$$f'(\psi) = 1 + 3\psi^2$$

Solution (a)

Substituting the base operating point into the non-linear function and its derivative,

$$f(\psi_b) = \sin(\omega t) + (\sin(\omega t))^3$$

$$f'(\psi_b) = 1 + 3(\sin(\omega t))^2$$

or, in terms of complex harmonics,

$$f(\psi_b) = j\frac{1}{8}e^{j3\omega t} - j\frac{7}{8}e^{j\omega t} + conj$$

and with the complex coefficients the linearized equation may be written,

$$\begin{pmatrix} I_{-3} \\ I_{-1} \\ I_1 \\ I_3 \end{pmatrix} = \frac{j}{8}\begin{pmatrix} -1 \\ 7 \\ -7 \\ 1 \end{pmatrix} + \begin{pmatrix} \frac{5}{2} & & \frac{-3}{4} & & & & \\ & \frac{5}{2} & & \frac{-3}{4} & & & \\ \frac{-3}{4} & & \frac{5}{2} & & \frac{-3}{4} & & \\ & \frac{-3}{4} & & \frac{5}{2} & & \frac{-3}{4} & \\ & & \frac{-3}{4} & & \frac{5}{2} & & \frac{-3}{4} \\ & & & \frac{-3}{4} & & \frac{5}{2} & \\ & & & & \frac{-3}{4} & & \frac{5}{2} \end{pmatrix} \begin{pmatrix} \Delta\psi_{-3} \\ \Delta\psi_{-1} \\ \Delta\psi_1 \\ \Delta\psi_3 \end{pmatrix}$$

Solution(b)

When a non-sinusoidal input force is used, the complexity of the problem grows although the procedure remains much the same. This becomes apparent when the input force in (b) is substituted into the non-linear function and its derivative.

$$f(\psi_b) = \sin(\omega t) + \sin(3\omega t) + (\sin(\omega t) + \sin(3\omega t))^3$$

$$f'(\psi_b) = 1 + 3(\sin(\omega t) + \sin(3\omega t))^2$$

or, in terms of complex harmonics,

$$f(\psi_b) = j\frac{1}{8}e^{j9\omega t} + j\frac{3}{8}e^{j7\omega t} - j\frac{3}{2}e^{j3\omega t} - j\frac{10}{8}e^{j\omega t} + conj$$

$$f'(\psi_b) = j\frac{3}{4}e^{j6\omega t} j\frac{3}{2}e^{j4\omega t} - j\frac{3}{4}e^{j2\omega t} + 2 + conj$$

A linearized model, similar to the one found in (a), can be written down with the complex coefficients computed above, although this linearized model will exhibit a wider band of non-zero coefficients.

4.3 Multivariable Static Circuits

4.3.1 A more general formulation

It is possible to generalize the non-linear relation (4.23) for several inputs and outputs:

$$Y_{(i)} = (X_{(1)}, X_{(2)}, ..., X_{(m)}) \qquad (i = 1, 2, ..., m) \tag{4.43}$$

Linearization about a base point X_b,Y_b yields

$$\Delta Y_{(i)} = \frac{\delta f_{(i)}}{\delta X_{(1)}}\Delta X_{(1)} + \frac{\delta f_{(i)}}{\delta X_{(2)}}\Delta X_{(2)} + \cdots \qquad (i = 1, 2, ..., m) \tag{4.44}$$

Equation (4.44) contains several terms which pose problems similar to those in (4.27). Using the same line of reasoning, equations similar to (4.35) are obtained

$$\Delta Y_{(i)} = [F_{(i,1)}]\Delta X_{(1)} + [F_{(i,2)}]\Delta X_{(2)} \qquad (i = 1, 2, ..., m) \tag{4.45}$$

which can be written in matrix form

$$[\Delta Y] = [F][\Delta X] \tag{4.46}$$

where the use of brackets indicates a higher order than in equation (4.35).

The linearized equivalent arrived at is:

$$[\Delta Y] = [F][X] + [Y_N] \tag{4.47}$$

4.3.2 Numerical Example 2

Linearize

$$Y = f(X_{(1)}, X_{(2)}) = X_{(1)}X_{(2)}^2(1 + X_{(2)})$$

around

$$X_{(1),b} = \sin(\omega t) + \sin(3\omega t)$$

$$X_{(2),b} = \cos(\omega t)$$

Substituting the base operating point into the non-linearity gives,

$$f(X_{(1)}, X_{(2)}) = -j\frac{1}{8}(e^{j6\omega t} + 2e^{j5\omega t} + 4e^{j4\omega t} + 6e^{j3\omega t} + 5e^{j2\omega t} + 4e^{j\omega t} - 1) + conj$$

and the partial derivatives are:

$$\frac{\delta f}{\delta X_{(1)}} = X_{(2)}^2\,(1 + X_{(2)})$$

$$\frac{\delta f}{\delta X_{(2)}} = X_{(1)}X_{(2)}\,(2 + 3X_{(2)})$$

When evaluated at the operational point, $X_{(1),b}$ $X_{(2),b}$, the partial derivatives become, in terms of complex harmonics,

$$\frac{\delta f}{\delta X_{(1)}} = \frac{1}{8}(e^{j3\omega t} + 2e^{j2\omega t} + 3e^{j\omega t} + 2) + conj$$

$$\frac{\delta f}{\delta X_{(2)}} = -j\frac{1}{8}(3e^{j5\omega t} + 4e^{j4\omega t} + 9e^{j3\omega t} + 8e^{j2\omega t} + 6e^{j\omega t}) + conj$$

With the complex coefficients obtained above the Toeplitz matrices $[F_{(1)}]$ and $[F_{(2)}]$ may be written down.

4.4 Dynamic Circuits

4.4.1 Linearizing the dynamic equations

In the previous sections it has been established that a function $f(x)$ of one or several variables can be linearized in the complex-conjugate harmonic space as $[F]X + I_N$. This result can be used for solving dynamic circuits for which non-linear state equations are written as

$$\dot{x} = f(x, u)$$

$$y = g(x, u) \tag{4.48}$$

The right hand sides of equations (4.48) can thus readily be linearized.The first equation is dynamic and the derivative x in the harmonic space is obtained by multiplying each component x_h by $jh\omega$. In matrix form this means the operation

$$diag\{jh\omega\}X \tag{4.49}$$

Accordingly, equations (4.48) becomes:

$$diag\{jh\omega\}\Delta X = [F_{(X)}]\Delta X + [F_{(u)}]\Delta U$$

$$\Delta Y = [G_{(X)}]\Delta X + [G_{(U)}]\Delta U \tag{4.50}$$

and eliminating ΔU from equation (4.50),

$$\Delta Y = [H]\Delta X \tag{4.51}$$

or

$$\Delta Y = [H]\Delta X + Y_N \tag{4.52}$$

which represents the linearization of a general non-linear dynamic circuit.

In most practical cases the problem can be formulated more simply than in the general case of equation (4.48).

4.4.2 Numerical Example 3

Consider the non-linear inductor

$$Ri + L\frac{di}{dt} + \frac{d\psi}{dt} = v$$

excited from a periodic voltage source $v(t)$ and with the magnetizing characteristic

$$i = f(\psi)$$

where $\psi = \phi N$ is the total flux linkage.

The non-linear state equations for the inductor are,

$$\dot{\psi} = -(R + j\omega L)f(\psi) + v$$

$$i = f(\psi)$$

and the linearization of the dynamic equations gives

$$diag\{jh\omega\}\psi = -(R + j\omega L)[F]\Delta\psi + \Delta V$$

$$\Delta I = [F]\Delta\psi$$

Therefore,

$$\Delta I = [H]\Delta V$$

$$I = [H]V + I_N$$

where $[H] = [F](diag\{jh\omega\} + diag\{R + j\omega L\}[F])^{-1}$, is the harmonic admittance matrix of the Norton equivalent.

For an ideal inductor the matrix [H] is reduced to

$$[H] = [F]diag\{\frac{1}{j\omega h}\}$$

4.5 Computer Tasks

4.5.1 The basic algorithm

At this stage the basic theory of linearization in the complex-conjugate harmonic space has been completely developed and applied to the solution of very simple problems by using only analytical calculations. For most practical cases, however, solutions must be numerical and computer-oriented as analytical calculations are possible only in contrived problems.

In this section a numerical application of the technique is made to the problem of single phase ferromagnetic cores. The necessary steps for actual computer implementation along with some important remarks and numerical examples are also given. Attention has been paid to the iterative process and the interfacing of the linear and linearized, non-linear elements of the network for an efficient solution.

The basic algorithm is as follows:

1. To initiate the process a base operating voltage $v_h(t)$ is established at the fundamental frequency for the voltage source $v_h^k(t)$ through a load flow solution.

2. The corresponding flux wave is obtained and impressed, point by point, upon the experimental characteristic $\psi - i$ and the associated magnetizing current $i_b^j(t)$ is thus determined in the time domain.

3. By means of a Fourier transform (FFT version), the magnetizing current $i_b^j(t)$ is solved in the frequency domain and the Fourier coefficients i_h and i_h^* are assembled into a base current vector I_b.

4. Using the magnetizing current and flux as determined in step 2, the derivative of the function $i = f(\psi)$ is evaluated.

5. The FFT is applied to the slope shape of step 4, and the Fourier coefficients c_h and c_h^* obtained from this exercise are used to assemble the Toeplitz matrices $[F]$ and $[G]$.

6. The harmonic admittance matrix $[H]$ and the Norton equivalent current source I_N, i.e. $I_N = I_b - [H]V_b$, are calculated.

7. The linear and linearized models are assembled using a nodal (or equivalent) approach and solved for the new state.

8. If the new state satisfies the chosen convergence criterion the process is stopped. Otherwise, the control is transfered back to step 2 to start a new iteration.

The points mentioned above are shown pictorially in figure 4.1, where the overall procedure may be better appreciated.

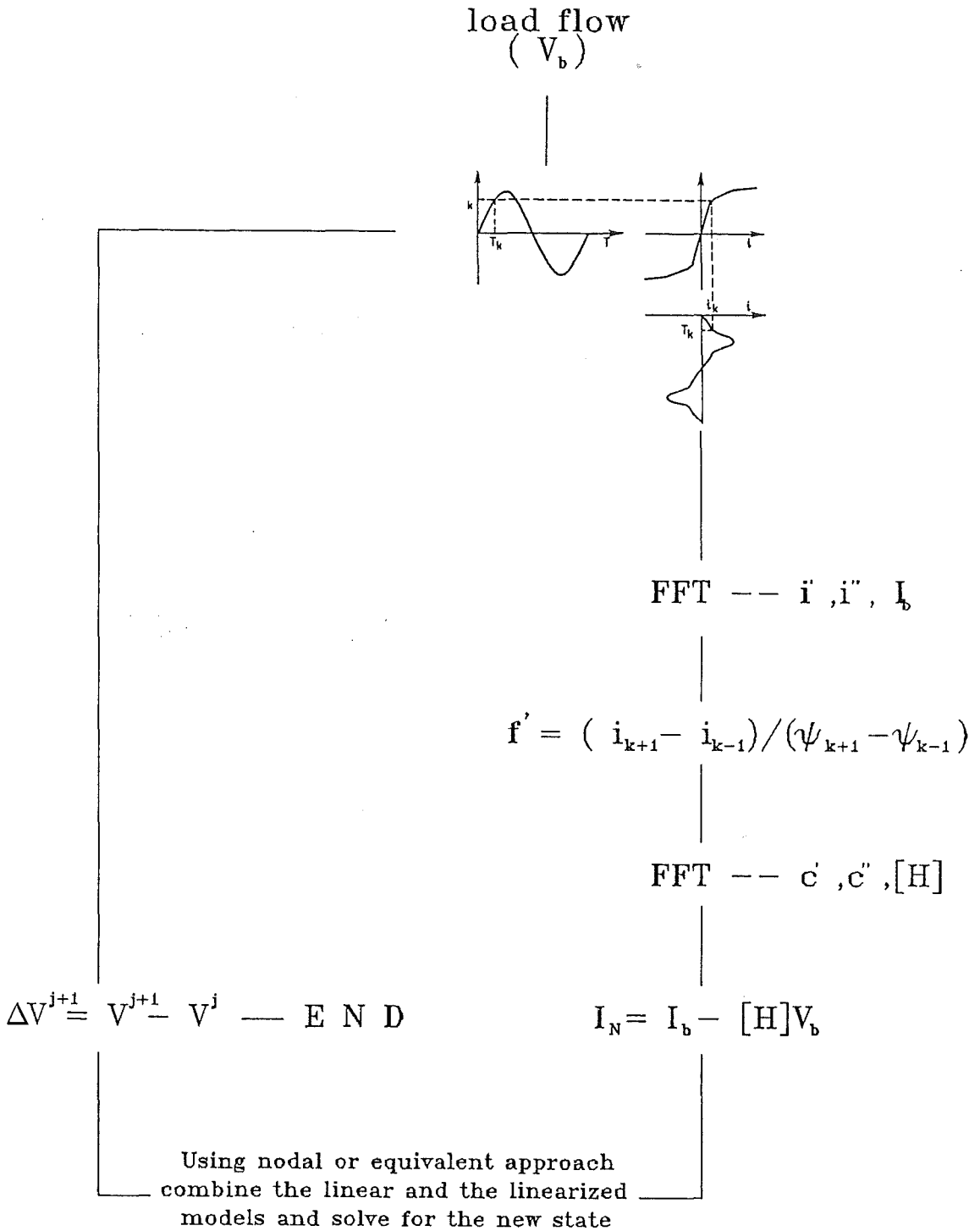

Figure 4-1: Basic iterative algorithm

4.5.2 Departing from the basic algorithm

The linearized harmonic model derived in this chapter provides a more powerful algorithm than that in the previous chapter because the present algorithm is not restricted to cases of sinusoidal excitation and offers the possibility of finding the harmonic solution of the non-linear network by a Newton-type approach.

The basic procedure, given above, combines both the linear and the linearized, non-linear components in the complex conjugate harmonic space. This form of solution is not, however, a full Newton-Raphson procedure because a part of the network is already linear and also because of the practical necessity of considering only a limited number of harmonics. Both factors are expected to affect adversely the quadratic convergence normally associated with the Newton-Raphson algorithm and the proposed method will be refered to as harmonic Newton-Raphson.

Two levels of variation are possible with regards to the basic algorithm. The first one relates to the way in which the elements of the network are treated. For instance, by taking advantage of the network's composition the linear and the linearized components can easily be identified and segregated for a sequential solution. This involves a diakoptical approach in the sense that the network is artificially torn and the individual parts are augmented by either current or voltage sources. The resultant subnetworks should represent correctly the behaviour of the original configuration. This provides an alternative to the unified solution of the basic algorithm.

The second level of variation refers to the way in which the Jacobian of the linearized model is handled. Three different possibilities, which are equally applicable to a unified or to a sequential solution, are:

- Solution
  - Unified
    - Multi-valued Jacobian
    - Single-valued Jacobian
    - Neglecting the Jacobian
  - Sequential
    - Multi-valued Jacobian
    - Single-valued Jacobian
    - Neglecting the Jacobian

For the case of a constant Jacobian, the evaluation takes place in the first iteration and then it is kept constant for the rest of the process.

4.5.3 Some notes in linearization

The complete linearization of a non-linearity in the harmonic space requires two FFT exercises. One determines the harmonic currents while the other determines the harmonic magnetic admittances.

When a unified solution of the network is sought with the non-linearity being linearized at each iterative step, large admittance matrices are inverted at each iteration. Furthermore, the convergence characteristic associated with the harmonic Newton-Raphson is not expected to be quadratic.

On the other hand, the approach based on single evaluation of the Jacobian matrix should reduce the computational burden. The number of FFTs equals the number of iteration plus one and the admittance matrix representing the network must be inverted only once. This approach can be seen as a Newton-type procedure with constant slope and still models the non-linearity as a Norton equivalent.

An even simpler procedure is to neglect the Jacobian matrix altogether. In doing this, the non-linearity is no longer modelled by a Norton equivalent but rather as a set of harmonic current sources. The number of FFTs equals the number of iterations and no need exists to use the harmonic space. Traditional phasors will model the non-linearity while nodal admittances will model the linear part. At this stage a great deal of simplification has been introduced when compared with the basic algorithm. However, the resultant algorithm is a sequential procedure of the Gauss-Seidel type. This particular case of the basic algorithm coincides with an heuristic approach proposed recently by Dommel and others.

The sequential solution for the harmonic response of the network that combines the characteristics of the Newton-Raphson and Gauss-Seidel techniques presents an attractive alternative to the unified approach. It will be refered to as a quasi-Newton procedure. This sequential technique avoids the repetitive inversion of large matrices, because the network is torn diakoptically and the admittances of the linear and linearized circuits are evaluated and solved separately.

A general view of the interaction taking place in a sequential solution, by the quasi-Newton approach, is presented below.

The network is first separated into a minimum number of linear subnetworks S_L^j, and a maximum number of non-linear subnetworks S_{NL}^k. The linear subnetworks S_L^j are augmented by a current source $i_h^j(t)$ while the non-linear subnetworks $S_{NL}^k$are augmented by a voltage source $v_h^k(t)$. where j = 1,...,number of linear subnetworks

k = 1,...,number of non-linear subnetworks

h = 1,...,number of considered harmonics

Once the network has been torn, the actual iterative process takes place. figure 4.2 highlights the mechanics of the iterative process for the case of one linear subnetwork and one non-linear subnetwork, in which, as stated in step 2 of the basic algorithm, an operational voltage $v_1(t)$ determined from a load flow solution is impressed on the non-linear ferromagnetic core, S_{n1}^k.

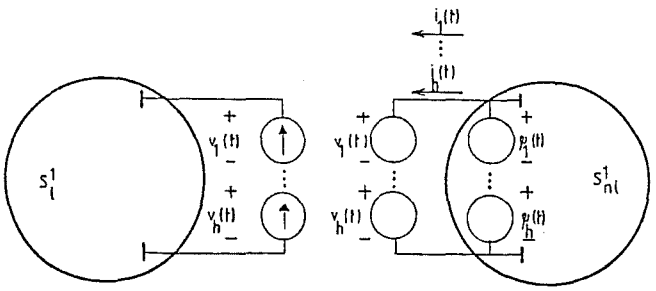

Figure 4.2: **The mechanics of the iterative sequential solution**

The output response is a set of currents of different frequencies equal in magnitude and phase to the current sources associated with the linear subnetwork.

The linear subnetwork is solved (its frequency dependence being taken into account) and a new set of harmonic voltages are found at the terminals of the linear subnetwork. In turn, these voltages are taken to be equal in magnitude and phase to a new state of the voltage sources associated with the non-linear subnetwork.

This routine is carried out until a specified criterion of convergence is satisfied. The one adopted here was a difference in voltage of 0.0005 *p.u.* between two successive iterations. This criterion applies to the fundamental and all its harmonics.

Since the non-linear elements are being treated in the complex-conjugate harmonic space, the usual positive phasors may not describe the phenomena here under discussion completely and the need arises to represent all the harmonics, both positive and negative ,explicitly.

Once the operating voltage and its associated flux has been established, a $50Hz$ period is subdivided in $N = 2^n$ time steps, Δt, such that the highest harmonic will be sufficiently well sampled. The discretized flux is impressed upon the experimental characteristic and a corresponding magnetizing current determined.

Provided that the magnetizing current is smooth, its derivative with respect to the magnetizing flux can be obtained simply and accurately using the central difference algorithm.

For instance, let t_k be a discrete time in the selected interval and ψ_k and i_k the corresponding values of the magnetizing characteristic as shown in figure 4.1. The derivative for this particular point (i.e. step 4 of the basic algorithm) is given as

$$f'_k = \frac{I_{k+1} - I_{k-1}}{\psi_{k+1} - \psi_{k-1}} \tag{4.53}$$

The remaining part of the algorithm contains the iterative solution of a number of linear and linearized equations of the form (4.52).

The linear subnetwork is described by

$$I_h = [Y]_h V_h \tag{4.54}$$

for each harmonic h.

For the non-linear components, the nodal equation for each harmonic are

$$I_h = \sum_j H_{hj} V_j + I_{Nh} \tag{4.55}$$

where H and I_N are as defined in step 6.

Equation (4.55) can also be written as

$$I_h = H_{hh} + I'_{Nh} \tag{4.56}$$

where

$$I'_{Nh} = I_{Nh} + \sum_j H_{hj} V_j \tag{4.57}$$

The iterative process starts from $h = 1$ with all V_j $(j \neq h)$ initialized to zero. Having obtained V_1, equation (4.57) is used to calculate V_{-1}. This is continued by making $h = 2, -2, etc.$, and updating V_h. With the latest set of V_h for all h, a new re-linearization is performed, until convergence is achieved.

It must be noted that, as in the Gauss-Seidel algorithm, the procedure uses the new values of V_h as soon as they are obtained.

4.5.4 Numerical Example 4

In this example a non-linear lossless reactor is fed from a lossless line of variable length and the magnetizing characteristic of the reactor is

$$f(\psi) = a\psi + b\psi^3$$

The line is supplied from an infinite busbar of 50 Hz and 1 p.u. fundamental voltage

$$V_\infty = \frac{e^{j\omega t} + e^{-j\omega t}}{2}$$

i.e. the sending end vector V_∞ has the following components

$V_{\infty,1} = \frac{1}{2}$, $V_{\infty,-1} = \frac{1}{2}$, all other $V_{\infty,h} = 0$

The equation of the line,for any harmonic h, is

$$V_{\infty,h} = \cosh(h\omega\tau t) \times V_h + jz_c \sinh(h\omega\tau t) \times I_h$$

The propagation constant and characteristic impedance of the line at fundamental frequency are:

$$\tau = j\sqrt{L_h C_h} = j\ 0.001 km^{-1}$$

$$z_c = \sqrt{\frac{L_h}{C_h}} = 378.52\Omega$$

The numerical evaluation of the line's equation up to the third harmonic for a line length of 400 km is

$$\begin{pmatrix} \vdots \\ \vdots \\ 1/2 \\ \vdots \\ 1/2 \\ \vdots \\ \vdots \end{pmatrix} = \begin{pmatrix} 0.282 & & & & & & & \\ & 0.655 & & & & & & \\ & & 0.909 & & & & & \\ & & & 1.000 & & & & \\ & & & & 0.909 & & & \\ & & & & & 0.655 & & \\ & & & & & & 0.282 & \end{pmatrix} \begin{pmatrix} V_{-3} \\ V_{-2} \\ V_{-1} \\ V_0 \\ V_1 \\ V_2 \\ V_3 \end{pmatrix}$$

$$+j \begin{pmatrix} -0.750 & & & & & & & \\ & -0.591 & & & & & & \\ & & -0.325 & & & & & \\ & & & 0.000 & & & & \\ & & & & 0.325 & & & \\ & & & & & 0.591 & & \\ & & & & & & 0.750 & \end{pmatrix} \begin{pmatrix} I_{-3} \\ I_{-2} \\ I_{-1} \\ I_0 \\ I_1 \\ I_2 \\ I_3 \end{pmatrix}$$

The dynamic equation of the reactor is

$$\dot{\psi} = v$$

which in the harmonic space becomes

$$\psi = diag\{\frac{1}{jh\omega}\}\, v$$

and the linearized form of the reactor characteristic, $i = f(\psi)$, in the harmonic space is

$$I = [F]\psi + I'_N$$

or, in terms of voltages,

$$I = [H]v + I_N$$

which, when numerically evaluated, becomes

$$\begin{pmatrix} I_{-3} \\ I_{-2} \\ I_{-1} \\ I_0 \\ I_1 \\ I_2 \\ I_3 \end{pmatrix} = \begin{pmatrix} 0.043 & & -0.064 & & & & \\ & 0.064 & & * & & & \\ -0.021 & & 0.128 & & 0.064 & & \\ & -0.032 & & * & & 0.032 & \\ & & -0.064 & & -0.128 & & 0.021 \\ & & & * & & -0.064 & \\ & & & & 0.064 & & -0.043 \end{pmatrix} \begin{pmatrix} V_{-3} \\ V_{-2} \\ V_{-1} \\ V_0 \\ V_1 \\ V_2 \\ V_3 \end{pmatrix} + j \begin{pmatrix} -0.011 \\ \\ 0.035 \\ \\ -0.035 \\ \\ 0.011 \end{pmatrix}$$

where the symbol $*$ indicates very large values.

As expected, no coupling between harmonics exists in the equation representing the linear subnetwork. Also, it shows that the positive and negative harmonics are related through the complex conjugate operation.

On the other hand, the equation representing the non-linear subnetwork, while symmetrical in structure, is numerically asymmetrical. Thus, the complete set of harmonics, i.e. +ve and -ve must be considered explicitly. The band-diagonal matrix $[H]$ is responsible for the coupling between harmonics in the complex conjugate harmonic space.

An harmonic Newton-Raphson algorithm would involve the joint solution of the linear and linearized matrix equations, i.e. a unified approach, requiring computations with large matrices. Alternatively, the quasi-Newton approach brings the linearized equation to the form of equation (4.57) and substitutes I_h into the linear equation to calculate V_h. This is a fast, scalar operation but several sweeps through all values of h would be needed to obtain the equivalent of the direct matrix solution.

Figure 4.3 shows the voltage magnitude V at the terminals of the lossless reactor for different line lengths.

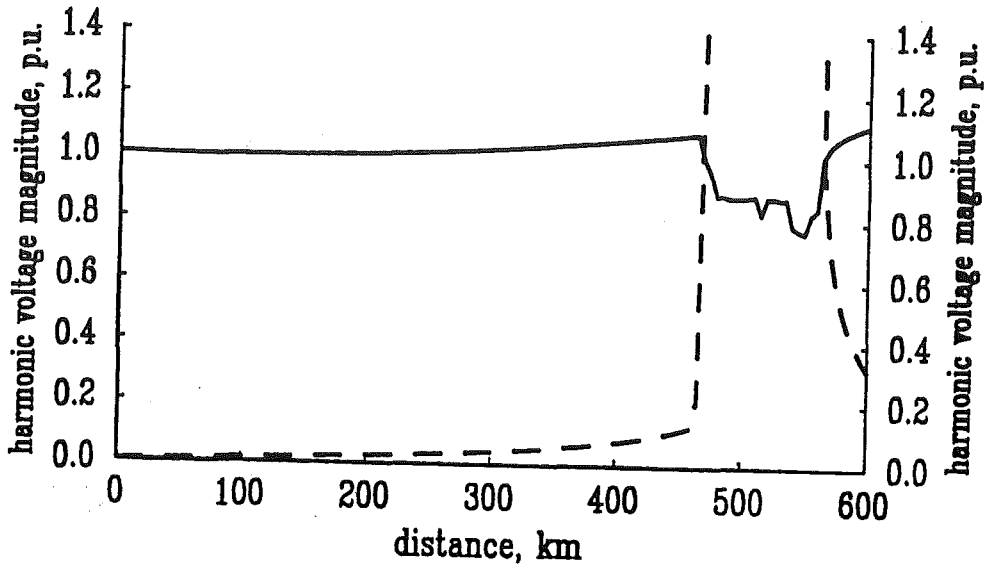

Figure 4.3: Fundamental and third harmonic voltage versus line length

For short distances the fundamental voltage is almost equal to unity and no harmonic distortion exists. As the reactor constitutes a very light load, the fundamental voltage rises as the length of the line is increased. The core can saturate as a result of fundamental and harmonic voltages, thus causing interaction between the fundamental and the harmonics as well as between the harmonics themselves. In figure 4.3, when the lossless line approaches its quarter wave length for the third harmonic, i.e. 500 km, because the initial fundamental flux is sufficiently high to saturate the core it will draw a distorted magnetizing current made up mainly of fundamental and third harmonic components.

At that distance the third harmonic current generated by the reactor excites an anti-resonance and establishes an extremely high third harmonic voltage (infinite theoretically) which drives the core to a state of deep saturation. Two combined effects are exhibited around this point, namely, the presence of an infinite voltage and the numerical algorithm failing to provide convergence.

4.5.5 Numerical example 5

The harmonic analysis for the test system of the numerical example 3-2 is now carried out by the technique of linearization in the complex conjugate harmonic space.

The equivalent circuit is given in figure 4.4.

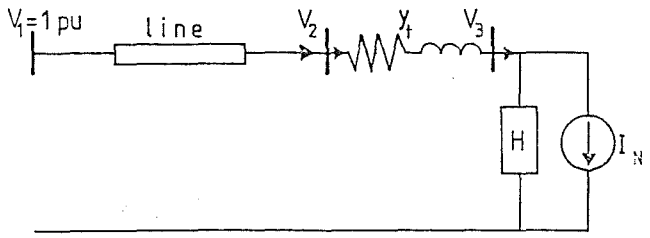

Figure 4.4: Equivalent circuit

Figure 4.5 shows the magnitude of the harmonic voltages at the point of connection between the transformer and the transmission line when the level of the excitation voltage at the infinite busbar is 1.0 p.u.

The iterative strategies discussed in section 4.5.2 have been applied to the solution of this example and a common solution has been obtained in every case. When connected to lines of short distance the transformer does not saturate and a negligible amount of harmonic distortion occurs. The various algorithms take the same number of iterations to converge. As the length of the line grows the fundamental voltage at the far end of the line grows, pushing the transformer into saturation. In turns, the transformer will draw a larger amount of distorted magnetizing current and, if resonant conditions exist, harmonic magnification will take place. In these cases the number of iterations taken by the algorithms to arrive at a solution differ from each other. The Newton-type methods find the solution in less iterations than cases when the Jacobian is being neglected, as shown below for selected lengths of line.

length(km)	100	200	300	400	500	600
Unified (a)	2	2	4	3	5	4
Quasi-Newton (a)	2	2	4	3	5	4
Unified (b)	2	2	4	3	5	4
Quasi-Newton (b)	2	2	4	3	5	4
Sequential	2	2	4	3	7	7

Table 4.1: Number of iterations required to converge

where (a) corresponds to the case of a multi-evaluated Jacobian and
(b) corresponds to the case of a constant Jacobian

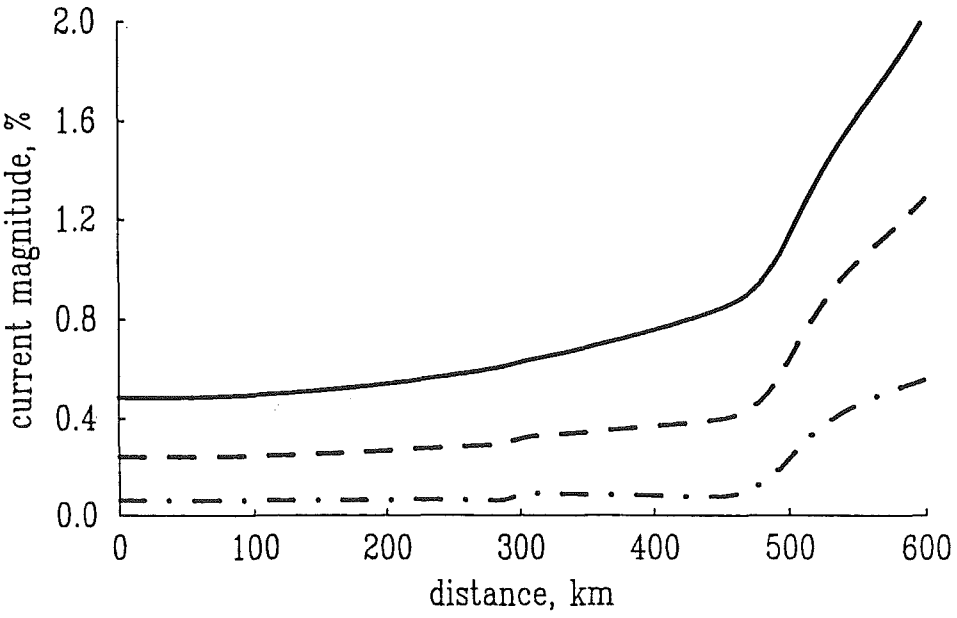

(a)

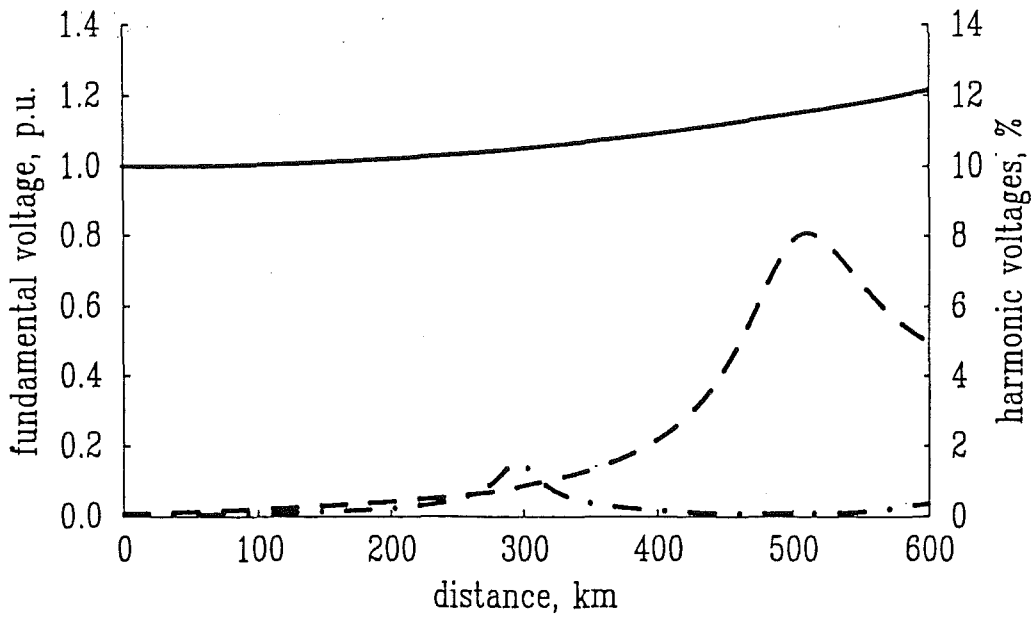

(b)

Figure 4-5: Harmonic information at busbar 2 versus line length
(a) Current (b) Voltage

fund. ——————
third — — —
fifth — · —

In cases of symmetrical or unsymmetrical over-excitation the transformer can be pushed into a state of deep saturation which causes it to draw a large amount of magnetizing current [Yacamini 1981]. This, in turn, may cause considerable harmonic voltage distortion at the transformer's terminals.

Figure 4.6 presents results when an excitation level of 1.1 p.u. is applied to the infinite busbar of figure 4-4. In this case the number of iterations taken by the different algorithms vary significantly from each other. The use of algorithms of the Newton-type achieve convergence, as shown in figure 4.6(a), while the algorithm that neglects the Jacobian matrix encounters problems for the levels of excitation involved, as illustrated in figure 4.6(b).

When solving circuits under these circumstances the number of iterations taken by the algorithms increases significantly because the resultant harmonic solution is very far away from the undistorted initial estimate and it has been observed that the solution is reached in an oscillatory or monotonic fashion. This may explain why sometimes the quasi-Newton methods reaches convergence in fewer iterations than the unified solutions. However, contrary to expectations, single-evaluated Jacobian solutions may require fewer iterations to converge than multi-evaluated Jacobian solutions.

To show the above points the number of iterations and their harmonic solutions are given below when the transmission line is 500 km long. In this case the approach that neglects the Jacobian matrix fails to converge.

	multi-evaluated Jacobian	single-evaluated jacobian
Unified	16 iterations	12 iterations
fundamental	1.249708 - j0.087701	1.249666 - j0.087703
third	0.041383 - j0.150975	0.041741 - j0.151166
fifth	-0.001086 + j0.002646	-0.001099 + j0.002646
seventh	-0.000975 + j0.006160	-0.001033 + j0.006157
Quasi-Newton	13 iterations	9 iterations
fundamental	1.249629 - j0.087690	1.249686 - j0.087698
third	0.041822 - j0.151575	0.041489 - j0.151340
fifth	-0.001096 + j0.002663	-0.001085 + j0.002660
seventh	-0.000992 + j0.006210	-0.000944 + j0.006192

Table 4.2: Harmonic content for a 500 km line

Future work is necessary on the theoretical convergence of the harmonic Newton-Raphson, but a possible explanation for this unexpected behaviour is the oscillatory and monotonic nature of the convergence mechanism.

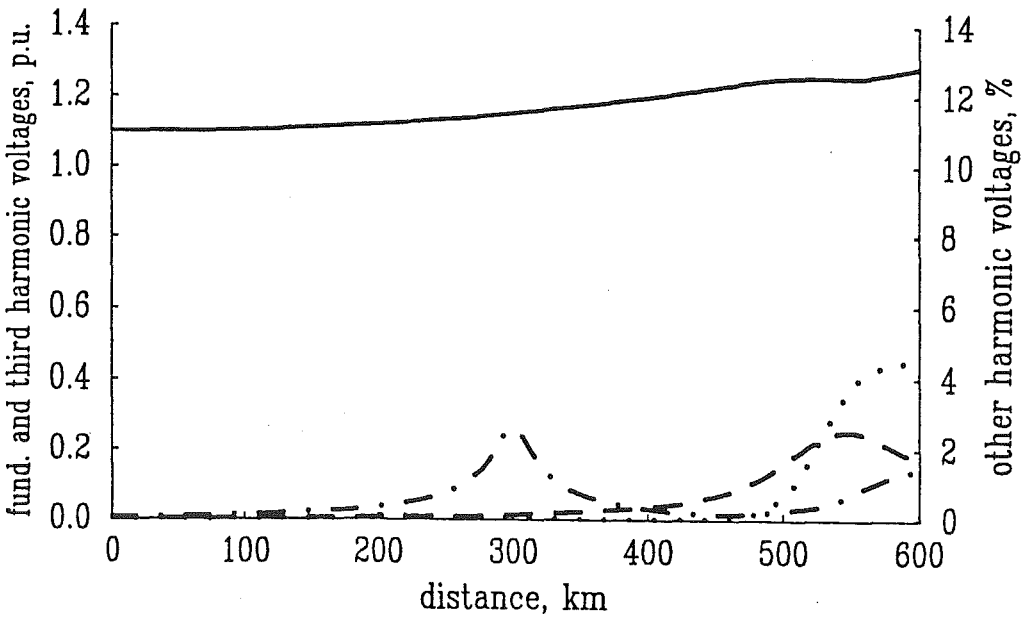

(a)

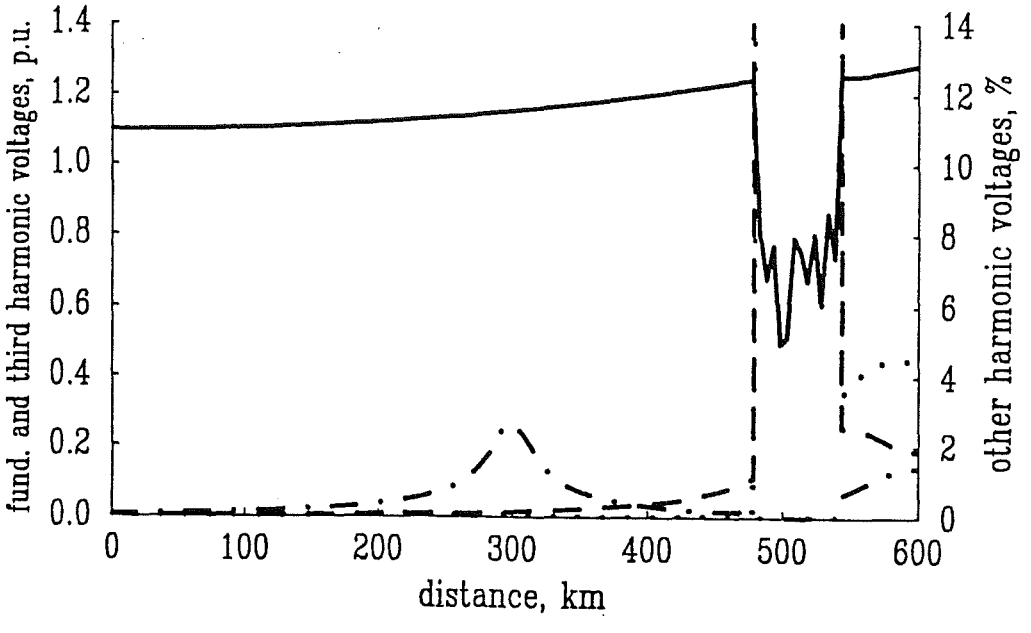

(b)

Figure 4-6: Harmonic voltages at busbar 2 versus line length
(a) Including the Jacobian (b) Neglecting the Jacobian

fund. ————
third — — -
fifth — . —
seventh . . . . .

4.6 Conclusions

A basic, generalized theory for the solution of harmonic problems has been developed capable of representing the coupling effects between different harmonic frequencies. It can be applied to sinusoidal or non-sinusoidal excitation, either symmetrical or unsymmetrical. It also includes correctly the voltage and the frequency dependent effects.

The individual linearized equations can be seen as a Newton-Raphson procedure with quadratic convergence. They may also be interpretated as an harmonic Norton equivalent and, if an unified solution is pursued, they are easily combined with the admittances of the linear part of the network. However, the linearized equations couple all harmonics while the linear part of the network has independent admittances for each harmonic and, hence, the global network equation is not a full Newton-Raphson and, therefore, no quadratic convergence is expected.

The Jacobian matrix of the linearized equation is a function of both the positive and the negative harmonic magnetic admittances and, while it is symmetrical in structure, it is numerically asymmetrical. The whole network equation must be treated explicitly in terms of +ve and -ve phasors which gives rise to the repetitive inversion of large matrices. The resultant network analysis is not of a conventional nature and therefore sufficient and detailed numerical examples have been presented.

Several iterative strategies have been compared in terms of their ability and the number of iterations taken to reach convergence. Among them are unified and sequential solutions with a single or multi-evaluated Jacobian.

In this case the network does not possess a global linearized equation. Unlike the load flow problem, where a global linearized equation exists because the whole network is non-linear. The reason is that the network is non-linear by sectors and is linked through linear components. This factor degrades convergence and it has been shown that sequential solutions of the quasi-Newton type are as good as unified ones. Furthermore, while the harmonic parameters of the non-linear subnetwork may change significantly from one iteration to the next, the harmonic parameters of the linear subnetwork are fixed and dominant by orders of magnitude. This produces very reliable, single-evaluated Jacobian solutions and a great reduction in the computational burden a result of some practical importance.

It has also been shown that Dommel's heuristic approach to the solution of this kind of problems corresponds to the most restricted case of the linearized equation presented in this chapter.

Chapter 5

Harmonic Models For Power Transformers

5.1 Introduction

This chapter capitalizes on the developments of the complex-conjugate harmonic space and, based on it, presents a new generation of steady state transformer models that are more general and possess better convergence characteristics than those already available in the literature.

It is true that the modelling of power transformers is an old discipline that has caught the attention of a great deal of researchers, however, different states of the power system requires different transformer models and, so far, almost every effort has been devoted to both the transient and the rms steady states. In contrast, very little work has been done for the periodic steady state which is the concern of this research.

The power frequency behaviour of this plant component and its influence upon the network was reasonably well understood very early. Transformer models based on sequence components have been available for many decades and when the need arose for representing power system imbalance, transformer models in the phase frame of reference were promptly offered [Laughton 1968] and [Chen and Dillon 1974].

Transformer models suitable for the study of conditions involving over-voltages and higher frequencies did not meet the same success. For instance, the problem of transformer transients, particularly inrush currents, was first observed as early as the last decade of the 19th century, and although much attention was paid to the problem, only qualitative analysis were made and some empirical models were established. A comprehensive solution was not easy to achieve mainly because of the difficulty in modelling the magnetic characteristic of the core, and most efforts were confined to the calculation of the first peak of the inrush current in single phase transformers.

Powerful digital computers and modern mathematical techniques have benefited contemporary research, which has been successful in establishing multilegged transformer models, based on time domain solutions, suitable for cases where the frequency dependence of the core may be overlooked, such as the inrush current problem [Nakra and Barton 1973]. Moreover, frequency dependant transformer models, which allows accurate and general solutions of problems associated with low transients, have been reported very recently [Avila-Rosales and Semlyen 1985].

In principle, time domain techniques can be applied to find the periodic steady state solution of power transformers but sometimes this is not without difficulty and the current trend is to avoid their use as steady state tools [Dommel,Yan,Ortiz de Marcano 1983]. Thus, the search for alternative formulations, based on harmonic phasors or equivalent approaches, was started a few years ago. Considerable progress has been reported for the case of single phase transformers [Semlyen,Acha and Arrillaga 1987(a)] and also for the case of grounded star bank of transformers [Dommel,Yan and Shi-Wei 1986]. More general three phase transformer models are now presented in this chapter.

Three phase bank of transformers consist of three separate units that keeps each magnetic circuit independent, allowing magnetic paths of low reluctance to be presented to the flux which remain almost entirely confined to the individual cores. In this situation, it is possible to derive harmonic models for three phase transformers using the technique of linearization in the harmonic space, almost as discussed in the previous chapters. Both the magnetic and the electric circuits are accommodated together to give a full representation for three phase bank of transformers.

5.2 Units with a single winding connected to a line of varying length

A transmission line of varying length has been a useful tool when analyzing the harmonic response of single phase transformers. The reason being that this hypothetical transmission line provides information of the resonant points at all the harmonics of interest.

Following the same trend, and to gain insight into three phase transformers, a lossles three phase bank is connected to a transmission line of a varying length and their harmonic behaviour is analyzed. Moreover, the individual magnetic units contain a single winding and are supplied from an infinite busbar through the transmission line of varying length.

Two different three phase arrangements are considered in this section, i.e. the grounded star and delta connection, respectively.

The grounded star arrangement is shown in figure 5.1.

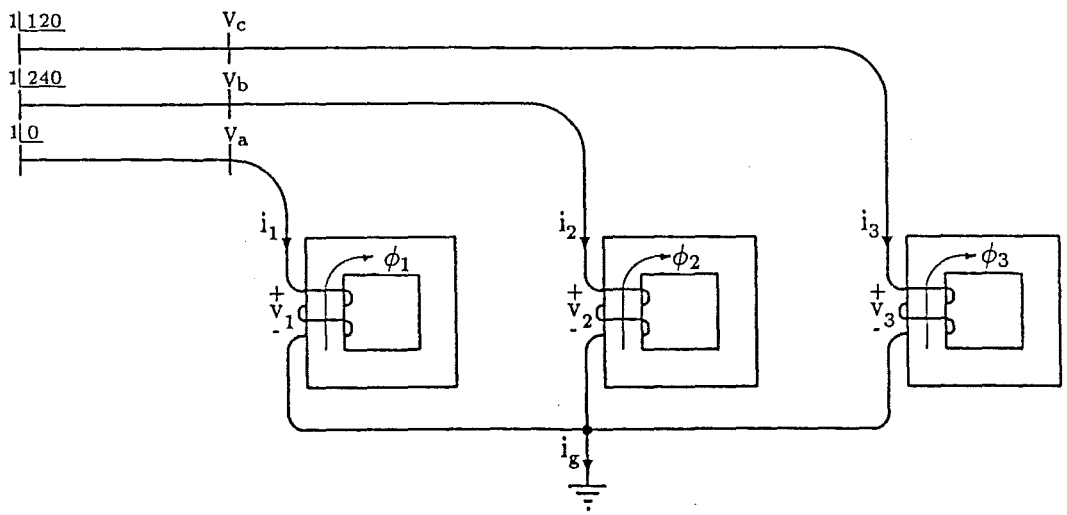

Figure 5.1: Lossles bank connected to a line of varying length

The three magnetic units are assumed to be identical, their magnetizing characteristic corresponding to that of figure 2-12. Furthermore, a Norton equivalent is used to represent the magnetizing branch of each core while a transfer function is used for the transmission line, which incorporates frequency dependent and long-line effects. The relevant information for the transmission line is provided in appendix number one.

The solution algorithm adopted for this problem has been to separate the linear and the linearized components and to start an iterative, sequential procedure until convergence is achieved.

The hybrid matrix equation

$$\begin{pmatrix} I_1^a \\ I_1^b \\ I_1^c \\ I_2^a \\ I_2^b \\ I_2^c \end{pmatrix}_h = \begin{pmatrix} [Y^{abc}] & [A^{abc}] \\ [A^{abc}] & [Z^{abc}] \end{pmatrix}_h \begin{pmatrix} V_1^a \\ V_1^b \\ V_1^c \\ V_2^a \\ V_2^b \\ V_2^c \end{pmatrix}_h \tag{5.1}$$

represents the linear part, while the linearized matrix equation

$$\begin{pmatrix} I_h^1 \\ I_h^2 \\ I_h^3 \end{pmatrix} = \begin{pmatrix} [H]_h^1 & & \\ & [H]_h^2 & \\ & & [H]_h^3 \end{pmatrix} \begin{pmatrix} V_h^1 \\ V_h^2 \\ V_h^3 \end{pmatrix} + \begin{pmatrix} I_{Nh}^1 \\ I_{Nh}^2 \\ I_{Nh}^3 \end{pmatrix} \tag{5.2}$$

models the three phase magnetic non-linearities. Moreover, for the electrical connection being discussed no additional restrictions are introduced, because of the homogeneity existing at the transformer and transmission line terminals, i.e.

$$\begin{pmatrix} I^a \\ I^b \\ I^c \end{pmatrix}_h = \begin{pmatrix} I^1 \\ I^2 \\ I^3 \end{pmatrix}_h \qquad \text{and} \qquad \begin{pmatrix} V^1 \\ V^2 \\ V^3 \end{pmatrix}_h = \begin{pmatrix} V^a \\ V^b \\ V^c \end{pmatrix}_h \tag{5.3}$$

The system under consideration is almost balanced and figure 5.2(a) shows the phase a of the fundamental, third, fifth and seventh harmonic frequency components of the magnetizing current of the three phase bank. As the line length increases and due to the Ferranti effect, the voltage fundamental at the far end of the line will grow and with it the harmonic currents resulting from transformer saturation.

In turn, the magnetizing harmonic currents drawn by the transformer will give rise to non-sinusoidal voltages. Figure 5.2(b) shows the fundamental and harmonic voltages of the phase a at the transformer terminals.

In this case, the most prominent harmonic voltage is the third, which reaches a maximum value of 6 per cent for a transmission line of 375 km long. It must be noticed that this length of line does not correspond to the quarter-wavelength for the third harmonic, i.e. 500 km. The fifth harmonic voltage, however, shows its highest value (one per cent) for a length of line of 300 km, which does correspond to its quarter wavelength.

For these levels of excitation the seventh harmonic voltage is seen to be negligible. However, if present, peaks should be expected for lengths of line corresponding to its quarter-wave length, i.e. 215 km, 645 km, ...

As has been shown in the last two Chapters, a single phase transformer connected to a positive sequence transmission circuit will produce its highest harmonic voltages for lengths of line corresponding to its quarter wavelength. As seen from the results presented in figure 5.2(b), this is not always the case for three phase circuits. An explanation is given below and further discussion is pursued in Appendix B.

Triplen harmonic currents tend to flow in phase causing the transmission circuit to behave no longer as a three phase one but, rather, as a three, single phase systems in parallel. The voltage wave travelling along single phase conductors over lossy ground will be both attenuated and retarded, and for the particular circuit being analysed, the third harmonic resonant peak is appearing at the quarter wavelength corresponding to the fourth harmonic, i.e. 375 km.

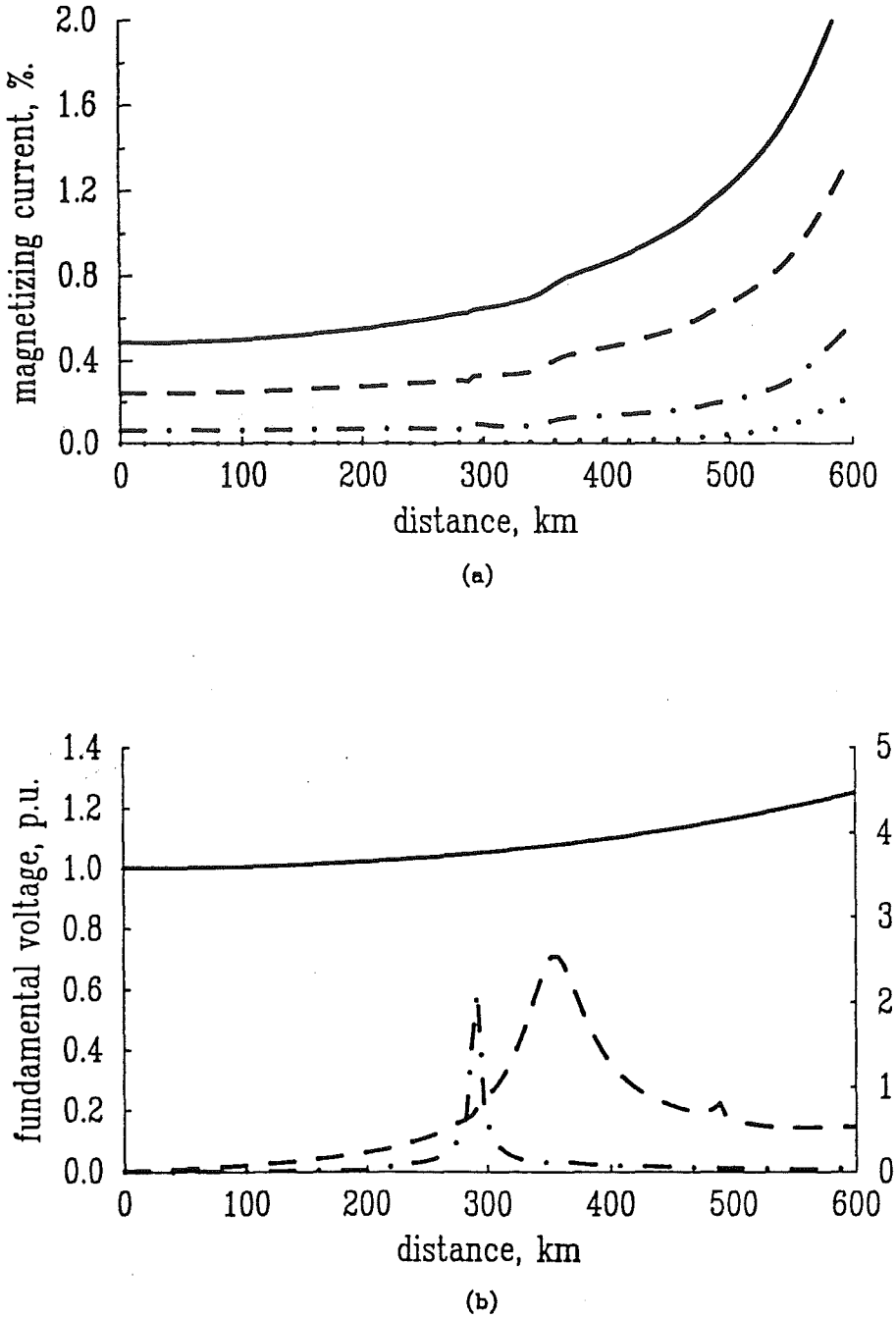

Figure 5-2: Harmonic information at the receiving end of the line
(a) Harmonic Currents (b) Harmonic Voltages

fund. ——————
third — — —
fifth — · —
seventh . . . . .

The current flowing through the solidly earthed star will consist mainly of third harmonic and because

$$I_g = I_1 + I_2 + I_3 \tag{5.4}$$

it will be almost three times the third harmonic current of one of the phases. This is shown in figure 5.3.

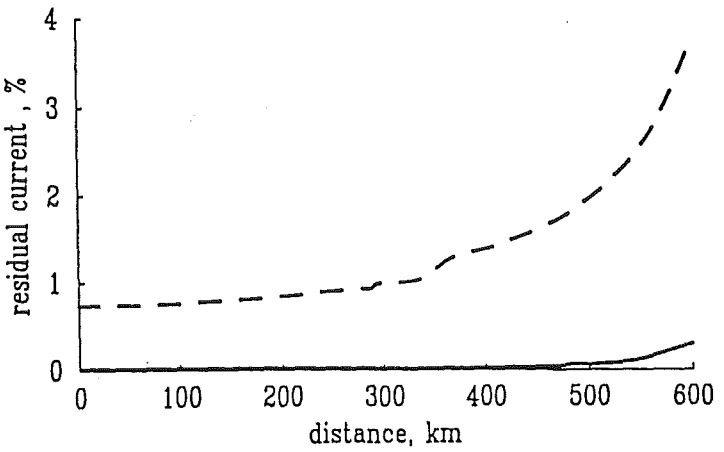

Figure 5.3: Harmonic currents flowing through the earthed star.

Along the same criteria, the delta connection is discussed below, and figure 5.4 shows the corresponding arrangement.

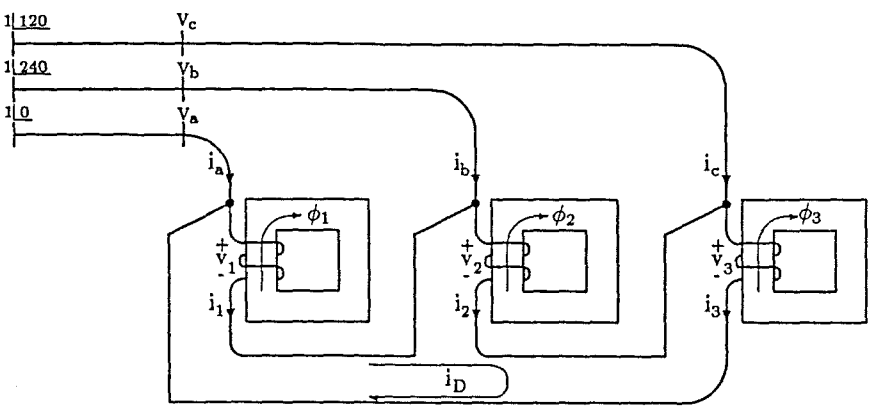

Figure 5.4: Lossless bank connected in delta

For this connection, the additional constraints

$$\begin{pmatrix} I^a \\ I^b \\ I^c \end{pmatrix}_h = \begin{pmatrix} I^1 - I^3 \\ I^2 - I^1 \\ I^3 - I^2 \end{pmatrix}_h \qquad \text{and} \qquad \begin{pmatrix} V^1 \\ V^2 \\ V^3 \end{pmatrix}_h = \begin{pmatrix} V^a - V^b \\ V^b - V^c \\ V^c - V^a \end{pmatrix}_h \tag{5.5}$$

are introduced in the solution process, acting as an interface between equations (5.2) and (5.1).

Because triplen harmonic currents flow in phase, the delta connection is effective in canceling them and its presence is due to unbalances. This is shown in figure 5.5(a), where small amounts of third harmonic are present only when long lengths of line are considered.

Harmonic currents, other than the triplets, are injected into the linear subnetwork given rise to the existence of harmonic voltages, which are shown in figure 5.5(b).

As expected, the presence of third harmonic voltage is negligible, and for the present excitation levels and chosen magnetizing characteristic, the fifth harmonic voltage is the only harmonic of significant value left, which maximum value takes place at its quarter wavelength.

The current circulating in the closed path of the delta consists mainly of third harmonic, i.e.

$$I_D = I_1 + I_2 + I_3 \tag{5.6}$$

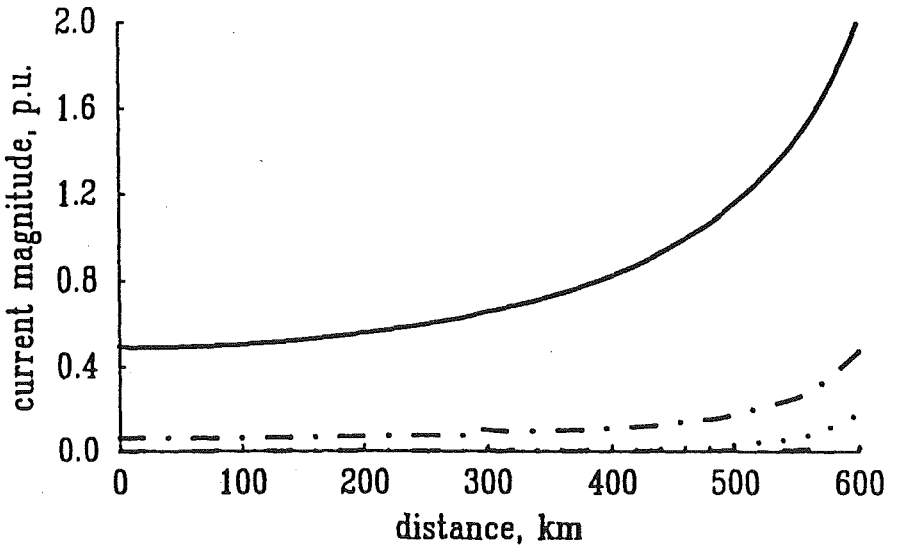

(a)

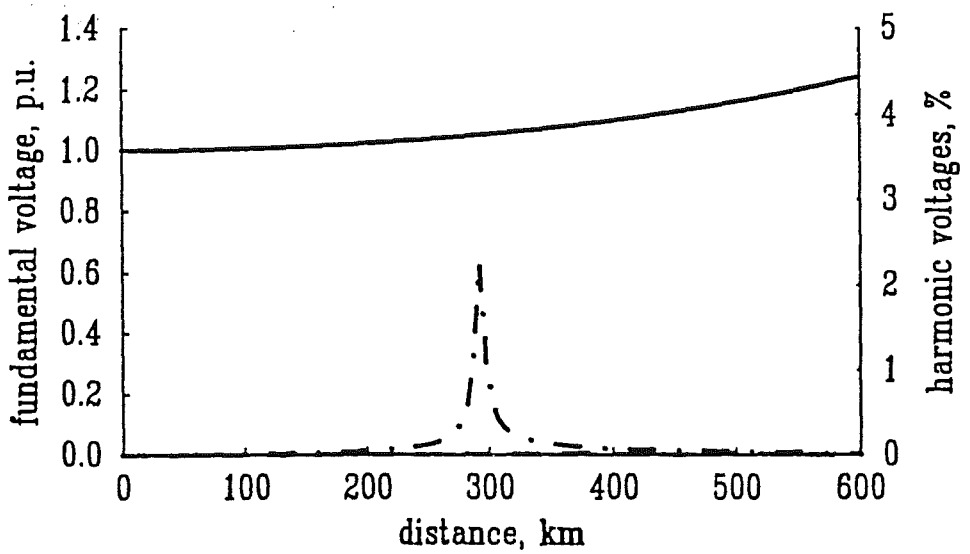

(b)

Figure 5-5: Harmonic information at the receiving end of the line
(a) Harmonic Currents (b) Harmonic Voltages

fund. ————
third — — -
fifth — . —
seventh . . . . .

5.3 Comparing Simulation Results With Field Measurements

This section compares simulation results provided by the technique of linearization in the harmonic space with field measurements and also EMTP solution are presented.

The Jaguara-Taquaril transmission circuit is used as a benchmark because field measurements are available [Dommel,Yan,Ortiz de Marcano 1983].The circuit is shown in figure 5.6 and consists of a power plant feeding an unloaded 345 kV-line through a step-up transformer.

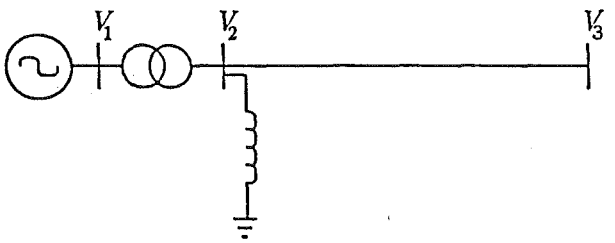

Figure 5.6: Test system

which goes into saturation when a balanced excitation voltage of 0.95 p.u. and 60 Hz exists at the power plant.

The field data available imposes some restrictions upon the simulation and an exact match between measurements and simulation results is not expected. For instance, the generator and the linear part of the transformer are represented as a single unit in the form of a Thevenin equivalent, which neglects the harmonic conversion process taking place in the generator [Semlyen,Eggleston and Arrillaga 1986] and allows no option but to connect the magnetizing branch of the transformer at the high voltage side. Furthermore, a two-slope representation is used for the magnetizing characteristic.

The recorded voltage at the sending end of the transmission line is shown if figure 5.7(a), together with the response provided by the technique of linearization in the harmonic space, where they appear to be in good agreement.The continuous line represents the recorded voltage while the broken line represents the simulation results. A similar comparison is shown in figure 5.7(b) for the case when the simulation results corresponds to an EMTP solution.

It must be said that the EMTP simulation does not correspond to a full steady state solution for it still contains a small portion of the transient [Dommel,Yan,Ortiz and Boscan 1984], and that favourable steady state solutions have only been obtained with excitations of 1 p.u. at the power plant [Yan 1986]. This is also the excitation value used by the simulation corresponding to this thesis.

The voltage wave forms shown in figure 5.7 show up a large amount of seventh harmonic, which is explained because of the length of the line involved (390 km, resonant point between the 6th and 7th harmonic frequency) and the transformer reaching saturation (it injects 7th harmonic current).

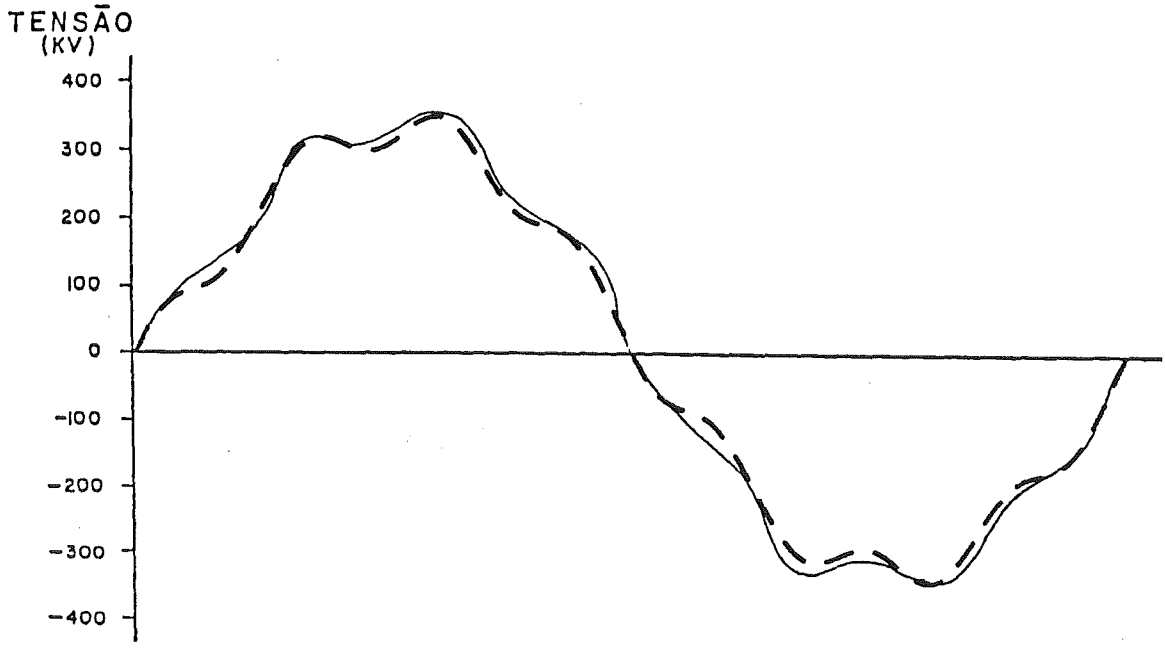

(a)

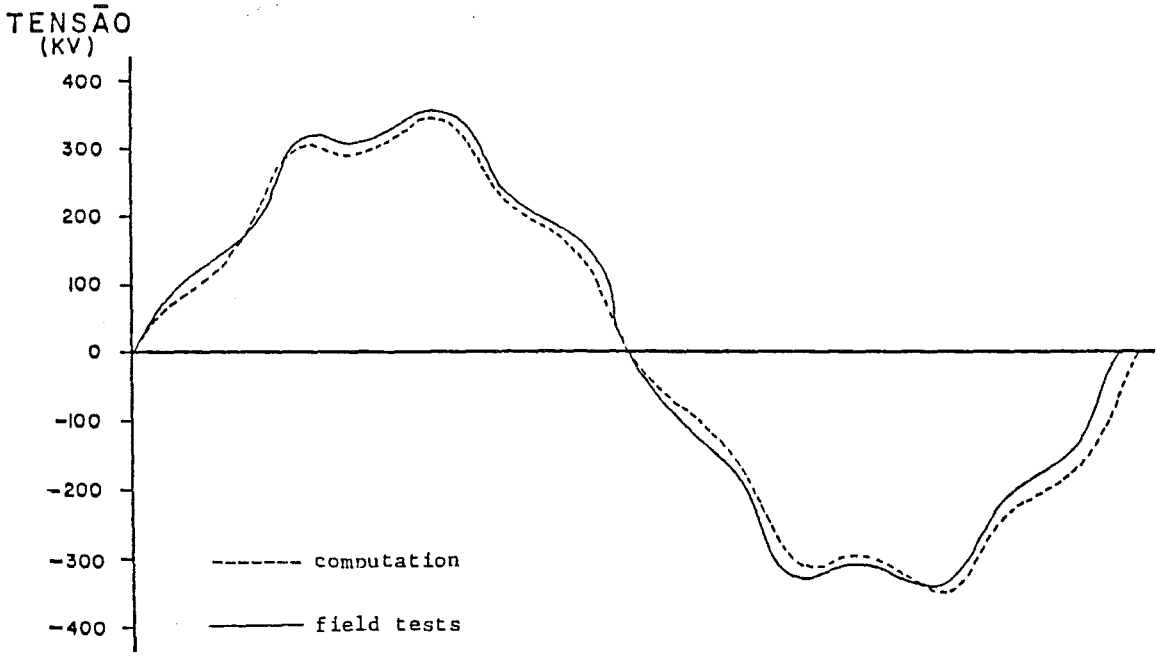

(b)

Figure 5-7: Measurement and simulation results
(a) Harmonic space solution (b) EMTP solution

The relevant data for the transmission system is as follows:
The linear part of the generator-transformer units are modelled by a Thevenin equivalent having self and mutual inductances $L_m = 4.4192\ H$ and $L_s = -1.2228\ H$, respectively.
The three phase reactor is modelled by a coupled inductor having self inductances $L_s = 4.4192\ H$ and mutual inductances $L_m = -1.2228\ H$.

The phase conductors of the transmission line are arranged in an horizontal configuration, with two 954 MCM-ACSR conductors per phase and two 3/8 in diameter galvanised steel earth wires. Some other parameters are:

phase conductor height = 13.10 m
phase spacing = 8.5 m
earth wires height = 22.97 m
earth wires spacing = 12.5 m
earth resistivity = 100 Ωm

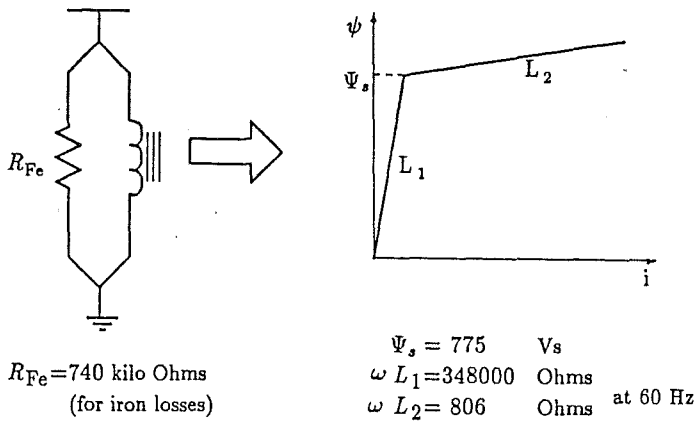

Figure 5.8: Magnetizing branch of the transformer.

5.4 A more general approach to the modelling of three phase bank of transformers

Harmonic models for the magnetizing branch of single phase magnetic cores, in the form of harmonic Norton equivalents , have been presented in the last two chapters, and extensions have been made to the case of three phase bank of transformers in the last two sections of this chapter. However, proper attention has yet to be paid to the electrical part of either single phase or three phase transformers.

A full harmonic representation of the transformer should combine both the magnetic and the electric circuits and complete models, based on the use of superposition, are derived in this chapter.

It has been experimentally corroborated that the magnetizing branch (harmonic Norton equivalent in this case) should be connected to a point where the voltage is proportional to the iron core flux [Dick and Watson 1981]. For instance, for the case of three phase units with cilindrical windings, the proportional effect between the voltage and the iron-core flux holds better across the winding closer to the iron-core, which is normally the tertiary winding or the low-voltage winding if the former does not exists.

This fact, however, may present some modelling problems because without any knowledge of the transformer design is not possible to define such a point. For the case of single phase transformer units with two windings it is not unrealistic to assume equal primary and secundary leakage impedances (refered to the same side), with the proportional effect taking place in between the two leakage impedances [Dommel 1975]. Thus, placing the harmonic Norton equivalent at this point would be reasonable and would also result in a harmonic T equivalent circuit for the single phase transformer with two windings.

Single phase transformer units with more than two windings possess a more difficult problem and the assumptions made above for two winding, single phase transformers do not hold any more. It is costumary to represent three winding transformers as star-equivalents, however, such a representation only provides the terminal conditions correctly and it may not have physical resemblance to the actual device at all. Therefore, there is no basis for assuming that the voltage and the iron-core flux are proportional at the center of the star. This picture becomes more complicated as the number of windings increases.

It has been recommended that unless knowledge of construction details are available, the per unit magnetizing admittance should be divided equally to all terminals. When applying this criteria to two winding, single phase transformers the resultant equivalent circuit is a π model, which is approximate because of the action of moving the magnetizing components to the terminals. This is the approach adopted below.

5.4.1 Basic equivalent circuit component

A full harmonic representation for the two winding, single phase transformer is shown schematically in figure 5.9(a). It consists of an ideal transformer with turns ratio 1:1, a diagonal matrix of harmonic leakage admittances $\{Y_l\}$ and the harmonic Norton equivalent (magnetizing branch) halfed and placed at both ends of the leakage admittance.

From the relationship across the ideal transformer and the terminal conditions in the side of the π circuit, nodal analysis can be applied to the four terminal schematic circuit of figure 5.9(a), resulting in the harmonic matrix equation (5.7).

Furthermore, by applying the algorithm that allows the nodal admittance matrix to be formed by inspection of the network topology, it is possible to derive the harmonic lattice equivalent circuit of figure 5.9(b) from equation (5.7).

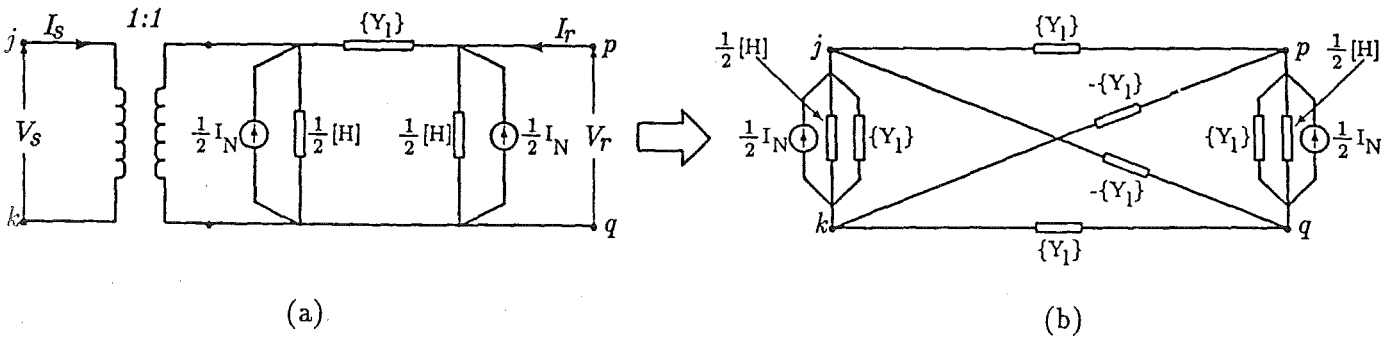

Figure 5.9: Full harmonic representation of the single phase transformer
(a) Schematic circuit (b) Harmonic lattice circuit.

$$\begin{pmatrix} I_j + \frac{1}{2}I_N \\ I_p + \frac{1}{2}I_N \\ I_k + \frac{1}{2}I_N \\ I_q + \frac{1}{2}I_N \end{pmatrix} = \begin{pmatrix} \{Y_l\} + \frac{1}{2}[H] & -\{Y_l\} & -\{Y_l\} - \frac{1}{2}[H] & \{Y_l\} \\ -\{Y_l\} & \{Y_l\} + \frac{1}{2}[H] & \{Y_l\} & -\{Y_l\} - \frac{1}{2}[H] \\ -\{Y_l\} - \frac{1}{2}[H] & \{Y_l\} & \{Y_l\} + \frac{1}{2}[H] & -\{Y_l\} \\ \{Y_l\} & -\{Y_l\} - \frac{1}{2}[H] & -\{Y_l\} & \{Y_l\} + \frac{1}{2}[H] \end{pmatrix} \begin{pmatrix} V_j \\ V_p \\ V_k \\ V_q \end{pmatrix} \tag{5.7}$$

The harmonic lattice equivalent circuit represents correctly the voltage and current relationships of the circuit of figure 5-9 (a), and harmonic representations for bank of transformers becomes readily available through suitable combinations of three of the harmonic lattice equivalent circuits. Parallel transformer windings are taken to represent a single phase unit.

5.4.2 Star-Star connection

The harmonic equivalent circuit for a three phase bank of transformers connected in a Star:Star arrangement is shown in figure 5.10, where only one single phase unit is fully represented.

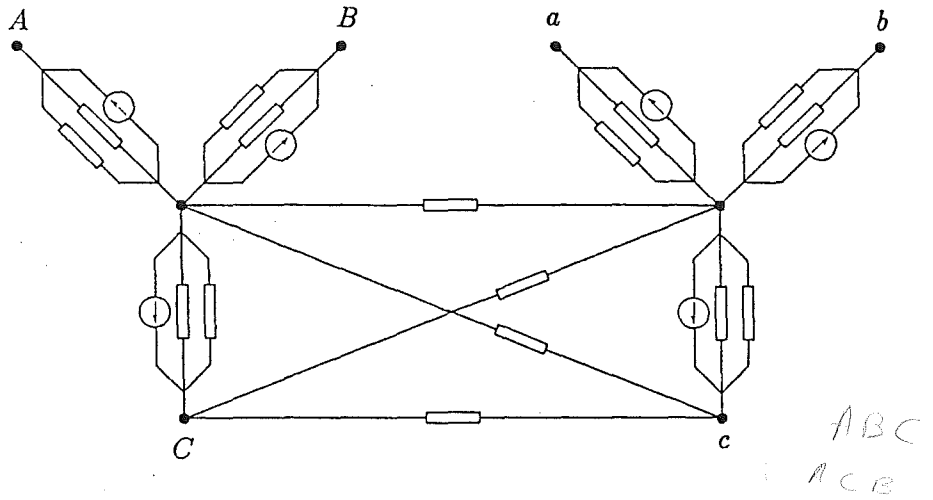

Figure 5.10: Star-Star connection

By inspection of the network topology of figure 5.10 or, alternatively, by applying the nodal transformations given in Appendix E, the harmonic nodal matrix equation (5.8) is derived. This matrix couples all the harmonics and the phases together.

$$
\begin{pmatrix}
I_A + \frac{1}{2}I_{N1} \\
I_B + \frac{1}{2}I_{N2} \\
I_C + \frac{1}{2}I_{N3} \\
I_a + \frac{1}{2}I_{N1} \\
I_b + \frac{1}{2}I_{N2} \\
I_c + \frac{1}{2}I_{N3} \\
I_N - \frac{1}{2}I_{N1} - \frac{1}{2}I_{N2} - \frac{1}{2}I_{N3} \\
I_n - \frac{1}{2}I_{N1} - \frac{1}{2}I_{N2} - \frac{1}{2}I_{N3}
\end{pmatrix}
=
\begin{pmatrix}
\{Y_l\} + \frac{1}{2}[H_1] & & & -\{Y_l\} \\
& \{Y_l\} + \frac{1}{2}[H_2] & & \\
& & \{Y_l\} + \frac{1}{2}[H_3] & \\
-\{Y_l\} & & & \{Y_l\} + \frac{1}{2}[H_1] \\
& -\{Y_l\} & & \\
& & -\{Y_l\} & \\
-\{Y_l\} - \frac{1}{2}[H_1] & -\{Y_l\} - \frac{1}{2}[H_2] & -\{Y_l\} - \frac{1}{2}[H_3] & \{Y_l\} \\
\{Y_l\} & \{Y_l\} & \{Y_l\} & -\{Y_l\} - \frac{1}{2}[H_1]
\end{pmatrix}
$$

$$
\begin{pmatrix}
& & -\{Y_l\} - \frac{1}{2}[H_1] & \{Y_l\} \\
-\{Y_l\} & & -\{Y_l\} - \frac{1}{2}[H_2] & \{Y_l\} \\
& -\{Y_l\} & -\{Y_l\} - \frac{1}{2}[H_3] & \{Y_l\} \\
& & \{Y_l\} & -\{Y_l\} - \frac{1}{2}[H_1] \\
\{Y_l\} + \frac{1}{2}[H_2] & & \{Y_l\} & -\{Y_l\} - \frac{1}{2}[H_2] \\
& \{Y_l\} + \frac{1}{2}[H_3] & \{Y_l\} & -\{Y_l\} - \frac{1}{2}[H_3] \\
\{Y_l\} & \{Y_l\} & 3\{Y_l\} + \frac{1}{2}[H_1] + \frac{1}{2}[H_2] + \frac{1}{2}[H_3] & -3\{Y_l\} \\
-\{Y_l\} - \frac{1}{2}[H_2] & -\{Y_l\} - \frac{1}{2}[H_3] & -3\{Y_l\} & 3\{Y_l\} + \frac{1}{2}[H_1] + \frac{1}{2}[H_2] + \frac{1}{2}[H_3]
\end{pmatrix}
\begin{pmatrix}
V_A \\ V_B \\ V_C \\ V_a \\ V_b \\ V_c \\ V_N \\ V_n
\end{pmatrix}
\tag{5.8}
$$

Deleting or adding appropriate rows and columns to the harmonic matrix equation (5.8) it is possible to incorporate different earthing schemes. For instance, the last two rows and columns will disappear from equation (5.8) when both neutrals are solidly earthed.

5.4.3 Delta-Delta connection

By a suitable combination of three of the harmonic lattice equivalent circuits of figure 5-9 (b), it is possible to build up a harmonic equivalent circuit for a three phase bank of transformers connected in a delta:delta arrangement. Figure 5.11 shows part of the resultant three phase equivalent circuit and its associated harmonic matrix equation (5.9) can be derived from inspection of the circuit or through matrix transformations.

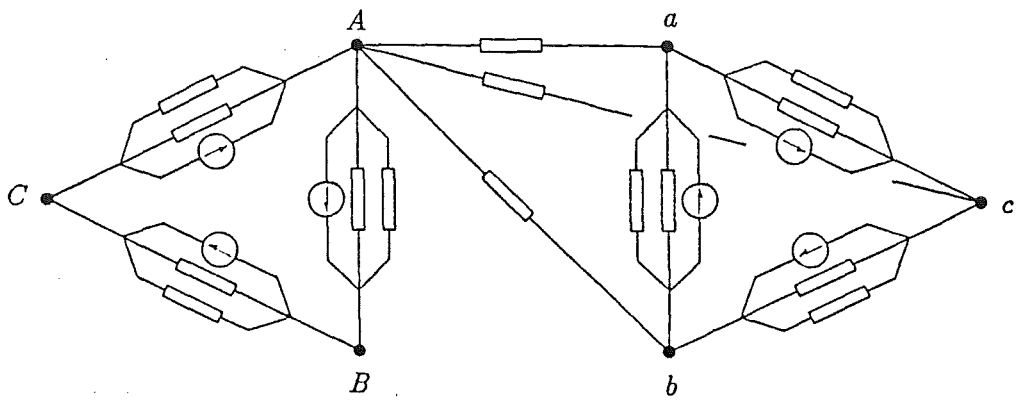

Figure 5-11: Delta - Delta connection

$$
\begin{pmatrix} I_A + \frac{1}{2}I_{N1} - \frac{1}{2}I_{N2} \\ I_B + \frac{1}{2}I_{N2} - \frac{1}{2}I_{N3} \\ I_C + \frac{1}{2}I_{N3} - \frac{1}{2}I_{N1} \\ I_a + \frac{1}{2}I_{N1} - \frac{1}{2}I_{N2} \\ I_b + \frac{1}{2}I_{N2} - \frac{1}{2}I_{N3} \\ I_c + \frac{1}{2}I_{N3} - \frac{1}{2}I_{N1} \end{pmatrix} =
\begin{pmatrix}
2\{Y_l\} + \frac{1}{2}[H_1] + \frac{1}{2}[H_2] & -\{Y_l\} - \frac{1}{2}[H_2] & -\{Y_l\} - \frac{1}{2}[H_1] \\
-\{Y_l\} - \frac{1}{2}[H_2] & 2\{Y_l\} + \frac{1}{2}[H_2] + \frac{1}{2}[H_3] & -\{Y_l\} - \frac{1}{2}[H_3] \\
-\{Y_l\} - \frac{1}{2}[H_1] & -\{Y_l\} - \frac{1}{2}[H_3] & 2\{Y_l\} + \frac{1}{2}[H_3] + \frac{1}{2}[H_1] \\
-2\{Y_l\} & \{Y_l\} & \{Y_l\} \\
\{Y_l\} & -2\{Y_l\} & \{Y_l\} \\
\{Y_l\} & \{Y_l\} & -2\{Y_l\}
\end{pmatrix}
$$

$$
\begin{pmatrix}
-2\{Y_l\} & \{Y_l\} & \{Y_l\} \\
\{Y_l\} & -2\{Y_l\} & \{Y_l\} \\
\{Y_l\} & \{Y_l\} & -2\{Y_l\} \\
2\{Y_l\} + \frac{1}{2}[H_1] + \frac{1}{2}[H_2] & -\{Y_l\} - \frac{1}{2}[H_2] & -\{Y_l\} - \frac{1}{2}[H_1] \\
-\{Y_l\} - \frac{1}{2}[H_2] & 2\{Y_l\} + \frac{1}{2}[H_2] + \frac{1}{2}[H_3] & -\{Y_l\} - \frac{1}{2}[H_3] \\
-\{Y_l\} - \frac{1}{2}[H_1] & -\{Y_l\} - \frac{1}{2}[H_3] & 2\{Y_l\} + \frac{1}{2}[H_3] + \frac{1}{2}[H_1]
\end{pmatrix}
\begin{pmatrix} V_A \\ V_B \\ V_C \\ V_a \\ V_b \\ V_c \end{pmatrix}
\tag{5.9}
$$

5.4.4 Grounded Star-Delta connection

By applying the same procedure the harmonic lattice equivalent circuit for the grounded star:delta arrangement is built up, and a part of it is shown in figure 5.12, while the resultant harmonic matrix is given by equation (5.10).

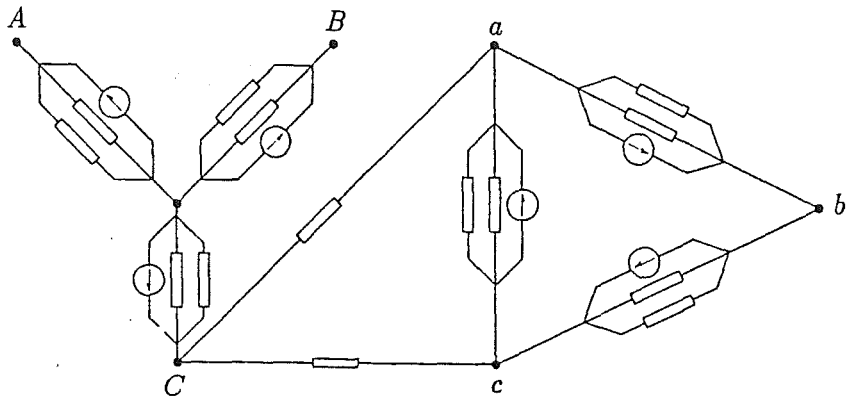

Figure 5-12: Grounded Star - Delta connection

$$
\begin{pmatrix} I_A + \frac{1}{2}I_{N1} \\ I_B + \frac{1}{2}I_{N2} \\ I_C + \frac{1}{2}I_{N3} \\ I_a + \frac{1}{2}I_{N1} - \frac{1}{2}I_{N2} \\ I_b + \frac{1}{2}I_{N2} - \frac{1}{2}I_{N3} \\ I_c + \frac{1}{2}I_{N3} - \frac{1}{2}I_{N1} \end{pmatrix} =
\begin{pmatrix}
\{Y_l\} + \frac{1}{2}[H_1] & & & -\{Y_l\} & & \{Y_l\} \\
& \{Y_l\} + \frac{1}{2}[H_2] & & & -\{Y_l\} & \\
& & \{Y_l\} + \frac{1}{2}[H_3] & \{Y_l\} & & -\{Y_l\} \\
-\{Y_l\} & \{Y_l\} & & 2\{Y_l\} + \frac{1}{2}[H_1] + \frac{1}{2}[H_2] & -\{Y_l\} - \frac{1}{2}[H_2] & -\{Y_l\} - \frac{1}{2}[H_1] \\
& -\{Y_l\} & \{Y_l\} & -\{Y_l\} - \frac{1}{2}[H_2] & 2\{Y_l\} + \frac{1}{2}[H_2] + \frac{1}{2}[H_3] & -\{Y_l\} - \frac{1}{2}[H_3] \\
\{Y_l\} & & -\{Y_l\} & -\{Y_l\} - \frac{1}{2}[H_1] & -\{Y_l\} - \frac{1}{2}[H_3] & 2\{Y_l\} + \frac{1}{2}[H_3] + \frac{1}{2}[H_1]
\end{pmatrix}
\begin{pmatrix} V_A \\ V_B \\ V_C \\ V_a \\ V_b \\ V_c \end{pmatrix}
\tag{5.10}
$$

5.4.5 Grounded Star:Grounded Star-Delta connection

The realization of harmonic equivalent circuits based on harmonic lattice diagrams are more difficult to achieve for the case of three phase bank of transformers with individual units containing more than two windings.

This difficulty, however, is overcome by applying the nodal relations and connectivity matrices given in Appendix E, which provides a convenient way of determining the harmonic nodal matrix equation (5.11).

$$
\begin{pmatrix}
I_A + \frac{1}{3}I_{N1} \\
I_B + \frac{1}{3}I_{N2} \\
I_C + \frac{1}{3}I_{N3} \\
I_a + \frac{1}{3}I_{N1} \\
I_b + \frac{1}{3}I_{N2} \\
I_c + \frac{1}{3}I_{N3} \\
I_{A'} + \frac{1}{3}I_{N1} - \frac{1}{3}I_{N2} \\
I_{B'} + \frac{1}{3}I_{N2} - \frac{1}{3}I_{N3} \\
I_{C'} + \frac{1}{3}I_{N3} - \frac{1}{3}I_{N1}
\end{pmatrix}
=
\begin{pmatrix}
\{Y_l\} + \frac{1}{3}[H_1] & & & -\{Y_l\} & & & & & \\
& \{Y_l\} + \frac{1}{2}[H_2] & & & & & & & \\
& & \{Y_l\} + \frac{1}{2}[H_3] & & & -\{Y_l\} & & & \\
-\{Y_l\} & & & \{Y_l\} + \frac{1}{3}[H_1] & & & & & \\
& -\{Y_l\} & & & & & & & \\
& & -\{Y_l\} & & & & \{Y_l\} + \frac{1}{2}[H_2] & & \\
-\{Y_l\} & \{Y_l\} & & -\{Y_l\} & & & & & \\
\{Y_l\} & -\{Y_l\} & \{Y_l\} & \{Y_l\} & \{Y_l\} & & & & \\
& & -\{Y_l\} & & -\{Y_l\} & & & &
\end{pmatrix}
$$

$$
\begin{pmatrix}
& -\{Y_l\} & \{Y_l\} & & \\
& & -\{Y_l\} & \{Y_l\} & \\
-\{Y_l\} & \{Y_l\} & & -\{Y_l\} & \\
& -\{Y_l\} & \{Y_l\} & & \\
& & -\{Y_l\} & \{Y_l\} & \\
\{Y_l\} + \frac{1}{2}[H_3] & \{Y_l\} & & -\{Y_l\} & \\
& 2\{Y_l\} + \frac{1}{2}[H_1] + \frac{1}{2}[H_2] & -\{Y_l\} - \frac{1}{2}[H_2] & -\{Y_l\} - \frac{1}{2}[H_1] & \\
\{Y_l\} & -\{Y_l\} - \frac{1}{2}[H_2] & 2\{Y_l\} + \frac{1}{2}[H_2] + \frac{1}{2}[H_3] & -\{Y_l\} - \frac{1}{2}[H_3] & \\
-\{Y_l\} & -\{Y_l\} - \frac{1}{2}[H_1] & -\{Y_l\} - \frac{1}{2}[H_3] & 2\{Y_l\} + \frac{1}{2}[H_3] + \frac{1}{2}[H_1] &
\end{pmatrix}
\begin{pmatrix}
V_A \\ V_B \\ V_C \\ V_a \\ V_b \\ V_c \\ V_{A'} \\ V_{B'} \\ V_{C'}
\end{pmatrix}
\tag{5.11}
$$

5.4.6 Numerical Example 1

In order to illustrate the theory just developed, the circuit of figure 5.13 has been chosen as a test system. It is based on the Infiernillo-Tula transmission circuit, which belongs to the 400 kV Mexican Central bulk system.

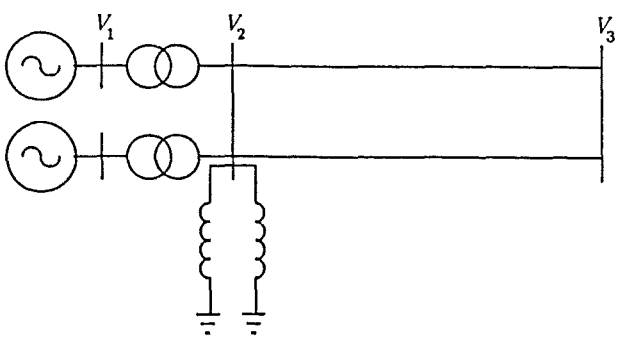

Figure 5.13: Layout of the transmission circuit.

	PHASE A	PHASE B	PHASE C
fundamental	1.1654 ∠−30	1.1987 ∠−158	1.1795 ∠88
third	0.0255 ∠−58	0.0244 ∠−56	0.0368 ∠−46
fifth	0.0158 ∠−261	0.0134 ∠−136	0.0121 ∠−21
seventh	0.0308 ∠−100	0.0264 ∠−233	0.0215 ∠18
ninth	0.0299 ∠−100	0.0234 ∠63	0.0172 ∠−261
eleventh	0.0071 ∠48	0.0058 ∠14	0.0063 ∠50
thirtieth	0.0006 ∠−71	0.0007 ∠20	0.0006 ∠−120

Table 5.1: Harmonic content of the voltage wave at the sending end.

It consists of a power plant supplying, at 60 Hz, a 416 km double circuit transmission line through delta-grounded star transformers, which go into saturation when a balanced excitation of 1 p.u. exists at the power plant. The system is operating under no load and reactors are connected at the sending end of the line.

It is realized that under no loading conditions only one line should be connected. However, it was chosen as a test case because the resultant equivalent circuit presents a case suceptible to harmonic distortion at frequencies in which saturated transformers draw most of their magnetizing current, i.e. third, fifth, seventh and nineth harmonic currents.

Figure 5.14(a) shows the voltage wave form at the sending end of the line while figure 5.14(b) shows the voltage wave form at the far end. Also Table 5.1 gives the harmonic content of the voltage existing at the sending end of the line.

The relevant data for the transmission system is as follows:

d-Axis subtransient reactance per generator : 0.1480 p.u.
q-Axis subtransient reactance per generator : 0.1008 p.u.
Zero sequence reactance per generator : 0.0422 p.u.
Leakage reactance per transformer : 0.0400 p.u.
Leakage reactance per reactor : 0.0250 p.u.

An earth resistivity of 100Ωm is assumed and the characteristic given in figure 2.12 is taken for each magnetic unit.

The Phase conductors are arranged in a double circuit configuration symmetricaly placed around the vertical axis of the tower, where each phase consists of two 954 MCM-ACSR conductors per phase, and also two 3/8 inch diameter galvanised steel earth wires are present. Taken from the center of the tower and the ground level, the coordinates of the conductors for one of the circuits are:

PHASE A	6.12 mt	,	34.10 mt
PHASE B	8.41 mt	,	26.63 mt
PHASE C	6.43 mt	,	20.08 mt
EARTH-WIRE	3.66 mt	,	41.32 mt

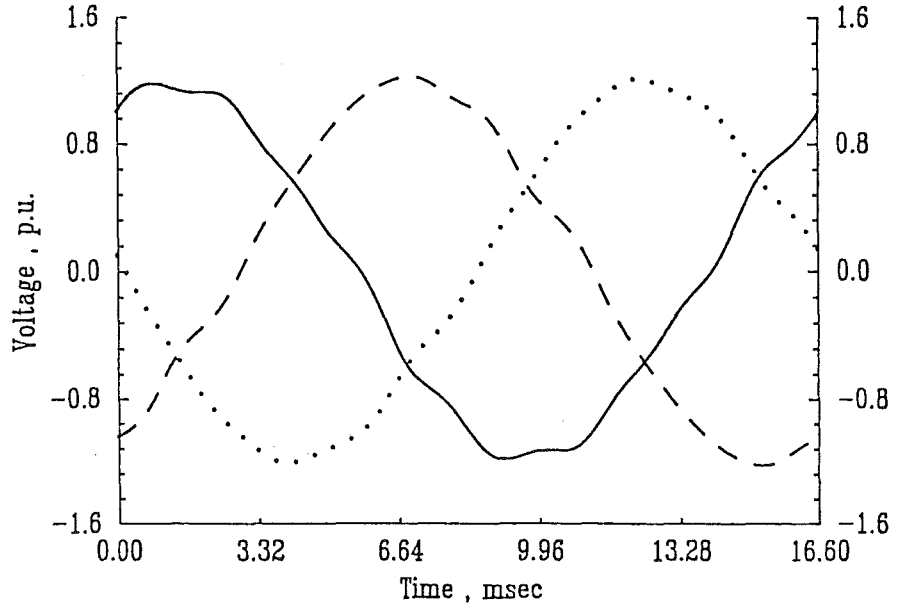

(a)

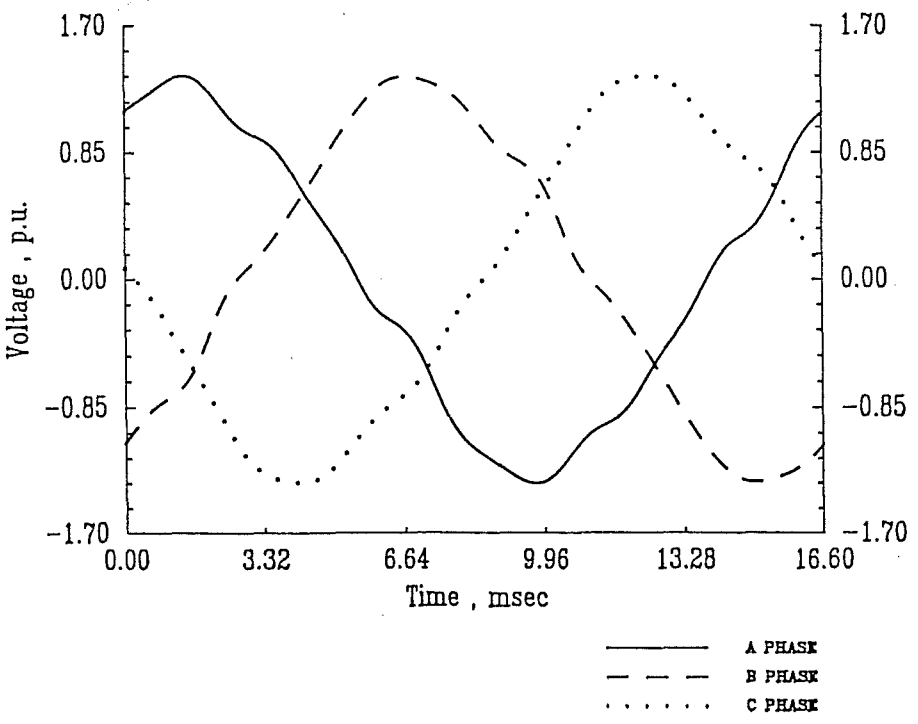

(b)

Figure 5-14: A full cycle of the voltage waveform
(a) Sending end (b) Receiving end

5.5 Conclusions

Based on the technique of linearization in the complex-conjugate harmonic space, a new generation of three phase transformer models have been developed. The proposed models are suitable for determining the harmonic response of three phase bank of transformers under any kind of periodic excitation and include correctly the voltage and frequency dependent effects, as well as the transformer's connection.

From the point of view of modelling, a single phase transformer may be thought as consisting of a magnetic part (magnetizing branch) and an electric part (leakage reactance). The former may be interpreted as an harmonic Norton equivalent while the later may be seen as a lattice-diagram at each harmonic frequency. Here, both representations were combined resulting in a new model for the single phase transformer in the form of an harmonic lattice equivalent circuit. Moreover, Three phase harmonic representations for the most commonly used three phase transformer connections were assembled by suitable combination of harmonic lattice equivalent circuits.

The resultant three phase harmonic models are combined easily with the external network in a sequential or in a unified solution. In this case, a sequential approach was used to solve the problem of a lossless core connected at the receiving end of a three phase line of varying distance. In every case an expected behaviour was observed, such as the in-phase flow of the third harmonic current and its associated effects.

Also, the response provided by a transformer model, based on the technique of linearization in the complex-conjugate harmonic space, compared well with an actual voltage waveform corresponding to a 345 kV transmission system.

The application cases presented in this chapter corresponds to radial transmission circuits, however, they have been useful as test cases and the results obtained should provide sufficient evidence about the veracity and usefulness of the harmonic transformer models presented here. More involved cases, corresponding to interconnected networks containing several transformers, are presented in Chapter 7.

Chapter 6

Linear Power Plant Components

6.1 Introduction

Realistic models of multiconductor transmission lines for the analysis of harmonic propagation studies are already well established [Arrillaga, Densem and Harker 1983] and [Dommel 1986]. These models take into account long-line effects, frequency dependence and line imbalance. However, a number of problems with regards to both flexibility and efficiency remains yet to be solved.

For instance, so far no proper attention has been paid to the representation of non-homogeneous transmission lines at harmonic frequencies. Accordingly, there is scarce information in the literature to the effect of either line transpositions and VAR compensating plant at harmonic frequencies and not at all in their combined effect.

Early computer models and network analysers were very restricted for the assessment of transpositions and VAR compensating plant at harmonic frequencies as they used simple nominal π circuits for the line modelling and most of the recent models appear to have no adequate provisions for this purpose. An early experimental attempt [Joint Committee on Inductive Interference 1915] made under very low voltage and relatively short distance, indicated that the balancing effect of the transpositions reduced considerably as the frequency increased.

Using digital simulation a thorough investigation was carried in the phase domain [Arrillaga, Acha, Densem and Bodger 1986], where it is shown that contrary to the unquestioned believe that transpositions restore the geometrical balance of the line, transpositions may not only render ineffective but, for most practical cases, they will degrade further the impedance asymmetry of the line at harmonic frequencies. New results are presented in Appendix C.

Harmonic studies normally consume large amounts of computer time. Information at several points along the line are sometimes required for assessment of harmonic interference or insulation coordination purposes and the harmonic analysis of electrical transmission systems require the values of self and mutual impedances of lines for a wide range of frequencies. It is also important to develop algorithms fast enough that permit the studies to be made in an interactive environment.

Existing harmonic transmission line models are based on the use of classical techniques that demand a considerable amount of computer time. For instance, the basic methods of calculating the frequency dependant part of transmission line impedances use infinite series, i.e. Carson's series for ground impedances and Bessel functions for the skin effect. It is therefore necessary to pursue ways of reducing time scales without degrading accuracy and several novel features are presented in this Chapter that allows accurate, interactive harmonic analysis of both homogeneous and non-homogeneous transmission lines.

6.2 Evaluation of Lumped Parameters

The lumped series impedance matrix $[Z]$ of a multiconductor transmission line consists of three components [Galloway, Shorrocks and Wedepohl 1964],

$$[Z] = [Z_c] + [Z_g] + [Z_e] \tag{6.1}$$

where $[Z_c]$ is the contribution of impedance due to the conductors,
$[Z_e]$ is the contribution of the earth return path and
$[Z_g]$ is the contribution of the physical geometry of the conductor's arrangement.

6.2.1 Earth Impedance Matrix $[Z_e]$

The impedance due to the earth path varies with the frequency in a non linear fashion and because of the non uniform nature of the land, as well as its lack of homogeneous conductivity, this is a problem for which an accurate solution may not exist. Nevertheless, the solution to the problem of impedances involving a perfectly flat earth, with homogeneous conductivity, is still of practical and also of theoretical significance. A satisfactory solution to the related problem of a current carrying wire above a lossy earth was first published more than half a century ago [Carson 1926]. The solution was given in the form of an infinite integral, which has not a closed form or analytical answer, but it is conveniently expressed as a set of infinite series.

Ever since, and perhaps because of the existence of these infinite series, this solution has been adopted worldwide, as the foundation for almost every study in the areas of electromagnetic fields, propagation characteristics and magnetic induction effects caused by power lines [Olsen and Pankaskie 1983]. Carson's integral was developed with the help of Maxwell's equation and some concepts of the circuit theory, although the latter restricted the validity of the solutions over the full span of frequencies.

More accurate solutions, based solely on the use of electromagnetic concepts (Maxwell's equations), have been pursued afterwards and two equivalent answers [Wedepohl and Efthymiadis 1978], [Wait 1972] in the form of infinite integrals have emerged. Furthermore, it has been demonstrated that Carson's integral corresponds to a particular case of the more accurate integrals of Wedepohl or Wait; but perhaps more important, it has been found that for most of the conditions prevailing in power system applications, Carson's solutions are as good as the more accurate approaches. Heavy computational burdens are associated with the numerical solution of any of the three infinite integrals that prevent their use in every day applications, and it is only in a reduced number of situations, such as conductors in close proximity to the ground and radio frequency applications, that the more accurate solutions should be used [Olsen and Pankaskie 1983].

As the need arises to calculate earth impedances for a wide spectrum of frequencies, and also because of the uncertainty in the available data, the tendency is to go for simpler formulations aiming at a reduction in computing time, while keeping the accuracy at a reasonable level.

With reference to figure 6.1, and based on Carson's work, the earth impedance can be concisely expressed as

$$z_e = \phi(J(r,\theta)) \tag{6.2}$$

where $z_e \in [Z_e]$

$\phi =$ function of $(\cdot)$

$J(r,\theta) = P(r,\theta) + jQ(r,\theta)$

$r_{lm} = \sqrt{\omega\mu\sigma}\, D_{lm}$

$D_{lm} = \sqrt{(h_l + h_m)^2 + d^2}$

$D_{ll} = 2h_l$

$\theta_{lm} = \arctan(\frac{d}{h_l + h_m})$

$\theta_{ll} = 0°$

$\mu = 4\pi\ 10^{-7}\ [H/m]$

$\omega = 2\pi\ f$

σ is the ground's conductivity in S/m

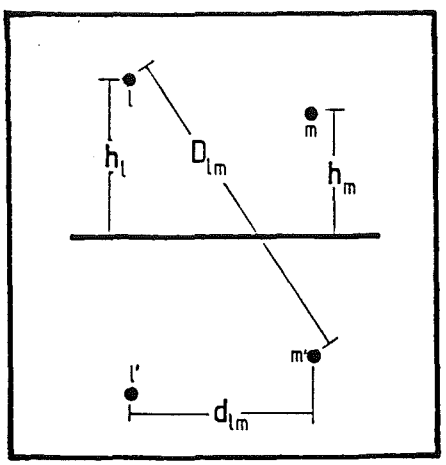

Figure 6.1: A line geometry and its image

Carson's solution to equation (6.2), in terms of infinite series, is

$$P = (1 - S_4) \times \frac{\pi}{8} + \ln\frac{2}{\gamma' r} \times \frac{S_2}{2} + \theta \times \frac{S_2'}{2} - \frac{\sigma_1}{\sqrt{2}} + \frac{\sigma_2}{2} + \frac{\sigma_3}{\sqrt{2}} \tag{6.3}$$

$$Q = \frac{1}{4} + \ln\frac{2}{\gamma' r} \times \frac{1 - S_4}{2} - \theta \times \frac{S_4'}{2} + \frac{\sigma_1}{\sqrt{2}} - S_2 \times \frac{\pi}{8} + \frac{\sigma_3}{\sqrt{2}} + \frac{\sigma_4}{2} \tag{6.4}$$

where γ' is the Euler's constant 1.7811 and S_2, S_2', S_4, S_4', σ_1, σ_2, σ_3 and σ_4 are infinite series [Carson 1926], which converge quickly for most power system applications, but the amount of required computation increases with frequency and the separation between conductors.

For very high frequency applications and when large distances are involved ($r > 6$) the series given in equations (6.3) and (6.4) present convergence problems and the following asymptotic series have also been presented by Carson,

$$P = \frac{\cos\theta}{\sqrt{2}r} - \frac{\cos 2\theta}{\sqrt{2}r^2} + \frac{\cos 3\theta}{\sqrt{2}r^3} + \frac{3\cos 5\theta}{\sqrt{2}r^5} + \cdots \tag{6.5}$$

$$Q = \frac{\cos\theta}{\sqrt{2}r} - \frac{\cos 3\theta}{\sqrt{2}r^3} + \frac{3\cos 5\theta}{\sqrt{2}r^5} + \cdots \tag{6.6}$$

These asymptotic series have been a useful and popular resource for most high frequency power system applications [Dommel 1969]. This has not been the case for interference calculation purposes where a great deal of restraint has been exercised due to the lack of accuracy of the asymptotic series at some special values of the parameters r and θ. Instead, numerical integrations have been carried in the past.

Very recently, it has been demonstrated that the mathematical validity of the asymptotic series of equations (6.5) and (6.6) is limited to values of the angle θ smaller than $\pi/4$. Furthermore, it has also been found that the complete solution [Tevan and Deri 1984] requires an additional series, which is complex, to be added to those given in equations (6.5) and (6.6).

$$(P + jQ)_{add} = \frac{\sqrt{\pi}}{16} \times \frac{e^s}{s\sqrt{s}} \times (1 - \frac{3}{16s} - \frac{15}{512s^2} - \frac{105}{8192s^3} - \cdots) \tag{6.7}$$

where $s = \frac{r}{2}e^{j(\frac{3\pi}{4}+\theta)}$

The complex series of equation (6.7) becomes increasingly important as both r and θ increases and it is shown later in this section that at large values of the parameter r ($5 < r < 9$) and values of the angle θ close to the ninety degrees the additional asymptotic series becomes the dominant factor in the numerical solution.

Equations (6.5), (6.6) and (6.7) provide the complete asymptotic solution to Carson's integral and a means for the evaluation of earth impedances when large values of the parameter r are present, regardless of the value of the angle θ ($0 < \theta < \pi/2$). Thus, in the range of validity of Carson's equations, solutions based on time consuming numerical integrations may not be necessary any more, though infinite series are still needed.

Nevertheless, once the P and Q terms have been computed, through either suitable set of infinite series, an scaled factor of $2.513274\, f\, 10^{-3}$ is applied to obtain the earth impedance in ohms per kilometer.

Alternatively, closed form formulations for the numerical evaluation of line-ground loops, based on the concept of a mirroring surface beneath the earth, at a certain complex depth, have appeared more recently in both the electrophysics [Wait and Spies 1969] and the power literature [Gary 1976], [Deri, Tevan, Semlyen and Castanheira 1981]. The concept of complex penetration has been developed intuitively and the heuristic equations based on this concept applied to actual calculations. Mathematical justification have followed next, showing these developments to be very good physical and mathematical approximations to the more formal approaches of Wait's and Carson's integrals. More recently, refinements have been introduced that provide more accurate, though, more complicated closed form formulations.

The three different approaches, based on the concept of complex penetration, vary slightly from each other but, in power system applications at least, the one which have had more appeal is that due to C. Dubanton [Gary 1976]. The reasons being its simplicity and its high degree of accuracy for the whole frequency span for which Carson's equations are valid, though, for a wide range of frequencies it becomes increasingly inaccurate as the angle θ approaches the $\pi/2$ radians.

Dubanton's formulae for the evaluation of the self and mutual impedances of the conductors l and m of figure 6.1 are,

$$z_{ll} = \frac{j\omega\mu_0}{2\pi} \times \ln \frac{2(h_l + p)}{r_l} \tag{6.8}$$

$$z_{lm} = \frac{j\omega\mu_0}{2\pi} \times \ln \frac{\sqrt{(h_l + h_m + p)^2 + d^2}}{\sqrt{(h_l - h_m)^2 + d^2}} \tag{6.9}$$

where $p = 1/\sqrt{j\omega\mu_0\sigma}$ is the complex depth below the earth at which the mirroring surface is located.

A third alternative, based on a piecewise-curve fitting exercise to a very accurate solution (i.e. carson's equations) and interpolation, is being proposed in this research for the first time. It is realised that the approach lacks the mathematical soundness of Carson's formulation or the elegance of the complex penetration model; it is rather a method of a very practical nature. It is remarkably simple and yields very accurate solutions when compared with those obtained using Carson's equations, but at a small fraction of the time. In fact, no error greater than 3 % is incurred for every situation in which the Carson's approach is valid, including cases of the angle θ close to the ninety degrees. Furthermore, in almost every case the curve fitting compares favourably to the complex penetration approach with regards to both execution time and accuracy.

The suggested formulae for the resistance and reactance of the ground in ohms per kilometer, at a given frequency, are:

$$R_e = (s_e - t_e \times r) \times 2.513274\, f\, 10^{-3} \tag{6.10}$$

$$X_e = (u_e - v_e \times \ln(r)) \times 2.513274\, f\, 10^{-3} \tag{6.11}$$

where the s_e, t_e, u_e, v_e coefficients are derived from curve fittings of any accurate formulation. In this case the Carson's series were chosen as the base case, however, there is no reason why a more accurate formulation, such as Wedepohl's integral or Wait's integral, should have not been used. Nevertheless, it is expected that for the range of values of r being considered here, this could have had little effect, if any, in our coefficients. The reason being the extremely high accuracy of Carson's equations, as has been previously established [Olsen and Pankaskie 1983].

The value of the parameter r increases rapidly with the separation between conductors and the frequency and, in some cases, it can take very large values, i.e. $r \simeq 10$ for $f = 1250\ Hz$, $\sigma = 0.01\ S/m$ and $d = 1\ km$, and $r \simeq 12$ for $f = 65\ kHz$, $\sigma = 0.01\ S/m$ and $d = 50\ m$. Nevertheless, the analysis and results presented in the rest of the section are limited to maximum values of the parameter r equal to twelve. This in itself is not because of a restriction of the approach, which should be accurate enough for the whole span of the parameter r and only restricted to the veracity of the base formulation (the Carson's equations in this case), but rather, a convenience for the presentation of results.

The linear and log-equations proposed for the fitting are very simple and not a single set of coefficients s_e, t_e, u_e, v_e are expected to match the whole span of the parameter r ($r \leq 12$), but at the same time, more elaborate fittings are not pursued because the simplicity of the equations (6.10) and (6.11) would be lost. Instead, a piecewise-curve fitting approach is adopted.

For this problem, smaller sections will result better fitted than larger ones, but this also will increase the set of coefficients s_e, t_e, u_e, v_e, which in the case of a computer oriented solution, have to be stored. Clearly, a compromise must be reached between accuracy and the number of sections in which the span is broken down. After an exhaustive search it was found that sections of 0.5 of r produces very accurate results, except for the first section, which has to be subdivided into two, i.e. $r \leq 0.2$ and $0.2 \leq r \leq 0.5$. Moreover, the exercise is only valid for a particular value of the angle θ, but fittings at fifteen degrees intervals, with linear interpolation in between, have been found to be sufficiently accurate. A complete set of coefficients is given in table 6-1.

This table of coefficients and the equations (6.10) and (6.11) are the only relevant information needed for the calculation of earth impedances through the approach being proposed here. Once the values of r and θ have been computed, the nearest *box* of table 6-1 is selected and the values used in equations (6.10) and (6.11).

The attraction of the curve fitting approach lies not just in the simplicity of its equations, but also in its ability to follow almost exactly the base formulation at the angle of fitting and, through interpolation, to give a reasonably accurate response at angles in which no fitting was carried.

This remarks are shown pictorially in figure 6-2(a), 6-3(a) and 6-4(a), in which the curve fitting approach is presented along with Carson's and Dubanton's solutions. Furthermore, figure 6-2(b) and (c), 6-3(b) and (c) and 6-4(b) and (c) compares the error of the curve fitting's and dubanton's solution with respect to Carson's solution.

The error criteria used here is the difference between the exact value (Carson) and the approximate values (Dubanton and curve fitting) of the real and imaginary part, related to the absolute values of the exact impedance [Tevan and Deri 1984], i.e.

$$\varepsilon_P = \frac{(R - R_0)}{\mid Z \mid} \tag{6.12}$$

$$\varepsilon_Q = \frac{(X - X_0)}{\mid Z \mid} \tag{6.13}$$

where ε_P and ε_Q are coefficients of error for the parameters P and Q,
R_0 and X_0 are the approximate resistance and reactance,
R and X are the resistance and reactance of the *exact* solution and
$\mid Z \mid$ is the absolute value of the *exact* impedance.

The results of figure 6.2 corresponds to the case when the angle θ takes a zero value (self term of the impedance), while the results of figure 6.3 belongs to the case when the angle θ equals the ninety degrees, which traditionally has been considered a difficult solution. Figure 6.3 also illustrates the inaccuracy of the complex penetration approach for this value of the angle θ and, in contrast, the accuracy of the curve fitting approach. The two cases above correspond to values of the angle θ for which fittings have been carried, and the error is kept low. For values of the angle θ different from those where a fitting was carried the accuracy is not as good as in the above two cases and the error increases with the angle θ. However, the error is always within the 1 to 2% mark and takes a maximum value of 3% only for cases when the angle θ is about 82.5^o. This case is shown in figure 6.4.

It is believed that the simplicity of this procedure is significant for computer oriented solutions and also for hand-calculations. The reason being that now it is possible to compute ground impedances for a very large range of frequencies, or cases of very wide separated conductors, even with a non programable calculator and within an error of 3% for the most extreme situation (when $\theta = 82.5^o$).

Table 6-1: Table of coefficients for the calculation of ground impedances

r/θ		0^o	15^o	30^o	45^o	60^o	75^o	90^o
	s_e	0.3910	0.3911	0.39150	0.39220	0.39290	0.39370	0.39440
0.2	t_e	0.1892	0.1854	0.17390	0.15450	0.12680	0.09050	0.04560
	u_e	0.3795	0.3773	0.37100	0.36060	0.34670	0.32990	0.31120
	v_e	0.4817	0.4822	0.48380	0.48640	0.49000	0.49420	0.49910
	s_e	0.3796	0.3804	0.38290	0.38690	0.39220	0.39830	0.40440
0.5	t_e	0.1426	0.1418	0.13910	0.13380	0.12480	0.11000	0.08700
	u_e	0.4652	0.4613	0.44960	0.43020	0.40320	0.36890	0.32810
	v_e	0.4248	0.4264	0.43140	0.43980	0.45180	0.46750	0.48690
	s_e	0.3591	0.3606	0.36540	0.37340	0.38470	0.39930	0.41670
1.0	t_e	0.1042	0.1047	0.10640	0.10870	0.11120	0.11270	0.11070
	u_e	0.5018	0.4978	0.48560	0.46500	0.43560	0.39710	0.34930
	v_e	0.3680	0.3699	0.37550	0.38550	0.40070	0.42240	0.45220
	s_e	0.3293	0.3313	0.33730	0.34800	0.36430	0.38760	0.41950
1.5	t_e	0.0740	0.0750	0.07800	0.08320	0.09090	0.10140	0.11430
	u_e	0.5033	0.4992	0.48700	0.46630	0.43670	0.39790	0.34950
	v_e	0.3073	0.3085	0.31260	0.32000	0.33220	0.35150	0.38190
	s_e	0.3019	0.3037	0.30950	0.32010	0.33710	0.36310	0.40250
2.0	t_e	0.0556	0.0565	0.05940	0.06460	0.07280	0.08510	0.10320
	u_e	0.4855	0.4812	0.46790	0.44540	0.41320	0.37060	0.31730
	v_e	0.2623	0.2628	0.26440	0.26750	0.27310	0.28310	0.30180
	s_e	0.2774	0.2790	0.28380	0.29270	0.30740	0.33100	0.36950
2.5	t_e	0.0433	0.0441	0.04650	0.05080	0.05790	0.06910	0.08680
	u_e	0.4618	0.4569	0.44210	0.41670	0.37960	0.32930	0.26400
	v_e	0.2278	0.2276	0.22690	0.22570	0.22420	0.22310	0.22440
	s_e	0.2559	0.2570	0.26050	0.26700	0.27790	0.29590	0.32680
3.0	t_e	0.0347	0.0353	0.03710	0.04050	0.04610	0.05500	0.06970
	u_e	0.4370	0.4316	0.41500	0.38640	0.34380	0.28410	0.20270
	v_e	0.2006	0.1998	0.19720	0.19240	0.18490	0.17360	0.15740
	s_e	0.2371	0.2377	0.23980	0.24370	0.25020	0.26110	0.28030
3.5	t_e	0.0284	0.0289	0.03020	0.03280	0.03690	0.04340	0.05420
	u_e	0.4130	0.4071	0.38900	0.35740	0.30970	0.24130	0.14390
	v_e	0.1788	0.1775	0.17340	0.16600	0.15390	0.13460	0.10370
	s_e	0.2205	0.2207	0.22160	0.22300	0.22520	0.22870	0.23480
4.0	t_e	0.0237	0.0240	0.02500	0.02680	0.02970	0.03410	0.04120
	u_e	0.3906	0.3843	0.36490	0.33090	0.27920	0.20400	0.09390
	v_e	0.1608	0.1592	0.15420	0.14490	0.12950	0.10470	0.06370
	s_e	0.2058	0.2057	0.20540	0.20460	0.20290	0.19970	0.19320
4.5	t_e	0.0200	0.0202	0.02096	0.02222	0.02413	0.02688	0.03081
	u_e	0.3699	0.3633	0.34300	0.30730	0.25280	0.17300	0.05524
	v_e	0.1459	0.1441	0.13840	0.12780	0.11040	0.08229	0.03572
	s_e	0.1929	0.1924	0.19120	0.18860	0.18380	0.17410	0.15730
5.0	t_e	0.0171	0.0173	0.01781	0.01866	0.01987	0.02120	0.02282
	u_e	0.3505	0.3445	0.32380	0.28550	0.22990	0.14830	0.02789
	v_e	0.1330	0.1316	0.12560	0.11330	0.09516	0.06582	0.01749
	s_e	0.1809	0.1812	0.17810	0.17270	0.16460	0.15510	0.127400
5.5	t_e	0.0147	0.0150	0.01519	0.01552	0.01609	0.01734	0.016840
	u_e	0.3375	0.3255	0.30260	0.27300	0.21270	0.12860	0.010340
	v_e	0.1247	0.1199	0.11260	0.10520	0.08436	0.05360	0.006572

Continuation of Table 6-1 ...

r/θ		0°	15°	30°	45°	60°	75°	90°
6.0	s_e	0.1709	0.1703	0.16690	0.16110	0.15080	0.13580	0.103400
	t_e	0.0129	0.0130	0.01316	0.01340	0.01359	0.01384	0.012479
	u_e	0.3202	0.3105	0.28820	0.25470	0.19570	0.11390	0.000229
	v_e	0.1146	0.1110	0.10410	0.09442	0.07436	0.04499	0.000628
6.5	s_e	0.1617	0.1608	0.15700	0.15040	0.13860	0.12020	0.084580
	t_e	0.0114	0.0114	0.01150	0.01161	0.01155	0.01122	0.009331
	u_e	0.3051	0.2965	0.27460	0.23920	0.18160	0.10250	-0.004619
	v_e	0.1062	0.1033	0.09649	0.08578	0.06650	0.03860	-0.002085
7.0	s_e	0.1534	0.1522	0.14810	0.14070	0.12780	0.10720	0.070060
	t_e	0.0101	0.0101	0.01013	0.01013	0.00989	0.00923	0.007094
	u_e	0.2916	0.2837	0.26200	0.22580	0.16970	0.09355	-0.006136
	v_e	0.0990	0.0964	0.08975	0.07866	0.06016	0.03382	-0.002899
7.5	s_e	0.1460	0.1444	0.13980	0.13220	0.11840	0.09621	0.058930
	t_e	0.0090	0.0090	0.00895	0.00891	0.00855	0.00766	0.005504
	u_e	0.2790	0.2720	0.25080	0.21390	0.15940	0.08693	-0.005799
	v_e	0.0925	0.0904	0.08399	0.07252	0.05485	0.03040	-0.002728
8.0	s_e	0.1390	0.1374	0.13260	0.12440	0.11010	0.08729	0.050410
	t_e	0.0081	0.0081	0.00800	0.00787	0.00743	0.00647	0.004367
	u_e	0.2681	0.2611	0.24010	0.20370	0.15070	0.08109	-0.004632
	v_e	0.0871	0.0850	0.07867	0.06746	0.05044	0.02751	-0.002149
8.5	s_e	0.1327	0.1310	0.12610	0.11740	0.10270	0.07973	0.043830
	t_e	0.0073	0.0073	0.00718	0.00699	0.00651	0.00553	0.003544
	u_e	0.2580	0.2511	0.23030	0.19460	0.14310	0.07633	-0.003265
	v_e	0.0822	0.0802	0.07397	0.06307	0.04689	0.02521	-0.001492
9.0	s_e	0.1269	0.1252	0.12010	0.11110	0.09621	0.07329	0.0386600
	t_e	0.0066	0.0066	0.00648	0.00625	0.00575	0.00477	0.0029350
	u_e	0.2486	0.2419	0.22130	0.18630	0.13640	0.07233	-0.0020390
	v_e	0.0778	0.0759	0.06979	0.05922	0.04375	0.02335	-0.0009185
9.5	s_e	0.1216	0.1199	0.11470	0.10540	0.09044	0.06774	0.0345100
	t_e	0.0060	0.0060	0.00588	0.00562	0.00511	0.00415	0.0024730
	u_e	0.2400	0.2333	0.21310	0.17890	0.13040	0.06890	-0.0010930
	v_e	0.0739	0.0720	0.06605	0.05583	0.04103	0.02179	-0.0004877
10.0	s_e	0.1167	0.1149	0.10970	0.10030	0.08529	0.06293	0.0310900
	t_e	0.0055	0.0055	0.00535	0.00508	0.00457	0.00365	0.0021130
	u_e	0.2320	0.2254	0.20560	0.17210	0.12500	0.06590	-0.0004458
	v_e	0.0703	0.0685	0.06269	0.05280	0.03864	0.02045	-0.0002001
10.5	s_e	0.1121	0.1104	0.10510	0.09560	0.08067	0.05872	0.0282100
	t_e	0.0051	0.0050	0.00489	0.00461	0.00410	0.00323	0.0018250
	u_e	0.2245	0.2180	0.19860	0.16580	0.12020	0.06323	-0.0000557
	v_e	0.0671	0.0653	0.05965	0.05010	0.03652	0.01929	-0.0000306
11.0	s_e	0.1079	0.1062	0.10090	0.09130	0.07650	0.05501	0.0257300
	t_e	0.0047	0.0046	0.00449	0.00421	0.00371	0.00287	0.0015890
	u_e	0.2175	0.2112	0.19210	0.16010	0.11570	0.06082	0.0001423
	v_e	0.0641	0.0623	0.05689	0.04766	0.03464	0.01827	0.0000537
11.5	s_e	0.1040	0.1023	0.09693	0.08742	0.07274	0.05172	0.0235700
	t_e	0.0043	0.0043	0.00413	0.00385	0.00336	0.00257	0.0013930
	u_e	0.2110	0.2048	0.18600	0.15480	0.11170	0.05862	0.0002129
	v_e	0.0614	0.0597	0.05437	0.04545	0.03295	0.01735	0.0000832

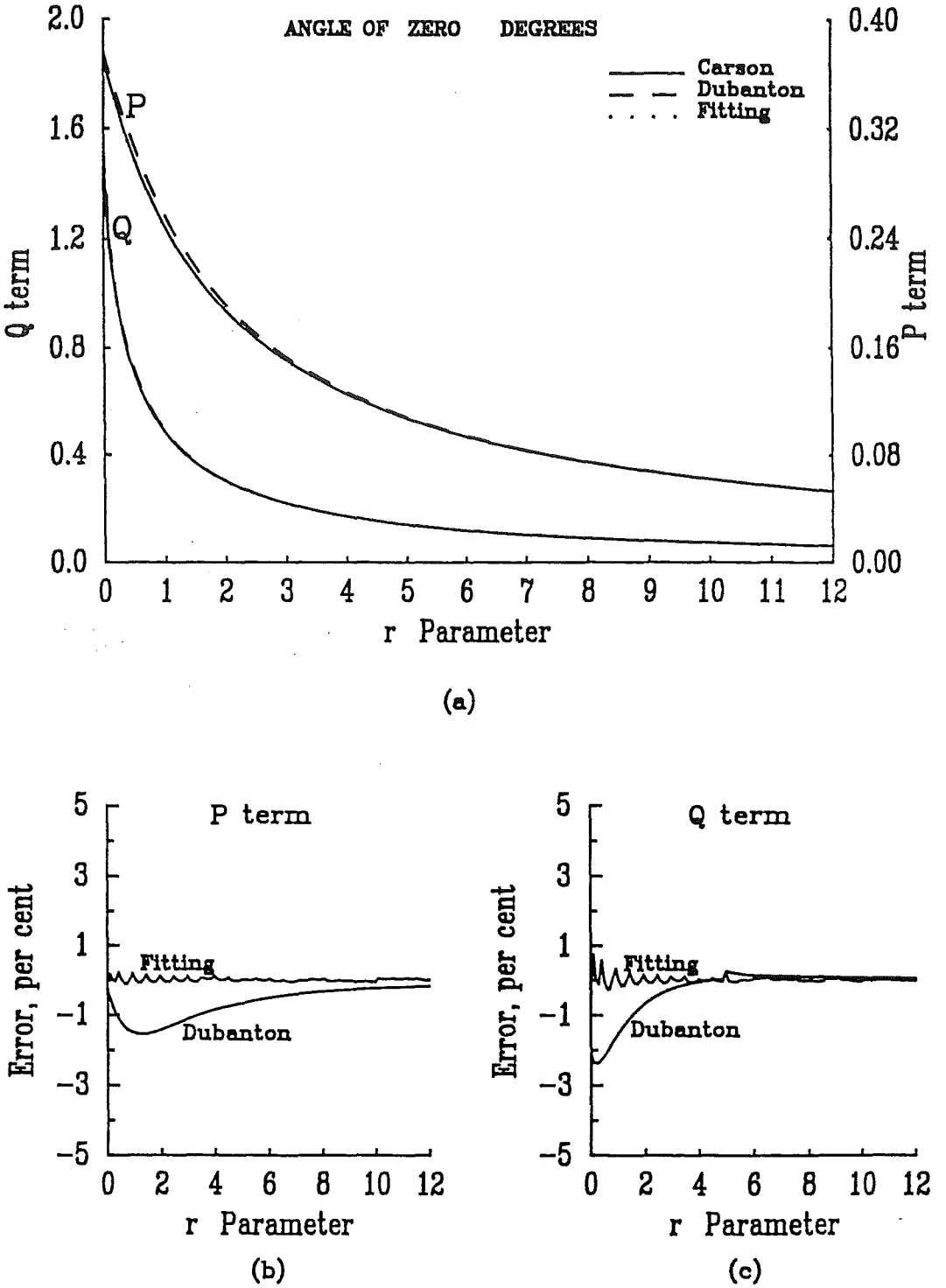

Figure 6-2: Comparison of Carson, Dubanton and curve fitting solutions for the self impedance of the ground

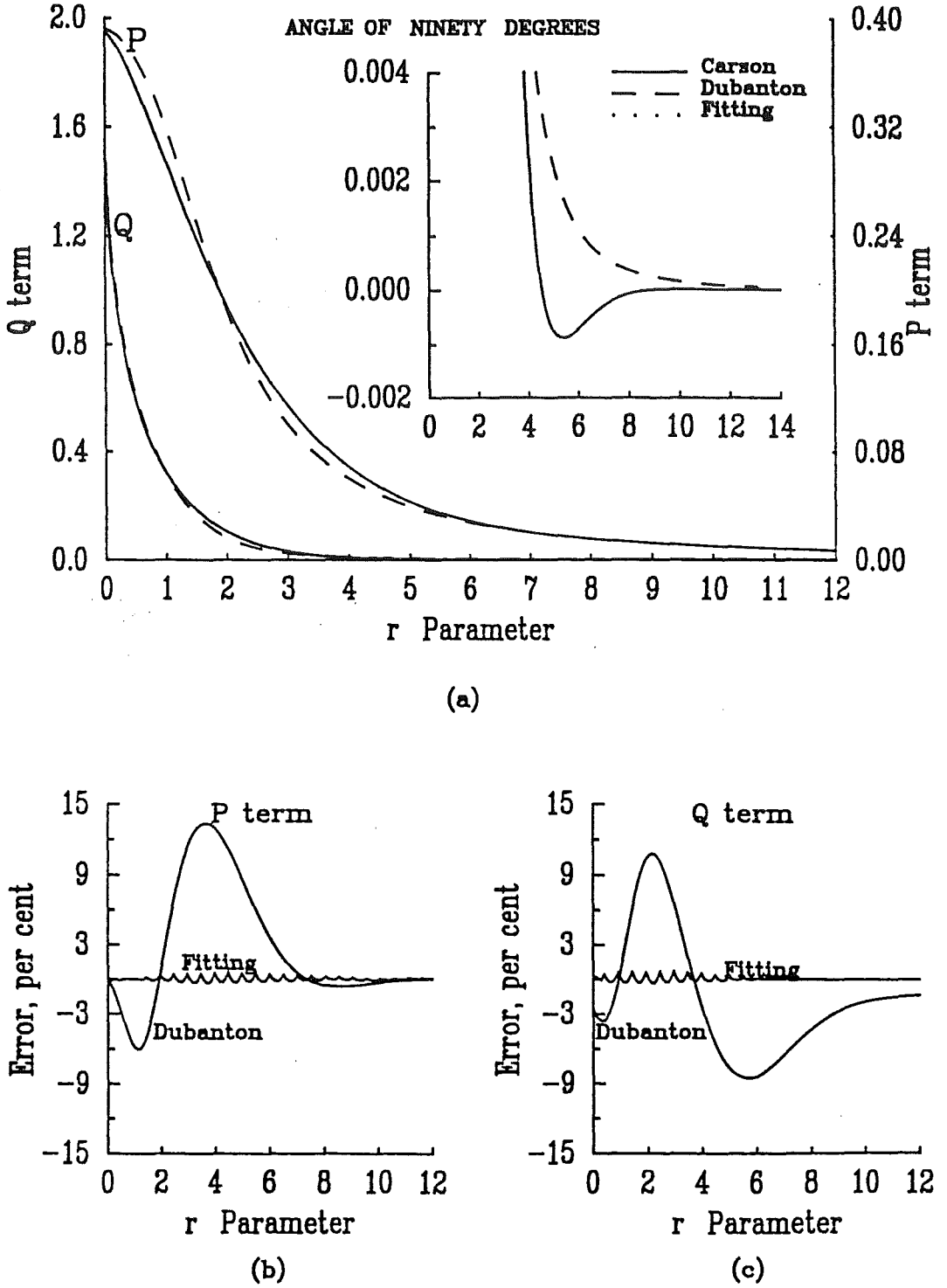

Figure 6-3: Comparison of Carson, Dubanton and curve fitting solutions for the mutual impedance of the ground, when $\theta = 90^{o}$

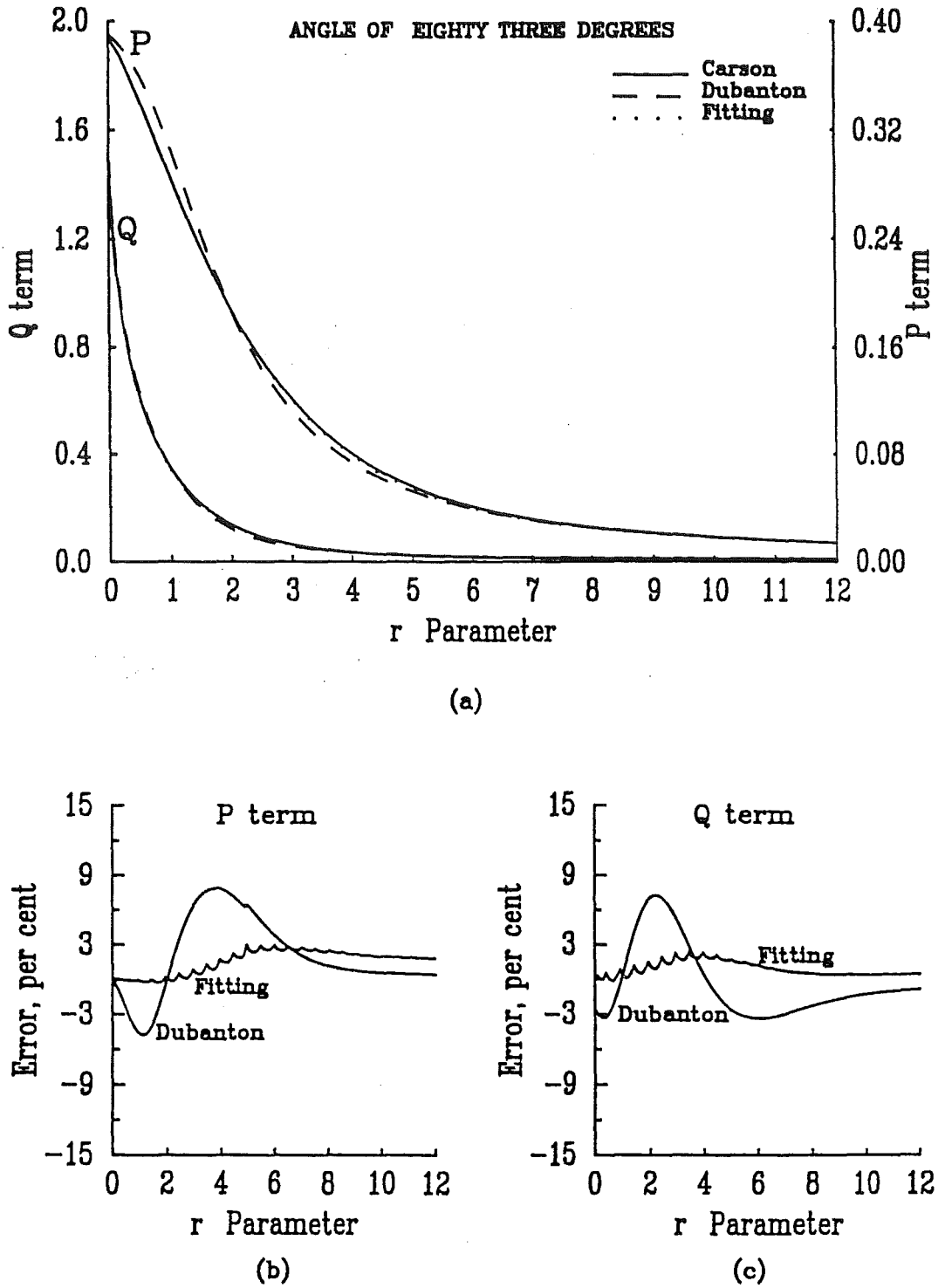

Figure 6-4: Comparison of Carson, Dubanton and curve fitting solutions for the mutual impedance of the ground, when $\theta = 82.5^{o}$

6.2.2 Conductor Impedance Matrix $[Z_c]$

This term accounts for the internal impedance of the conductors. Both resistance and inductance vary with frequency in a non-linear manner and need to be computed at each particular harmonic frequency.

The reasons behind the non-linear variation of these parameters with frequency have been very early recognized [Kenelly, Laws and Pierce 1915] and are attributable mainly to the fact that the current flowing in the conductor does not distribute itself uniformly over the full area available, rather, it tends to flow on the surface. The overall effect is an increase in the resistance and a decrease in its internal inductance. This trend increases with the frequency and it is termed *skin* effect [Densem 1983].

In the past, extensive research both theoretical and practical has been carried for conductors with regular and non regular shapes. Solid conductors, annular conductors (tubes), rounded, squared, stranded, etc. have been investigated and different models have been proposed [Zaborszky 1953], [Silvester 1969] and [King 1970]. In power system applications the most successful approach has been the one that models the power conductor as a tube [Lewis and Tuttle 1958]. The reason being that modern power transmission circuits utilize almost exclusively ACSR (Aluminium Conductor Steel Reinforced) conductors and, under the assumption that a negligible amount of current flows through the path of high resistance (the steel), the conductor can be approximated to a tube. The diameter of the conductor being the outer diameter of the tube and the diameter of the steel reinforcement being the inner diameter of the tube.

The formula for the evaluation of the internal impedance of an annular conductor with outer radio r_e and inner radio r_i, at a given frequency [Semlyen and Abdel-Rahman 1982], is:

$$Z_c = \frac{j\omega\mu_0}{2\pi}\frac{1}{x_e}\frac{J_0(x_e)N_0'(x_i) - N_0(x_e)J_0'(x_i)}{J_0'(x_e)N_0'(x_i) - N_0'(x_e)J_0'(x_i)} \tag{6.14}$$

and the function arguments x_e and x_i obtained from $x = j\sqrt{j\omega\mu_0\sigma_c}\, r$, where $r = r_e$ or $r = r_i$.

Furthermore, J_0 and N_0 represent the Bessel functions of first kind and second kind of zero order, J_0' and N_0' their derivatives and σ_c the conductivity of the conductor.

The Bessel functions and their derivatives are solved, within a specified accuracy, by means of their associated infinite series. In some cases this is not without difficulties, because the series present convergence problems and their asymptotic expansions have to be used. This is particularly the case at high frequencies and low ratios of thickness to external radius, i.e. t/r_e or $(r_e - r_i)/r_e$. An additional problem is also the time required for them to converge.

Once again the complex penetration concept has been successfully invoked, and based on it, an alternative solution has been proposed recently [Semlyen and Deri 1985]. The new formulation supersedes the problems encountered by the infinite series of the Bessel functions. It is a closed form solution, and although errors up to the 6.5 per cent exist at low frequencies, its accuracy increases with the frequency. The method appeals to the two extreme cases of the impedance, the zero frequency solution and the infinite frequency solution,

$$R_0 = \frac{1}{\pi(r_e^2 - r_i^2)\sigma_c} \tag{6.15}$$

$$Z_\infty = \frac{1}{2\pi\sigma_c r_e p_c} \tag{6.16}$$

$$Z_c = \sqrt{R_0^2 + Z_\infty^2} \tag{6.17}$$

where $p_c = 1/\sqrt{j\omega\mu_0\sigma_c}$

This research is concerned mainly with the low range of frequencies (harmonic frequencies), and trying to circumvent the slow convergence of the bessel functions and the error of the complex penetration approach at low frequencies, an alternative solution has been developed. It has been inspired by the successful application of the curve fitting approach to the earth impedance problem.

In this case the formula used to fit the internal impedance of the conductor, at a given frequency, are,

$$R_c = (s_c + t_c \times c) \times R_{dc} \tag{6.18}$$

$$X_c = (u_c + v_c \times c) \times R_{dc} \tag{6.19}$$

where $c = \sqrt{f/R_{dc}}$

R_{dc} is the resistance of the conductor at zero frequency and
s_c, t_c, u_c, v_c are coefficients derived from piecewise-curve fittings of the formulation based on Bessel functions, equation (6.14).

In this case a maximum value of the parameter c equal to 300 and ratios of thickness to radius between 1.0 and 0.4 were considered. The span of the parameter c is conveniently covered by six sets of s_c, t_c, u_c, v_c coefficients, i.e. $0 < c_1 \leq 25 < c_2 \leq 50 < c_3 \leq 75 < c_4 \leq 100 < c_5 \leq 150 < c_6 \leq 300$.

Furthermore, this exercise is repeated at selected values of the ratio thickness to radius, and it was found that fittings at 1.0,0.8,0.6 and 0.4 values of the ratio allow accurate solutions for the intermediate ratios, through linear interpolation. The coefficients are given in table 6-3.

$\sqrt{f/R_{dc}}$		thick./rad. 1.0	0.8	0.6	0.4
25	s_c	0.997000	0.997600	0.998600	0.999400
	t_c	0.000446	0.000362	0.000213	0.000091
	u_c	-0.036490	-0.033920	-0.027560	-0.019150
	v_c	0.008132	0.007553	0.006132	0.004257
50	s_c	0.823000	0.850500	0.906900	0.958700
	t_c	0.006667	0.005599	0.003458	0.001528
	u_c	-0.360600	-0.350100	-0.304300	-0.221400
	v_c	0.021280	0.020270	0.017130	0.012230
75	s_c	0.320000	0.342100	0.483200	0.725400
	t_c	0.016780	0.015720	0.011750	0.006039
	u_c	-0.398100	-0.463500	-0.562100	-0.527900
	v_c	0.022480	0.022960	0.022530	0.018410
100	s_c	0.212700	0.137300	0.039790	0.250600
	t_c	0.018370	0.018630	0.017780	0.012330
	u_c	-0.096000	-0.122600	-0.329300	-0.630600
	v_c	0.018410	0.018440	0.019570	0.019890
150	s_c	0.294600	0.283000	0.150000	-0.120100
	t_c	0.017540	0.017190	0.016830	0.016090
	u_c	-0.050160	-0.022840	0.035870	-0.179000
	v_c	0.017910	0.017370	0.015910	0.015610
300	s_c	0.278300	0.266100	0.237500	0.188500
	t_c	0.017650	0.017300	0.016160	0.014080
	u_c	-0.035970	-0.033730	-0.032480	0.014060
	v_c	0.017830	0.017460	0.016350	0.014110

Figure 6.5(a) and figure 6.6(a) present the solutions for the real and imaginary components for the case of a solid conductor (ratio of thickness to radius equals to unity). This value of the ratio corresponds to a case where a fitting was carried and it is observed that the solution provided by the approach proposed in this research follows that given by the base formulation (Bessel functions) very closely. In contrast, some deviations are observed for the approach based on the complex penetration concept.

Based on a similar criteria as that used for the case of ground impedances, an assessment of the errors introduced by the two simplified approaches are shown in figures 6.5(b) and 6.6(b), where maximum errors of 2 and 6.5 % are observed for the real component of the curve fitting and complex penetration approaches, respectively. The maximum errors for the imaginary component of the curve fitting approach is slightly higher than that of the real component, 3 % ; while for the complex penetration approach remains much the same, 6.5 %.

It is interesting to observe the deviations incurred by the curve fitting approach with respect to the rigorous solution at a particular value of the ratio thickness to radius where no fitting was performed. For the range of parameters being considered here, the maximum deviations are observed for the case when the ratio thickness to radius takes a value of 0.5. This result is presented in figure 6.7(a) and 6.7(a) for the real and imaginary components, respectively. The errors incurred are also evaluated and given in figure 6.7(b) and 6.8(b), where it is shown that the maximum error is kept below the 2 % mark.

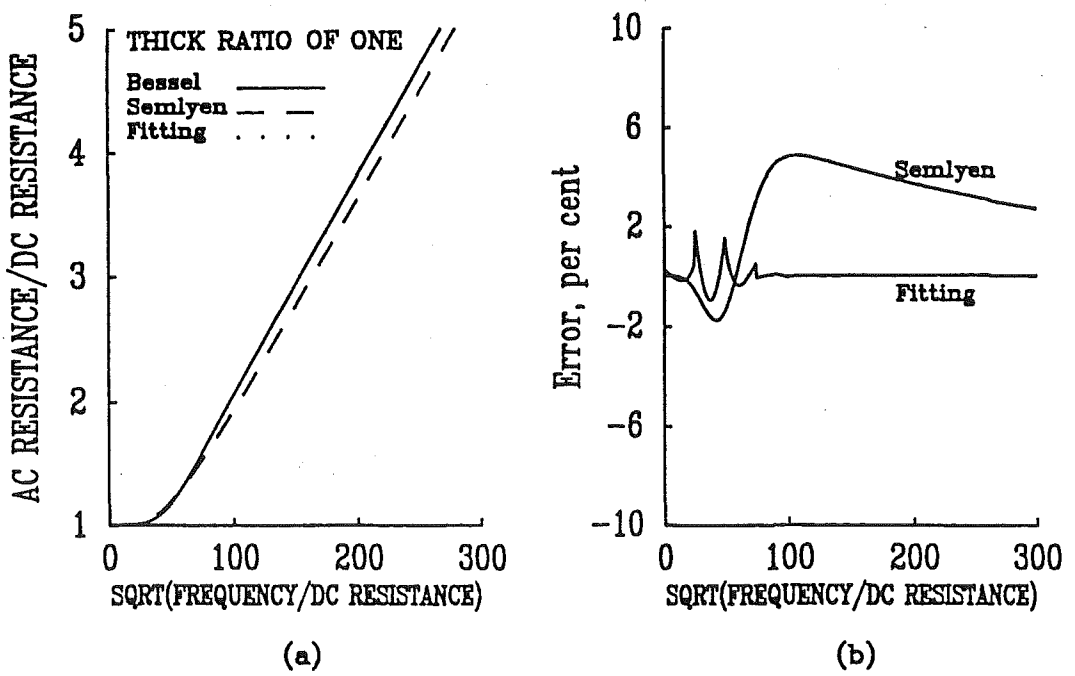

Figure 6-5: Comparison of Bessel, Semlyen and curve fitting solutions for the resistance of solid conductors

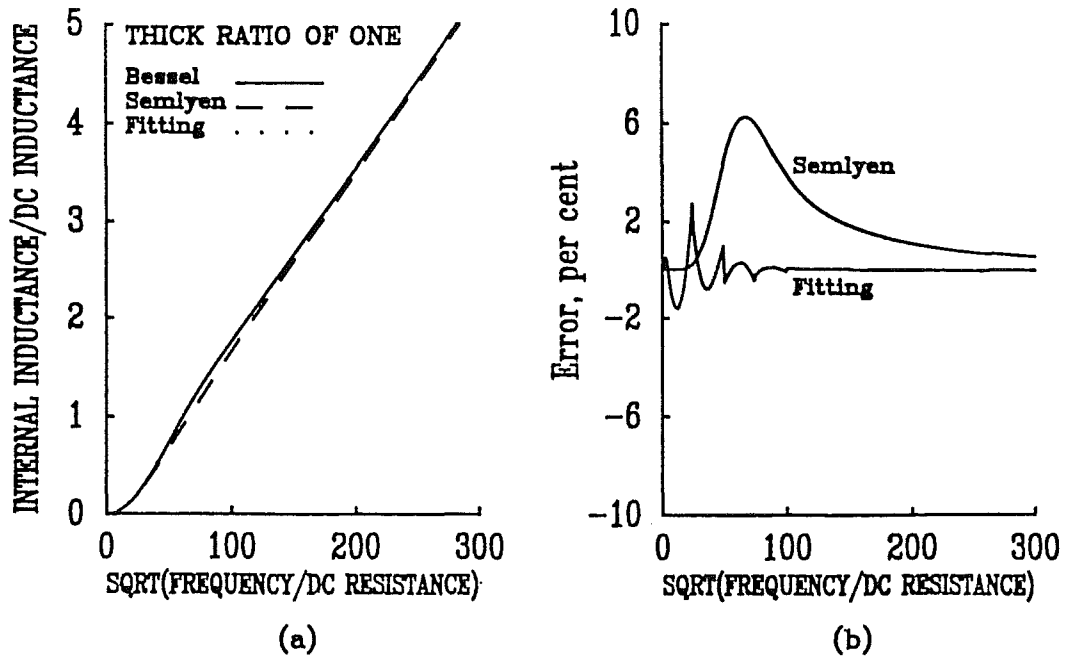

Figure 6-6: Comparison of Bessel, Semlyen and curve fitting solutions for the inductance of solid conductors

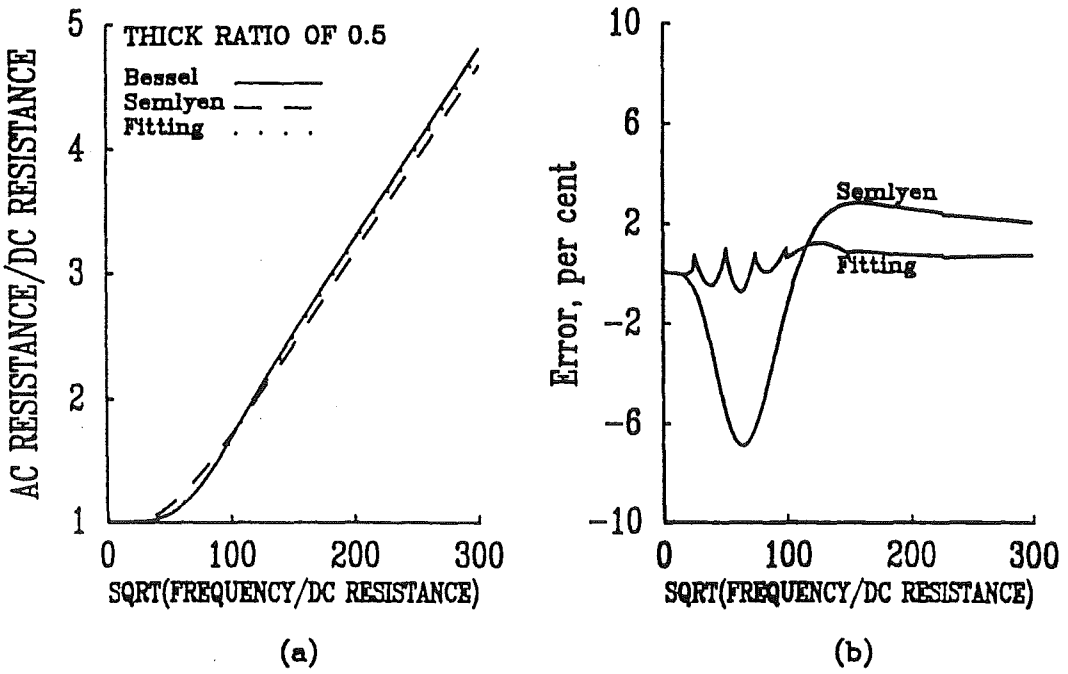

Figure 6-7: Comparison of Bessel, Semlyen and curve fitting solutions for the resistance of conductors with thick ratio of 0.5

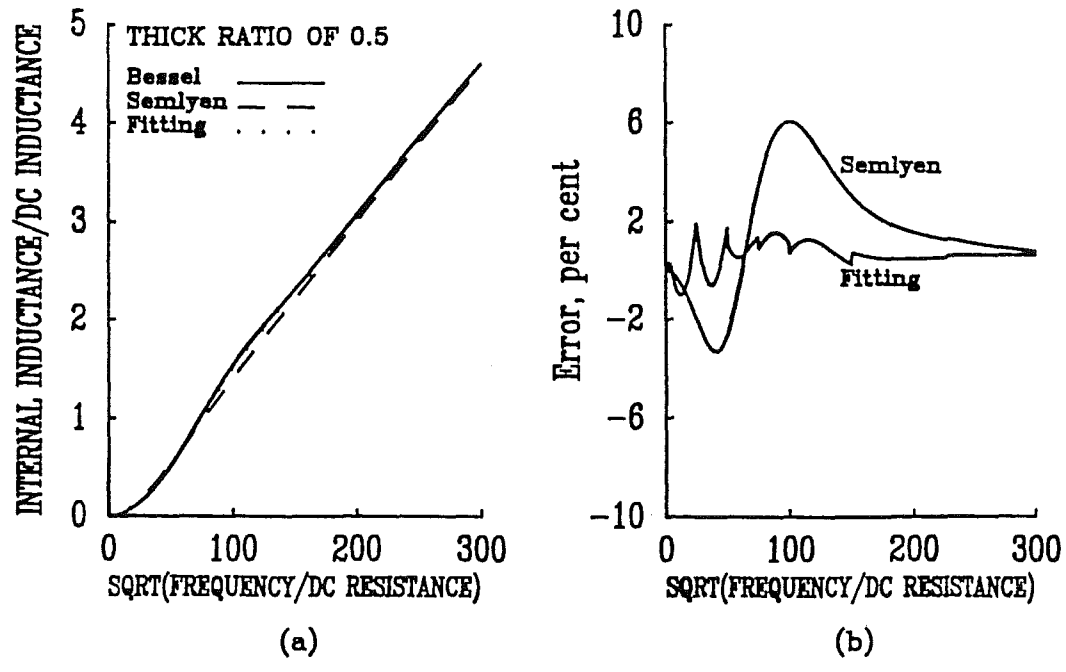

Figure 6-8: Comparison of Bessel, Semlyen and curve fitting solutions for the inductance of conductors with thick ratio of 0.5

6.2.3 Geometrical Impedance Matrix $[Z_g]$

If the conductors and the earth are assumed to be equipotential surfaces, the geometrical impedance can be formulated in terms of the potential coefficients theory.

The self-potential coefficient ψ_{ll} for the lth conductor and the mutual potential coefficient ψ_{lm} between the lth and mth conductors of figure 6-1 are defined as follows,

$$\psi_{ll} = \ln \frac{2h_l}{r_l} \tag{6.20}$$

$$\psi_{lm} = \ln \frac{D_{lm}}{d_{lm}} \tag{6.21}$$

where r_l is the radius of the l th conductor while the other variables are shown in figure 6-1.

Potential Coefficients depend entirely on the physical arrangement of the conductors and they must be evaluated once. For practical purposes the air is assumed to have zero conductance, and

$$[Z_g] = j\omega K'[\Psi]\ (\Omega/km) \tag{6.22}$$

where $[Z_g]$ varies linearly with frequency
$[\Psi]$ is a matrix of potential coefficients and
$K' = 2 \times 10^{-4}$

Also, if the corona threshold is not transversed, lumped shunt admittance parameters $[Y]$ are voltage independent and, thereby, completely defined by the inverse relation of the potential coefficients matrix [Ovick and Kusic 1984],

$$[Y] = j\omega K''[\Psi]^{-1}\ (S/km) \tag{6.23}$$

where $K'' = 5.5606 \times 10^{-2}$

6.2.4 Reduced Equivalent Matrices $[Z']$ and $[\Psi']$

Although AC Extra High Voltage transmission lines contain a large number of conductors, i.e. earth wires and several bundle conductors per phase, the interest of harmonic studies is not the individual conductors but the individual phases and steps must be taken to find reduced equivalent matrices, which should correctly account for the original configuration while keeping essential information only, i.e. one equivalent conductor per phase.

This can be achieved in two different ways. One of them, the Geometrical Mean Radius (GMR) concept [Dommel 1984], although frequency independent, provides an efficient computational solution.

The second method uses matrix reduction techniques. It includes frequency dependence for the series impedance but requires considerable computation, with the following three steps carried out for each frequency (except for $[\Psi]$, since this matrix is frequency independent).

1. Setting up of $[Z]$ and $[\Psi]$ with an order equal to the total number of conductors plus earth-wires.
2. By assuming that the voltage from line to ground is exactly the same for all the conductors in the bundle, the transformation matrices $[B]$ and $[B]^t$ are built up, so that modified matrices $[Z'']$ and $[\Psi'']$ are obtained, i.e.

$$[Z''] = [B]^t[Z][B] \tag{6.24}$$

$$[\Psi''] = [B]^t[\Psi][B] \tag{6.25}$$

3. Next a partial inversion is applied to the matrices $[Z'']$ and $[\Psi'']$. All but a number of elements equal to the number of phases are inverted and each of the non inverted locations correspond to one conductor per phase. Thus, final reduced equivalent matrices $[Z']$ and $[\Psi']$ are arrived at, whose order equals the number of phases but implicitly account for the original configuration.

Furthermore, this procedure can be applied to the case of multi-circuit transmission lines operating in parallel, resulting in a single equivalent circuit that properly represents any number of circuits, bundle conductors and earth-wires.

6.2.5 Numerical Example 1

Based on the geometrical configuration of figure 6.9, an illustrative numerical example is presented below. The series impedance matrix is formed for the case when the frequency is 1000 Hz and the conductivity of the earth is 0.01 S/m.

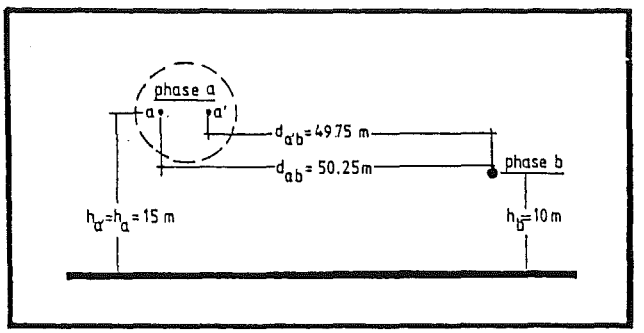

Figure 6.9: Line geometry for example 1

The data for the conductor is also needed:
-DC resistance
$R_{dc,a} = R_{dc,a'} = 0.0709\Omega/km$
$R_{dc,b} = 0.1840\Omega/km$
-geometrical mean radius
$GMR_a = GMR_{a'} = 1.155cm$
$GMR_b = 0.485cm$
-external radius
$r_{e,a} = r_{e,a'} = 1.429cm$
$r_{e,b} = 0.615cm$
-internal radius
$r_{i,a} = r_{i,a'} = 0.477cm$
$r_{i,b} = 0.0cm$

The three constituent parts of the series impedance are evaluated separately and then added up to obtain a full series impedance matrix, representing explicitly the three conductors of the circuit of figure 6.9.

The earth impedance matrix is evaluated first, and the parameters r and angles θ are as follow:

$$r_{aa} = r_{a'a'} = \sqrt{2\pi \times 1000 \times 4\pi E - 7 \times 0.01}\, 30 =$$
$$= 8.885766\, E - 3 \times 30 = 0.266573; \theta_{aa} = \theta_{a'a'} = 0°$$

$r_{bb} = 8.885766\,E - 3 \times 20 = 0.177715; \theta_{bb} = 0^o$
$r_{ab} = 8.885766\,E - 3 \times 56.125418 = 0.498717; \theta_{ab} = 63.5^o$
$r_{aa'} = 8.885766\,E - 3 \times 30.004166 = 0.266610; \theta_{aa'} = 1^o$
$r_{a'b} = 8.885766\,E - 3 \times 55.678205 = 0.494743; \theta_{a'b} = 63.3^o$

Now that the parameters r and the angle θ are known for the three conductors making up the configuration, the appropriate coefficients s_e, t_e, u_e and v_e are picked up from table 6-1 and substituted in equations (6.10) and (6.11). The resultant values for the earth impedances, in Ohms per kilometer, are

$$[Z_e] = \begin{pmatrix} 0.858502 + j2.580708 & 0.829280 + j1.803337 & 0.858487 + j2.580559 \\ 0.829280 + j1.803337 & 0.898184 + j3.045264 & 0.830526 + j1.812420 \\ 0.858487 + j2.580559 & 0.830526 + j1.812420 & 0.858502 + j2.580708 \end{pmatrix} \tag{6.26}$$

For the conductors impedance matrix the parameters c and the ratio of thickness to radius are needed,

$c_a = c_{a'} = \sqrt{\frac{1000}{0.07009}} = 119.446$
$c_b = \sqrt{\frac{1000}{0.184}} = 73.721$
$T_a = T_{a'} = \frac{1.429 - 0.477}{1.429} = 0.6662$
$T_b = 1.0$

and the appropriate coefficients are selected from table 6-2 and substituted in equations (6.18) and (6.19).

The resultant impedance matrix for the conductors is,

$$[Z_c] = \begin{pmatrix} 0.129649 + j0.120491 & & \\ & 0.286495 + j0.231683 & \\ & & 0.129649 + j0.120491 \end{pmatrix} \tag{6.27}$$

The geometric impedance matrix is found by substituting the relevant data into equations (6.20) and (6.21).

$$[Z_g] = \begin{pmatrix} j9.880016 & j0.132766 & j5.145279 \\ j0.132766 & j10.460887 & j0.135155 \\ j5.145279 & j0.135155 & j9.880016 \end{pmatrix} \tag{6.28}$$

The three constituent parts are added up to give the total series impedance matrix,

$$[Z] = \begin{pmatrix} 0.988151 + j12.581215 & 0.829280 + j1.936103 & 0.858487 + j7.725838 \\ 0.829280 + j1.936103 & 1.184679 + j13.737834 & 0.830526 + j1.947575 \\ 0.858487 + j7.725838 & 0.830526 + j1.947575 & 0.988151 + j12.581215 \end{pmatrix} \tag{6.29}$$

Now, if it is assumed that the conductors a and a' belong to the same phase, a reduced equivalent matrix that relates the phases a and b only, rather than the three conductors, is found by using the linear transformations of equations (6.24) and then, applying a partial inversion. The resultant matrix is,

$$[Z'] = \begin{pmatrix} 0.914982 + j10.153526 & 0.829903 + j1.941839 \\ 0.829903 + j1.941839 & 1.184677 + j13.737821 \end{pmatrix} \tag{6.30}$$

where

$$[B] = \begin{pmatrix} 1 & 0 & -1 \\ 0 & 1 & 0 \\ 0 & 0 & 1 \end{pmatrix} \tag{6.31}$$

6.2.6 Computation Efficiency

The transmission line given in appendix A was used to illustrate the computation economy achieved with the alternative approaches to the earth impedance and the conductor impedance (**skin effect**) problems. This example was used first to compare the cpu times of Carson's, Dubanton's and the curve fitting technique for the earth impedance problem and then, to compare the cpu times of the method that uses Bessel functions, Semlyen's approach and the curve fitting technique for the **skin effect**. In each case the study was limited to the first fifty harmonics, the programming was carried in Fortran 77 and the computer was a VAX-750.

Table 6-3 shows the cpu times taken by the earth impedance, conductor impedance and also the nominal π solutions.

Earth impedances (using GMR approach) :		
Carson	2.69 sec	
Dubanton	0.13 sec	
Curve fitting	0.04 sec	
Conductor impedances (using GMR approach) :		
Bessel functions	2.51 sec	
Semlyen	0.10 sec	
Curve fitting	0.03 sec	
Normal π (in p.u.) matrix reduction		GMR approach
Infinite series	53.05 sec	5.31 sec
Complex penetration	4.30 sec	0.30 sec
Curve fitting	2.95 sec	0.12 sec

6.3 Distributed Parameters

As the electrical distance increases with frequency long-line effects must be taken into account in harmonic propagation analysis. The modelling of transmission lines by nominal π circuits, described in the previous section, is no longer valid. Instead the use of equivalent π circuits or analogous formulations, derived from the wave propagation equation, is essential.

To date only equivalent π circuits have been used for harmonic distortion applications [Arrillaga,Densem and Harker 1983] and [Dommel 1986]. However, the transfer function approach seems to be a more efficient alternative [Semlyen and Abdel-Rahman 1982].

6.3.1 Modal Analysis at Harmonic Frequencies

The incorporation of long-line effects into multiconductor transmission lines is not as simple as for single phase lines, because it involves matrix rather than scalar operations.

Operations such as square roots, logarithms, circular and hyperbolic functions, etc. are not directly defined in matrix theory. The solution adopted in power transmission line problems has been to diagonalize the matrices [Wedepohl 1963] and [Dommel 1969], through modal analysis, and then normal scalar operations are carried out for the decoupled matrices. More recently, less time demanding, yet accurate solutions, have been proposed [Semlyen and Deri 1985].

In general, diagonalization procedures of matrices associated with three phase transmission lines are performed by means of iterative algorithms,i.e. QR methods and idempotents; and analytical formulas exists for the special case of configurations with center-phase symmetry [Naredo,Silva,Romero and Moreno 1987].

An alternative, closed form approach, which has apparently not been used is presented in Appendix E. It is based on the solution of the cubic equation and applies to cases of three phase transmission lines having an arbitrary configuration. However, the procedure does not solve the rather theoretical problem of irregular eigenvalues [Brandao Faria and Borges Da Silva 1986].

In transmission line theory two transformation matrices are needed. One defines the modal voltages and the other the modal currents, i.e.

$$V_p = [T_v]V_m \tag{6.32}$$

$$I_p = [T_i]I_m \tag{6.33}$$

where V_p and I_p are vectors of phase quantities, V_m and I_m are vectors of modal quantities, $[T_v]$ and $[T_i]$ are linear transformation matrices that require the eigen-solution of the product $[Z][Y]$ and $[Y][Z]$, respectively. The matrices $[Z]$ and $[Y]$ are the lumped parameter matrices derived in the previous section.

Also, as an extension,

$$[Z_m] = [T_v]^{-1}[Z][T_i] \tag{6.34}$$

$$[Y_m] = [T_i]^{-1}[Y][T_v] \tag{6.35}$$

At this stage, both $[Z_m]$ and $[Y_m]$ are fully diagonal and scalar operations are permitted. For instance,

$$\gamma_m = \sqrt{z_m y_m} \tag{6.36}$$

$$z_{0m} = \sqrt{\frac{z_m}{y_m}} \tag{6.37}$$

where $z_m \in [Z_m]$ and $y_m \in [Y_m]$

The same is true for all of the hyperbolic and transfer functions discussed in the next two sections.

Furthermore, a transformation from modal to phase domain is also defined,

$$[Z] = [T_v][Z_m][T_i]^{-1} \tag{6.38}$$

$$[Y] = [T_i][Y_m][T_v]^{-1} \tag{6.39}$$

For an efficient numerical solution, the proposed algorithm uses the following simplifications:

1. Theoretically, transformation matrices $[T_v]$ and $[T_i]$ must be obtained at each harmonic frequency, as modal transformations are unique and frequency dependent. However it has been observed that they do not vary much for wide range of frequencies [Semlyen and Deri 1986]. Our investigation has found that a single eigen-analysis, carried at the fundamental frequency, is sufficiently accurate for use in harmonic frequencies.

2. The transformation matrices $[T_v]$ and $[T_i]$ are non-singular and the following relationship exists between them,
   $[T_i]^t = [T_v]^{-1}$

6.3.2 Homogeneous Line

In an homogeneous line the relationship between sending and receiving end harmonic voltages and currents is a transfer impedance matrix, i.e.

$$\begin{pmatrix} V_S \\ V_R \end{pmatrix} = \begin{pmatrix} [Z'] & [Z''] \\ [Z''] & [Z'] \end{pmatrix} \begin{pmatrix} I_S \\ I_R \end{pmatrix} \tag{6.40}$$

where $[Z'] = [T_v] \times Diag\{z_{0m} \times \coth(\gamma_m l)\} \times [T_i]^{-1}$
$[Z''] = [T_v] \times Diag\{z_{0m} \times \frac{1}{\sinh}(\gamma_m l)\} \times [T_i]^{-1}$

Alternatively, the use of the equivalent π concept, leads to the following equation,

$$\begin{pmatrix} V_S \\ V_R \end{pmatrix} = \begin{pmatrix} [Z_{eq}]^{-1} + \frac{1}{2}[Y_{eq}] & -[Z_{eq}]^{-1} \\ -[Z_{eq}]^{-1} & [Z_{eq}]^{-1} + \frac{1}{2}[Y_{eq}] \end{pmatrix}^{-1} \begin{pmatrix} I_S \\ I_R \end{pmatrix} \tag{6.41}$$

where $[Z_{eq}] = l\,[Z][T_i] \times Diag\{\frac{\sinh(\gamma_m l)}{\gamma_m l}\} \times [T_i]^{-1}$
$[Y_{eq}] = l\,[T_i] \times Diag\{\frac{\tanh(\frac{\gamma_m l}{2})}{\frac{\gamma_m l}{2}}\} \times [T_i]^{-1}[Y]$

Either, equation (6.40) or equation (6.41), is solved as many times as the number of harmonics to be considered.

When harmonic voltages rather than currents are to be injected (at the sending end) the following equation applies instead of equation (6.40).

$$\begin{pmatrix} V_R \\ -I_S \end{pmatrix} = \begin{pmatrix} [L] & [M] \\ [N] & [L] \end{pmatrix} \begin{pmatrix} V_S \\ I_R \end{pmatrix} \tag{6.42}$$

where $[L] = [T_v] \times Diag\{\frac{1}{\coth(\gamma_m l)}\} \times [T_i]^{-1}$

$[M] = [T_v] \times Diag\{z_{0m} \times \tanh(\gamma_m l)\} \times [T_i]^{-1}$

$[N] = -[T_i] \times Diag\{\frac{1}{z_{0m}} \times \tanh(\gamma_m l)\} \times [T_v]^{-1}$

Again, the use of the equivalent π concept is possible, although its application is not as direct as the above procedure [Arrillaga,Acha,Densem and Bodger 1986].

Finally when the aim of the analysis is the observation of standing waves along the line or the distribution of harmonic levels in a mesh of lines, it is necessary to obtain the line's parameters in the form of an admittance.

$$\begin{pmatrix} I_S \\ I_R \end{pmatrix} = \begin{pmatrix} [Y'] & [Y''] \\ [Y''] & [Y'] \end{pmatrix} \begin{pmatrix} V_S \\ V_R \end{pmatrix} \tag{6.43}$$

where $[Y'] = [T_i] \times Diag\{\frac{1}{z_{0m}} \times \coth(\gamma_m l)\} \times [T_v]^{-1}$

$$= [Z_{eq}]^{-1} + \tfrac{1}{2}[Y_{eq}]$$

$$[Y''] = -[T_i] \times Diag\{\frac{1}{z_{0m}} \times \frac{1}{\sinh}(\gamma_m l)\} \times [T_v]^{-1}$$

$$= [Z_{eq}]^{-1}$$

6.3.3 Numerical example 2

This example relates to an unloaded, 230 km long homogeneous transmission line with 1 p.u. harmonic current being injected at the sending end. The configuration corresponds to that given in appendix A and, as expected, for lines of this length, a resonance point is established at 650 Hz (13th harmonic for 50 Hz fundamental). Although the analysis is carried in the phase frame of reference the sending end harmonic voltage magnitudes, plotted in figure 6.10 are shown in sequence components form.

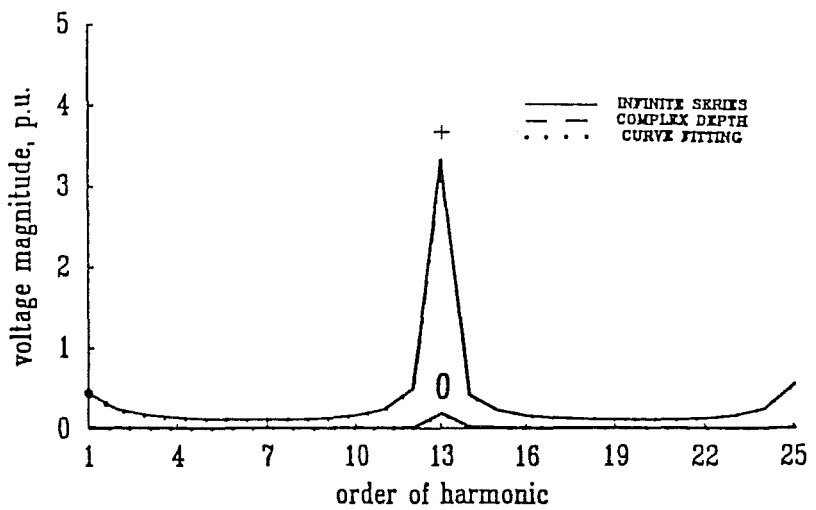

Figure 6.10: Harmonic voltage at the sending end of the line

The three different approaches for the frequency dependant part of the transmission line discussed earlier, i.e. infinite series(Carson plus Bessel), complex penetration (Dubanton plus Semlyen) and curve fitting, were applied to the solution of this example and the results differ little at the point of resonance. The difference between the matrix elimination and GMR approaches were also insignificant for this test system. Finally, the repeated use of the eigen-analysis at every harmonic frequency showed no advantage over the case where this was only carried out at the fundamental frequency. Thus, the approximations suggested in the formulation to make the computation more efficient are justified.

6.3.4 Non-homogeneous lines

Long lines will often include series and shunt compensation as well as transpositions. In such case each individual section of the transmission system needs to be represented as an independent unit. All the units are then cascaded to derive an equivalent matrix equation of ABCD parameters, which effectively relates the input to the output taking into consideration all the discontinuities along the transmission system.

Capacitors produce no harmonic distortion and their reactance varies linearly with frequency. Reactors, on the other hand, are non-linear elements and their magnetizing branches are rich in harmonics. It has been shown in the previous chapters that this introduces considerable complexities into the analysis. However, under the assumption that no saturation takes place, the reactances vary linearly with frequency and no harmonic distortion is produced. To simplify the analysis this assumption is made in this section, leaving the complexities of magnetic non-linearities for the other chapters.

The ABCD parameters matrix equation for a distributed element, e.g. a transmission line section, is

$$\begin{pmatrix} V_S \\ I_S \end{pmatrix} = \begin{pmatrix} [A] & [B] \\ [C] & [D] \end{pmatrix} \begin{pmatrix} V_R \\ -I_R \end{pmatrix} \tag{6.44}$$

where $[A] = [T_i] \times Diag\{\cosh(\gamma_m l)\} \times [T_v]^{-1}$

$[B] = [T_v] \times Diag\{z_{0m} \times \sinh(\gamma_m l)\} \times [T_i]^{-1}$

$[C] = -[T_i] \times Diag\{\frac{1}{z_{0m}} \times \sinh(\gamma_m l)\} \times [T_i]^{-1}$

$[D] = [A]$

For a lumped series element, the ABCD parameters matrix equation is,

$$\begin{pmatrix} V_S \\ I_S \end{pmatrix} = \begin{pmatrix} [U] & [Z] \\ & [U] \end{pmatrix} \begin{pmatrix} V_R \\ -I_R \end{pmatrix} \tag{6.45}$$

where $[Z_{se}] = Diag\{\frac{-j}{\omega C}\}$ for series capacitive compensation

$[U]$ = is a unity matrix

While for a shunt element,

$$\begin{pmatrix} V_S \\ I_S \end{pmatrix} = \begin{pmatrix} [U] & \\ [Y] & [U] \end{pmatrix} \begin{pmatrix} V_R \\ -I_R \end{pmatrix} \tag{6.46}$$

where

$[Y_{sh}] = Diag\{\frac{-j}{\omega L}\}$ for shunt inductive compensation

$= Diag\{j\omega C\}$ for shunt capacitive compensation

So that, for a transmission system with n individual sections,

$$\begin{pmatrix} V_S \\ I_S \end{pmatrix} = \begin{pmatrix} [A_1] & [B_1] \\ [C_1] & [D_1] \end{pmatrix} \begin{pmatrix} [A_2] & [B_2] \\ [C_2] & [D_2] \end{pmatrix} \times \cdots \times \begin{pmatrix} [A_n] & [B_n] \\ [C_n] & [D_n] \end{pmatrix} \begin{pmatrix} V_R \\ -I_R \end{pmatrix}$$

$$\begin{pmatrix} V_S \\ I_S \end{pmatrix} = \begin{pmatrix} [A] & [B] \\ [C] & [D] \end{pmatrix} \begin{pmatrix} V_R \\ -I_R \end{pmatrix} \tag{6.47}$$

However, an equivalent matrix equation in the form of ABCD parameters may not be the most desirable answer, as it will depend on the source to be injected and the response to be observed,i.e. voltages or currents. Thus, a systematic way of transforming a particular transfer function into another is presented next. The partial inversion algorithm [Shipley and Coleman 1959] is central to the present approach.

For instance, for converting equation (6.47) into a nodal impedance matrix equation, the following steps are needed,
Interchanging block columns,

$$\begin{pmatrix} V_S \\ I_S \end{pmatrix} = \begin{pmatrix} [B] & [A] \\ [D] & [C] \end{pmatrix} \begin{pmatrix} -I_R \\ V_R \end{pmatrix} \tag{6.48}$$

Partial invertion,

$$\begin{pmatrix} V_S \\ V_R \end{pmatrix} = \begin{pmatrix} [Z''] & [Z'] \\ [Z'] & [Z''] \end{pmatrix} \begin{pmatrix} I_R \\ I_S \end{pmatrix} \tag{6.49}$$

Interchanging block columns,

$$\begin{pmatrix} V_S \\ V_R \end{pmatrix} = \begin{pmatrix} [Z'] & [Z''] \\ [Z''] & [Z'] \end{pmatrix} \begin{pmatrix} I_S \\ I_R \end{pmatrix} \tag{6.50}$$

6.3.5 Numerical Example 3

This example illustrates the case of a fully loaded long distance non-homogeneous transmission system. It relates to El Chocon [Jones 1974], a 1000 Km, double line operating at 500 kV, 50 Hz. The scheme layout and equivalent circuit (per line), shown in figure 6.11, include two identical compensation units symmetrically placed along the line. The configuration of the transmission line is that shown in appendix A.

When the line carries maximum power (i.e. 1650 MW) requires two series capacitors each of -j0.0188 p.u. reactance (to provide a total of 40 per cent series compensation) combined with two sets of shunt inductance compensation (to provide 30 per cent shunt compensation).

A very large number of arrangements for the placement of combined compensation is possible [Iliceto and Cinieri 1977], but the case when the shunt inductive compensation units are placed before the series capacitors gives a more regular profile for the fundamental voltage (this is shown in the next section).

Compensation is designed solely on fundamental frequency requirements and therefore it will not provide a flat voltage profile at harmonic frequencies, as shown in figure 6.12. The overall effect of compensation is a reduction in the electrical length of the line, and the appearance of the first resonant peak at 2.3 multiple of the fundamental frequency shows it.

Figure 6.12(a) shows the harmonic voltage magnitude at the receiving end of the transmission system for the case when a balanced excitation of 1 p.u. is applied at the sending end. The presence of 1 p.u. harmonic voltage is unrealistic, however, the figure provides a good reference for comparability between the effects at different frequencies. The expected harmonic voltage levels are likely to be about 1 to 3 per cent of the fundamental and the harmonic voltages should be scaled down proportionately.

Due to the increasing number of static converters of large rating and also to the large amount of power transformers existing in a network, harmonic current injections is a more practical case. Figure 6.12(b) presents the result for the case when a balanced current source of 1 p.u. is applied at the receiving end, while the sending end is kept short circuited.

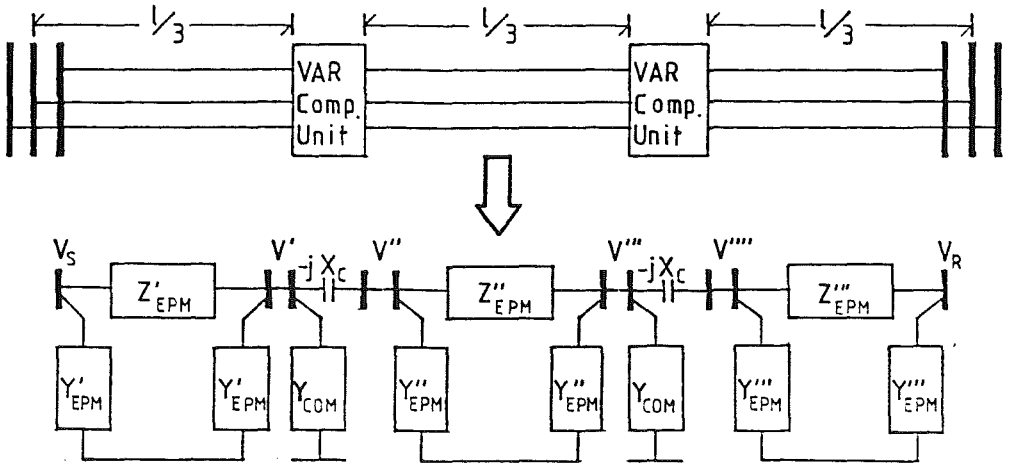

Figure 6.11: Layout and equivalent circuit of a non-homogeneous long distance transmission line

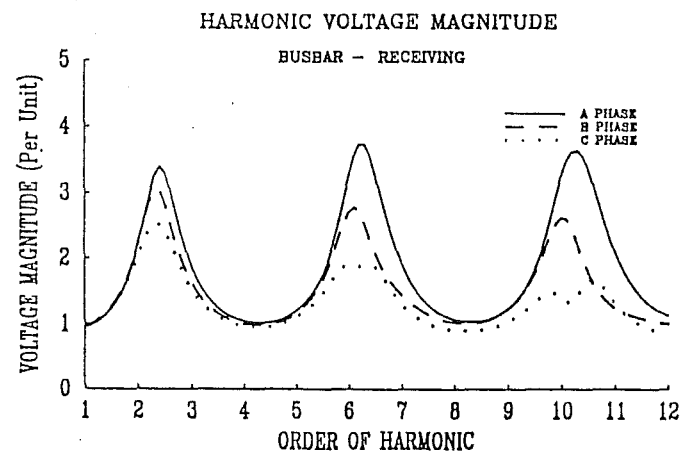

(a)

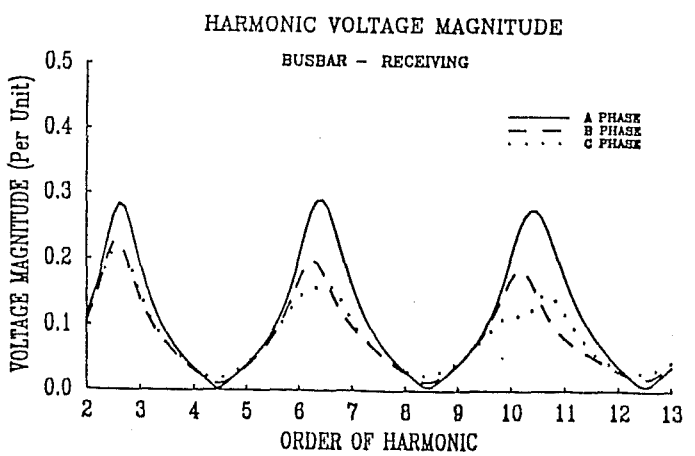

(b)

Figure 6-12: Harmonic voltage magnitudes at the receiving end of the compensated line (a) With 1 p.u. voltage injection at the sending end (b) With 1 p.u. current injection at the receiving end

6.3.6 Network Nodal Analysis

If only input-output voltage information is required, the cascading approach described in the previous section is sufficient. However, if extra information along the line is required appropriate fictitious nodes are created at specified points and/or at regular intervals and either nodal or laddering techniques are applied. The former approach is adopted in this section because it seems to be a more systematic way of solving any number of three phase sections (including discontinuities). The following matrix equation is formed, inverted (factorized) and solved. The resultant vectors provide the harmonic voltage profile along the line. The analysis applies to both homogeneous and non-homogeneous lines.

$$\begin{pmatrix} I_S \\ I_1 \\ I_2 \\ \vdots \\ I_n \\ I_R \end{pmatrix} = \begin{pmatrix} [Y_1'] & [Y_1''] & & & & \\ [Y_1''] & [Y_1'] + [Y_2'] & [Y_2''] & & & \\ & [Y_2''] & [Y_2'] + [Y_3'] & & & \\ & & & \ddots & & \\ & & & & [Y_{n-1}'] + [Y_n'] & [Y_n''] \\ & & & & [Y_n''] & [Y_n'] \end{pmatrix} \begin{pmatrix} V_S \\ V_1 \\ V_2 \\ \vdots \\ V_n \\ V_R \end{pmatrix} \tag{6.51}$$

6.3.7 Numerical Example 4

The compensated transmission system of the previous section (example 3) is solved this time using the nodal approach. The voltage profile of the transmission system is shown in figure 6.13 for the **phase a** of the fundamental, second, third and sixth harmonics, while figure 6.14 shows different views of the harmonic order and voltage magnitudes at the sending, receiving and intermediate points of the transmission line for the fundamental and harmonics (up to the 12th).

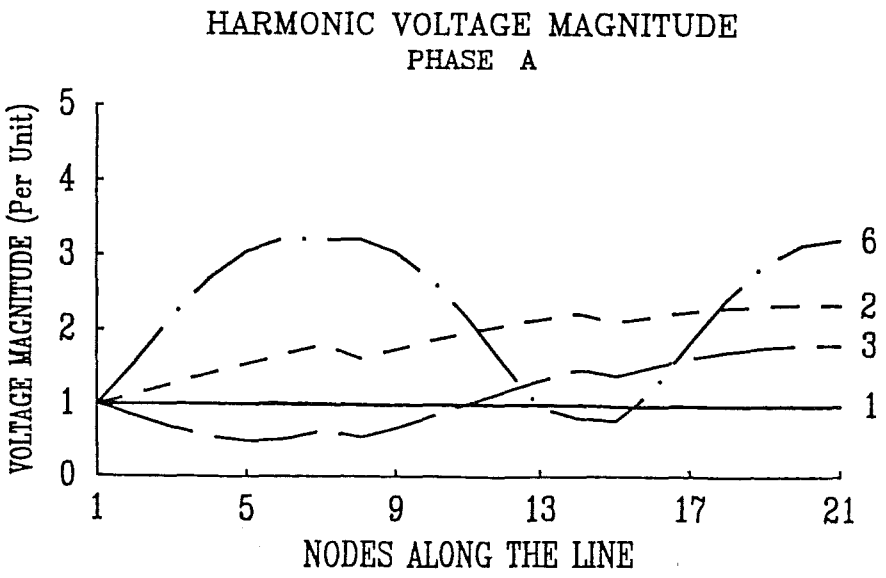

Figure 6-13: Standing waves along the compensated line of example 3

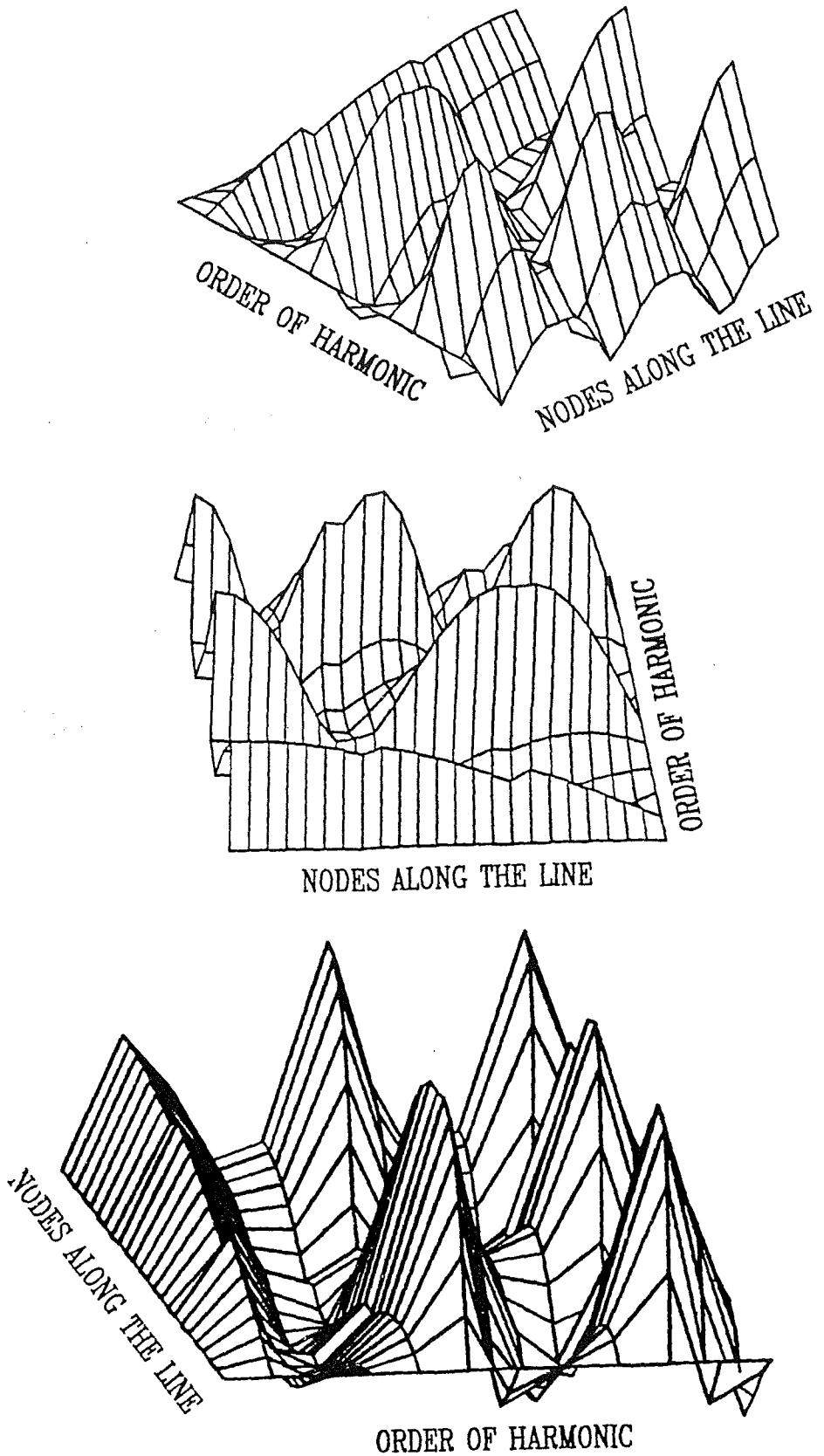

Figure 6-14: Standing Voltage waves for the compensated line of example 3 together with the harmonic order to produce three-dimensional plots as observed from different positions

6.4 Modelling Linear Components In The Complex Conjugate Harmonic Space

For harmonic network analysis purposes, non-linear power plant components are conveniently represented as harmonic Norton equivalents, while linear power plant components are modelled as harmonic transfer admittances. The resultant Norton equivalent consists of a current source and a transfer admittance that exhibit cross-couplings between frequencies.

Transfer admittances associated with linear elements do not exhibit cross-couplings and they can be represented independently at each harmonic frequency. For instance,the case of a coupled, three phase branch is represented by the following transfer function (it corresponds to an explicit form of equation (6.43))

$$\begin{pmatrix} I_{a,S} \\ I_{b,S} \\ I_{c,S} \\ I_{a,R} \\ I_{b,R} \\ I_{c,R} \end{pmatrix}_h \begin{pmatrix} y'_{aa} & y'_{ab} & y'_{ac} & y''_{aa} & y''_{ab} & y''_{ac} \\ y'_{ba} & y'_{bb} & y'_{bc} & y''_{ba} & y''_{bb} & y''_{bc} \\ y'_{ca} & y'_{cb} & y'_{cc} & y''_{ca} & y''_{cb} & y''_{cc} \\ y''_{aa} & y''_{ab} & y''_{ac} & y'_{aa} & y'_{ab} & y'_{ac} \\ y''_{ba} & y''_{bb} & y''_{bc} & y'_{ba} & y'_{bb} & y'_{bc} \\ y''_{ca} & y''_{cb} & y''_{cc} & y'_{ca} & y'_{cb} & y'_{cc} \end{pmatrix}_h \begin{pmatrix} V_{a,S} \\ V_{b,S} \\ V_{c,S} \\ V_{a,R} \\ V_{b,R} \\ V_{c,R} \end{pmatrix}_h \tag{6.52}$$

where h represents the harmonic order.

In harmonic studies geometrical imbalance plays an important role and it should be represented correctly if accurate solutions are needed. To this end, only representations of the form of equation (6.52) have been used so far for the modelling of three phase linear components, i.e. phase frame of reference.

An alternative representation based on the complex conjugate harmonic space is possible. However, if the non-linear components are modelled as current or voltage sources, there is no need for using the harmonics space and the phases are the correct frame of reference for the linear components.

A different situation arises when the non-linearities are modelled as harmonic Norton equivalents. The transfer admittance of non linear elements can not be represented in the phase frame of reference because cross-couplings exists between frequencies, rather, they are well framed in the harmonic space. At this point still is possible to represent linear components in the phase frame of reference, however, the solution of the entire network must be carried then through a sequential approach.

It will be shown in the next chapter that both linear and non-linear polyphase elements can be combined together in the complex conjugate harmonic space for an unified solution of the Newton type. This fact provides enough reasons for representing linear elements in the complex conjugate harmonic space, where equation (6.53) is a fully equivalent representation of equation (6.52).

$$\begin{pmatrix} I_{a,S} \\ I_{b,S} \\ I_{c,S} \\ I_{a,R} \\ I_{b,R} \\ I_{c,R} \end{pmatrix} = \begin{pmatrix} \{y'_{aa}\} & \{y'_{ab}\} & \{y'_{ac}\} & \{y''_{aa}\} & \{y''_{ab}\} & \{y''_{ac}\} \\ \{y'_{ba}\} & \{y'_{bb}\} & \{y'_{bc}\} & \{y''_{ba}\} & \{y''_{bb}\} & \{y''_{bc}\} \\ \{y'_{ca}\} & \{y'_{cb}\} & \{y'_{cc}\} & \{y''_{ca}\} & \{y''_{cb}\} & \{y''_{cc}\} \\ \{y''_{aa}\} & \{y''_{ab}\} & \{y''_{ac}\} & \{y'_{aa}\} & \{y'_{ab}\} & \{y'_{ac}\} \\ \{y''_{ba}\} & \{y''_{bb}\} & \{y''_{bc}\} & \{y'_{ba}\} & \{y'_{bb}\} & \{y'_{bc}\} \\ \{y''_{ca}\} & \{y''_{cb}\} & \{y''_{cc}\} & \{y'_{ca}\} & \{y'_{cb}\} & \{y'_{cc}\} \end{pmatrix} \begin{pmatrix} V_{a,S} \\ V_{b,S} \\ V_{c,S} \\ V_{a,R} \\ V_{b,R} \\ V_{c,R} \end{pmatrix} \tag{6.53}$$

where the matrix $\{y'_{aa}\}$ has dimensions $(2h+1) \times (2h+1)$.

For the case when the three phase branch is uncoupled, i.e. VAR compensating plant, the same structure exists but elements other than *aa*, *bb* and *cc* are not present.

6.5 Conclusions

A comprehensive theory for the modelling of linear power plant components has been presented. Due to its distributed nature and non-linear variation with frequency, most of the material relates to transmission lines, however, lumped elements have also received attention.

Both distributed and lumped components have been interfaced together to represent non-homogeneous transmission lines, and applications have been made to the solution of problems hitherto neglected. Among such problems are the effects of conventional VAR compensation at harmonic frequencies and the effect that conventional voltage balancing techniques have on the propagation of harmonics, i.e. transpositions.

When dealing with harmonic frequencies transmission line models should incorporate provisions for representing several effects which, normally, are of no concern in fundamental frequency studies. Available techniques for the representation of such effects demand a considerable amount of cpu time which, coupled with the necessity of computing parameters for a wide range of frequencies, makes existing harmonic transmission line algorithms unsuitable for interactive studies. Keeping this in mind, alternative proposals have been successfully developed that reduces substantially the computing requirements without loss of accuracy.

Both the traditional and the new tools have been presented and comparisons, based on their accuracy and cpu time requirements, made. Particular attention has been given to the frequency dependant part of the transmission line in which the more rigorous formulations based on the evaluation of infinite series have been replaced by piecewise-curve fitting solutions.

The approach proposed in this research gives answers with errors within the 0 to 2 per cent mark for most cases, and take maximum values of 3 per cent for a reduced number of situations. These remarks are observed for the whole range of values for which Carson's solutions are valid and should be significant in the area of electromagnetic interference. Also, comparisons have been made with alternative, closed form solutions, based on the concept of complex penetration. The curve-fitting approach compares favourable with the complex penetration methods with regards to both execution time and accuracy, except but few cases where the errors introduced by the two approximate solutions is less than, say, 1 per cent.

Most of the information discussed in this chapter together with a powerful graphic package, has been implemented in an extremely fast, yet accurate, harmonic multiphase transmission line program. Furthermore, because of the incorporation of non-homogeneous transmission lines, transfer functions and matrix manipulation facilities, it is also a very versatile program.

Finally, a way of modelling coupled, three phase linear components in the complex conjugate harmonic space has been presented at the closure of the chapter.

Chapter 7

A New and More General Frame of Reference for Harmonic Studies

7.1 Introduction

If carried by hand-calculations, quantitative analysis of three phase power systems are cumbersome and time consuming, even for the most basic configurations. Digital computers were not in existence in the early days of the power industry and means of performing simplified quantitative analysis were developed. For instance, more comprehensive studies were possible with the appearance of the symmetrical components theory [Fortescue 1918], which allows a single phase interpretation of a balanced three phase plant component and also of the entire network. It quickly gain popularity as a frame of reference for several of the power system studies.

The awareness of the network being unbalanced, however, never faded away and a number of unwanted characteristics of the grid, such as additional losses, ill-tripping of protection devices, generation of non-characteristic harmonics, etc., were directly associated with geometrical imbalance. Nevertheless, no comprehensive analysis could be undertaken because of the numerical task involved. It was the digital computer that paved the way for the emergence of the phases as a more general frame of reference, where all the geometrical and operational unbalances of the power system can be represented explicitly.

More recently, a problem which has risen serious concern is the marked increase of harmonics on the network and their damaging consequences. Many contributions have appeared in the literature and different models, with a varying degree of sofistication, have been applied to the problem of power system harmonics. Some approaches use the phases as their frame of reference [Densem,Bodger and Arrillaga 1983], while other approaches use the sequences [Mahmoud and Schultz 1982] and, therefore, are of a more restricted nature.

The harmonic behaviour of the power network is a non-linear problem and cross-couplings exist between frequencies [Semlyen,Acha and Arrillaga 1987], [Semlyen,Eggleston and Arrillaga 1986] and [Mizuma,Sagisaka and Sekine 1985], which can not be represented explicitly in existing frames of reference. Therefore, the harmonic numerical solution, which is iterative, has to be performed on a sequential fashion.

Iterative unified solutions, on the other hand, are possible but they require the realization of a new frame of reference so that all the busbars, phases, harmonics and cross-couplings between harmonics can be represented explicitly. The complex conjugate harmonic space is shown to meet such expectations and, in this chapter, it is applied to find the harmonic solution of an actual power network with multiple non-linearities of the transformer type.

7.2 The Harmonic Multiphase Nodal Matrix Equation

The combined use of nodal analysis and the technique of linearization in the complex-conjugate harmonic space allows, in principle at least, a global harmonic representation for the entire network in the form of equation (7.1).

$$[Y_J]\Delta V = \Delta I \tag{7.1}$$

where $[Y_J]$ is a harmonic admittance matrix for the entire network,
ΔV is a vector of incremental voltages and
ΔI is a vector of incremental currents.

The nodal matrix equation (7.1) accommodates all the nodes, phases and the full spectrum of harmonics, i.e. +ve and -ve. This realization is one of a very general nature and provides a new frame of reference in which all the power plant components of the system can be setted.

The formation of the admittance matrix obeys the same basic rules as those used to make up the well known single and three phase admittance matrices [Arrillaga,Arnold and Harker,1981]. However, in the present case the building units are not scalars or 3×3 matrices as is the case for +ve sequence or three phase studies but, rather, a matrix which contains the phases and the full spectrum of harmonics (truncated because of practical purposes).

The order of each building-unit is equal to the number of phases $\times$(2$\times$ number of considered harmonics + DC term) and, for most conditions, they are highly sparse.

The vector of nodal injections of the harmonic matrix equation consists of the internal sources associated with the linearized power plant components, infinite busbars and external contributions from outside the network.

The nodal matrix equation (7.1) may be interpreted as a Norton equivalent which means that a particular state of the entire network has also the interpretation of a Norton equivalent which is harmonic, polyphase and multinodal.

Furthermore, the admittance matrix of equation (7.1) is non-singular and, therefore, equation (7.2) exists

$$\Delta V = [Y_J]^{-1}\Delta I \tag{7.2}$$

which has the interpretation of a Thevenin equivalent and is the dual of the Norton equivalent of equation (7.1).

In this thesis only magnetic non-linearities of the transformer type are considered, however, recent research shows that other non-linearities such as the generator [Semlyen,Eggleston and Arrillaga 1986] and the static power converter [Mizuma,Sagisaka and Sekine 1985], can also be modelled in the complex harmonic space. Furthermore, very preliminary work indicates that a representation for these two non-linearities in the more general complex conjugate harmonic space is a possibility.

By way of example, figure 7.1(b) shows the structure of the admittance matrix, up to the third harmonic, corresponding to the radial system of figure 7.1 (a).

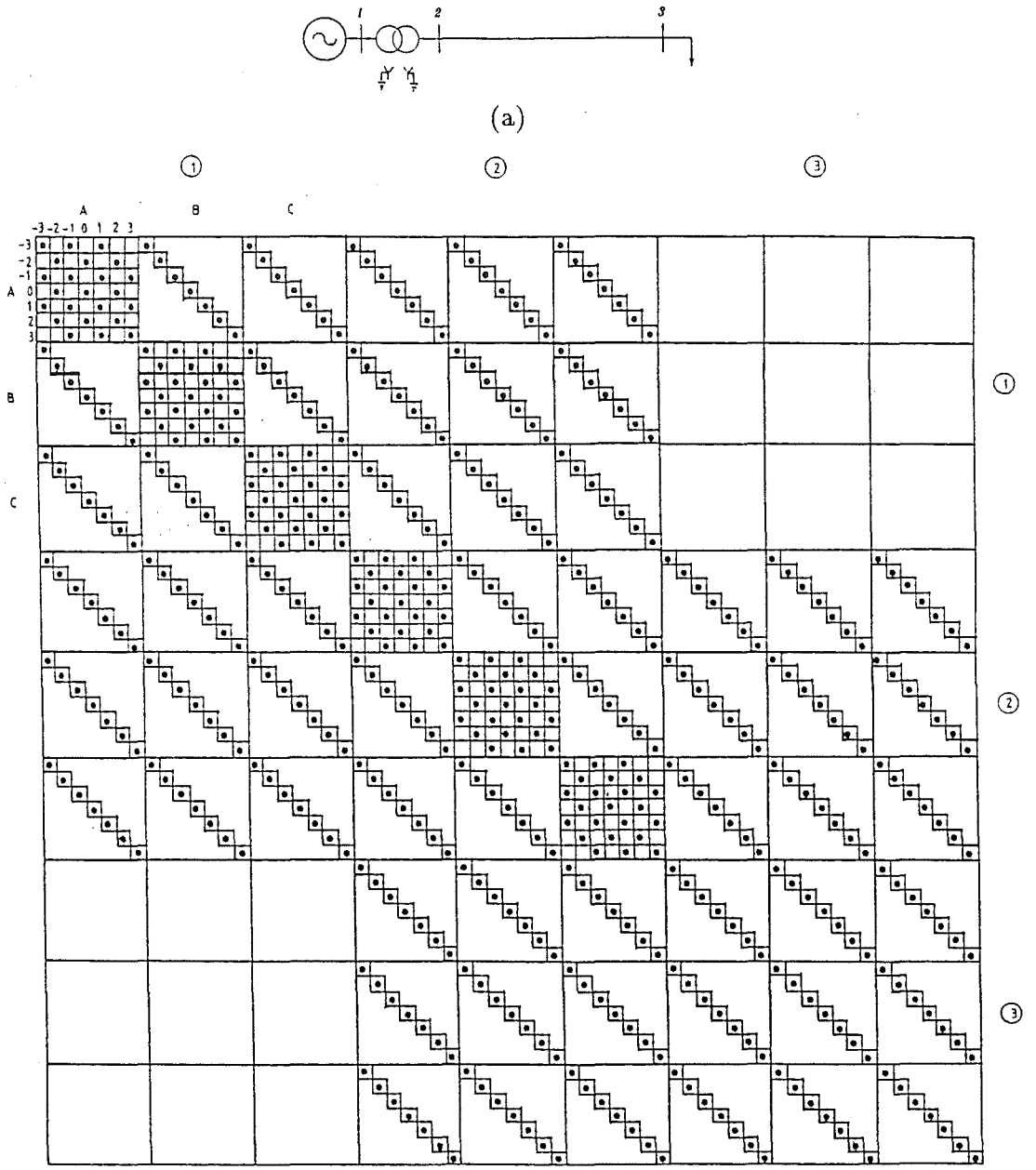

Figure 7-1: Structure of the Jacobian-admittance matrix corresponding to a radial system

7.3 A Unified Solution Of The Newton Type

The harmonic matrix equation (7.1) combines the linear and the linearized, non-linear components and, therefore, the solution process based on an iterative scheme becomes one of necessity. This implies a re-linearization of the non-linear components at each iterative step which may also be interpreted as a re-linearization of the entire system and, thus, finding the harmonic solution through a Newton-type procedure, where the admittance matrix of equation (7.1) play the role of a Jacobian. Once the iterative algorithm settles down to a solution all the harmonics in the network will be in balance.

This is not, however, a true Newton-Raphson algorithm because part of the network is already linear and also because of the practical need of considering only a limited number of harmonics. Moreover, because the network contains both voltage and current excitations, the harmonic Jacobian matrix needs to be inverted only partially.

One would expect all these factors to affect adversely the good convergence characteristics normally associated with the Newton-Raphson algorithm but, so far, the method has proved very reliable towards convergence requiring a reduced number of iterations to do so. Admittedly, the method has only been applied to the harmonic solution of a few networks and a full scale test has yet to take place.

It is also realized that the method, as it stands, can not be used in every-day applications and that sparsity techniques are to be included. An enormous amount of research has been done about the solution of sparse matrices over the last twenty years and, nowadays, it is considered a straightforward, though, time consuming exercise. However, the problem at hand imposes some additional restrictions because the nodal matrix has to be partially factorized only, and existing sparsity routines are of no use in this case.

It is interesting to observe that the iterative algorithm behaves reasonable well not only when the Jacobian matrix is evaluated at each iterative step, but also when the Jacobian matrix is single evaluated, i.e. this is done in the first iteration and then it is kept constant for the rest of the process. All the results presented in this chapter were obtained by using a single-evaluated Jacobian approach and, in every case, the harmonic solution was obtained in less than five iterations.

The harmonic solution of the network consists in solving equation (7.1) as many times as required until a change, between successive iterations, smaller than 0.001 per cent is observed for all the variables involved.

A three phase load flow provides the starting point for the harmonic solution. In this case, a sequential algorithm, based on a partial inversion and voltage and current injections, was used. After convergence the PQ loads are modelled as admittances which, for the purpose of the harmonic solution, are assumed to vary linearly with frequency.

By way of example, a ten bus system (including the internal busbars of the generators) which is part of the actual New Zealand grid is used as a benchmark [Densem 1983]. Above Roxburgh the rest of the network is ignored and the reduced system is shown in figure 7.2.

No load is assumed at Tiwai and the relevant data is given at Appendix F. The magnetizing characteristic of figure 2-12 has been assumed for each one of the transformers existing in the network.

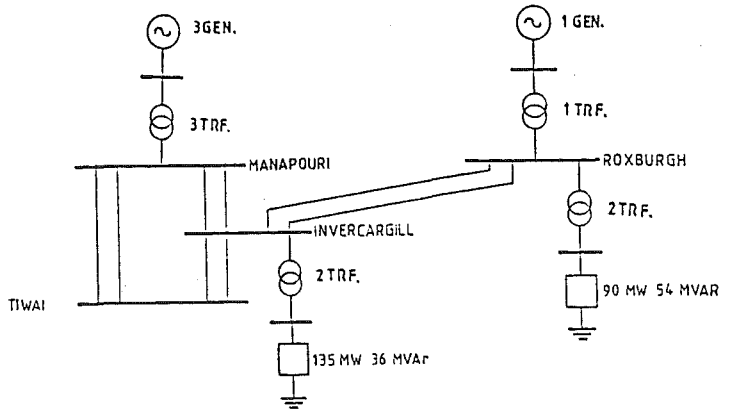

Figure 7.2: New Zealand grid below Roxburgh

It has been shown [Demsem 1983] that, when seen from Tiwai, the system of figure 7.2 contains a parallel resonance at a frequency laying somewhere between the fourth and the fifth harmonic frequency. This observation, of course, is not exclusive to Tiwai but, to a greater or lesser extent, to several of the nodes of the network. This can be verified by taking one node at the time in the Thevenin equivalent of equation (7.2).

Saturated transformers draw fifth harmonic current and it is expected that if any, or several, of the transformers existing in the network saturates, distorted voltage waves containing fifth harmonic will take place.

Table 7.3 Harmonic content of the voltage wave at Tiwai-220.

	Phase A	Phase B	Phase C
fundamental	$1.0159\ \angle -0.9^o$	$1.0172\ \angle 238.9^o$	$1.0142\ \angle 118.7^o$
third	$0.0162\ \angle -5.7^o$	$0.0156\ \angle -6.0^o$	$0.0159\ \angle -6.4^o$
fifth	$0.0507\ \angle 149.5^o$	$0.0656\ \angle -76.0^o$	$0.0526\ \angle 62.6^o$
seventh	$0.0186\ \angle 159.2^o$	$0.0100\ \angle 72.4^o$	$0.0125\ \angle -69.6^o$
ninth	$0.0069\ \angle -9.0^o$	$0.0068\ \angle -8.4^o$	$0.0073\ \angle -9.9^o$
eleventh	$0.0018\ \angle -157.1^o$	$0.0003\ \angle -64.7^o$	$0.0019\ \angle 40.3^o$
thirteenth	$0.0014\ \angle -18.7^o$	$0.0003\ \angle 244.7^o$	$0.0012\ \angle 82.7^o$

Due to the absence of load in Tiwai and also due to the Ferranti effect, the fundamental and harmonics voltages will be higher at this busbar and its harmonic content is given in table 7.3. The voltage waveforms are shown in figure 7.3 for the relevant busbars of the network.

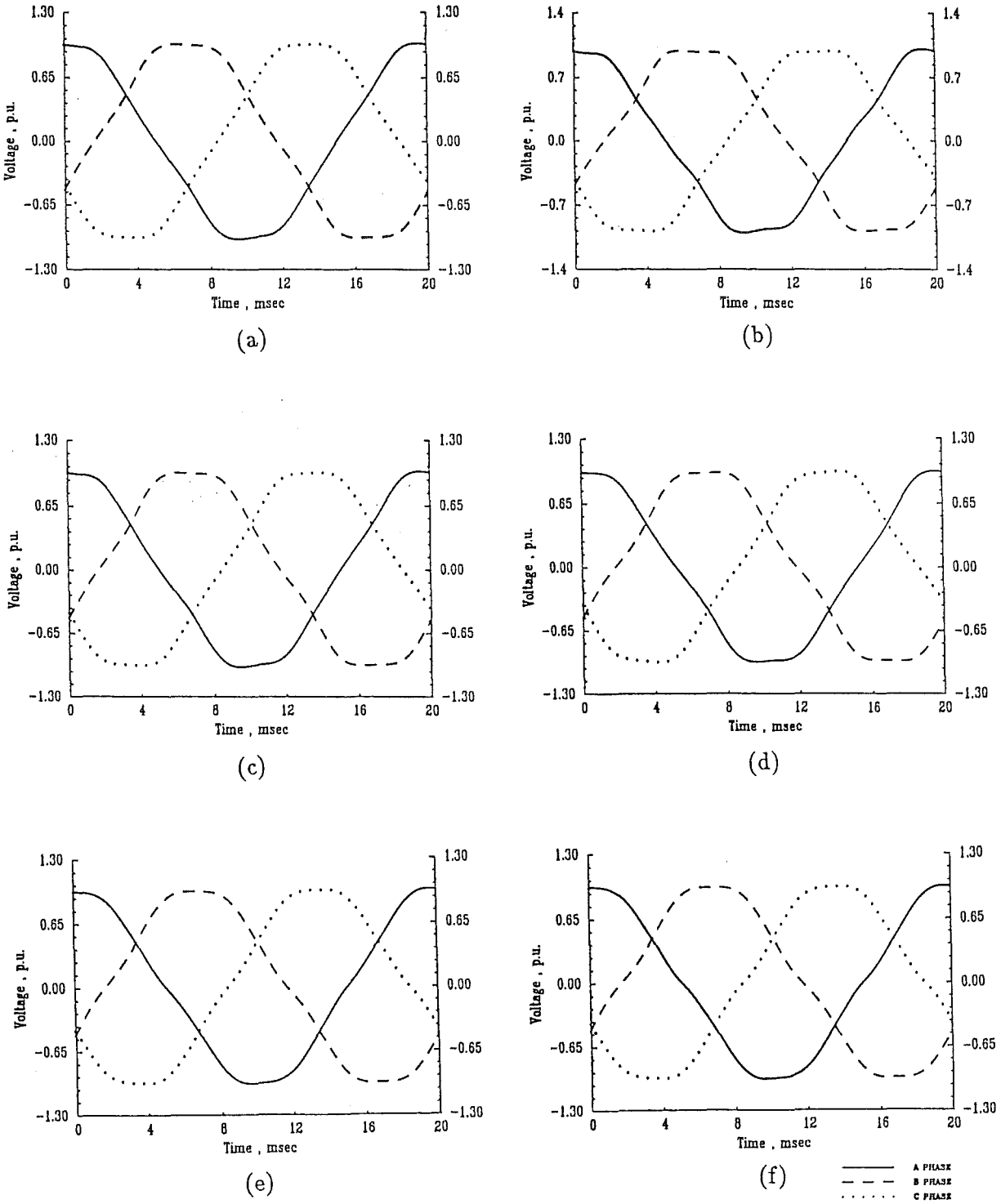

Figure 7-3: A full cycle of the voltage waveform existing at :
(a) Manapouri-014 (b) Manapouri-220 (c) Tiwai-220
(d) Invercargill-220 (e) Invercargill-033 (f) Roxburgh-220

7.4 Conclusions

A new and more general frame of reference suitable for the harmonic solution of power systems has been introduced. It is based on the concept of the complex-conjugate harmonic space and it allows a unified representation of all the busbars, phases, harmonics and cross-couplings between harmonics existing in the network. It is also a more general frame of reference than that provided by the phases.

The entire network, when modelled in the complex-conjugate harmonic space, may be interpreted as an harmonic Norton equivalent and because the associated admittance matrix is non-singular, a dual interpretation in the form of a Thevenin equivalent, also exists. Both representations are related to each other by a matrix inversion or, more efficiently, by a process of matrix factorization.

Framing non-linear components into the complex-conjugate harmonic space involves a linearization procedure for each non-linearity present in the network and the overall process could be seen a single linearization for the entire network. In most cases, the harmonic solution will require the network to be re-linearized several times, which implies an iterative solution through a Newton-type procedure.

A more efficient alternative, which also shows good reliability towards the convergence, is to keep constant the Jacobian-admittance matrix after it has been evaluated in the first iteration.

The new frame of reference has been used to obtain the harmonic solution of a portion of an actual 220 kV network containing several transformers and the results show that magnetizing harmonics may cause substantial voltage distortion in interconnected networks if a low order parallel resonance exists.

It is realized that the circuit under analysis is only a fraction of the New Zealand grid and, therefore, a parallel resonance at the fifth harmonic is not expected in the complete network neither the marked amount of distortion existing at the fifth harmonic for the circuit of figure 7-2.

Nevertheless, the results have practical significance because so far magnetizing harmonics in interconnected networks have received no attention and the general believe is that they cause no problems. However, the preliminary results shown in this chapter indicates that more analysis of this kind are needed to accurately determine the sources of harmonic distortion and, accordingly, to take appropriate measures.

Chapter 8

Conclusion

The harmonic distortion of the electrical waveform of power networks has reappered as a problem having practical significance and, accordingly, a great deal of effort has been devoted to its solution, worldwide.

Many contributions have appeared in the technical literature over the last ten years, however, no solution so far put forward copes with the problem satisfactorily in all its complexities.

The power network is multiphase and unbalanced, and the number of plant components capable of producing harmonic distortion is large and varied. Moreover, all non-linear plant components exhibit cross-couplings between harmonics. Traditional harmonic models and existing frames of reference have no provision for representing the later effect and, therefore, the development of a new generation of mathematical models for all the power plant components has been considered a priority.

In this research, as well as in contemporary research, it has been found that the harmonic space presents a convenient vehicle for the representation of the cross-couplings between harmonics. Other researchers have represented the synchronous generator and the static power converter in the harmonic space whereas this author has focused on magnetic non-linearities of the transformer type and also linear components.

To this end, a basic theory for the solution of harmonic problems has been developed and the mathematical analysis carried in this thesis shows the existence of several harmonic spaces. Among them are the real harmonic space, the complex harmonic space and also the more general complex-conjugate harmonic space, where the magnetizing branch of the transformer is better represented.

It has been shown that the resultant linearized equations may be interpreted as a harmonic Norton equivalent and that the linearization exercise could be seen as a Newton-Raphson procedure, where the matrix of magnetic admittances plays the role of a harmonic Jacobian. It has also been shown that linear components can be well represented in the complex-conjugate harmonic space as admittance matrices and that both linear and linearized, non-linear components can be represented together and solved in a unified, harmonic solution.

A more general model for the single phase transformer, in the form of a harmonic lattice equivalent circuit, has also been presented and this representation has been used to assemble harmonic models for three phase bank of transformers taking proper account of the electrical connection.

Also, a product of this research has been the development of a new and more general frame of reference, suitable for the harmonic solution of power system harmonics. It is based on the complex-conjugate harmonic space and allows a unified representation of all the busbars, phases, harmonics and cross-couplings between harmonics existing in the network. Furthermore, it presents a means for the iterative harmonic solution of the network through a Newton-type procedure.

A small, but realistic, three phase network containing several transformers has been represented in this new frame of reference and the results show that, contrary to the current thinking, magnetizing harmonics may cause unacceptable harmonic distortion of the voltage waveform.

Another important aspect of the harmonic problem that has received attention in this research

is the development of fast and accurate transmission line models that allows interactive harmonic analysis of the transmission line. This has been possible because the new model uses a transfer function approach rather than the equivalent-pi concept and also because new formulas have been found for the frequency dependent part which have shown to be the fastest today and yet keeping a high degree of accuracy.

The new transmission line model is also capable of modelling non-homogeneous transmission lines correctly and it has been applied to the solution of problems hitherto neglected, such as the effect of conventional VAR compensation and phase transpositions at harmonic frequencies. The results have shown that while both practices fulfil their duty at the fundamental frequency they may produce the opposite effect at harmonic frequencies. Moreover, by carrying analysis in the modal domain a better understanding of the effect that single and multiple set of transpositions have on the propagation of harmonics.

It is realized that the problem at hand is one of a very complicated nature and it was not expected that a single research project, such as the present one, could provide a final answer to it, however, there are hopes that positive elements have been incorporated into the knowledge of the problem of harmonics in power systems.

Chapter 9

References

[Aprille,Jr. and Trick 1972] T. J. Aprille,Jr. and T. N. Trick. A computer algorithm to determine the steady-state response of nonlinear oscillators. *IEEE Transactions on Circuit Theory*, CT-19(4):354–360, July 1972.

[Arrillaga 1981] J. Arrillaga. Harmonic monitoring. *Conference on harmonics in power systems*, 159–174, 1981. UMIST, Manchester.

[Arrillaga 1983] J. Arrillaga. *High voltage direct current transmission. IEE Power Engineering series 6*, Peter Peregrinus Ltd., London, UK, 1983.

[Arrillaga *et al.* 1983a] J. Arrillaga, C. P. Arnold, and B. J. Harker. *Computer modelling of electric Power systems.* John Wiley & Sons, London, 1983.

[Arrillaga *et al.* 1983b] J. Arrillaga, T. J. Densem, and B. J. Harker. Zero sequence harmonic current generation in transmission lines connected to large convertor plant. *IEEE Transactions on Power Apparatus and Systems*, PAS-102(7):2357–2363, July 1983.

[Arrillaga *et al.* 1986] J. Arrillaga, E. Acha, T. J. Densem, and P. S. Bodger. Ineffectiveness of transmission line transpositions at harmonic frequencies. *Proceedings IEE Part C*, 133(2):99–104, March 1986.

[Avila-Rosales and Semlyen 1985] J. Avila-Rosales and A. Semlyen. Iron core modeling for electrical transients. *IEEE Transactions on Power Apparatus and Systems*, PAS-104(11):3189, November 1985.

[Boon and Robey 1968] C. R. Boon and J. A. Robey. Effect of domain wall motion on power loss in grain-orientated silicon-iron sheet. *Proceedings IEE*, 115(10):1535–1540, October 1968.

[Bradley *et al.* 1985] D. A. Bradley, P. J. Morfee, and L. A. Wilson. The New Zealand harmonic legislation. *Proceedings IEE*, 132(4):177–184, July 1985.

[Brailsford and Fogg 1964] F. Brailsford and R. Fogg. Anomalous iron losses in cold-reduced grain-oriented transformer steel. *Proceedings IEE*, 11(8):1463–1467, August 1964.

[Brandão Faria and Borges da Silva 1986] J. A. Brandão Faria and J. F. Borges da Silva. Wave propagation in polyphase transmission lines a general solution to include cases where ordinary modal theory fails. *IEEE Transactions on Power Systems*, PWRD-1(2):182–189, April 1986.

[Breuer *et al.* 1982] G. B. Breuer, J. H. Chow, T. Gentile, and C. B. Lindh. HVDC-AC harmonic interaction - AC system harmonic model with comparisons of calculated and measured data. *IEEE Transactions on Power Apparatus and Systems*, PAS-101(3):709–718, March 1982.

[Calabro *et al.* 1986] S. Calabro, F. Coppadoro, and S. Crepaz. The measurement of the magnetization characteristics of large power transformers and reactors through D.C. excitation. *IEEE Transactions on Power Delivery*, PWRD-1(4):224, October 1986.

[Carson 1926] J. R. Carson. Wave propagation in overhead wires with ground return. *Bell System Technical Journal*, 539–554, October 1926.

[Chen and Dillon 1974] M. Chen and W. E. Dillon. Power system modeling. *Proceedings IEEE*, 62(7):901, July 1974.

[Clinker 1914] C. R. Clinker. Harmonic voltages and currents in Y- and Delta -connected transformers. *AIEE Transactions*, 33:723–733, 1914.

[de Carvalho 1983] M. A. de Carvalho. *Steady state representation of reactive compensators in HVDC convertor stations.* PhD thesis, The Victoria University of Mancester, University of Mancester Institute of Science and Technology (UMIST), September 1983.

[Densem 1983] T. J. Densem. *Three phase power system harmonic penetration.* PhD thesis, University of Canterbury, Christchurch, New Zealand, 1983.

[Densem *et al.* 1983] T. J. Densem, P. S. Bodger, and J. Arrillaga. Three phase transmission system modelling for harmonic penetration studies. In *IEEE Power Engineering Society Summer Meeting*, pages Paper No. 83SM444–7, Los Angeles, 1983.

[Deri *et al.* 1981] A. Deri, G. Tevan, A. Semlyen, and A. Castanheira. The complex ground return plane, simplified model for homogeneous and multi-layer earth return. In *PES Winter Meeting*, pages no. 81 WM 222–9, Atlanta, 1981.

[Dick and Watson 1981] E. P. Dick and W. Watson. Transformer models for transient studies based on field measurements. *IEEE Transactions on Power Apparatus and Systems*, PAS-100(1):409, January 1981.

[Director and Wayne 1976] S. W. Director and K. Wayne. Optimization of forced nonlinear periodic circuits. *IEEE Transactions on Circuits and Systems*, CAS-23(6):329, June 1976.

[Dommel 1969] H. W. Dommel. Digital computer solution of electromagnetic transients in single and multiphase networks. *IEEE Transactions on Power Apparatus and Systems*, PAS-88:388–399, April 1969.

[Dommel 1975] H. W. Dommel. Transformer models in simulation of electromagnetic transients. In *5th Power Systems Computation Conference*, page Paper No 3.1/4, Cambridge, England, September 1-5 1975.

[Dommel 1984] H. W. Dommel. Transmission line models for harmonic studies. In *International Conference on Harmonics in Power Systems, Worcester, Mass.*, pages 127–131, October 22-23 1984.

[Dommel 1985] H. W. Dommel. Overhead line parameters from harmonic formulas and computer programs. *IEEE Transactions on Power Apparatus and Systems*, PAS-104(2):366–372, February 1985.

[Dommel *et al.* 1983] H. W. Dommel, A. Yan, and R. J. O. de Marcano. Case studies for electromagnetic transients. Internal Report, Department of Electrical Engineering, University of British Columbia, Vancouver, Canada, May 1983.

[Dommel *et al.* 1986] H. W. Dommel, A. Yan, and S. Wei. Harmonics from transformer saturation. *IEEE Transactions on Power Apparatus and Systems*, PWRD-1(2):209–214, April 1986.

[Emanuel 1977] A. E. Emanuel. Energetical factors in power systems with non-linear loads. *Archiv für Elektrotechnik*, 59:183–189, 1977.

[Fortescue 1918] C. L. Fortescue. Method of symmetrical coordinates applied to the solution of ploy phase networks. *AIEE Transactions Part II*, 37:1027–1140, 1918.

[Galloway *et al.* 1964] R. H. Galloway, W. B. Shorrocks, and L. M. Wedepohl. Calculation of electrical parameters for short and long polyphase transmission lines. *Proceedings IEE*, 111(12):2051, December 1964.

[Gary 1976] C. Gary. Approche complète de la propagation multifilaire en haute fréquency par utilisation des matrices complexes. *E.D.F. Bulletin de la direction des études et recherches - Series B*, 4(3):5–20, 1976.

[Gauper *et al.* 1971] H. A. Gauper, J. D. Harnden, and A. M. McQuarrie. Power supply aspects of semiconductor equipment. *IEEE Spectrum*, 32–43, October 1971.

[Hale and Richardson 1953] J. W. Hale and F. R. Richardson. Mathematical description of core losses. *Transactions American Institute of Electrical Engineers Part I*, 72:495–501, 1953.

[IEEE Working Group 1974] IEEE Working Group. Discussion of electromagnetic effects of overhead lines. *IEEE Transactions on Power Apparatus and Systems*, PAS-93:900–901, May/June 1974.

[Iliceto and Cinieri 1977] F. Iliceto and E. Cinieri. Comparative analysis of series and shunt compensation schemes for AC transmission systems. *IEEE Transactions on Power Apparatus and Systems*, PAS-96(6):1819–1830, November/December 1977.

[Joint Conference on Inductive Interference 1914] Joint Conference on Inductive Interference. Report to the railroad commission of the state of California. *AIEE Transactions*, 33:1441–1508, 1914.

[Joint Conference on Inductive Interference 1915] Joint Conference on Inductive Interference. Progress of the investigation of inductive interference. *Transactions AIEE*, XXXIV(II):2113–2125, 1915.

[Jones 1974] K. M. Jones. AC system network control methods compensation. In *Symposium on Power System Dynamics, Control and Compensation*, IEE, IEE North Eastern Centre, Newcastle upon Tyne, 1974.

[Kennelly *et al.* 1915] A. E. Kennelly, F. A. Laws, and P. H. Pierce. Experimental researches on skin effect in conduction. *AIEE Transactions*, 34:1935–2018, 1915.

[King 1970] S. Y. King. Electromagnetic characteristics of isolated bundle conductors. *Proceedings IEE*, 117(4):753–760, 1970.

[Laughton 1968] M. A. Laughton. Analysis of unbalanced polyphase networks by the method of phase co-ordinates. *Proceedings IEE*, 115(8):1163–1172, August 1968.

[Lewis and Tuttle 1958] V. A. Lewis and P. D. Tuttle. The resistance and reactance of aluminium conductors steel reinforced. *AIEE Transactions*, PAS-77:1189–1215, 1958.

[Mahmoud and Shultz 1982] A. A. Mahmoud and R. D. Shultz. A method for analyzing harmonic distribution in AC power systems. *IEEE Transactions on power apparatus and systems*, PAS-101(6):1815–1823, June 1982.

[Mizuma *et al.* 1985a] T. Mizuma, Y. Sagisaka, K. Neri, and Y. Sekine. Harmonic analysis of synchronous machine with AC/DC converter: Part I, Harmonic voltage characteristics of AC/DC converter. *Electrical Engineering in Japan*, 105(3):71–79, March 1985.

[Mizuma *et al.* 1985b] T. Mizuma, Y. Sagisaka, K. Neri, and Y. Sekine. Harmonic analysis of synchronous machine with converter load: Part II. *Electrical Engineering in Japan*, 105(5):77–84, May 1985.

[Nakhla and Branin 1977] M. S. Nakhla and F. H. Branin. Determining the periodic response of nonlinear systems by a gradient method. *Circuit Theory and Applications*, 5:255–273, 1977.

[Nakhla and Vlach 1976] M. S. Nakhla and J. Vlach. A piecewise harmonic balance technique for determination of periodic response of nonlinear systems. *IEEE Transactions on Circuits and Systems*, CAS-23(2):85–91, February 1976.

[Nakra and Barton 1973] H. L. Nakra and T. H. Barton. Three phase transformer transients. In *PES Winter Meeting*, pages 1810–1819, IEEE Power Engineering Society, New York, November 26 1973.

[Naredo *et al.* 1987] J. L. Naredo, J. L. Silva, R. Romero, and P. Moreno. Application of approximated modal analysis methods for PLC system design. *IEEE Transactions on Power Delivery*, PWRD-2(1):57–63, January 1987.

[Olsen and Pankaskie 1983] R. G. Olsen and T. A. Pankaskie. On the exact, carson and image theories for wires at or above the earth's interface. *IEEE Transactions on Power Apparatus and Systems*, PAS-102(4):769–777, April 1983.

[Ovick and Kusic 1984] N. L. Ovick and G. L. Kusic. Including corona effects for travelling waves on transmission lines. *IEEE Transactions on Power Apparatus and Systems*, PAS-103(12):3643–3649, December 1984.

[Robinson 1966] G. H. Robinson. Harmonic phenomena associated with the Benmore-Haywards hvdc transmission scheme. *New Zealand Engineering*, 21(1):16–29, 1966.

[Semlyen and Abdel-Rahman 1982] A. Semlyen and M. H. Abdel-Rahman. Transmission line modelling by rational transfer functions. *IEEE Transactions on Power Apparatus and Systems*, PAS-101(9):3576–3584, September 1982.

[Semlyen and Deri 1985] A. Semlyen and A. Deri. Time domain modelling of frequency dependent three-phase transmission line impedance. *IEEE Transactions on Power Apparatus and Systems*, PAS-104(6):1549, June 1985.

[Semlyen *et al.* 1986] A. Semlyen, J. F. Eggleston, and J. Arrillaga. Admittance matrix model of a synchronous machine for harmonic analysis. *IEEE Summer Power Meeting, Mexico City*, SM 350-3(86), 1985.

[Semlyen *et al.* 1987a] A. Semlyen, E. Acha, and J. Arrillaga. Harmonic Norton equivalent for the magnetising branch of a transformer. *Proceedings IEE Part C*, 134(2):162–169, March 1987.

[Semlyen *et al.* 1987b] A. Semlyen, E. Acha, and J. Arrillaga. Newton-type algorithm for the harmonic analysis of non linear power circuits in periodical steady state with special reference to magnetic non-linearities. In *PES Winter Meeting*, IEEE Power Engineering Society, New Orleans, Louisiana, November 17 1987.

[Shipley and Coleman 1959] R. B. Shipley and D. Coleman. A new direct matrix inversion method. *AIEE Transactions Part I*, 78:568–572, November 1959.

[Silvester 1969] P. Silvester. Impedence of nonmagnetic overhead power transmission conductors. *IEEE Transactions on Power Apparatus and Systems*, PAS-88(5):731–737, 1969.

[Swift 1971] G. W. Swift. Power transformer core behaviour under transient conditions. In *PES winter meeting*, pages 2206–2210, IEEE Power Engineering Society, New York, N. Y., January 31-February 5 1971.

[Tevan and Déri 1984] G. Tevan and A. Déri. Some remarks about the accurate evaluation of the Carson integral for mutual impedance of lines with earth return. *Arkiv für Elektrotechnik*, 67:83–90, 1984.

[Wait and Spies 1969] J. R. Wait and K. P. Spies. On the image representation of the quasi-static fields of a line current source above the ground. *Canadian Journal of Physics*, 47:2731, 1969.

[Wait 1972] J. R. Wait. Theory of wave propagation along a thin wire parallel to an interface. *Radio Science*, 7:675–679, June 1972.

[Wedepohl and Efthymiadis 1978] L. M. Wedepohl and A. E. Efthymiadis. Wave propagation in transmission lines over lossy ground: a new, complete field solution. *Proceedings IEE*, 125(6):505–510, June 1978.

[Wedepohl 1963] L. M. Wedepohl. Application of matrix methods to the solution of travelling wave phenomena in poly-phase systems. *Proceedings IEE*, 110(12):2200–2212, 1963.

[Yacamini and De Oliveira 1980] R. Yacamini and J. C. De Oliveira. Harmonics in multiple converter systems: a generalized approach. *Proceedings IEE Part B*, 127(2):96–106, 1980.

[Yacamini 1981] R. Yacamini. Harmonics caused by transformer saturation. In *Harmonics in power systems*, UMIST, 1981.

[Yan 1986] A. Yan. Private communication. Department of Electrical Engineering, University of British Columbia, Vancouver, Canada, 1986.

[Zaborszky 1953] J. Zaborszky. Skin and spiralling effect in stranded conductors. *AIEE Transactions*, 72:599–603, 1953.

Appendix A

Data for a 500 kV Transmission Line

The 500 kV, three phase transmission line of flat configuration shown in figure A.1 has been used for most of the transmission line results presented in this thesis.

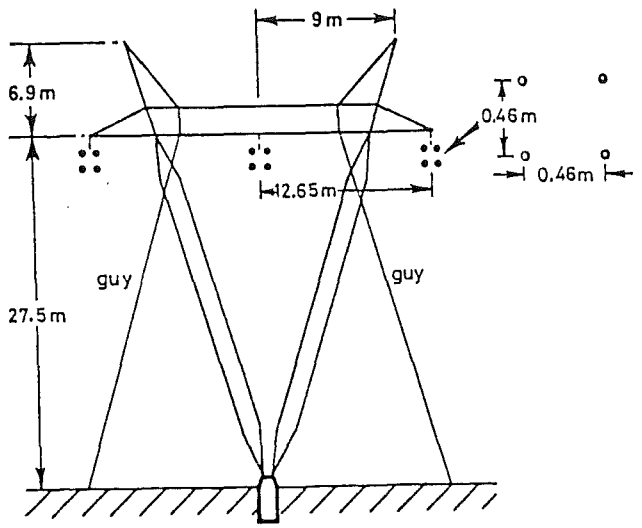

Figure A.1: Transmission line

Configuration without earth wires and the main parameters are:
Nominal voltage = 500 KV
Conductor type: Panther (30/3.00 + 7/3.00 ACSR)
Resistivity = 100Ω/m
Base power = 100 MVA
Base frequency = 50 Hz
Lumped parameters at 50 Hz:

$$[Z] = \begin{pmatrix} 0.0809 + j0.5383 & 0.0464 + j0.2733 & 0.0464 + j0.2297 \\ 0.0464 + j0.2733 & 0.0809 + j0.5383 & 0.0464 + j0.2733 \\ 0.0464 + j0.2297 & 0.0464 + j0.2733 & 0.0809 + j0.5383 \end{pmatrix} \Omega/km \tag{A.1}$$

$$[Y] = j \begin{pmatrix} 3.3544 & -0.8083 & -0.3044 \\ -0.8083 & 3.5215 & -0.8083 \\ -0.3044 & -0.8083 & 3.3544 \end{pmatrix} \mu S/km \tag{A.2}$$

and the natural impedance matrix

$$[Z_o] = \begin{pmatrix} 414.976 - j30.613 & 165.370 - j14.821 & 121.974 - j13.958 \\ 165.370 - j14.821 & 415.888 - j31.167 & 159.937 - j13.838 \\ 121.974 - j13.958 & 159.937 - j13.838 & 410.732 - j29.788 \end{pmatrix} \Omega \qquad \text{(A.3)}$$

Appendix B

Propagation of Voltage Waves in Lines Over Lossy Ground

B.1 Introduction

The characteristics of propagation and attenuation of the voltage waves travelling along a transmission line above ground depend heavily on the length of the line and the number of phases involved. The velocity of propagation of the voltage wave associated with a single line conductor will differ from those of a three phase transmission line of the same length, and so does its attenuation.

The analysis of the propagation of the voltage wave can be carried out in either the phase domain or the modal domain. Mutual couplings exist between the phases in the phase domain analysis and changes of voltage in one phase are functions of the changes of voltage in the other phases. In general, a complex interaction takes place which becomes more complicated as the number of phases increases. In the modal domain analysis, a number of modal voltage waves equal to the number of active conductors is assumed to exist. Each mode is independent of the others, with its own characteristics of propagation and attenuation.

In transmission circuits with more than one conductor, one of the modes will travel with a smaller velocity and higher attenuation than the rest. This is mainly due to ground penetration effects and is called the **ground mode**. In cases of a continuously transposed, three phase transmission line, the **ground mode** is also known as the **zero sequence component**.

The harmonic voltages of transmission lines with different number of phases are presented below together with an analysis of their characteristics of propagation and attenuation. The parameters used are based on the transmission line shown in appendix A.

B.2 Single Phase Lines

An equivalent positive sequence open circuit line is discussed first. It is expected to show a resonant peak at a harmonic order which is a function of both the length of the line and the fundamental frequency.

$$harmonic\ order = \frac{\lambda}{kl} \tag{B.1}$$

where λ is the wavelength for the fundamental frequency,
l is the length of the line and
k is equal to 2 when the excitation is produced by a current source and
is equal to 4 when the excitation is produced by a voltage source.

An alternating series of resonant and antirresonant peaks will also be present, with a regular span equal to the harmonic order given above. In the particular case of a line 500 km long and a fundamental frequency of 50 Hz, resonant peaks will be observed for the 3rd, 9th, 15th, 21th ... harmonics.

However, the answer provided by equation (B.1) is an idealized, theoretical harmonic order which, strictly, is valid only for voltage waves travelling with zero delay. In the case of a single phase above earth, the voltage wave travelling along it will be considerably retarded and attenuated , mainly because of earth penetration effects. Figure B.1 shows the harmonic voltage magnitude at the receiving end, up to the fifth harmonic, for a line conductor 500 km long when 1 p.u. voltage excitation is applied at the sending end. For this line conductor it is assumed that only one phase of the line given in Appendix A exists.

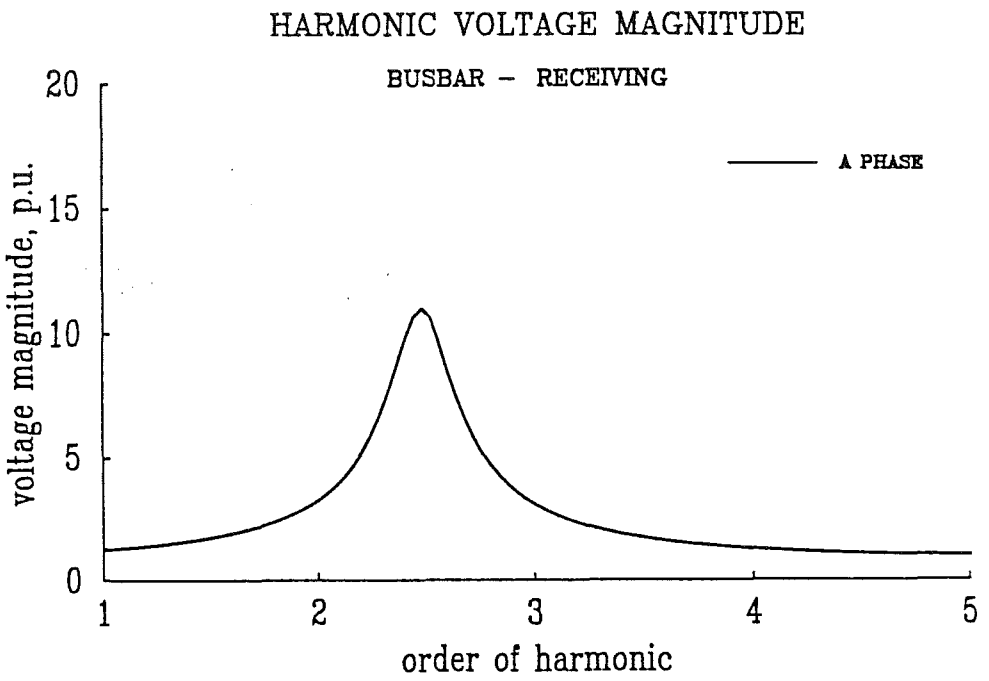

Figure B.1: Harmonic voltage magnitude for a single phase line above a lossy ground

From the above result it can be seen that the resonant peak has been shifted to the left of the expected theoretical harmonic order. Moreover, when compared with the corresponding peak of an equivalent positive sequence transmission line (not shown), it has also been reduced in magnitude, i.e. attenuated. In the terminology of modal analysis this circuit is said to contain one mode of propagation called the ground mode because of its relatively high attenuation and delay.

B.3 Double Phase Lines

Consider a transmission line 500 km long with two parallel conductors above earth and energized with a harmonic voltage source of

$$1 \angle 0^{o} \text{ and } 1 \angle 90^{o}$$

The harmonic voltage response is shown in figure B.2 . In this case, two adjacent phases of the three phase transmission line of Appendix A were used, with the third phase assumed not to exist.

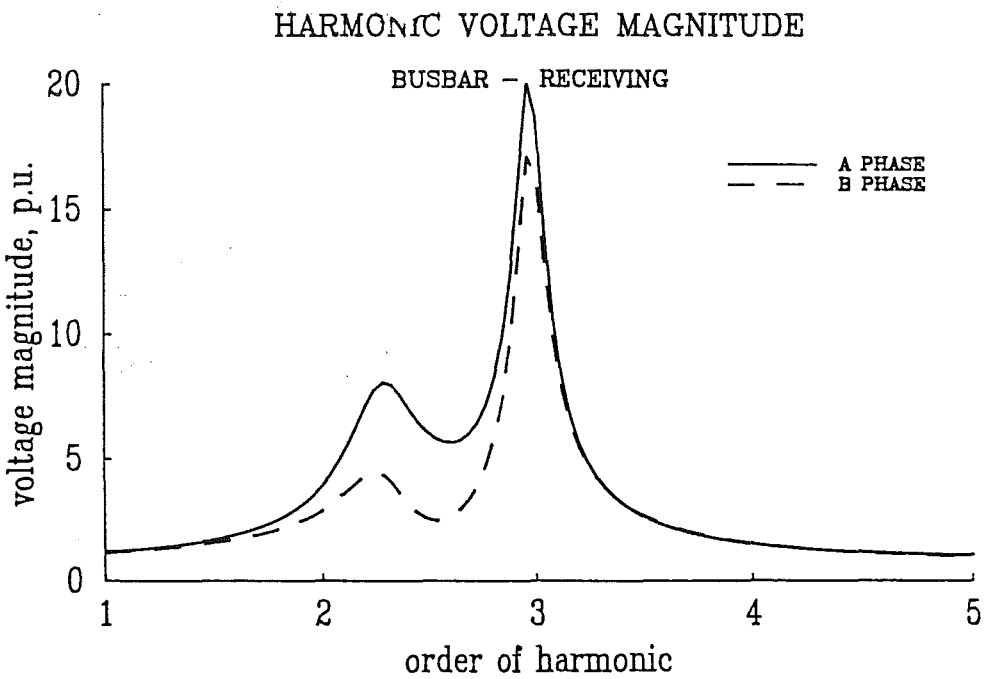

Figure B.2: Harmonic voltage magnitude for a double phase line above a lossy ground

The result shows twin resonant peaks, rather than the single peak associated with the circuit of a single phase. One of the twin peaks coincides with the theoretical harmonic order while the other shows a high degree of attenuation and appears well to the left of the other. There are two modes of propagation associated with two phase transmission circuits. One of them contains a high degree of attenuation while the other contains very little attenuation. The two modes resonate at different frequencies because of their different speeds of travel and this is the cause of the twin, resonant peaks shown by the two phase system.

B.4 Three Phase Lines

Figure B.3 shows the magnitude of the harmonic voltage for the three phases of the transmission line given in Appendix A. It is excited by a three phase harmonic voltage source of

$$1\angle 0^{o},\ 1\angle 240^{o} \text{ and } 1\angle 120^{o}$$

with the receiving end operating under no load.

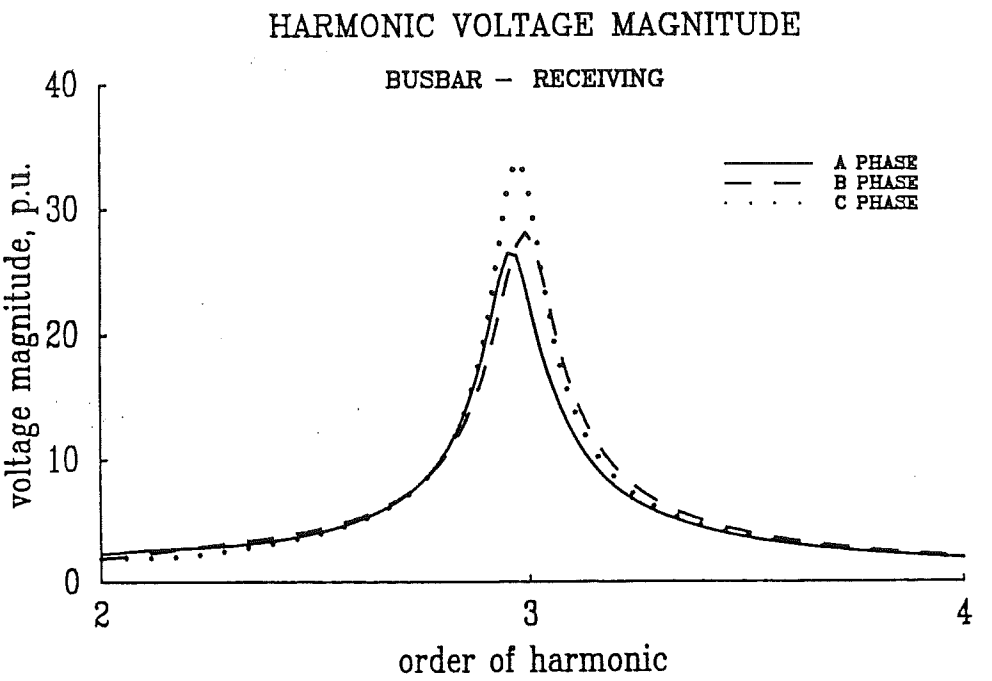

Figure B.3: Harmonic voltage magnitude for a three phase line above a lossy ground

In this case the response is smoother than the one presented by the two phase transmission circuit, and each phase has a single resonant peak in close proximity to the theoretical harmonic order, although some delay is present. Due to the larger number of mutual couplings, a stronger interaction exists between the voltage of the phases. This typical response suggests a more efficient form of transmission.

Three phase transmission lines contain three modes of propagation, one of them is the ground mode while the other two are line modes. They resonate at different frequencies, however, this effect is not apparent on the voltage wave of the phases because of the more robust mechanism of transmission. If specific information of the resonant frequencies of the modes is required, analysis in the modal domain must be pursued.

Figure B.4 shows the magnitude of the harmonic voltage response for the same transmission line discussed above, but when the harmonic voltage excitation applied is:

$1\angle 0^o$, $1\angle 0^o$ and $1\angle 0^o$

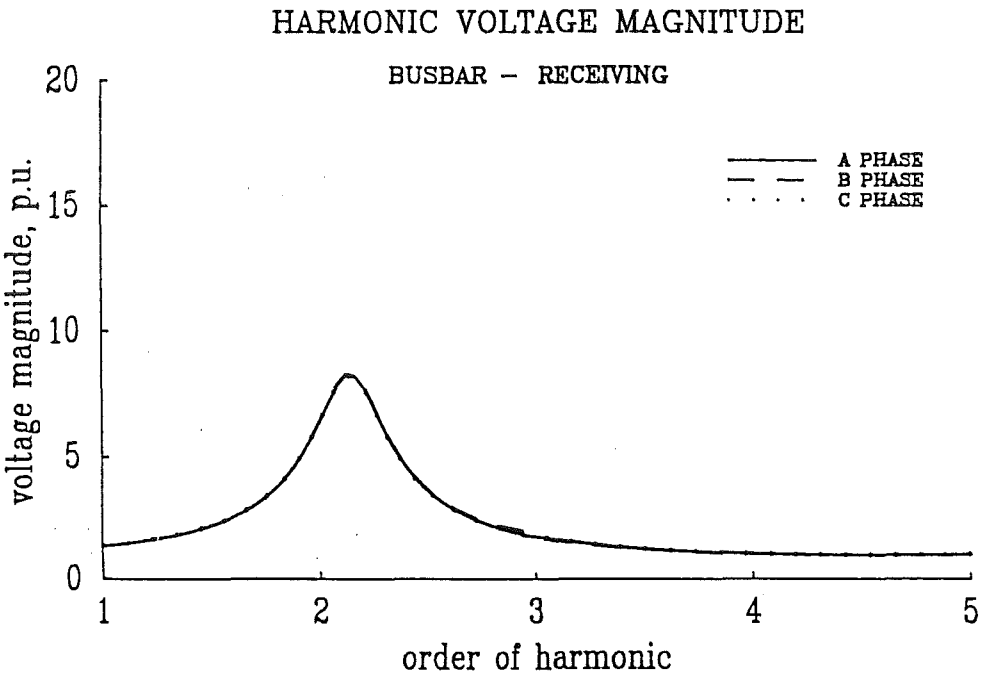

Figure B.4: Harmonic voltage magnitude for three single phase lines in parallel

This result is strikingly different from that presented in figure B.3, with the later case resembling more the behaviour of the single phase shown in figure B.1. Both cases relates to the same three phase transmission line and both results are correct. The reason for the difference in results lies in the excitation.

The case presented in figure B.3 corresponds to a full three phase transmission system whereas the case presented in figure B.4 corresponds to three single phase systems in parallel which explains the high attenuation and marked delay of the three voltage waves, which are almost **zero sequence** exclusively.

Appendix C

Transpositions: A Means for Creating Further Unbalances

C.1 Introduction

The conductor geometries of high voltage transmission lines produce considerable impedance asymmetry, which in turn causes corresponding voltage imbalance at the far end of the line and transpositions are often used in long distance transmission as a means of balancing the impedances of the line.

With the rapidly increasing numbers and ratings of static converters and thyristor-controlled compensators, the harmonic voltage and current levels present in high voltage transmission systems are growing considerably. It is thus important to assess the effect that conventional voltage balancing techniques have on the propagation of harmonics, particularly in long distance transmission lines.

There is practically no reference in the literature to the effect of line transpositions at harmonic frequencies. An early experimental attempt [Joint committee on electromagnetic interference 1915] made under very low voltage and relatively short distance, indicated that the balancing effect of the transpositions reduced considerably as the frequency increased.

In fundamental frequency studies the effect of transpositions is generally accounted for by averaging the lumped parameters of the transposed sections and using them in a single nominal or equivalent π-circuit. Such a method, however, assumes that the line geometry is perfectly symmetrical at all points, whereas the transpositions occur at discrete distances. In contrast, the method adopted in this research considers each transposed section as an independent subsystem and subsequently cascades the individual matrices to obtain an overall equivalent matrix.

A transmission line with a full set of transpositions included consists of three subsystems, as shown in figure C.1 where each section can be viewed as an equivalent π-circuit.

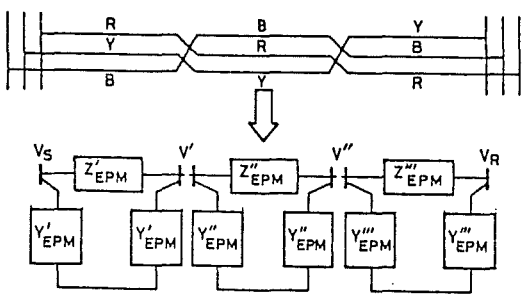

Figure C.1: Transposed line diagram and equivalent π sections

C.2 ABCD Transfer functions of transposed lines

The electrical distance increases with frequency and therefore long line effects must be included when modelling harmonic distortion. This requires the use of equivalent π circuits or transfer functions derived from the wave propagation equations [Bowman and Mc Namme 1964]. Moreover, the distributed parameters of these equivalent circuits must include their frequency dependence. Finally, the coupling between phases and parallel lines must be accurately represented.

The ABCD transfer function representation for the transposed line of figure C.1, is as follows:

$$\begin{pmatrix} V_S \\ I_S \end{pmatrix}_h = \begin{pmatrix} [A'] & [B'] \\ [C'] & [D'] \end{pmatrix}_h \times \begin{pmatrix} [A''] & [B''] \\ [C''] & [D''] \end{pmatrix}_h \times \begin{pmatrix} [A'''] & [B'''] \\ [C'''] & [D'''] \end{pmatrix}_h \begin{pmatrix} V_R \\ -I_R \end{pmatrix}_h$$

$$\begin{pmatrix} V_S \\ I_S \end{pmatrix}_h = \begin{pmatrix} [A] & [B] \\ [C] & [D] \end{pmatrix}_h \begin{pmatrix} V_R \\ -I_R \end{pmatrix}_h \tag{C.1}$$

where h is the harmonic order.

For the particular case of harmonic voltage excited open ended line shown in figure C.2 (a), equation (C.2) is of interest,

$$V_S = [A]V_R$$

$$V_R = [A]^{-1}V_S \tag{C.2}$$

while for the case of harmonic current excited short circuit ended line of figure C.2 (b), equation (C.3) applies,

$$0 = [A]V_R - [B]I_R$$

$$V_R = [A]^{-1}[B]I_R \tag{C.3}$$

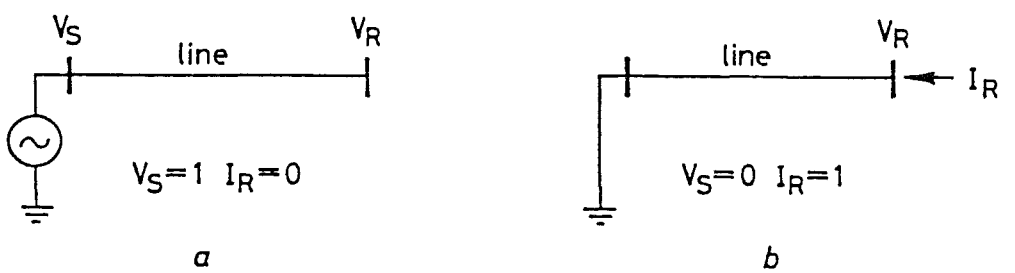

Figure C.2: Diagram of terminal conditions
(a) Voltage source and open ended line
(b) Current source and short-circuited line

The later case is likely to be of more practical interest because most of the non-linear power plant components acts as harmonic current sources, i.e. static converters and power transformers. However, balanced voltage excitations offers a better opportunity for assessing voltage unbalances at the far end of the line and, therefore, the only case considered in this appendix. A previous study [Arrillaga,Acha,Densem and Bodger 1986] considers current excitations and the effect of the load in addition to voltage excitations.

Equation (C.2), when expressed in the phase frame of reference, takes the form,

$$\begin{pmatrix} V_R^a \\ V_R^b \\ V_R^c \end{pmatrix}_h = \begin{pmatrix} a_{aa} & a_{ab} & a_{ac} \\ a_{ba} & a_{bb} & a_{bc} \\ a_{ca} & a_{cb} & a_{cc} \end{pmatrix}_h^{-1} \begin{pmatrix} V_S^a \\ V_S^b \\ V_S^c \end{pmatrix}_h \tag{C.4}$$

while, when expressed in the modal frame of reference, is

$$\begin{pmatrix} V_R^\alpha \\ V_R^\beta \\ V_R^0 \end{pmatrix}_h = \begin{pmatrix} \frac{1}{a_\alpha} & & \\ & \frac{1}{a_\beta} & \\ & & \frac{1}{a_0} \end{pmatrix}_h \begin{pmatrix} V_S^\alpha \\ V_S^\beta \\ V_S^0 \end{pmatrix}_h \tag{C.5}$$

C.3 Ineffectiveness of transpositions

The computer solution described in Chapter 6 has been used to calculate the harmonic voltages at the far end of a 500 kV line of flat configuration (details given in appendix A) fed from 1 p.u. voltage source at fundamental and harmonic frequencies.

It is realised that the presence of 1 p.u. harmonic voltage source is unrealistic, but such a figure provides a good reference for comparability between the effects at different frequencies. The expected harmonic voltage levels are likely to be 1-3 per cent of the fundamental and therefore the results plotted in later figures should be scaled down proportionally.

The fundamental frequency behaviour of the open ended line is illustrated in figure C-3 (a) and (b) for the line untransposed and transposed, respectively. In each case the receiving end voltages are plotted for line distances varying from 50 to 1500 km.

These figures indicate that in the absence of voltage compensation, the effectiveness of transpositions is limited to line distances under one eight of the wavelength (i.e. 750 km at 50 Hz). For distances approaching the quarter wavelength the transposed line produces considerably greater imbalance than the untransposed.

Although such transmission distances are impractical without compensation, the results provide some indication of the behaviour to be expected with shorter lines at harmonic frequencies. Such behaviour is exemplified in figure C.4 which corresponds to the case of a line excited by 1 p.u. third harmonic voltage. However, the results plotted in figure C.4, obtained at 50 km intervals, are not sufficiently discriminating around the points of resonance. Thus the region of resonant distances has been expanded in figure C.5 to illustrate more clearly the greatly increased imbalance caused by the transpositions. The resonant peaks of the three phases occur at very different distances, e.g. figure C.5 (b) shows 50 km diversity between the peaks. Therefore for a given line distance the resonant frequencies will vary,thus increasing the risk of a resonant condition.

The voltage wave travelling in a particular phase is function of the voltage waves travelling along the other phases and, accordingly, a complex relationship between the phase voltages will take place at the far end of the line.

Modal analysis, on the other hand, offers the possibility of analyzing independent circuits that, through linear combinations, fully reproduce the behaviour of the original circuit. Thus, using the frame of reference of the modes, a complementary analysis is presented below which provides further insight into the mechanism of imbalance associated with line transpositions.

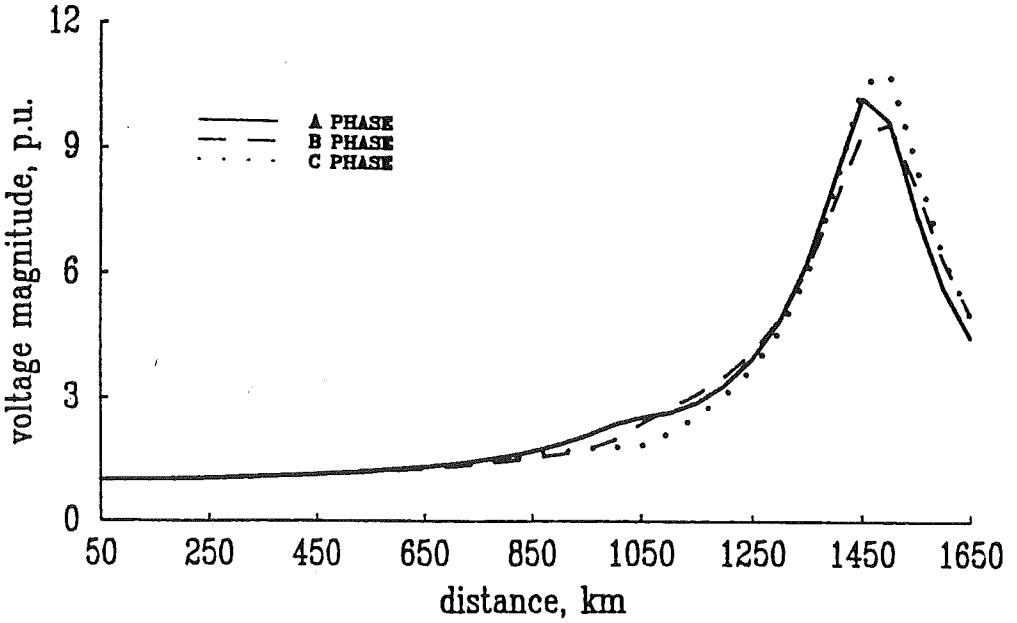

(a)

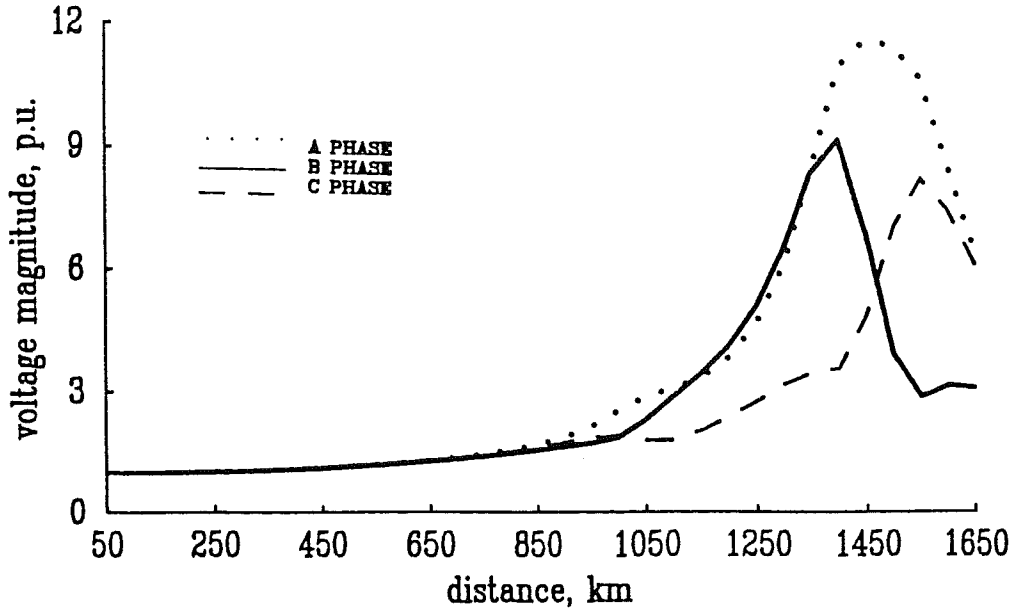

(b)

Figure C-3: Fundamental frequency three phase voltages at the end of the test line (open circuited) versus line distance
(a) With no transpositions (b) With transpositions

Three modes are associated with a three phase transmission line. Furthermore, each mode has its own speed of travel and attenuation characteristics and it is expected that they will resonate at different line lengths. This is shown in figures C-6 and C-7, where equivalent results to those of figures C-3 and C-5 are presented.

One of the modes, termed the ground or zero sequence mode, will travel with a reduced speed and higher attenuation than the rest, termed α and β or line modes. Moreover, it is expected that in a transmission line of flat configuration both the α and β modes will resonate at line distances of close vecinity. The above remarks are more or less well known facts and they are correct for the case of homogeneous lines. This is clearly shown in figures C-6 (a) and C-7 (a) for the fundamental and third harmonic voltages, respectively. The α and β modes resonate at line distances of about one quarter of the wave length, whereas the ground mode resonates at line distances of about one sixth of the wave length.

Unknown facts, however, concern modal propagation in non-homogeneous transmission lines, i.e. transposed lines, which have received no attention so far. figure C.6 (b) and C-7 (b) present results for the case when the transmission line has been transposed and it is shown that line transpositions leave unchanged the propagation characteristics of the ground mode. However, they have a marked effect on the propagation characteristics of the α and β modes, which resonate at very different line distances.

Phase voltages can be seen as linear combinations of modal voltages and the further apart the α and β modes resonate, the greater the unbalance in the phase voltages will be. Furthermore, a point to point comparison of the phase and modal results helps to explain the unbalances and the presence of twin resonant peaks taking place in the phase voltages.

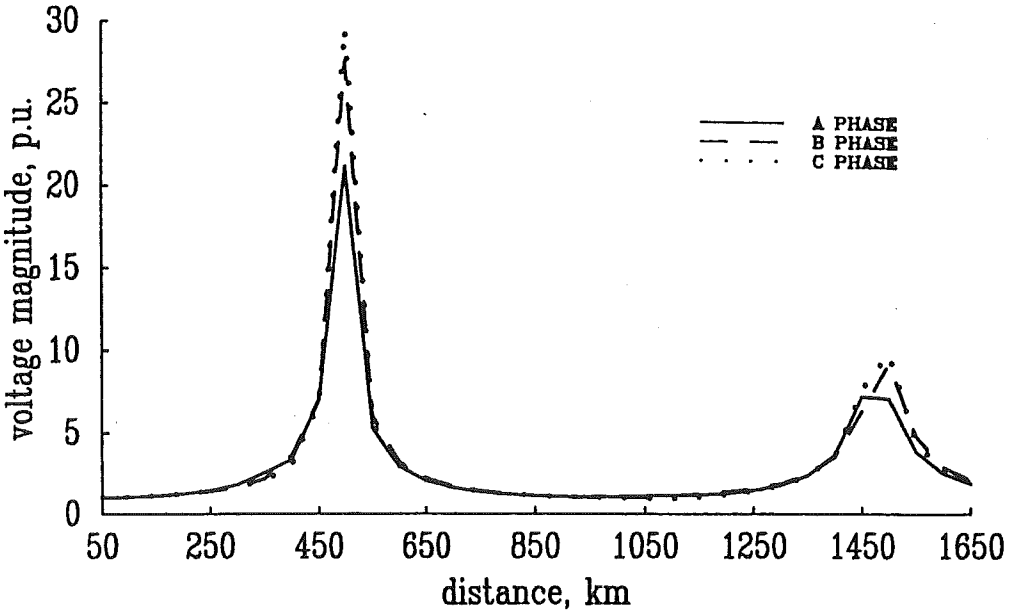

(a)

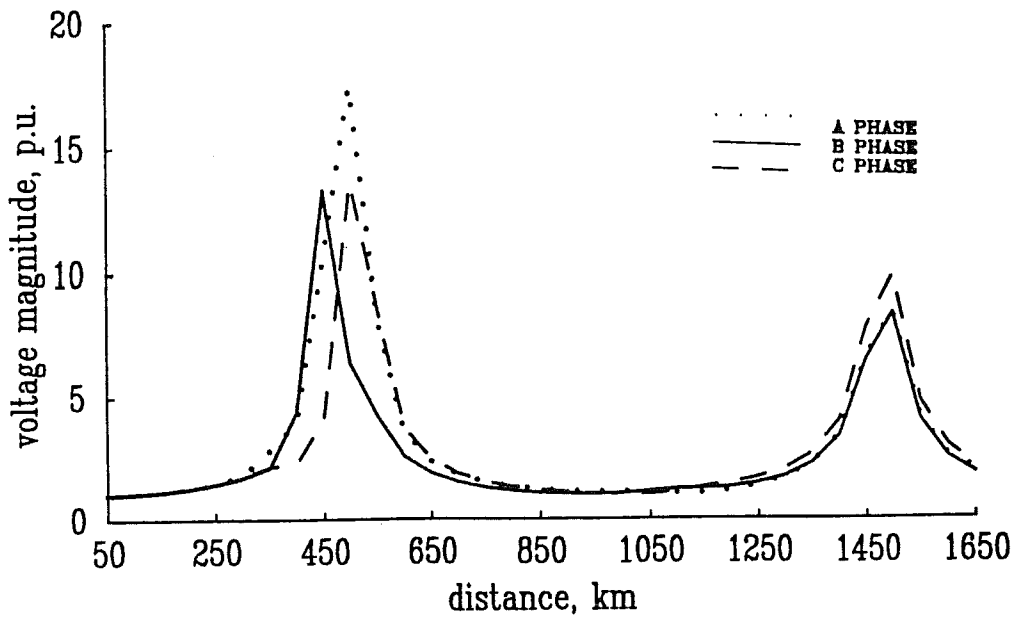

(b)

Figure C-4: Three phase third harmonic voltages at the end of the test line (open circuited) versus line distance
(a) With no transpositions (b) With transpositions

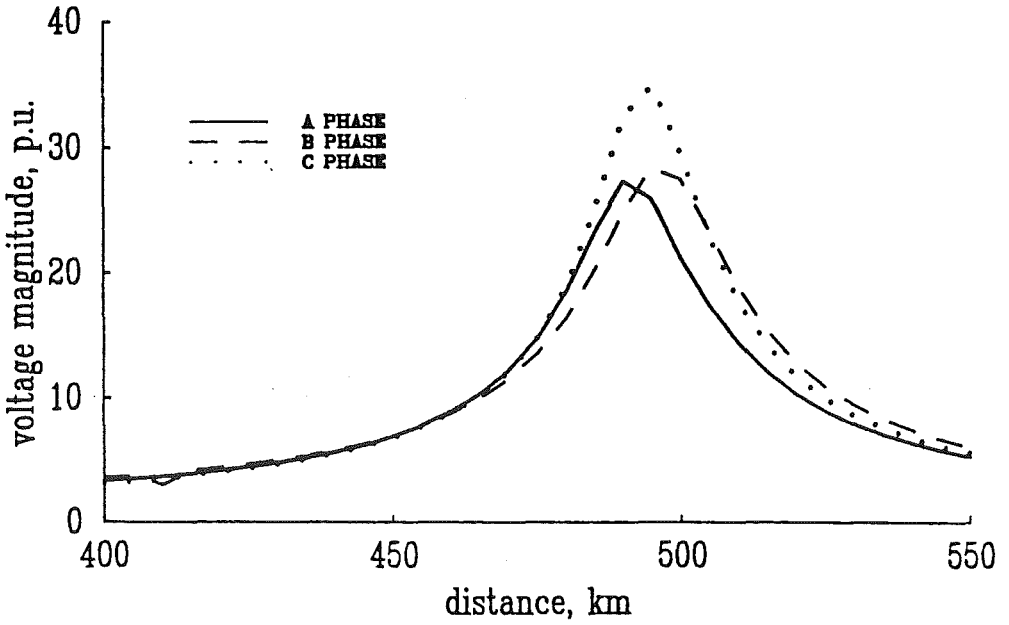

(a)

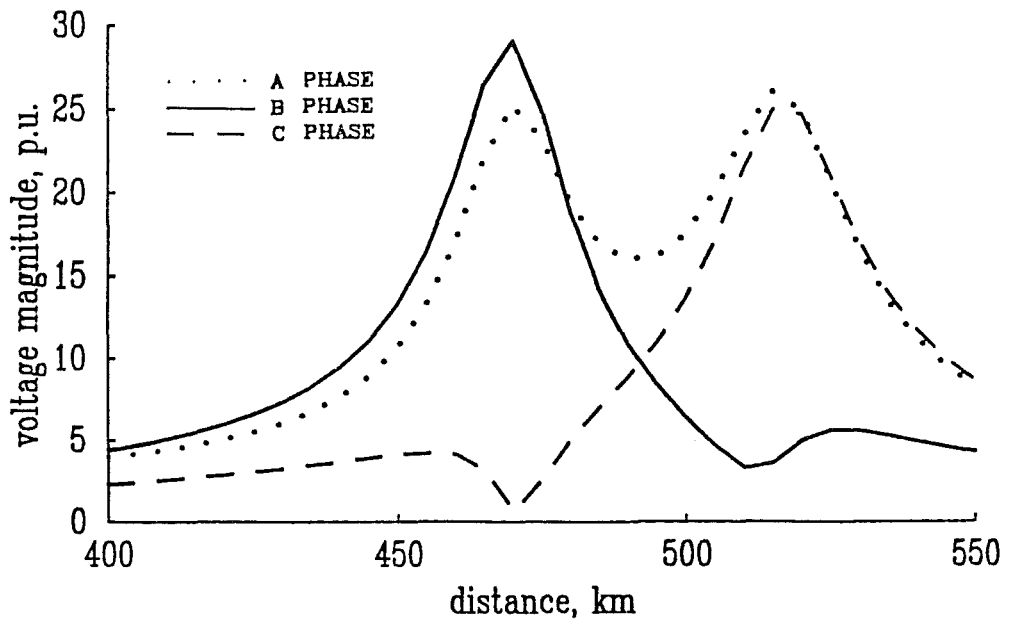

(b)

Figure C-5: Results of figure C-4 expanded at the region of resonance

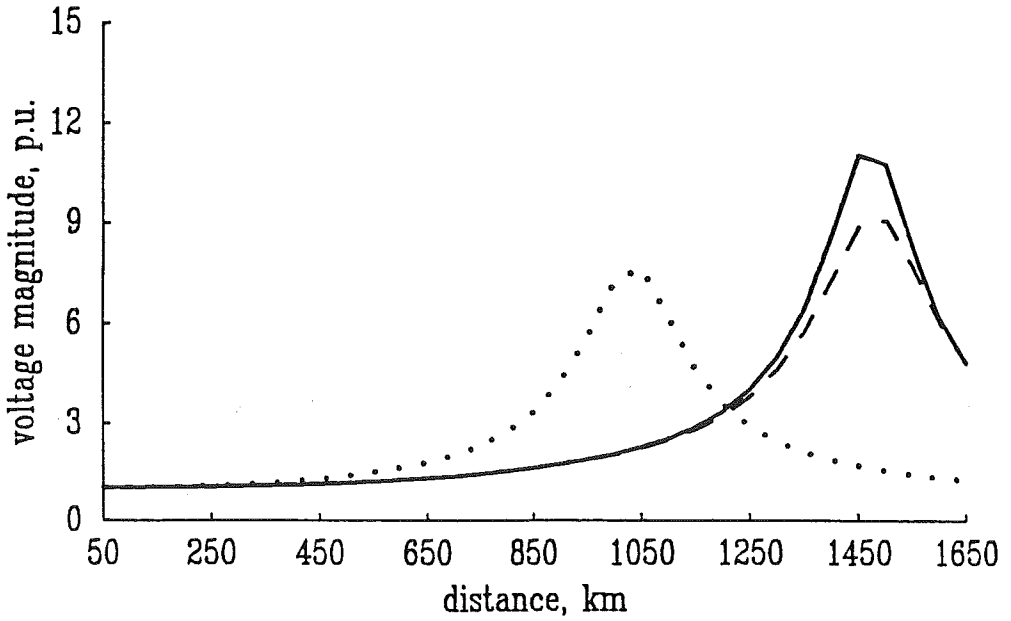

(a)

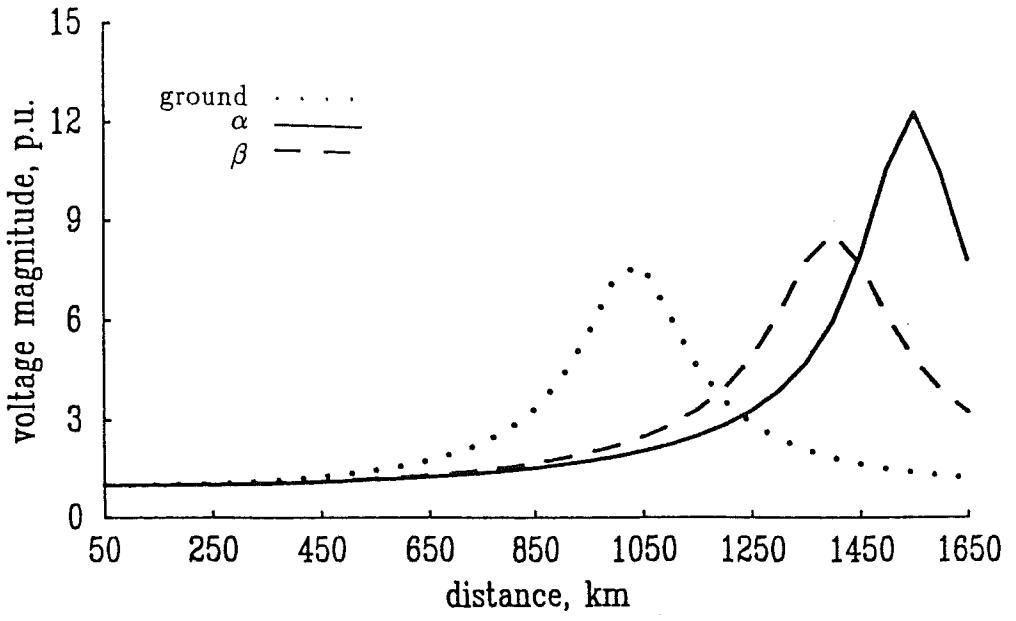

(b)

Figure C-6: Fundamental α, β and ground mode voltages at the end of the test line (open circuited) versus line distance (a) With no transpositions (b) With transpositions

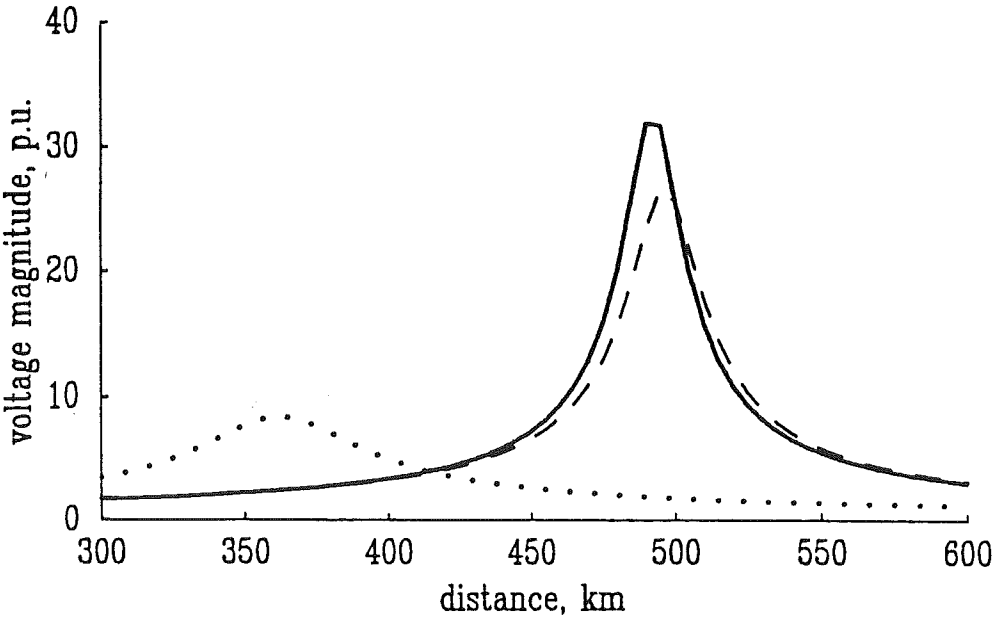

(a)

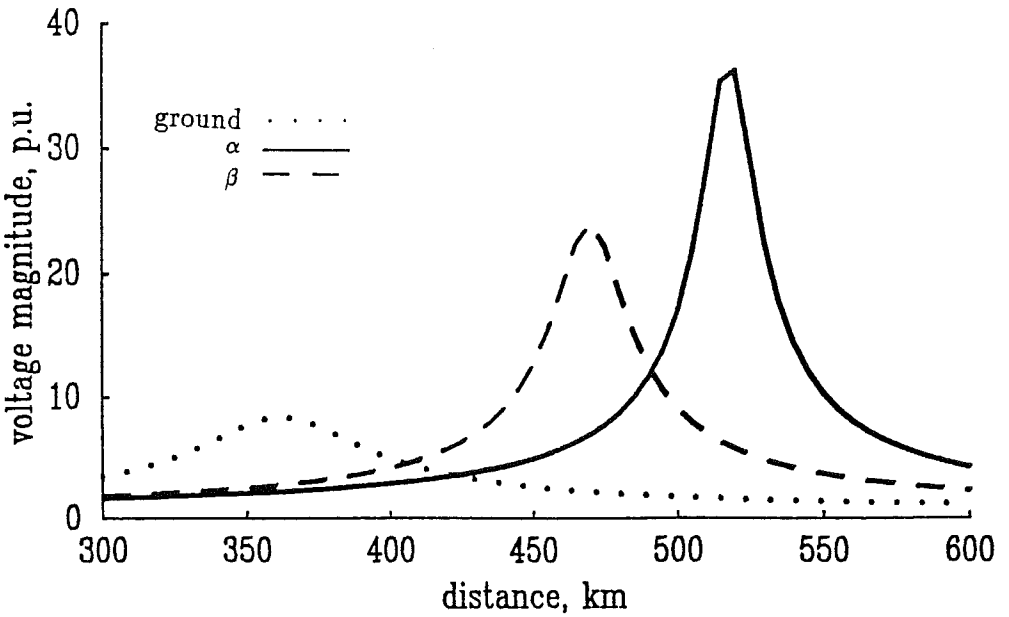

(b)

Figure C-7: Third harmonic α, β and ground mode voltages at the end of the test line (open circuited) versus line distance (a) With no transpositions (b) With transpositions

C.4 Multiple transpositions

The more practical situation under which transpositions are carried has been analyzed in the previous section and the results show that the effectiveness of transpositions are limited to short distances of the wave length and beyond one eight of the wave length introduces substantial adverse effects.

An observation of perhaps less practical nature but still of theoretical significance is the balancing effects that multiple set of transpositions impose upon the harmonic voltages. The reason being that the literature is plagued with mathematical derivations claiming to be valid for **transposed lines**, which is clearly inappropriate. Instead, they should be read to be valid for **continuously transposed lines** which, at harmonic frequencies, resembles more the untransposed than the transposed line. In general it is expected that the adverse effects introduced by a single set of transpositions beyond one eight of the wave length will be alleviated by increasing the number of transpositions. figure C.8 shows the fundamental modal voltages appearing at the far end of the line for the case when two full cycle of transpositions have been included, i.e. in each case the line has been broken down in six segments of equal length. This result adds weight to the observation that line transpositions do not alter the propagation characteristics of the ground mode but, rather, they have a profound effect in the propagation characteristics of the α and β modes, which have been shifted to resonate at line lengths of close vecinity and, therefore, more balanced phase voltages at the far end of the line are expected to result.

This trend will follow with the number of transpositions, however, an increasingly large number of them may be needed to balance the harmonic voltages as the harmonic order progresses. This is shown in figure C.9 for the case when the transmission line is 300 km long and includes no transpositions, one set, two sets and ten sets of transpositions, respectively.

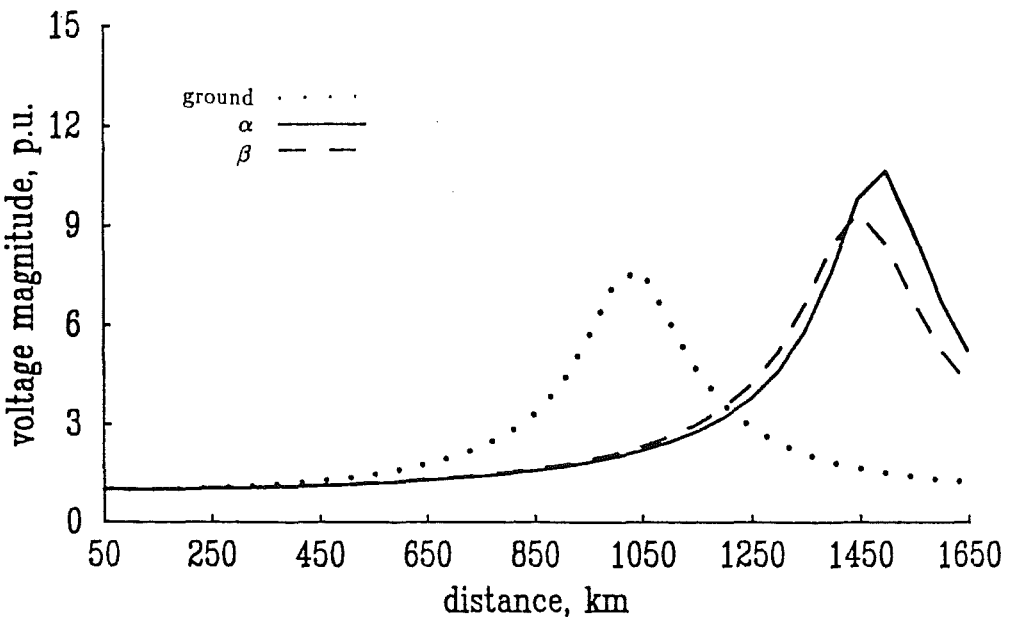

Figure C-8: Fundamental α, β and ground mode voltages at the end of the test line including two sets of transpositions

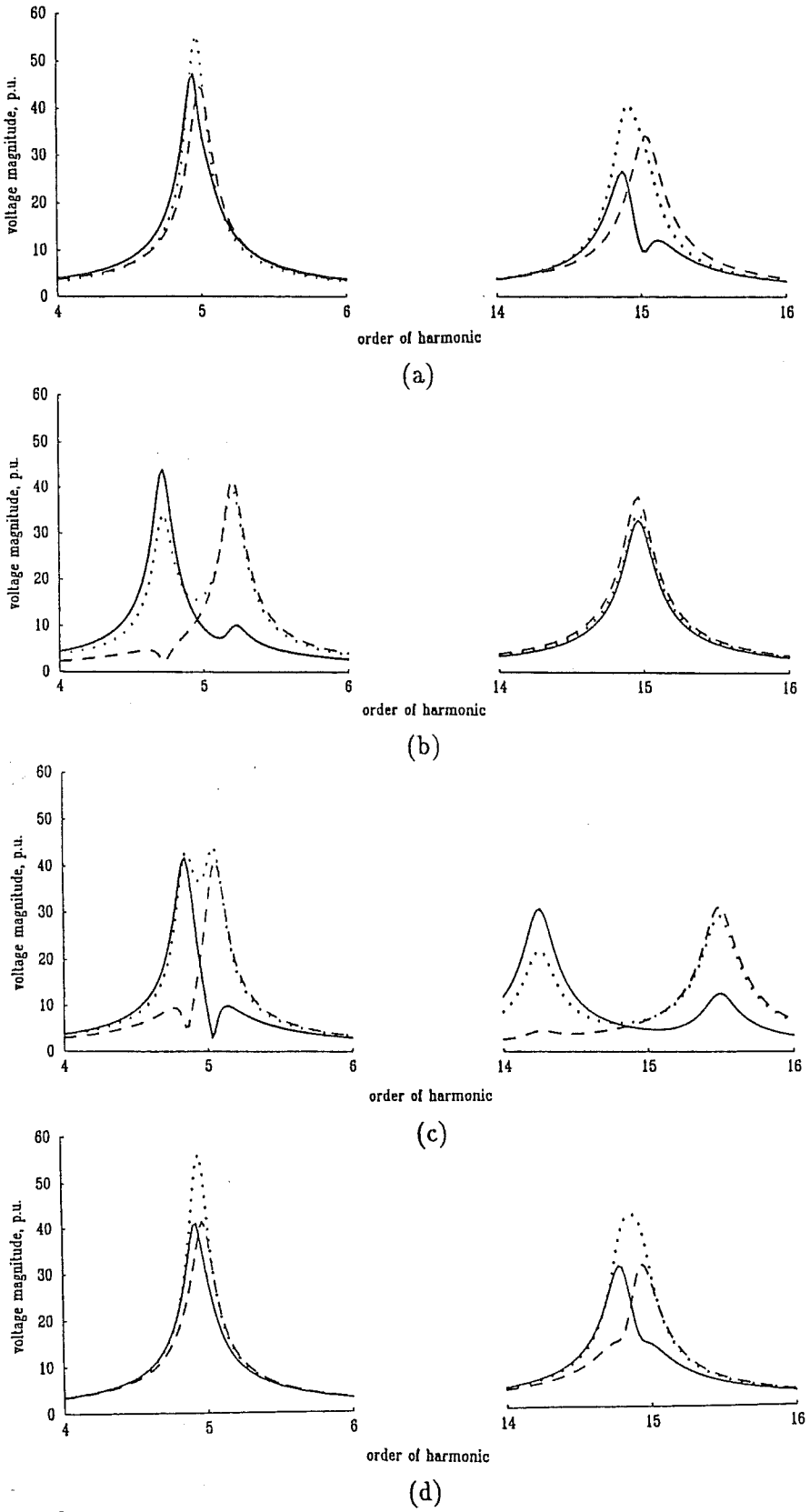

Figure C.9: First and second resonant peaks of a 300 km line with
(a) no transpositions
(b) one set of transpositions
(c) two sets of transpositions
(d) ten sets of transpositions

C.5 Compensated lines including transpositions

The realistic assessment of line transposition effects in long distance transmission requires the incorporation of VAR compensating plant, because transmission distances of one eight of the wave length are not practical without compensation.

In this section VAR compensating plant and line transpositions are combined together and applied to the solution of the lightly loaded case of the transmission system shown in figure 6-11. Under this operating conditions a single line is used to transmit 300 MW and two sets of shunt inductive compensation are included to provide 40 per cent shunt compensation.

Figure C.10 (a) presents the three phase voltages along the line for the fundamental and second harmonic of the untransposed transmission system, while figure C.10 (b) presents the case when the transmission system has been transposed. This result shows the balancing effects taking place at the fundamental voltage and, in contrast, the dramatic unbalance amplification occurring for the second harmonic.

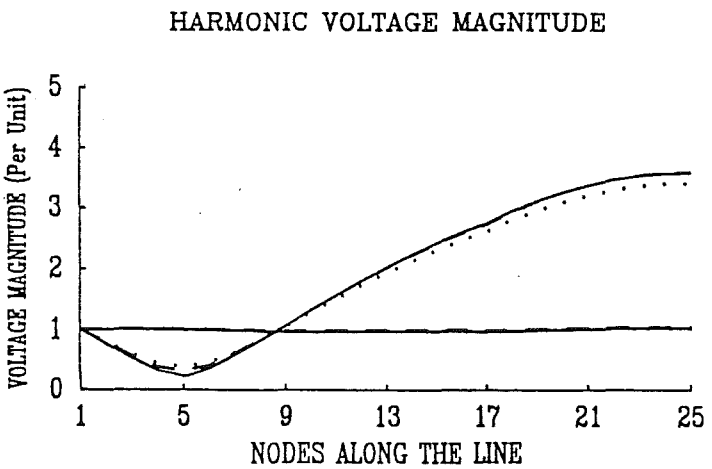

(a)

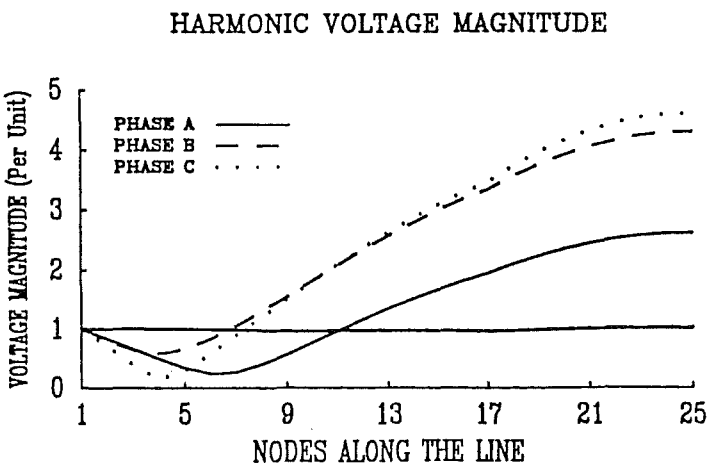

(b)

Figure C-10: Three phase voltages along the compensated line with (a) no transpositions (b) one set of transpositions

Appendix D

Closed Form Modal Analysis

The characteristic equation

$$([A] - \lambda[U])x = 0 \tag{D.1}$$

provides the foundations for the modal propagation theory, and the procedure involves the diagonalization of the matrix $[A] = [Z][Y]$.

The number of active conductors (phases) determines the order of the analysis, and for a three phase line the following characteristic polynomial exists,

$$\lambda^3 + p\lambda^2 + q\lambda + r = 0 \tag{D.2}$$

where $p = -(a_{11} + a_{22} + a_{33})$
$q = a_{11}a_{33} + a_{22}a_{33} + a_{11}a_{22} - a_{12}a21 - a_{13}a_{31} - a_{23}a_{32}$
$r = -(a_{11}a_{22}a_{33} + a_{12}a_{23}a_{31} + a_{13}a_{32}a_{21} - a_{31}a_{13}a_{22} - a_{32}a_{23}a_{11} - a_{21}a_{12}a_{33})$

while for the case of a DC link, the characteristic polynomial is,

$$\lambda^2 + q'\lambda + r' = 0 \tag{D.3}$$

where $p' = -(a_{11} + a_{22})$
$r' = a_{11}a_{22} - a_{12}a_{21}$

Both characteristic polynomials possess closed form solutions.

In the case of equation (D.2) the change of variable

$$\lambda = \zeta - \frac{p}{3}$$

is needed, so that

$$\zeta^3 + s\zeta + t = 0 \cdot \tag{D.4}$$

where $s = \frac{3q-p^2}{3}$

$t = \frac{2p^3-9pq+27r}{27}$

and the solution is,

$$\zeta_1 = S + T$$

$$\zeta_2 = \frac{-(S+T)}{2} + \frac{\sqrt{-3(S-T)}}{2}$$

$$\zeta_3 = \frac{-(S+T)}{2} - \frac{\sqrt{-3(S-T)}}{2}$$

where $S = (\frac{-t}{2} + \sqrt{\frac{t^2}{4} + \frac{s^3}{27}})^{\frac{1}{3}}$

$T = (\frac{-t}{2} - \sqrt{\frac{t^2}{4} + \frac{s^3}{27}})^{\frac{1}{3}}$

The solution for the characteristic polynomial (D.2) is,

$$\lambda_1 = S + T - \frac{s}{3}$$

$$\lambda_2 = \frac{-(S+T)}{2} + \sqrt{\frac{-3}{2}(S-T) - \frac{s}{3}}$$

$$\lambda_3 = \frac{-(S+T)}{2} - \sqrt{\frac{-3}{2}(S-T) - \frac{s}{3}}$$

The solution of the characteristic polynomial associated with the DC link ,equation (D.3), is a more straightforward procedure,

$$\lambda_1 = \frac{a_{11}+a_{22}}{2} + \frac{\sqrt{(a_{11}+a_{22})^2 - 4(a_{11}a_{22}-a_{12}a_{21})}}{2}$$

$$\lambda_2 = \frac{a_{11}+a_{22}}{2} - \frac{\sqrt{(a_{11}+a_{22})^2 - 4(a_{11}a_{22}-a_{12}a_{21})}}{2}$$

and for the case when conductors are located at the same height above ground, the previous solution is reduced to the well known expressions,

$$\lambda_1 = a_{11} + a_{12}$$

$$\lambda_2 = a_{11} - a_{12}$$

Once the eigenvalues $\lambda's$ have been determined the eigenvectors that diagonalize the matrix $[A]$ are found by substituting the $\lambda's$ into the characteristic equation (D.1).

For instance, by applying the above procedure to the matrix

$$[A] = \begin{pmatrix} 5 & 2 & 1 \\ 1 & 3 & 1 \\ 1 & 2 & 5 \end{pmatrix}$$

the following eigenvalues are obtained

$$\lambda_1 = 4, \lambda_2 = 2, \lambda_3 = 7$$

$$[T] = \begin{pmatrix} 1 & 1 & 2 \\ 0 & -2 & 1 \\ -1 & 1 & 2 \end{pmatrix}$$

Appendix E

Nodal Analysis

E.1 Introduction

The three phase transformer models presented in Chapter 5 may be obtained by a suitable combination of three harmonic lattice equivalent circuits or, alternatively, by using nodal transformations. The former approach has an intuitive appeal while the later has a more sounded mathematical basis. Both approaches should provide the answer.

The nodal analysis presented below is based on the use of a matrix of unconnected elements, termed primitive matrix, and nodal transformation matrices that relates the unconnected elements to the wanted connection. The mathematical derivations and transformation matrices for the most commonly used transformer connections are presented below.

E.2 Mathematical Derivations

The voltage and current relations existing in an unconnected circuit are,

$$I_\psi = [Y_{\psi\psi}]V_\psi \tag{E.1}$$

while the voltages and currents existing in the unconnected circuit and those existing in a connected circuit are,

$$V_\psi = [C_{\psi\alpha}]^t V_\alpha \tag{E.2}$$

$$I_\alpha = [C_{\alpha\psi}]I_\psi \tag{E.3}$$

Substituting equation (E.2) into equation (E.1),

$$I_\psi = [Y_{\psi\psi}][C_{\psi\alpha}]^t V_\alpha \tag{E.4}$$

and substituting equation (E.4) into equation (E.3),

$$I_\alpha = [C_{\alpha\psi}][Y_{\psi\psi}][C_{\psi\alpha}]^t V_\alpha \tag{E.5}$$

or

$$I_\alpha = [Y_{\alpha\alpha}]V_\alpha \tag{E.6}$$

where

$$Y_{\alpha\alpha} = [C_{\alpha\psi}][Y_{\psi\psi}][C_{\psi\alpha}]^t \tag{E.7}$$

E.3 Primitive Matrix

In this case the unconnected circuit consists of three single phase transformers, as shown in figure A.1. The magnetizing branch, represented by a Norton equivalent, has been halfed and placed it at both ends.

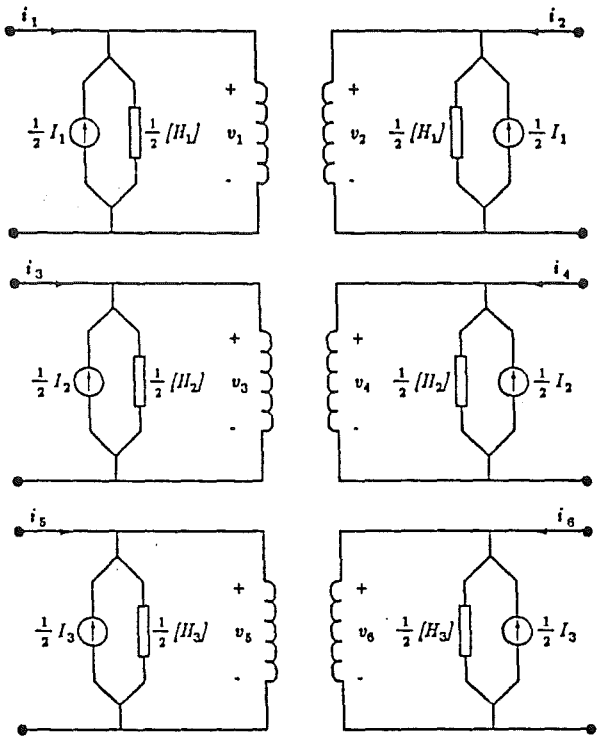

Figure E.1: Three unconnected single phase transformers

The primitive matrix equation for the circuit of figure A.1 is,

$$\begin{pmatrix} i_1+\frac{1}{2}I_{N1} \\ i_2+\frac{1}{2}I_{N1} \\ i_3+\frac{1}{2}I_{N2} \\ i_4+\frac{1}{2}I_{N2} \\ i_5+\frac{1}{2}I_{N3} \\ i_6+\frac{1}{2}I_{N3} \end{pmatrix} = \begin{pmatrix} \{Y_l\}+\frac{1}{2}[H]_1 & -\{Y_l\} & & & & \\ -\{Y_l\} & \{Y_l\}+\frac{1}{2}[H]_1 & & & & \\ & & \{Y_l\}+\frac{1}{2}[H]_2 & -\{Y_l\} & & \\ & & -\{Y_l\} & \{Y_l\}+\frac{1}{2}[H]_2 & & \\ & & & & \{Y_l\}+\frac{1}{2}[H]_3 & -\{Y_l\} \\ & & & & -\{Y_l\} & \{Y_l\}+\frac{1}{2}[H]_3 \end{pmatrix} \begin{pmatrix} v_1 \\ v_2 \\ v_3 \\ v_4 \\ v_5 \\ v_6 \end{pmatrix} \tag{E.8}$$

E.4 Grounded Star : Grounded Star Connection

Figure A.2 shows the case when both the primary and the secondary sides of the three phase transformer are grounded star connected,

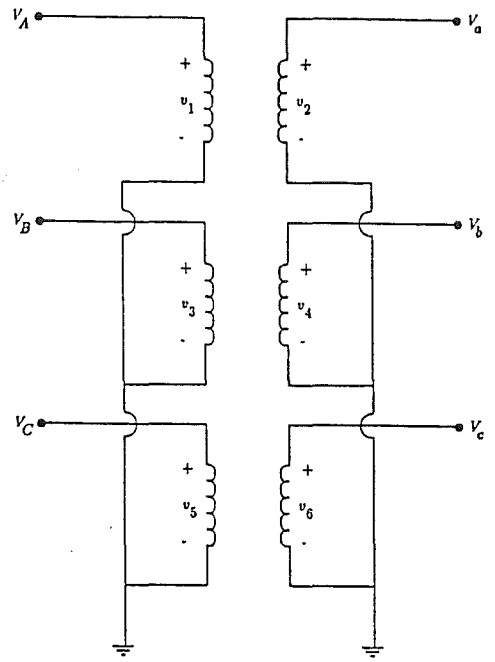

Figure E.2: Grounded star : grounded star connection

and equation (E.9) gives the transformation that relates the voltages existing in the unconnected transformers to the voltages existing in a three phase transformer having both neutrals solidly earthed.

$$\begin{pmatrix} v_1 \\ v_2 \\ v_3 \\ v_4 \\ v_5 \\ v_6 \end{pmatrix} = \begin{pmatrix} 1 & & & & & \\ & 1 & & & & \\ & & 1 & & & \\ & & & 1 & & \\ & & & & 1 & \\ & & & & & 1 \end{pmatrix} \begin{pmatrix} V_A \\ V_a \\ V_B \\ V_b \\ V_C \\ V_c \end{pmatrix} \tag{E.9}$$

E.5 Star : Star Connection

Figure E.3 shows the case when both the primary and the secondary sides of the three phase transformer are star connected but with unearthed neutrals

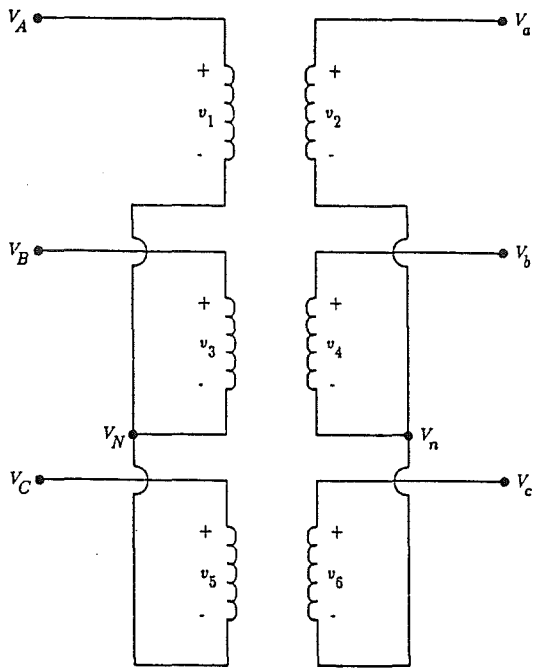

Figure E.3: Star : star connection

and the transformation matrix equation is given in (E.10).

$$\begin{pmatrix} v_1 \\ v_2 \\ v_3 \\ v_4 \\ v_5 \\ v_6 \end{pmatrix} = \begin{pmatrix} 1 & & & & -1 & \\ & 1 & & & & -1 \\ & & 1 & & -1 & \\ & & & 1 & & -1 \\ & & & & 1 & -1 \\ & & & & & -1 \end{pmatrix} \begin{pmatrix} V_A \\ V_a \\ V_B \\ V_b \\ V_C \\ V_c \\ V_N \\ V_n \end{pmatrix} \tag{E.10}$$

E.6 Delta : Delta Connection

Figure E.4 shows the case when both the primary and the secondary sides of the three phase transformer are delta connected

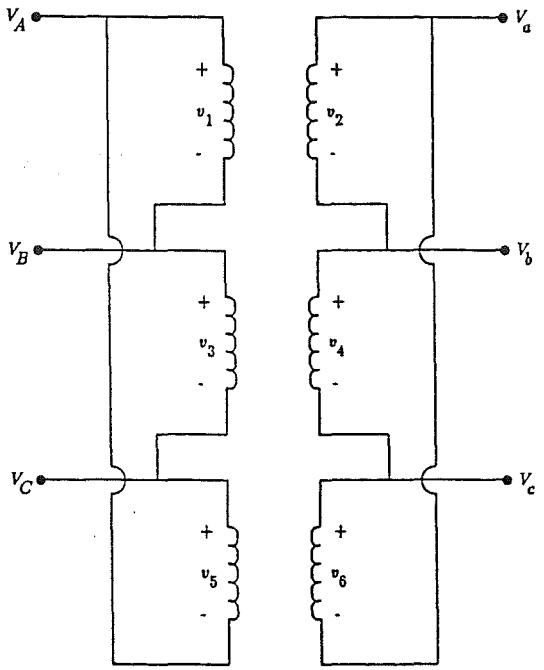

Figure E.4: Delta : delta connection

and the transformation matrix equation is given in (E.11).

$$\begin{pmatrix} v_1 \\ v_2 \\ v_3 \\ v_4 \\ v_5 \\ v_6 \end{pmatrix} = \begin{pmatrix} 1 & & -1 & & & \\ & 1 & & -1 & & \\ & & 1 & & -1 & \\ & & & 1 & & -1 \\ -1 & & & & 1 & \\ & -1 & & & & 1 \end{pmatrix} \begin{pmatrix} V_A \\ V_a \\ V_B \\ V_b \\ V_C \\ V_c \end{pmatrix} \tag{E.11}$$

E.7 Grounded star : Delta Connection

Figure E.5 shows the case when both the primary side has a grounded star connection while the secondary side has a delta connection

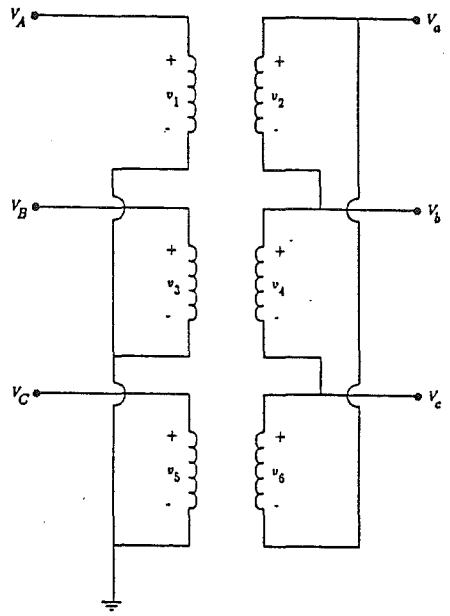

Figure E.5: Grounded star : delta connection

and the transformation matrix equation is given in (E.12).

$$\begin{pmatrix} v_1 \\ v_2 \\ v_3 \\ v_4 \\ v_5 \\ v_6 \end{pmatrix} = \begin{pmatrix} 1 & & & & & \\ & & 1 & -1 & & \\ & 1 & & & & \\ & & & 1 & -1 & \\ & & 1 & & & \\ & & & -1 & & 1 \end{pmatrix} \begin{pmatrix} V_A \\ V_a \\ V_B \\ V_b \\ V_C \\ V_c \end{pmatrix} \tag{E.12}$$

Appendix F

Data for the Reduced System of the South Island

The relevant information for the three phase network [Densem,1983] used in Chapter 7 is as follows:

Transmission Lines(earth resistivity equal to 100 Ohms-mt):

The phase conductors of the first three transmission lines presented below are arranged in a double circuit configuration and they are symmetricaly placed around the vertical axis of the tower. There are two conductors per phase and the coordinates, taken from the center of the tower and the ground level, are given for one of the circuits.

Invercargo220-Manapouri220 :

The length of the line is 152.9 km and the conductor type is GOAT (30/3.71 + 7/3.71 ACSR) There is also one earth-wire (7/3.05 Gehss).

Phase a	4.80 mt , 12.50 mt
Phase b	6.34 mt , 18.00 mt
Phase c	4.42 mt , 23.50 mt
Earth-wire	0.00 mt , 29.00 mt

Manapouri220-Tiwai220 :

The length of the line is 175.60 km, otherwise, it is taken to be identical to the line Invercargo220-Manapouri220.

Invercargo220-Tiwai220 :

The length of the line is 24.3 km and the conductor type is GOAT (30/3.71 + 7/3.71 ACSR) There are also two earth-wire (7/3.05 Alumoweld).

Phase a	4.77 mt , 12.50 mt
Phase b	6.29 mt , 17.95 mt
Phase c	4.41 mt , 23.41 mt
Earth-wire	1.52 mt , 28.26 mt

The next transmission line consists of two single-circuit lines of flat configuration having one conductor per phase. The coordinates taken from the extreme left conductor and the ground level, are given for the two circuits.

Invercargo220-Roxburgh220 :

The length of the line is 131 km and the conductor type is Zebra (54/3.18 + 7/3.18 ACSR). The circuit number one contains two earth-wires (7/3.18 Gehss).

Circuit one

Phase a	0.00 mt , 12.50 mt
Phase b	6.47 mt , 12.50 mt
Phase c	12.94 mt , 12.50 mt
Earth-wire	1.86 mt , 18.41 mt
Earth-wire	11.08 mt , 18.41 mt

Circuit two

Phase a	22.94 mt , 12.50 mt
Phase b	30.14 mt , 12.50 mt
Phase c	37.34 mt , 12.50 mt

Generators.

Manapouri1014	$X''_d = 0.0370$ $X''_0 = 0.0197$
Manapouri2014	$X''_d = 0.1480$ $X''_0 = 0.0788$
Manapouri3014	$X''_d = 0.1480$ $X''_0 = 0.0788$
Roxburgh1011	$X''_d = 0.0620$ $X''_0 = 0.0323$

Transformers.

Manapouri220 Manapouri1014	$X_1 = 0.0269$
Manapouri220 Manapouri2014	$X_1 = 0.1072$
Manapouri220 Manapouri3014	$X_1 = 0.1072$
Invercarg033 Invergcarg220	$X_1 = 0.1029$
Invercarg033 Invergcarg220	$X_1 = 0.1029$
Roxburgh-220 Roxburgh1011	$X_1 = 0.0382$
Roxburgh-011 Roxburgh-220	$X_1 = 0.7632$
Roxburgh-011 Roxburgh-220	$X_1 = 0.7632$

Loads.

Roxburgh-011	P = 90 Q = 54
Invercarg033	P = 135 Q = 36

System Parameters.

Base frequency = 50 Hz
Base power = 100 MVA
Base Voltage = 220 kV